

NMR Investigations of the Self-Organization and Dynamics of Mutated Amyloid Protein Fibrils

Von der Fakultät für Lebenswissenschaften
der Universität Leipzig
genehmigte

DISSERTATION

zur Erlangung des akademischen Grades

Doctor rerum naturalium
Dr. rer. nat.

vorgelegt
von

M. Sc. (Molecular Life Science) Alexander Korn
geboren am 15.5.1990 in Saalfeld

Dekan: Prof. Dr. Marc Schönwiesner
Gutachter: Prof. Dr. Tilo Pompe
Prof. Dr. Jochen Balbach

Tag der Verteidigung

Leipzig, den 2.9.2022

Supervisor

Herr Prof. Dr. Daniel Huster

Co-Supervisor

Herr Prof. Dr. Tilo Pompe

Bibliographic Data

Alexander Korn

NMR Investigations of the Self-Organization and Dynamics of Mutated Amyloid Protein Fibrils

Leipzig University, Faculty of Life Sciences

Dissertation

125 pages, 140 references, 33 figures, 1 table

This work investigates the influence of mutations at selected positions on the structure formation of the Alzheimer's disease peptide amyloid β . Amyloid β is a member of the class of intrinsically disordered proteins that can aggregate into fibrils, which are characterized by a highly stable secondary structure, called cross- β structure. A central contact during fibrillation is the hydrophobic F19-L34 contact, which is located within the core of the cross- β structure. Modifications of this contact are known to influence the local molecular structure whereas the fibril morphology and the cross- β structure remain stable. In contrast, toxicity of amyloid β was completely lost for all previously investigated mutants of F19 and L34.

This work characterizes the properties of this contact and answers the question what the minimally tolerated modifications are. To characterize the structure, structure formation process and biological activity of the A β variants a set of experiments was carried out. The local structure and dynamics were investigated using NMR experiments focusing on ^{13}C -chemical shift changes and ^1H - ^{13}C dipolar couplings, respectively. The fibril morphology and cross- β structure was verified by electron microscopy, circular dichroism spectroscopy and X-ray diffraction. Toxicity and biological activity was investigated using complementary cell culture experiments.

The work was divided in three parts. First, L34 was substituted with three highly similar amino acids: the isomer isoleucine, valine that is one methylene group shorter but also a branched chain amino acid and the stereoisomer *D*-leucine. The L34 position proved to be important for the initiation of the structure formation, oligomer stability, fibril growth and the biological activity of amyloid β . These characteristics and properties were highly sensitive also to minor modifications but the different mutants showed no specific but qualitatively similar effects.

The second part complemented previous mutation studies of the F19 position. Four new mutants were designed testing mild modification of the F19-L34 contact: phenylglycine and the homophenylalanine (S)-2-amino-4-phenyl-butyric acid change the length of the side chain, cyclohexyl-alanine eliminates the π -aromaticity of the ring system and increases the 3D steric demand, and (1-naphthyl)-alanine increases the 2D steric demand while maintaining the aromaticity. Mutations at the F19 position caused qualitatively similar effects as L34 modifications but proved to have quantitatively greater impact. Furthermore, they showed some specificity as steric constraints caused larger changes than modifications of the ring system.

The third part investigates the influence of β -methylamino-L-alanine (BMAA) substitutions at positions F19, S8, and S26. The serine to BMAA substitutions were included because of their potential medical relevance. A F19BMAA substitution caused similar effects like other modifications at this position. Replacement of serine lead to a structural reorientation of the A β N-terminus and turn region. Furthermore, the pathways of the cell response changed from mitochondrial activity and plasma membrane integrity to apoptosis and neuronal stress reaction.

Summarizing, it could be shown that, although the formation and structure of amyloid β fibrils is robust against different modifications the fibrillation kinetics, local structure and especially biological activity is highly sensitive and to some extend specific to even minor modifications.

Table of content

Directories	III
List of figures	III
List of tables	III
List of abbreviations	IV
1 Summary	1
1.1 References	8
2 Zusammenfassung	9
2.1 Referenzen	17
3 Introduction	19
3.1 Protein fibrils and their medical relevance	19
3.2 Proteins and their 3D structure	22
3.2.1 Properties of amino acids	22
3.2.2 IDPs and unstructured proteins	24
3.2.3 Native protein structure	25
3.2.4 Protein misfolding: cross- β structure	28
3.3 Guiding physicochemical properties and interactions in protein structure formation	31
3.4 The process of protein folding	36
3.5 Amyloid β peptide and amyloid fibril formation	40
3.5.1 A β and its structure formation process	40
3.5.2 The F19-L34 contact in previous investigations	45
3.6 Biological relevance of A β modifications	49
3.6.1 A β mutations in early onset Alzheimer's disease	49
3.6.2 Posttranslational modification	52
3.6.3 Peptide length	52
3.7 Methods for the investigation of fibril formation and structure	54
3.7.1 Fibril formation kinetics	54
3.7.2 Fibril morphology	57
3.7.3 Secondary structure composition and characteristics	57
3.7.4 Local structure	58
3.7.5 Biological activity	62
4 Research questions and motivation	65

Table of content

5	Articles	71
5.1	Amyloid β (1-40) Toxicity Depends on the Molecular Contact between Phenylalanine 19 and Leucine 34	71
5.2	Ring structure modifications of phenylalanine 19 increase fibrillation kinetics and reduce toxicity of amyloid β (1-40)	83
5.3	Incorporation of the Nonproteinogenic Amino Acid β -Methylamino-alanine Affects Amyloid β Properties and Toxicity.....	89
6	References	101
	Acknowledgement	111
	Curriculum vitae	113
	Publications, presentations, posters	115
	Declaration of independent work	117

Directories

List of figures

Figure 1:	Key questions and major findings. ⁴⁻⁶	3
Figure 2:	Classification of proteopathies and risk factors for Alzheimer's disease.	20
Figure 3:	A β related cell death mechanisms contributing to neurodegeneration in Alzheimer's disease.	21
Figure 4:	Peptide bond formation.	23
Figure 5:	The 20 canonical amino acids.	23
Figure 6:	Venn diagram.	24
Figure 7:	Comparison of structure properties and function between proteins with intrinsic disorder and a stable native conformation.	25
Figure 8:	Structure hierarchy of proteins.	27
Figure 9:	Protein folding and misfolding pathways.	29
Figure 10:	Top and side view of a class 1 steric zipper conformation.	30
Figure 11:	Cross- β structure.	30
Figure 12:	Forces and interactions guiding protein folding (I).	33
Figure 13:	Forces and interactions guiding protein folding (II).	35
Figure 14:	Schematic folding energy landscape of proteins.	37
Figure 15:	Structure formation models.	38
Figure 16:	Extended folding energy landscape with intermolecular contacts.	39
Figure 17:	The fibril formation process.	40
Figure 18:	A β monomer structure.	41
Figure 19:	A β oligomer structure.	42
Figure 20:	A β protofibril model.	43
Figure 21:	A β fibril structure.	44
Figure 22:	Sterically constrained F19 mutants.	46
Figure 23:	F19 mutants with additional hydrogen bond donating chemical groups.	47
Figure 24:	F19 mutants introducing charged amino acids and F19-L34 double mutants introducing attractive or repulsive charges.	48
Figure 25:	Selected A β mutations and modifications.	49
Figure 26:	Genetic factors in the etiology of Alzheimer's disease.	52
Figure 27:	APP cleavage pathways.	53
Figure 28:	Thioflavin T fluorescence assay.	56
Figure 29:	Circular dichroism spectroscopy.	58
Figure 30:	Schematic comparison of the carbon chemical shifts of valine in different secondary structures.	60
Figure 31:	DipShift experiment.	62
Figure 32:	Cell response assays.	63
Figure 33:	Research questions and experimental setup.	68

List of tables

Table 1	A β variants.	50
---------	--------------------------	----

List of abbreviations

2D	two-dimensional
3D	three-dimensional
ADAM	a disintegrin and metalloproteinase
APP	amyloid precursor protein
A β	amyloid beta
BACE	beta-secretase; beta-site amyloid precursor protein cleaving enzyme
BMAA	β -methylamino-L-alanine
CD	circular dichroism
Cha	cyclohexyl-alanine
C-terminus	carboxy-terminus
DipShift	dipolar-coupling chemical-shift correlation
DNA	deoxyribonucleic acid
EM	electron microscopy
EWSR	Ewing's sarcoma ribonucleic acid-binding protein
FET	FUS/EWS/TAF
FTLD	frontotemporal lobar degeneration
FUS	fused in sarcoma protein
hPhe	homophenylalanine; (S)-2-amino-4-phenylbutanoic acid
IDP	intrinsically disordered peptide
LDH	lactate dehydrogenase
MAS	magic angle spinning
MND	moto neuron disease
MTT	3-(4,5-dimethylthiazol-2-yl)-2,5-diphenyltetrazolium bromide
Nal	(1-naphthyl)-alanine
NDD	newly diagnosed diabetes
NMR	nuclear magnetic resonance
N-terminus	amino-terminus
PDB	protein data base
Phg	phenylglycine
PI	propidium iodide
TAF	TATA-binding protein-associated factor
TAR	transactive response
TDP	transactive response deoxyribonucleic acid-binding protein
TEM	transmission electron microscopy
t_{fib}	fibrillation time
ThT	Thioflavin T
TICT	twisted intramolecular charge transfer
t_{lag}	lag time
tRNA	transfer ribonucleic acid
WHO	World Health Organization
WT	wildtype

1 Summary

The function of a protein essentially depends on its correct three-dimensional structure. Therefore, it is not surprising that protein misfolding contributes to the pathology of many diseases. For a large group of diseases, called proteopathies, it is even the central pathological mechanism. Although the protein structure is determined by the sequence and the properties of the amino acids forming the polypeptide chain, especially intermolecular forces can interfere with the folding process that is commonly dominated by intramolecular forces. A dominant misfolding pathway of many proteopathies, especially neurodegenerative diseases, is the formation of amyloid fibrils. The best-known example is the formation of amyloid β (A β) fibrils in Alzheimer's disease.

In the case of amyloids, a large number of peptides with the same amino acid sequence assembles in a fibril like fashion. Each protein contributes typically at least two β -strands to form extended β -sheets that are stabilized by intermolecular backbone hydrogen bonds. Stacking of at least two of these intermolecular β -sheets in a way that hydrophobic residues are buried between the sheets and hydrophilic residues are exposed to the solvent results in the formation of the characteristic cross- β structure. This hallmark structure of amyloid fibrils is extraordinarily stable as the formation of a large number of hydrogen bonds and the high energy contribution of the hydrophobic effect result in a folding energy that is typically even lower than the native conformation of the monomeric protein.

Understanding this process and its underlying mechanisms is not only substantial for the identification of the pathology of many diseases but also of the physiological protein folding mechanisms. It is likely that all proteins are able to form fibrils regardless of their sequence provided that the conditions during the folding process promote aggregation. This makes the fibril formation a generic property of all proteins reflecting fundamental physical laws and principles, which determine protein structure formation.

This work addresses the questions which characteristics of the fundamental physical forces govern amyloid fibril formation and which physicochemical interactions determine the peptide self-organization, the amylogenic folding pathway and the subsequent cross- β structure formation. To this end, the influence of perturbations and constraints, locally introduced in the primary structure, were examined. Finally, investigations on how mechanisms of structure formation translate to protein function and activity were performed (see Figure 1).

This was done using mutational studies on A β . This peptide is not only noted for its role in Alzheimer's disease but also because it is a well-established model peptide for the process of fibril formation. In this work, the 40 amino acids long alloform that is most abundant in the human brain was used. The peptide structure can be divided into five parts: (1) a flexible N-terminus, (2) a first hydrophobic region with pronounced β -sheet formation propensity, (3) a linker region, (4) a second hydrophobic region with pronounced β -sheet formation propensity, and (5) a short C-terminus. Whereas the monomer is intrinsically disordered, the typical cross- β structure is formed during fibrillation. There, the two hydrophobic regions form β -strands that contribute to β -sheets stabilized by intermolecular hydrogen bonds between consecutive A β monomers. The hydrophobic areas of the two β sheets stack together, which results in the formation of the cross- β structure typical for amyloid fibrils.

For A β it was shown that the hydrophobic contact between phenylalanine 19 (F19) and leucine 34 (L34) is of key importance for fibril formation. The two amino acids are located within the two β -sheet forming regions of the peptide, namely the hydrophobic core and the

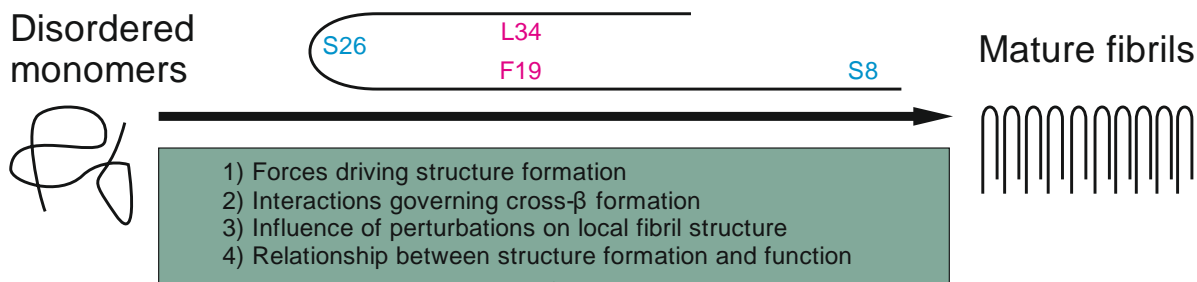
C-terminus. The interaction between these residues is a conserved, early step in the fibril formation process. In the mature fibril structure, these residues are located within the hydrophobic core of the cross- β structure. In previous mutation studies of the F19-L34 contact it could be shown that the cross- β structure remains highly conserved and tolerates various perturbations introduced at the position of the contact.¹ These constraints comprised (1) changes of the structural flexibility of the peptide backbone, (2) the introduction of additional hydrogen bond forming moieties at the side chains, the influence of (3) positive as well as (4) negative charges and the substitution of the contact by (5) a salt bridge and (6) two repulsive positively charged amino acids. For all mutants the global fibril morphology and the cross- β structure remained conserved with exception of the salt bridge variant that did not form fibrils. The introduced constraints resulted in an alteration of the local structure and modified amino residue dynamics caused by a change in the packing density within the fibril core. Strong effects could also be observed on the fibril formation kinetics. This reflects the interactions between the solvent environment and forces at the peptide surface, which are crucial for the stability and structure transition of transient folding intermediates but less important for the mature fibril structure. For example, these can be interactions of charged amino acids with solvent salt ions or the protonation of amino acid residues caused by a high solvent pH. The largest difference to the wildtype that was generic for all variants independent of the nature of the substitution concerns the cellular activity of the mutants. MTT assays showed that exclusively the wildtype impaired mitochondrial activity whereas the mutations completely abolished this effect.

This rises several fundamental questions concerning the fibrillation formation process of A β : How specific is the F19-L34 contact? What forces and interactions determine this potential specificity? What are the individual contributions of the F19 and the L34 respectively to the contact? How sensitive is the biological activity of A β to modifications of this contact? Are the observed effects exclusive to the F19-L34 contact or can other mutations cause similar changes?

To address these questions, a library of mutations was prepared. Mutational studies are a well-established approach to study the properties of A β . This strategy is suitable as several naturally occurring mutations are known that are often linked to familial forms of Alzheimer's disease or specific pathologies.² Furthermore, A β has a number of sites for posttranslational modifications.³ This shows that single side alterations of the peptide sequence are on the one hand well tolerated, but on the other hand lead to observable changes in the properties and function of the peptide. Because of this, mutational studies on A β are a well-established experimental approach already used in a number of other investigations and were also chosen to address the questions asked in this work.

Selected amino acids were substituted to moderately alter the van der Waals volume, hydrophobicity, dielectric properties, stereospecific configurations, and aromatic ring systems at chosen positions in the fibril structure. Different characteristics of the mature fibrils and the folding process were investigated for these mutations, namely: (1) global fibril morphology, (2) secondary structure composition, (3) characteristics of the cross- β structure, (4) local structure and (5) dynamics of amino acids in the fibrillar state, (6) kinetics of the fibril formation process and (7) cytotoxic activity, which is mainly caused by transient oligomer species.

The first part of the work focuses on the local environment of L34, whereas the second part investigates new mutations at the F19 side. In the third and final part, the scope was extended to two additional regions of the peptide, namely the N-terminus and the loop region. There, the positions S8 and S26 were substituted by the microbial, non-proteinogenic amino acid β -Methylamino-L-alanine (BMAA), which also gave insights to the questions, which pathological effects could be expected by such possibly medically relevant modification.



F19-L34 contact		BMAA misincorporation	
<p>Position L34</p> <chem>CC(C)C</chem>	<p>Position F19</p> <chem>c1ccccc1</chem>	<p>F19</p> <chem>c1ccccc1</chem>	<p>S8</p> <chem>CO</chem>
<p>Wildtype</p>			
<p>Mutations</p> <p>V: <chem>CC(C)C</chem></p> <p>I: <chem>CC(C)C</chem></p> <p>D-L: <chem>CC(C)C</chem></p> <p>Nal: <chem>c1ccc2ccccc2c1</chem></p> <p>Cha: <chem>C1CCCCC1</chem></p> <p>hPhe: <chem>c1ccc(cc1)CC</chem></p> <p>Phg: <chem>c1ccccc1</chem></p>			<p>BMAA</p> <chem>CNC</chem>
<p>Results: <u>Role of the position L34</u></p> <ul style="list-style-type: none"> - Initiation of the structure formation process - Stabilization of transient oligomeric structures - Fibril elongation by monomer recruitment - Cellular activity <p><u>Contribution of different physicochemical forces:</u></p> <ul style="list-style-type: none"> - High sensitivity of all effects also to minor constraints - No specificity to different forces observed 	<p>Results: <u>Role of the position F19</u></p> <ul style="list-style-type: none"> - Greater influence than L34 - Fibril formation kinetics - Aggregation propensity - Destabilization of transient oligomeric structure - Fibril elongation by monomer recruitment - Cellular activity <p><u>Contribution of different physicochemical forces:</u></p> <ul style="list-style-type: none"> - High sensitivity of all effects also to minor constraints - Major role of steric constraints - less impact of ring system modifications 	<p>Results: <u>F19 substitution:</u></p> <ul style="list-style-type: none"> - Behaves like a severe mutation - Major effects on: fibril formation kinetics, local structure, local dynamics and cellular activity <p><u>S8 and S26 substitution:</u></p> <ul style="list-style-type: none"> - Similar effects at both positions - Greater influence of the S26 than the S8 position - Structural reorientation of the N-terminus as well as the turn region - Switch of the cellular response pathway from mitochondrial activity and cell membrane integrity to apoptosis and neuronal stress reactions 	

Figure 1: Key questions and major findings.⁴⁻⁶

At the L34 position investigated in the first part, three mutations were introduced: The first variant contained *D*-leucine, the enantiomer of the proteinogenic *L*-leucine, which only changes the stereochemistry at the C_α position. The second mutant was L34I where the isomeric relocation of one methyl group caused a change in the steric properties of the side chain. The third substituent was valine, which is also a terminally branched amino acid but one methylene group shorter than the leucine in the wildtype, which reduces the van der Waals volume of the side chain. This mutation is characteristic for cerebral amyloid angiopathy.⁷ However, our investigations do not directly relate to this form of disease but molecular dynamics simulations addressing this aspect match our findings.⁸ All three mutants influenced the fibrillation kinetics and biological activity of Aβ but caused only minor changes of the local structure and did not affect the fibril morphology, the secondary structure composition of the mature fibrils or the characteristics of the cross-β structure. This indicates that the Aβ oligomers, as transient folding intermediates, are sensitive to constraints affecting the interaction forces at the L34 position, which guide the folding process. The fibril formation kinetics indicate that on one hand the oligomer structure was destabilized and on the other hand the fibril elongation was enhanced. This shows that, besides the predominant hydrophobicity, the exact stereospecificity of interactions and the transitions between folding intermediates are also of utter importance. These interactions are not restricted to the neighboring amino acids of L34 but more importantly affect the non-local interaction with F19 and adjacent amino acids.⁴

The most significant differences between the wildtype and the mutants could be seen in the kinetics measurements and especially the cell response assays. As structural investigations are only possible to a limited extent for transient species, these functional assays proved to be an important method for oligomer characterization. Overall, in this part of the work it could be demonstrated, that even minor modifications of the forces located at the L34 side are important for (1) the initiation of the structure formation process, (2) the stabilization of transient oligomeric structures, (3) the recruitment of monomers for fibril elongation, (4) to a minor extend local structure and dynamics, and (5) neuronal toxicity of Aβ. (7) No specificity of the observed effects correlating with distinct constraints could be identified by the substitution pattern applied. However, (8) a high sensitivity of the cellular response could be demonstrated even for minimal modifications of the local forces.⁴

The second part of the work answers questions that remained open in previous studies concerning the F19 position. As the mutations at the L34 side demonstrated, already minor alterations of the physical forces at the F19-L34 contact result in clear changes in the fibril formation process and cell response. Therefore, also at the F19 positions the influence of minor modifications on fibril formation and biological activity had to be investigated. The canonical amino acids most similar to phenylalanine, tyrosine and tryptophane have already been investigated. Whereas they showed the main commonality with the wildtype in aspects of structure and fibril formation kinetics, they also completely abolished the toxic properties of Aβ.¹ This demonstrates, that the presence of a ring system is of key importance for the fibril formation as well as the local structure and dynamics of the mature fibril. It also shows, that the characteristics of the ring system, like aromaticity, 2D, and 3D steric demand, determine the biological activity of the Aβ variant. To get a deeper insight in the involved mechanisms, four mutants were synthesized using non-canonical phenylalanine derivatives. The first amino acid was cyclohexyl-*L*-alanine, which carries a saturated ring instead of a conjugated ring system. This changes not only the electronic properties but also the dipole moment and the planarity of the residue. The second mutation, which was introduced was (1-naphthyl)-*L*-alanine based on two condensed benzene rings. This changes the van der Waals volume of the residue and to some extent also the dipole moment but conserves the other characteristics of the residue. The final pair of substitutions are phenylglycine and *L*-homophenylalanine, which remove or add a methylene

group, respectively. These represent the smallest changes as only the distance between the two opposing amino acids at positions 19 and 34 was altered. All mutants of this part of the work showed effects similar to the L34 mutants. Also, in the cases of the altered distances, the global structure remained unaffected and only moderate changes on the molecular level could be observed. Again, the fibrillation kinetics and the biological activity were much more sensitive towards modifications. Overall, the non-canonical amino acids all caused a higher aggregation propensity, destabilized oligomeric structure and caused a faster recruitment of unstructured monomers to preformed fibril structures reflected by a faster growth rate in the kinetics measurements of the fibril formation process. Furthermore, they showed a strongly reduced cell response, which, however, was still significantly different from control and wildtype. Compared to the L34 position, the constraints introduced at the F19 side had stronger effects on the cellular response in terms of mitochondrial activity and plasma membrane integrity. Furthermore, similar to the L34 mutations, the steric characteristics of the contact is of highest importance. Changes of the hydrophobicity or the π -electron ring system caused still detectable but less pronounced effects showing a specificity of the local interactions towards steric constraints. Again, the modifications act on level of the transient folding intermediates rather than the mature structure.⁵

The direct comparison between the F19 and the L34 mutations confirms the importance of this contact but indicates that the contribution of the F19 side is larger than the contribution of the L34 position, especially regarding the consequences of modifications on the cellular response. In both cases, the investigated modifications caused qualitatively comparable but quantitatively distinct effects. Particularly, stereospecific mechanisms determine the properties of this contact even though other forces like van der Waals interactions or the π -electrons of the phenyl ring system contribute. In general, constraints at the F19 position caused more severe effects on structure formation and biological activity than at the L34 position. The propagation of the local structural changes to the opposing β -sheet at the F19 position is another important feature of L34 mutations.⁵

In the third part, the non-canonical amino acid β -Methylamino-L-alanine (BMAA) was introduced at the F19 position as well as S8 and S26, which are located at the N-terminus and the turn-region, respectively. BMAA is suspected to be a risk factor for neurodegenerative diseases. One of the discussed pathological pathways of BMAA is its misincorporation in proteins leading to misfolding and subsequently to aggregations. This is indicated by the possibility that the Ser-tRNA synthetase can accept BMAA instead of serine. The S8 and S26 positions were used as mutation sites because of this capability of Ser-tRNA synthetase to accept BMAA instead of serine. Both BMAA and serine contain a hydrogen donating group in their side chain for formation of potential hydrogen bonds.⁶

When BMAA is introduced at position F19 within the hydrophobic core region, it strongly affects local structure and dynamics, the fibril formation kinetics, and the biological activity of A β , while the global fibril morphology and secondary structure composition were conserved. Thus, in this case it behaves like a severe mutation rather than a mild one. BMAA substitutions for serine are of more interest. Although such modifications could not be shown in vivo, their possible relevance is discussed based on the capability of serine tRNA synthetase to accept BMAA as substitute in vitro. Synthetic A β peptides with a S8BMAA or a S26BMAA mutation showed that such substitutions result in a characteristic change of A β properties: The hydrophobic core with the cross- β structure remains unaffected but structural alterations occur at the N-terminus (S8BMAA) as well as within the turn structure (S26BMAA). Most prominent are the changes in the biological activity of A β as in both cases no longer the mitochondrial activity is impaired but apoptotic caspase 3 activation and a stress induced neurite length shortening is induced. Both serine substitutions show comparable effects that are slightly more pronounced in case of

S26BMAA. This functional similarity might be caused by a S8-S26 interaction, which was shown for an A β fibril structure relevant to Alzheimer's disease.⁹ The correlation between fibrillation kinetics and biological activity was different between the Ser-BMAA substitutions and the other mutations tested in this work indicating a distinct fibril formation pathway, which favors more stable oligomers. Furthermore, the serine substitutions showed a distinct cell activity. Instead of acting through mitochondria-cell membrane mediated mechanisms they induced apoptosis and a neuronal stress response. This shows that more than one mode of action contributes to A β toxicity. Also, this observed change of activity might be useful to answer the question if BMAA misincorporation is a relevant risk factor for Alzheimer's disease as this should be revealed by Caspase 3 activation instead of mitochondrial dehydrogenase inhibition, which seems to be characteristic for non-BMAA misincorporation A β pathology. Additionally, such activity switches might be relevant to explain different forms and etiologies of Alzheimer's disease and the activity of different risk factors.⁶

All of our findings can be interpreted using the classical U-shape model of the A β fibril structure, which is guided by intramolecular contacts. However, it cannot be ruled out that the investigated contacts form intermolecular contacts. This can result in a U-shaped structure with an offset between the β -sheets along the fibril axis or even an extended structure where two straight filaments align in opposing orientation.^{10,11} A distinction between intramolecular and intermolecular contacts could be made by NMR experiments comparing fully labeled with mixtures of labeled and non-labeled or differently labeled peptides. However, this was not done in this work as the investigated physicochemical characteristics of the interactions were supposed to be identical in both cases.

In conclusion, this work shows that modulations of the local physicochemical forces and interactions of A β strongly affect its structural properties, the folding process and biological activity. Depending on the mutation side and the introduced constraints, mutations not only modulate the strength of the cellular response but are also capable of changing the involved signaling pathways for neurotoxicity. This has to be caused by a change of the self-organization of the polypeptide and the involved structure formation pathways. Subsequently, this links the fundamental physicochemical characteristics of the amino acid chain to the various etiologies and modes of action of potential risk factors contributing to the pathology of Alzheimer's disease and other proteinopathies. The key features of A β fibrils are not only the fibril morphology and cross- β structure but also their outstanding stability and resistance to side chain modifications, which can be introduced by various mutations. All mutants investigated in this and previous works caused structural rearrangements and changes in dynamics, which were restricted to the local environment of the affected amino acids. However, not only amino acids neighboring the mutation side were affected but also amino acids in close proximity of direct interaction partners. This could be demonstrated for interactions between S8 and S26 as well as in detail for the F19-L34 contact.

The characteristics of this contact are mainly determined by the steric properties, which are more sensitive to modifications of the F19 position with the bulky ring system whereas the smaller L34 side chain has a lower impact. It could be shown that the fibril formation is not only driven by the aggregation propensity of the peptide, which is caused by the enthalpic and entropic contribution of the interaction forces. At both positions, the steric features were the key factors of the involved amino acid residues. For the F19 position, the conjugation of the ring system also proved to be important. Constraints addressing other physicochemical characteristics displayed only moderate effects on the self-organization, folding pathway and mature fibril structure of A β . The importance of the steric specificity of the interactions guiding the fibril formation process is also reflected on the level of oligomers and other transient structural species, which were indirectly investigated by fibril formation kinetics measurements. This links

the demonstrated steric specificity of the guiding F19-L34 interaction to the sensitivity of the biological activity to introduced constraints, which explains the fact that not the mature fibrils, but oligomers are shown to be the toxic species in Alzheimer's disease pathology.

A recent work shows, that the influence of steric constraints is not limited to the amino acid side chains but also the backbone contributes significantly. By using non-proteinaceous amino acids with methylated backbone amino groups, it could be shown that also constraints in the backbone lead to similar changes in the fibrillation behavior, structure and biological activity of A β . In this case, besides steric constraints the prevention of the hydrogen bond formation of the amino group also contributes to the effect. In contrast, introducing a methylene or ethylene spacer between the amino and carboxy group within the backbone increased the fibrillation propensity by introduction of additional degrees of freedom.¹²

Furthermore, the observed effects are not exclusive for the amino acids, which form the hydrophobic contact, but also neighboring amino acids within the cross- β region contribute. This could be shown in the case of F20 and G33. Also, for these amino acids the fibril structure remained robust and the strongest effects could be observed for the fibrillation kinetics and toxicity of the peptides. Interestingly, the effects of a substitution of G33 with alanine caused similar but stronger effects than the substitution of either amino acid involved in the F19-L34 contact. This could be attributed to the fact that the G33A mutation prevented the formation of a salt bridge in the turn region on the oligomeric but not on the fibrillar level. This shows that not only the F19-L34 contact is critical for the initiation of the fibril formation, the fibrillation kinetics and the properties of the oligomers. Also other amino acids within the cross- β structure determine the structure formation process and are capable to guide it to alternative pathways.¹³

Subsequent investigations should be invested in the question if the amino acid contacts, which are reported to be critical for the structure formation process are indeed intramolecular contacts. Although this would be in agreement with the widely used U-shape structural model recent research indicates that also other conformations comprising an intermolecular arrangement of the contacts have to be considered. This also touches the question if the classical U-shape model can be maintained or if other models should be preferred. It is also still not clear, if the wildtype is the primary toxic species and which are contributions of mutated or posttranslationally modified variants. Both cases can lead to different structures and therefore other molecular contacts and other physicochemical interactions might be critical.

This work focuses on the hydrophobic contact between F19 and L34 within the cross- β region. However, also other contacts are known to be important, for example the formation of a salt bridge within the turn formation that electrostatic interactions should be the predominant force. A detailed investigation of such other contacts could yield similar important insights in the structure formation process.

Overall, this work contributes to the understanding of protein folding and misfolding mechanisms and gives indications for the development of new approaches to treat proteinopathies.

1.1 References

1. Adler, J., Scheidt, H. A., Krüger, M., Thomas, L. & Huster, D. Local interactions influence the fibrillation kinetics, structure and dynamics of A β (1-40) but leave the general fibril structure unchanged. *PHYSICAL CHEMISTRY CHEMICAL PHYSICS : PCCP* **16**, 7461–7471; 10.1039/c3cp54501f (2014).
2. Bateman, R. J. *et al.* Autosomal-dominant Alzheimer's disease: a review and proposal for the prevention of Alzheimer's disease. *ALZHEIMER'S RESEARCH & THERAPY* **3**, 1; 10.1186/alzrt59 (2011).
3. Atwood, C. S., Martins, R. N., Smith, M. A. & Perry, G. Senile plaque composition and posttranslational modification of amyloid- β peptide and associated proteins. *PEPTIDES* **23**, 1343–1350; 10.1016/S0196-9781(02)00070-0 (2002).
4. Korn, A. *et al.* Amyloid β (1-40) Toxicity Depends on the Molecular Contact between Phenylalanine 19 and Leucine 34. *ACS CHEMICAL NEUROSCIENCE* **9**, 790–799; 10.1021/acschemneuro.7b00360 (2018).
5. Korn, A., Surendran, D., Krueger, M., Maiti, S. & Huster, D. Ring structure modifications of phenylalanine 19 increase fibrillation kinetics and reduce toxicity of amyloid β (1-40). *CHEMICAL COMMUNICATIONS (CAMBRIDGE, ENGLAND)* **54**, 5430–5433; 10.1039/c8cc01733f (2018).
6. Korn, A. *et al.* Incorporation of the Nonproteinogenic Amino Acid β -Methylamino-alanine Affects Amyloid β Fibril Properties and Toxicity. *ACS CHEMICAL NEUROSCIENCE* **11**, 1038–1047; 10.1021/acschemneuro.9b00660 (2020).
7. Obici, L. *et al.* A novel AbetaPP mutation exclusively associated with cerebral amyloid angiopathy. *ANNALS OF NEUROLOGY* **58**, 639–644; 10.1002/ana.20571 (2005).
8. Saini, R. K., Thakur, H. & Goyal, B. Effect of Piedmont mutation (L34V) on the structure, dynamics, and aggregation of Alzheimer's A β 40 peptide. *JOURNAL OF MOLECULAR GRAPHICS & MODELLING* **97**, 107571; 10.1016/j.jmgm.2020.107571 (2020).
9. Lu, J.-X. *et al.* Molecular structure of β -amyloid fibrils in Alzheimer's disease brain tissue. *CELL* **154**, 1257–1268; 10.1016/j.cell.2013.08.035 (2013).
10. Paravastu, A. K., Leapman, R. D., Yau, W.-M. & Tycko, R. Molecular structural basis for polymorphism in Alzheimer's beta-amyloid fibrils. *PROCEEDINGS OF THE NATIONAL ACADEMY OF SCIENCES OF THE UNITED STATES OF AMERICA* **105**, 18349–18354; 10.1073/pnas.0806270105 (2008).
11. Ghosh, U., Thurber, K. R., Yau, W.-M. & Tycko, R. Molecular structure of a prevalent amyloid- β fibril polymorph from Alzheimer's disease brain tissue. *PROCEEDINGS OF THE NATIONAL ACADEMY OF SCIENCES OF THE UNITED STATES OF AMERICA* **118**; 10.1073/pnas.2023089118 (2021).
12. Schwarze, B. *et al.* Peptide backbone modifications of amyloid β (1-40) impact fibrillation behavior and neuronal toxicity. *SCIENTIFIC REPORTS* **11**, 23767; 10.1038/s41598-021-03091-4 (2021).
13. Fritsch, J. *et al.* Probing the Influence of Single-Site Mutations in the Central Cross- β Region of Amyloid β (1-40) Peptides. *BIOMOLECULES* **11**; 10.3390/biom11121848 (2021).

2 Zusammenfassung

Die Funktion eines Proteins hängt im Wesentlichen von seiner korrekten dreidimensionalen Struktur ab. Daher ist es nicht überraschend, dass Proteinfehlfaltung zur Pathologie vieler Krankheiten beiträgt. Bei einer großen Gruppe von Erkrankungen, den sogenannten Proteopathien, ist sie sogar der zentrale Krankheitsmechanismus. Obwohl die Proteinstruktur durch die Sequenz und die Eigenschaften der Aminosäuren, die die Polypeptidkette bilden, bestimmt wird, können insbesondere intermolekulare Kräfte den Faltungsprozess beeinträchtigen, der üblicherweise von intramolekularen Kräften dominiert wird. Ein vorherrschender Fehlfaltungsweg vieler Proteopathien, insbesondere neurodegenerativer Erkrankungen, ist die Bildung von Amyloidfibrillen. Das bekannteste Beispiel ist die Bildung von A β -Fibrillen bei der Alzheimer-Krankheit.

Im Falle von Amyloiden lagert sich eine große Anzahl von Peptiden mit gleicher Aminosäuresequenz perlenkettenartig zusammen. Jedes Protein trägt typischerweise mindestens zwei β -Stränge zur Bildung ausgedehnter β -Faltblätter bei, die durch intermolekulare Wasserstoffbrücken zwischen den Hauptketten stabilisiert werden. Das Aneinanderlagern von mindestens zwei dieser intermolekularen β -Faltblätter in einer Form, dass hydrophobe Reste zwischen den Blättern begraben und hydrophile Reste dem Lösungsmittel zugewendet sind, führt zur Bildung der charakteristischen Cross- β -Struktur. Diese charakteristische Struktur der Amyloidfibrillen ist außerordentlich stabil, da die Bildung einer großen Anzahl von Wasserstoffbrückenbindungen sowie der hohe Energiebeitrag des hydrophoben Effekts zu einer Faltungsenergie führen, die typischerweise sogar niedriger ist als die native Konformation des monomeren Proteins.

Das Verständnis dieses Prozesses und der ihm zugrundeliegenden Mechanismen ist nicht nur wesentlich für die Identifizierung der Pathologie vieler Krankheiten, sondern auch für die physiologischen Proteinfaltungsmechanismen. Es ist wahrscheinlich, dass alle Proteine in der Lage sind, unabhängig von ihrer Sequenz Fibrillen zu bilden, vorausgesetzt, die Bedingungen während des Faltungsprozesses fördern die Aggregation. Dies macht die Fibrillenbildung zu einer generischen Eigenschaft aller Proteine, die grundlegende physikalische Gesetze und Prinzipien widerspiegelt, die die Proteinstrukturbildung bestimmen.

Diese Arbeit beschäftigt sich mit den Fragen, welche Eigenschaften die grundlegenden physikalischen Kräfte haben, die die Bildung von Amyloidfibrillen regeln und welche physikalisch-chemischen Wechselwirkungen die strukturelle Selbstorganisation von Peptiden, den amyloiden Faltungsweg und die anschließende Cross- β -Strukturbildung bestimmen. Zu diesem Zweck wurde der Einfluss von lokalen Störungen und Beeinträchtigungen der Primärstruktur betrachtet. Schlussendlich wurde untersucht, wie sich die Mechanismen der Strukturbildung auf die Funktion und Aktivität auswirken (siehe Abbildung 1).

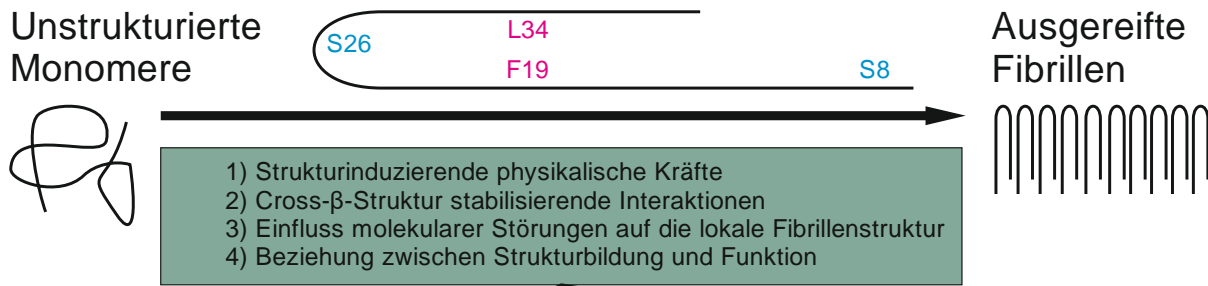
Dafür wurden Mutationsstudien an Amyloid β (A β) durchgeführt. Dieses Peptid ist nicht nur bekannt für seine Rolle bei der Alzheimer-Krankheit, sondern auch, weil es ein fest etabliertes Modellpeptid für den Prozess der Fibrillenbildung ist. In dieser Arbeit wurde die 40 Aminosäuren lange Alloform genutzt, die im menschlichen Gehirn am häufigsten vorkommt. Die Peptidstruktur lässt sich in fünf Teile unterteilen: (1) einen flexiblen N-Terminus, (2) eine erste hydrophobe Region mit ausgeprägter Neigung zur Bildung von β -Faltblättern, (3) eine Linker-Region, (4) eine zweite hydrophobe Region mit ausgeprägter Neigung zur Bildung von β -Faltblättern und (5) ein kurzer C-Terminus. Während das Monomer intrinsisch ungeordnet ist, wird während der Fibrillenbildung die typische Cross- β -Struktur gebildet. Darin bilden die beiden

hydrophoben Regionen β -Stränge, die zu β -Faltblättern beitragen, die durch intermolekulare Wasserstoffbrückenbindungen zwischen aufeinanderfolgenden A β -Monomeren stabilisiert werden. Die hydrophoben Bereiche der beiden β -Faltblätter lagern sich schlussendlich aneinander, was zur Bildung der für Amyloidfibrillen typischen Cross- β -Struktur führt.

Für A β wurde gezeigt, dass der hydrophobe Kontakt zwischen Phenylalanin 19 (F19) und Leucin 34 (L34) von zentraler Bedeutung für die Fibrillenbildung ist. Die beiden Aminosäuren befinden sich innerhalb der hydrophoben Kernregion und des C-Terminus, der beiden β -Faltblattbildenden Regionen des Peptids. Die Interaktion zwischen diesen Seitenketten ist ein konservierter, früher Schritt im Fibrillenbildungsprozess. In der finalen Fibrillenstruktur befinden sich diese Reste innerhalb des hydrophoben Kerns der Cross- β -Struktur. In früheren Mutationsstudien des F19-L34-Kontakts konnte gezeigt werden, dass die Cross- β -Struktur weitestgehend unverändert bleibt und verschiedene an der Kontaktstelle eingeführte Störungen toleriert.¹ Diese Störungen umfassten (1) die Änderungen der strukturellen Flexibilität des Peptidrückgrats, (2) die Einführung weiterer Wasserstoffbrücken bildender chemischer Gruppen an den Seitenketten, den Einfluss (3) positiver sowie (4) negativer Ladungen und die Substitution des Kontaktes durch (5) eine Salzbrücke und (6) zwei abstoßende, positiv geladene Aminosäuren. Bei allen Mutanten blieben die globale Fibrillenmorphologie und die Cross- β -Struktur erhalten, mit Ausnahme der Salzbrückenvariante, die keine Fibrillen bildete. Die eingeführten Beschränkungen führten zu einer Änderung der lokalen Struktur und einer modifizierten Dynamik der Seitenketten, die durch eine Änderung der Packungsdichte innerhalb des Fibrillenkerns verursacht wurde. Starke Effekte konnten auch auf die Kinetik der Fibrillenbildung beobachtet werden. Dies spiegelt die Wechselwirkungen zwischen der Lösungsumgebung und den Kräften an der Peptidoberfläche wider, die für die Stabilität und den Strukturübergang kurzlebiger Faltungsintermediate entscheidend sind, aber weniger wichtig für die finale Fibrillenstruktur. Dies können beispielsweise Wechselwirkungen geladener Aminosäuren mit Salzionen des Lösungsmittels oder die Protonierung von Aminosäureresten durch einen hohen pH Wert des Lösungsmittels sein. Der größte Unterschied zum Wildtyp, der unabhängig von der Art der Substitution und generisch für alle Varianten war, betrifft die zelluläre Aktivität der Mutanten. MTT-Assays zeigten, dass ausschließlich der Wildtyp die mitochondriale Aktivität beeinträchtigte, während die Mutationen diesen Effekt vollständig aufhoben.

Dies wirft mehrere grundlegende Fragen zum Bildungsprozess von A β -Fibrillen auf: Wie spezifisch ist der F19-L34-Kontakt? Welche Kräfte und Wechselwirkungen bestimmen diese potentielle Spezifität? Was sind die individuellen Beiträge des F19 bzw. des L34 zum Kontakt? Wie sensitiv ist die biologische Aktivität von A β gegenüber Modifikationen dieses Kontakts? Sind die beobachteten Effekte ausschließlich auf den F19-L34-Kontakt beschränkt oder können andere Mutationen ähnliche Veränderungen hervorrufen?

Um diese Fragen zu beantworten, wurde eine Bibliothek von Mutanten erstellt. Mutationsstudien sind ein etablierter Ansatz, um die Eigenschaften von A β zu untersuchen. Dieser Ansatz bietet sich an, da mehrere natürlich vorkommende Mutationen bekannt sind, die häufig mit familiären Formen der Alzheimer-Krankheit oder spezifischen Pathologien verbunden sind.² Außerdem besitzt A β eine Reihe von Aminosäuren die posttranslational modifiziert werden können.³ Dies zeigt, dass einzelne Änderungen der Peptidsequenz einerseits gut akzeptiert werden, andererseits aber zu erkennbaren Veränderungen der Eigenschaften und Funktion des Peptids führen. Da diese Mutationsstudien an A β ein etablierter experimenteller Ansatz sind, der bereits in einer Reihe anderer Untersuchungen erfolgreich Verwendung fand, wurde er auch hier gewählt, um die in dieser Arbeit gestellten Fragen zu adressieren.



F19-L34-Kontakt		BMAA Fehleinlagerung	
Position L34	Position F19	F19	S8 S26
$\begin{array}{c} \\ \text{CH}_2 \\ \\ \text{CH} \\ / \quad \backslash \\ \text{H}_3\text{C} \quad \text{CH}_3 \end{array}$	$\begin{array}{c} \\ \text{CH}_2 \\ \\ \text{C}_6\text{H}_5 \end{array}$	$\begin{array}{c} \\ \text{CH}_2 \\ \\ \text{C}_6\text{H}_5 \end{array}$	$\begin{array}{c} \\ \text{CH}_2 \\ \\ \text{OH} \end{array}$
Wildtyp			
V $\begin{array}{c} \\ \text{CH} \\ / \quad \backslash \\ \text{H}_3\text{C} \quad \text{CH}_3 \end{array}$	I $\begin{array}{c} \\ \text{CH} \\ / \quad \backslash \\ \text{CH}_2 \quad \text{CH}_3 \\ \\ \text{CH}_3 \end{array}$	D-L $\begin{array}{c} \\ \text{CH}_2 \\ \\ \text{CH} \\ / \quad \backslash \\ \text{H}_3\text{C} \quad \text{CH}_3 \end{array}$	Nal $\begin{array}{c} \\ \text{CH}_2 \\ \\ \text{CH}_2 \\ \\ \text{C}_6\text{H}_4 \end{array}$
Mutationen	Cha $\begin{array}{c} \\ \text{CH}_2 \\ \\ \text{C}_6\text{H}_{11} \end{array}$	hPhe $\begin{array}{c} \\ \text{CH}_2 \\ \\ \text{CH}_2 \\ \\ \text{C}_6\text{H}_5 \end{array}$	Phg $\begin{array}{c} \\ \text{CH}_2 \\ \\ \text{C}_6\text{H}_5 \end{array}$
BMAA			$\begin{array}{c} \\ \text{NH} \\ \\ \text{CH}_3 \end{array}$
Ergebnisse <u>Funktion der L34-Position</u>	Ergebnisse: <u>Funktion der F19-Position</u>	Ergebnisse: <u>F19-Substitution:</u>	
<ul style="list-style-type: none"> - Initiierung des Strukturbildungsprozesses - Stabilisation transienter Oligomerstrukturen - Fibrillenwachstum durch Monomeranlagerung - Zelluläre Aktivität 	<ul style="list-style-type: none"> - Größerer Einfluss als L34 - Fibrillierungskinetik - Aggregationsneigung - Destabilisation der transienten Oligomere - Fibrillenverlängerung durch Monomeranlagerung - Zellaktivität 	<ul style="list-style-type: none"> - Einfluss ähnlich einer schwerwiegenden Mutation - Hauptsächlich Einfluss auf: Fibrillierungskinetik, lokale Struktur, lokale Dynamik und Zellaktivität 	
<u>Beitrag unterschiedlicher physikochemischer Kräfte</u>	<u>Beitrag unterschiedlicher physikochemischer Kräfte</u>	<u>S8- und S26-Substitution</u>	
<ul style="list-style-type: none"> - Hohe Sensitivität sämtlicher Effekte selbst auf geringfügige Beschränkungen - Keine Spezifität für unterschiedliche Kräfte beobachtbar 	<ul style="list-style-type: none"> - Hohe Sensitivität aller Effekte auch auf geringere Beeinträchtigungen - Hauptrolle spielen sterische Beschränkungen - Geringerer Einfluss von Modifikationen des Ringsystems 	<ul style="list-style-type: none"> - Ähnliche Effekte an beiden Positionen - Stärker ausgeprägt an S26 als an S8 Position - Umstrukturierung von N-Terminus und Turn-Region - Geänderte Zellantwort: Apoptose und Stressreaktion statt mitochondriale Antwort und Zellmembranschäden 	

Abbildung 1: Schlüsselfragen und wichtigste Erkenntnisse.⁴⁻⁶

Wir haben ausgewählte Aminosäuren substituiert, um das van-der-Waals-Volumen, die Hydrophobizität, die dielektrischen Eigenschaften, die stereospezifischen Konfigurationen und die aromatischen Ringsysteme an ausgewählten Positionen in der Fibrillenstruktur moderat zu verändern. Für diese Mutationen wurden verschiedene Charakteristika der ausgereiften Fibrillen und des Faltungsprozesses untersucht, nämlich: (1) die globale Fibrillenmorphologie, (2) die Zusammensetzung der Sekundärstruktur, (3) die Charakteristika der Cross- β -Struktur, (4) die lokale Struktur und (5) die Dynamik der Aminosäuren im fibrillären Zustand, (6) die Kinetik des Fibrillenbildungsprozesses und (7) die zytotoxische Aktivität, die hauptsächlich durch transiente Oligomer-Spezies verursacht wird.

Der erste Teil der Arbeit konzentriert sich auf die L34-Region, während der zweite Teil neue Mutationen der F19-Position untersucht. Im dritten und letzten Teil wurde der Blick auf zwei zusätzliche Regionen des Peptids erweitert, nämlich den N-Terminus und die Loop-Region. Dort wurden die Serine S8 und S26 durch die mikrobielle, nicht-proteinogene Aminosäure β -Methylamino-L-alanin (BMAA) ersetzt, was auch Aufschluss darüber gab, welche pathologischen Wirkungen bei einer solchen möglicherweise medizinisch relevanten Modifikation zu erwarten sind.

An der im ersten Teil untersuchten L34-Position wurden drei Mutationen eingeführt: Die erste Variante enthielt *D*-Leucin, das Enantiomer des proteinogenen *L*-Leucin, das nur die Stereochemie an der C_α -Position verändert. Die zweite Mutante war L34I, bei der die isomere Verlagerung einer Methylgruppe eine Veränderung der sterischen Eigenschaften der Seitenkette bewirkt. Der dritte Substituent war Valin, das ebenfalls eine endständig verzweigte Aminosäure ist, aber eine Methylengruppe kürzer als das Leucin im Wildtyp, was das van-der-Waals-Volumen der Seitenkette reduziert. Diese Mutation ist charakteristisch für die zerebrale Amyloidangiopathie.⁷ Unsere Untersuchungen beziehen sich jedoch nicht direkt auf diese Form der Krankheit, aber eine Arbeit die dies auf Basis von Molekulardynamik-Simulationen untersucht, stützt unsere Ergebnisse.⁸ Alle drei Mutanten beeinflussten die Fibrillationskinetik und die biologische Aktivität von A β , verursachten aber nur geringfügige Veränderungen der lokalen Struktur und hatten keinen Einfluss auf die Fibrillenmorphologie, die Sekundärstrukturzusammensetzung der ausgereiften Fibrillen oder die Eigenschaften der Cross- β -Struktur. Dies deutet darauf hin, dass die A β -Oligomere als transiente Faltungsintermediate empfindlich auf Einschränkungen reagieren, die die Interaktionskräfte an der L34-Position betreffen, welche den Faltungsprozess steuern. Die Kinetik der Fibrillenbildung deutet darauf hin, dass einerseits die Oligomerstruktur destabilisiert und andererseits das Fibrillenwachstum verstärkt wurde. Dies zeigt, dass neben der vorherrschenden Hydrophobie auch die genaue Stereospezifität der Wechselwirkungen sowie die Übergänge zwischen den Faltungsintermediaten von großer Bedeutung sind. Diese Wechselwirkungen sind nicht auf die benachbarten Aminosäuren von L34 beschränkt, sondern betreffen vor allem die nichtlokale Wechselwirkung mit F19 und benachbarten Aminosäuren.⁴

Die deutlichsten Unterschiede zwischen dem Wildtyp und den Mutanten zeigten sich bei den Kinetikmessungen und insbesondere bei den Zellkultur-Assays. Da Strukturuntersuchungen für transiente Spezies nur bedingt möglich sind, erwiesen sich diese funktionellen Assays als wichtige Methode zur Oligomercharakterisierung. Insgesamt konnte in diesem Teil der Arbeit gezeigt werden, dass bereits geringe Modifikationen der an der L34-Seite wirkenden Kräfte wichtig sind für (1) die Initiierung des Strukturbildungsprozesses, (2) die Stabilisierung transienter Oligomerstrukturen, (3) die Rekrutierung von Monomeren für das Fibrillenwachstum, (4) in geringem Maße für die lokale Struktur und Dynamik und (5) die neuronale Toxizität von A β . (7) Durch das angewandte Substitutionsmuster konnte keine Spezifität der beobachteten Effekte identifiziert werden, die mit bestimmten Einschränkungen korrelieren. Allerdings

konnte (8) eine hohe Sensitivität der zellulären Antwort auch für minimale Modifikationen der lokalen Kräfte nachgewiesen werden.⁴

Der zweite Teil der Arbeit beantwortet Fragen, die in früheren Studien bezüglich der F19-Position offenblieben. Wie die Mutationen an der L34-Seite gezeigt haben, führen bereits geringe Veränderungen der physikalischen Kräfte am F19-L34-Kontakt zu deutlichen Veränderungen im Fibrillenbildungsprozess und der Zellantwort. Daher musste auch an den F19-Positionen der Einfluss geringfügiger Modifikationen auf die Fibrillenbildung und die biologische Aktivität untersucht werden. Die kanonischen Aminosäuren, die dem Phenylalanin am ähnlichsten sind, Tyrosin und Tryptophan, wurden bereits untersucht. Während sie in Bezug auf Struktur und Fibrillenbildungskinetik die größte Gemeinsamkeit mit dem Wildtyp aufwiesen, hoben auch sie die toxischen Eigenschaften von A β vollständig auf. Dies zeigt, dass das Vorhandensein eines Ringsystems von zentraler Bedeutung für die Fibrillenbildung sowie die lokale Struktur und Dynamik der ausgereiften Fibrille ist und dass die Eigenschaften des Ringsystems, wie Aromatizität oder zwei- und dreidimensionaler Raumanpruch, die biologische Aktivität der A β -Variante bestimmen. Um einen tieferen Einblick in die beteiligten Mechanismen zu erhalten, wurden vier Mutanten unter Verwendung nicht-kanonischer Phenylalanin-Derivate synthetisiert. Die erste verwendete Aminosäure war Cyclohexyl-*L*-alanin, das einen gesättigten Ring anstelle eines konjugierten Ringsystems trägt. Dadurch ändern sich nicht nur die elektrischen Eigenschaften, sondern auch das Dipolmoment und die Planarität der Seitenkette. Die zweite Mutation, die eingeführt wurde, ist (1-Naphthyl)-*L*-Alanin, welches auf zwei kondensierten Benzolringen basiert. Dies verändert das van-der-Waals-Volumen der Seitenkette und bis zu einem gewissen Grad auch das Dipolmoment, erhält aber die anderen Eigenschaften. Das letzte Paar von Substitutionen sind Phenylglycin und *L*-Homophenylalanin, die eine Methylengruppe entfernen bzw. hinzufügen. Diese stellen die kleinsten Änderungen dar, da nur der Abstand zwischen den beiden gegenüberliegenden Aminosäuren an den Positionen 19 und 34 verändert wird. Alle Mutanten dieses Teils der Arbeit zeigten ähnliche Effekte wie die L34-Mutanten. Auch in den Fällen der veränderten Abstände blieb die globale Struktur unbeeinflusst und es konnten nur moderate Veränderungen auf molekularer Ebene beobachtet werden. Auch hier waren die Fibrillationskinetik und die biologische Aktivität deutlich empfindlicher gegenüber den Modifikationen. Insgesamt verursachten die verwendeten nicht-kanonischen Aminosäuren alle eine höhere Aggregationsneigung, destabilisierten die oligomere Struktur und bewirkten eine schnellere Rekrutierung von unstrukturierten Monomeren in vorgebildete Fibrillenstrukturen, was sich in einer schnelleren Wachstumsrate in den Kinetikmessungen des Fibrillenbildungsprozesses widerspiegelte. Darüber hinaus zeigten sie eine stark reduzierte Zellantwort, die sich jedoch immer noch signifikant von der Kontrolle und dem Wildtyp unterschied. Im Vergleich zur L34-Position hatten die an der F19-Seite eingeführten Einschränkungen stärkere Auswirkungen auf die zelluläre Antwort in Bezug auf die mitochondriale Aktivität und die Plasmamembranintegrität. Darüber hinaus ist, ähnlich wie bei den L34-Mutationen, die sterische Charakteristik des Kontakts von höchster Bedeutung. Veränderungen der Hydrophobizität oder des π -Elektronenringsystems verursachten immer noch nachweisbare, aber weniger ausgeprägte Effekte, die eine Spezifität der lokalen Wechselwirkungen gegenüber sterischen Einschränkungen zeigen. Auch hier wirken die Modifikationen eher auf der Ebene der transienten Faltungsintermediate als auf der Ebene der ausgereiften Struktur.⁵

Der direkte Vergleich zwischen den F19- und den L34-Mutationen bestätigt die Bedeutung dieses Kontakts, zeigt aber, dass der Beitrag der F19-Seite größer ist als der Beitrag der L34-Position, vor allem im Hinblick auf die Konsequenzen der Modifikationen auf die zelluläre Antwort. In beiden Fällen verursachten die untersuchten Modifikationen qualitativ vergleichbare, aber quantitativ unterschiedliche Effekte. Insbesondere stereospezifische Mechanismen bestimmen die Eigenschaften dieses Kontakts, obwohl auch andere Kräfte wie van-der-Waals-

Wechselwirkungen oder die π -Elektronen des Phenylringsystems dazu beitragen. Im Allgemeinen verursachten Modifikationen an der F19-Position stärkere Auswirkungen auf die Strukturbildung und biologische Aktivität als an der L34-Position. Ein wichtiges Merkmal von L34-Mutationen ist außerdem, dass sich lokale Strukturveränderungen auf das gegenüberliegende β -Faltblatt an der F19-Position ausbreiten.⁵

Im dritten Teil wurde die nicht-kanonische Aminosäure β -Methylamino-L-alanin (BMAA) an der Position F19 sowie an S8 und S26 eingeführt, die sich am N-Terminus bzw. der Turn-Region befinden. BMAA steht im Verdacht, ein Risikofaktor für neurodegenerative Erkrankungen zu sein. Einer der diskutierten pathologischen Mechanismen von BMAA ist sein Fehleinbau in Proteine, der zu Fehlfaltungen und anschließend zu Aggregationen führt. Dies wird durch die Möglichkeit angezeigt, dass die Serin-tRNA-Synthetase BMAA anstelle von Serin akzeptieren kann. Als Mutationsstellen wurden die Positionen S8 und S26 wegen dieser Fähigkeit der Serin-tRNA-Synthetase BMAA anstelle von Serin aufzunehmen verwendet. Sowohl BMAA als auch Serin enthalten in ihrer Seitenkette einen Wasserstoffdonor zur Bildung von potentiellen Wasserstoffbrücken.⁶

Wenn BMAA an Position F19 innerhalb der hydrophoben Kernregion eingeführt wird, beeinflusst es stark die lokale Struktur und Dynamik, die Kinetik der Fibrillenbildung und die biologische Aktivität von A β , während die globale Fibrillenmorphologie und Sekundärstrukturzusammensetzung konserviert blieben. In diesem Fall verhält es sich also eher wie eine starke Mutation als eine moderate. Von größerem Interesse sind BMAA-Substitutionen für Serin. Obwohl solche Modifikationen in vivo nicht gezeigt werden konnten, wird ihre mögliche Relevanz basierend auf der Fähigkeit der Serin-tRNA-Synthetase diskutiert, BMAA als Ersatz in vitro zu akzeptieren. Synthetische A β -Peptide mit einer S8BMAA oder einer S26BMAA Mutation zeigte, dass solche Substitutionen in einer charakteristischen Änderung eines A β Eigenschaften resultiert: Der hydrophobe Kern mit der Cross- β -Struktur bleibt unberührt, aber strukturelle Veränderungen treten am N-Terminus (S8BMAA) sowie innerhalb der turn-Struktur (S26BMAA) auf. Am deutlichsten sind die Veränderungen der biologischen Aktivität von A β , da in beiden Fällen nicht mehr die mitochondriale Aktivität beeinträchtigt wird, sondern eine apoptotische Caspase-3-Aktivierung und eine stressinduzierte Verkürzung der Neuritenlängen induziert wird. Beide Serin-Substitutionen zeigen vergleichbare Effekte, die bei S26BMAA etwas stärker ausgeprägt sind. Diese funktionelle Ähnlichkeit könnte durch eine S8-S26-Interaktion erklärt werden, die für eine Fibrillenstruktur gezeigt wurde, die für die Alzheimer-Krankheit relevant sein könnte.⁹ Die Korrelation zwischen der Fibrillenkinetik und der biologischen Aktivität war zwischen den S-BMAA-Substitutionen und den anderen in dieser Arbeit getesteten Mutationen unterschiedlich, was auf einen veränderten Weg der Fibrillenbildung hindeutet, der stabilere Oligomere begünstigt. Darüber hinaus zeigten die Serin-Substitutionen eine deutliche Zellaktivität. Anstatt über mitochondrial-zellmembranvermittelte Mechanismen zu wirken, induzierten sie Apoptose und eine neuronale Stressantwort. Das zeigt, dass mehr als ein Wirkmechanismus zur A β -Toxizität beiträgt. Diese beobachtete Aktivitätsänderung könnte auch nützlich sein, um die Frage zu beantworten, ob der BMAA-Fehleinbau ein relevanter Risikofaktor für die Alzheimer-Krankheit ist. Dies sollte sich durch die Caspase-3-Aktivierung zeigen, die für den BMAA-Fehleinbau charakteristisch ist und anstelle der mitochondrialen Dehydrogenase-Hemmung auftritt. Darüber hinaus könnten solche Aktivitätswechsel relevant sein, um verschiedene Formen und Ätiologien der Alzheimer-Krankheit und die Aktivität verschiedener Risikofaktoren zu erklären.⁶

All unsere Ergebnisse können unter Verwendung des klassischen U-förmigen Modells der A β -Fibrillenstruktur interpretiert werden, das durch intramolekulare Kontakte gesteuert wird. Es ist jedoch nicht auszuschließen, dass die untersuchten Kontakte intermolekulare Kontakte sind. Dies kann zu einer U-förmigen Struktur mit einem Versatz zwischen den β -Faltblättern

entlang der Fibrillenachse oder sogar zu einer gestreckten Struktur führen, bei der zwei geradlinige Filamente in entgegengesetzter Richtung ausgerichtet sind.^{10,11} Eine Unterscheidung zwischen intramolekularen und intermolekularen Kontakten kann durch NMR-Experimente getroffen werden, bei denen vollständig markierte Peptide mit Mischungen von markierten und nicht markierten oder unterschiedlich markierten Peptiden verglichen wird. Das wurde in dieser Arbeit jedoch nicht getan, da die untersuchten physikalisch-chemischen Eigenschaften der Wechselwirkungen in beiden Fällen identisch sein sollten.

Zusammenfassend zeigt diese Arbeit, dass Modulationen der lokalen physikalisch-chemischen Kräfte und Wechselwirkungen von A β dessen strukturelle Eigenschaften, den Faltungsprozess und die biologische Aktivität stark beeinflussen. Abhängig von der Mutationsstelle und den eingeführten Beschränkungen verändern Mutationen nicht nur die Stärke der zellulären Antwort, sondern sind auch in der Lage, die beteiligten Signalwege für Neurotoxizität zu verändern. Dies muss durch eine Veränderung der Selbstorganisation des Polypeptids und der beteiligten Strukturbildungswege verursacht werden. In Folge ergeben sich die verschiedenen Ätiologien und Wirkungsweisen potenzieller Risikofaktoren, die zur Pathologie der Alzheimer-Krankheit und anderer Proteinopathien beitragen, aus den grundlegenden physikalisch-chemischen Eigenschaften der Aminosäurekette. Die Hauptmerkmale von A β -Fibrillen sind nicht nur die Fibrillenmorphologie und die Cross- β -Struktur an sich, sondern auch deren herausragende Stabilität und Resistenz gegenüber Seitenkettenmodifikationen, die durch verschiedene Mutationen erzeugt werden können. Alle in dieser und früheren Arbeiten untersuchten Mutanten verursachten Strukturumlagerungen und Dynamikänderungen, die auf die lokale Umgebung der betroffenen Aminosäuren beschränkt waren. Betroffen waren jedoch nicht nur Aminosäuren in unmittelbarer Nachbarschaft der Mutationsstelle, sondern auch Aminosäuren in der Nähe direkter Interaktionspartner. Dies konnte für Interaktionen zwischen S8 und S26 sowie im Detail für den F19-L34-Kontakt nachgewiesen werden.

Die Eigenschaften dieses Kontakts werden hauptsächlich durch die sterischen Charakteristika bestimmt, die bei dem raumgreifenderen Ringsystem empfindlicher auf Modifikationen der F19-Position reagieren, während die kleinere L34-Seitenkette weniger Einfluss hat. Es konnte gezeigt werden, dass die Fibrillenbildung nicht nur durch die Aggregationsneigung des Peptids getrieben wird, die durch den enthalpischen und entropischen Beitrag der Wechselwirkungskräfte verursacht wird. An beiden Positionen waren die sterischen Eigenschaften die Schlüsselfaktoren der beteiligten Aminosäurereste. Für die F19-Position erwies sich auch die Konjugation des Ringsystems als wichtig. Einschränkungen bezüglich anderer physikalisch-chemischer Eigenschaften zeigten nur mäßige Auswirkungen auf die Selbstorganisation, den Faltungsweg und die finale Fibrillenstruktur von A β . Die Bedeutung der sterischen Spezifität der Wechselwirkungen, die den Fibrillenbildungsprozess leiten, spiegelt sich auch auf der Ebene der Oligomere und anderer transientser Strukturspezies wider, die indirekt durch Messungen der Fibrillenbildungskinetik untersucht wurden. Dies verknüpft die nachgewiesene sterische Spezifität der den Gesamtprozess leitenden F19-L34-Interaktion mit der Empfindlichkeit der biologischen Aktivität gegenüber eingefügten Beschränkungen, was die Tatsache erklärt, dass nicht die ausgebildeten Fibrillen, sondern Oligomere die toxischen Spezies bei der Pathologie der Alzheimer-Krankheit sind.

Eine neuere Arbeit zeigt, dass der Einfluss sterischer Beschränkungen nicht auf die Aminosäureseitenketten beschränkt ist, sondern auch das Rückgrat einen wichtigen Beitrag leistet. Durch die Verwendung von nicht-proteinogenen Aminosäuren mit methylierten Rückgrat-Aminogruppen konnte gezeigt werden, dass auch Restriktionen im Rückgrat zu ähnlichen Veränderungen im Fibrillationsverhalten, der Struktur und der biologischen Aktivität von A β führen. In diesem Fall trägt neben sterischen Zwängen auch die Verhinderung der Wasserstoffbrückenbindungen der Aminogruppe zu diesem Effekt bei. Im Gegensatz dazu erhöhte das

Einfügen eines Methylen- oder Ethylenspacers zwischen der Amino- und der Carboxygruppe innerhalb des Rückgrats die Fibrillationsneigung durch die Ermöglichung zusätzlicher Freiheitsgrade.¹²

Darüber hinaus gelten die beobachteten Wirkungen nicht ausschließlich für die Aminosäuren, die den hydrophoben Kontakt bilden, sondern es tragen auch benachbarte Aminosäuren innerhalb der Cross- β -Region bei. Dies konnte im Fall von F20 und G33 gezeigt werden. Auch bei diesen Aminosäuren blieb die Fibrillenstruktur stabil, und die stärksten Auswirkungen konnten bei der Fibrillationskinetik und Toxizität der Peptide beobachtet werden. Interessanterweise hatte die Substitution von G33 durch Alanin ähnliche, aber stärkere Auswirkungen als die Substitution einer der beiden am F19-L34-Kontakt beteiligten Aminosäuren. Dies könnte darauf zurückzuführen sein, dass die G33A-Mutation die Bildung einer Salzbrücke in der Turn-Region auf oligomerer, aber nicht auf fibrillärer Ebene verhindert. Dies zeigt, dass, obwohl der F19-L34-Kontakt entscheidend für die Initiierung der Fibrillenbildung, die Fibrillenkinetik und die Eigenschaften der Oligomere ist, auch andere Aminosäuren innerhalb der Cross- β -Struktur den Strukturbildungsprozess bestimmen und auf alternative Verläufe führen können.¹³

An die vorliegende Arbeit anschließende Untersuchungen sollten sich mit der Frage befassen, ob die Aminosäurekontakte, die als für die Strukturbildung entscheidend beschrieben wurden, tatsächlich intramolekulare Kontakte sind, was mit dem weit verbreiteten U-förmigen Strukturmodell übereinstimmt, oder ob diese Kontakte intermolekular sind. Dies berührt auch die Frage, ob das klassische U-förmige Modell beibehalten werden kann oder ob andere Modelle in Betracht gezogen werden müssen. Es ist ebenfalls noch nicht klar, ob der Wildtyp die primäre toxische Spezies ist und welchen Beitrag mutierte oder posttranslational veränderte Varianten leisten. Beide Fälle können zu unterschiedlichen Strukturen führen, so dass andere molekulare Kontakte und andere physikalisch-chemische Wechselwirkungen entscheidend sein können.

Diese Arbeit konzentriert sich auf den hydrophoben Kontakt zwischen F19 und L34 innerhalb der Cross- β -Region. Es ist jedoch bekannt, dass auch andere Kontakte wichtig sind, z.B. die Bildung einer Salzbrücke innerhalb der Turn-Region, wobei elektrostatische Wechselwirkungen und nicht sterische Beschränkungen die vorherrschende Kraft hervorbringen sollten. Eine detaillierte Untersuchung dieser anderen Kontakte könnte ähnlich wichtige Erkenntnisse über den Strukturbildungsprozess liefern.

Insgesamt trägt diese Arbeit zum Verständnis von Proteinfaltung und Fehlfaltungsmechanismen bei und gibt Hinweise für die Entwicklung neuer Ansätze zur Behandlung von Proteopathien.

2.1 Referenzen

1. Adler, J., Scheidt, H. A., Krüger, M., Thomas, L. & Huster, D. Local interactions influence the fibrillation kinetics, structure and dynamics of A β (1-40) but leave the general fibril structure unchanged. *PHYSICAL CHEMISTRY CHEMICAL PHYSICS : PCCP* **16**, 7461–7471; 10.1039/c3cp54501f (2014).
2. Bateman, R. J. *et al.* Autosomal-dominant Alzheimer's disease: a review and proposal for the prevention of Alzheimer's disease. *ALZHEIMER'S RESEARCH & THERAPY* **3**, 1; 10.1186/alzrt59 (2011).
3. Atwood, C. S., Martins, R. N., Smith, M. A. & Perry, G. Senile plaque composition and posttranslational modification of amyloid- β peptide and associated proteins. *PEPTIDES* **23**, 1343–1350; 10.1016/S0196-9781(02)00070-0 (2002).
4. Korn, A. *et al.* Amyloid β (1-40) Toxicity Depends on the Molecular Contact between Phenylalanine 19 and Leucine 34. *ACS CHEMICAL NEUROSCIENCE* **9**, 790–799; 10.1021/acscchemneuro.7b00360 (2018).
5. Korn, A., Surendran, D., Krueger, M., Maiti, S. & Huster, D. Ring structure modifications of phenylalanine 19 increase fibrillation kinetics and reduce toxicity of amyloid β (1-40). *CHEMICAL COMMUNICATIONS (CAMBRIDGE, ENGLAND)* **54**, 5430–5433; 10.1039/c8cc01733f (2018).
6. Korn, A. *et al.* Incorporation of the Nonproteinogenic Amino Acid β -Methylamino-alanine Affects Amyloid β Fibril Properties and Toxicity. *ACS CHEMICAL NEUROSCIENCE* **11**, 1038–1047; 10.1021/acscchemneuro.9b00660 (2020).
7. Obici, L. *et al.* A novel AbetaPP mutation exclusively associated with cerebral amyloid angiopathy. *ANNALS OF NEUROLOGY* **58**, 639–644; 10.1002/ana.20571 (2005).
8. Saini, R. K., Thakur, H. & Goyal, B. Effect of Piedmont mutation (L34V) on the structure, dynamics, and aggregation of Alzheimer's A β 40 peptide. *JOURNAL OF MOLECULAR GRAPHICS & MODELLING* **97**, 107571; 10.1016/j.jmgm.2020.107571 (2020).
9. Lu, J.-X. *et al.* Molecular structure of β -amyloid fibrils in Alzheimer's disease brain tissue. *CELL* **154**, 1257–1268; 10.1016/j.cell.2013.08.035 (2013).
10. Paravastu, A. K., Leapman, R. D., Yau, W.-M. & Tycko, R. Molecular structural basis for polymorphism in Alzheimer's beta-amyloid fibrils. *PROCEEDINGS OF THE NATIONAL ACADEMY OF SCIENCES OF THE UNITED STATES OF AMERICA* **105**, 18349–18354; 10.1073/pnas.0806270105 (2008).
11. Ghosh, U., Thurber, K. R., Yau, W.-M. & Tycko, R. Molecular structure of a prevalent amyloid- β fibril polymorph from Alzheimer's disease brain tissue. *PROCEEDINGS OF THE NATIONAL ACADEMY OF SCIENCES OF THE UNITED STATES OF AMERICA* **118**; 10.1073/pnas.2023089118 (2021).
12. Schwarze, B. *et al.* Peptide backbone modifications of amyloid β (1-40) impact fibrillation behavior and neuronal toxicity. *SCIENTIFIC REPORTS* **11**, 23767; 10.1038/s41598-021-03091-4 (2021).
13. Fritzsche, J. *et al.* Probing the Influence of Single-Site Mutations in the Central Cross- β Region of Amyloid β (1-40) Peptides. *BIOMOLECULES* **11**; 10.3390/biom11121848 (2021).

3 Introduction

3.1 Protein fibrils and their medical relevance

The correct three-dimensional structure is mandatory for a protein to fulfill its function. Therefore, it is not surprising that errors in the process of protein folding can cause diseases. It is speculated that protein misfolding might contribute to half of all human diseases.¹ The family of these diseases is called protein conformational disorders or proteopathies. These can be grouped in two classes: the first is characterized by a loss of the physiological protein function, either by losing activity or by altered protein trafficking, sorting and localization. The second class is characterized by a gain of pathological activity like toxicity.²

The largest group of proteopathies form neurodegenerative diseases (see Figure 2A). The common hallmark of these diseases is the loss of function and degeneration of neuronal cells leading to similar symptoms comprising cognitive symptoms like impairment of memory, language, visuo-spatial functioning and executive control as well as emotional and behavioral symptoms like anxiety, mood, apathy, disinhibition, loss of empathy or elation.³

The various diseases of this family can be classified by protein characteristics. Six major characteristic proteins and corresponding disease groups are described: (1) Tau protein for tauopathies, (2) amyloid β ($A\beta$) together with Tau for Alzheimer's disease, (3) α -Synuclein for α -synucleinopathies, (4) Prion protein for Prion disease, (5) Transactive response (TAR) DNA-binding protein 43 (TDP-43) for TDP-43 proteinopathies, (6) Fused in sarcoma protein (FUS), Ewing's sarcoma RNA-binding protein 1 (EWSR1), and TATA-binding protein-associated factor 15 (TAF15), taken together to FET proteins for FUS (FET)-proteinopathy frontotemporal lobar degeneration (FTLD) / Motor neuron disease MND-FUS (FET). These six major groups are complemented by a group of proteins, which is characterized by the fact that their pathological potential arises by a trinucleotide repeat, causing trinucleotide repeat expansion disorders and a group of different not further related proteins causing distinct diseases (for example neuroserpinopathy, ferritin-related NDDs, familial cerebral amyloidosis).⁴

One of the most prominent neurodegenerative diseases is Alzheimer's disease. According to the WHO, Alzheimer's disease and other dementias contributed the fifth most common cause of death globally in 2016 with a doubling of death rates since 2000 to a number of 1'992'000 cases.⁵ It is estimated that in 2015 there were 46.8 million dementia patients worldwide causing costs of US \$ 818 billion. Extrapolating the observed trends, it is expected that these numbers will rise to ~45 million patients and US \$ 2 trillion by 2030.⁶ Recent studies indicate that these predictions might underestimate the actual increase.⁷

While the final consequence of Alzheimer's disease is death, the clinical history of patients comprises years of severe symptoms and substantially reduced quality of life. In many cases, affected people show early symptoms like amnesia, loss of episodic memory, cognitive impairment, difficulties in multi-tasking and topographical impairment, and in later stages behavioral changes and loss of mobility. The onset of symptoms is gradual. They start with mild manifestation but deteriorate. In most cases intensive support or institutionalization becomes necessary.^{8,9} While a cure for Alzheimer's disease is not available, symptomatic treatment and a slowing of the progression of the disease is possible.

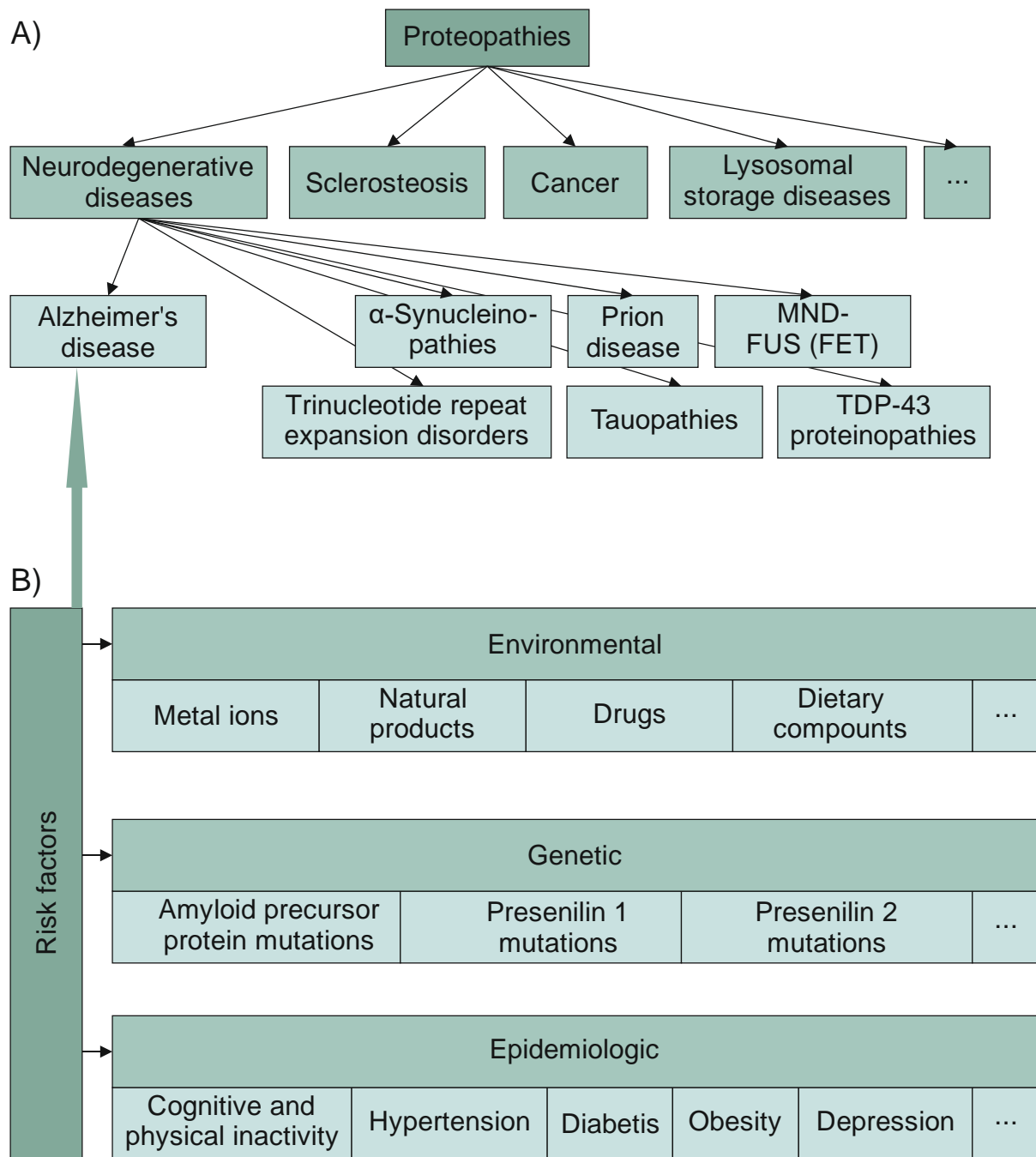


Figure 2: Classification of proteopathies and risk factors for Alzheimer's disease.

A) Classification of proteopathies. Proteopathies are a family of diseases comprising for example neurodegenerative diseases, sclerosteosis, cancer, lysosomal storage diseases and other. The largest subgroup are neurodegenerative diseases, which can themselves be categorized by the characteristic proteins of the diseases.⁴ B) Risk factors for Alzheimer's disease. The major group of Alzheimer's disease risk factors are environmental, genetic and epidemiologic factors.¹⁰

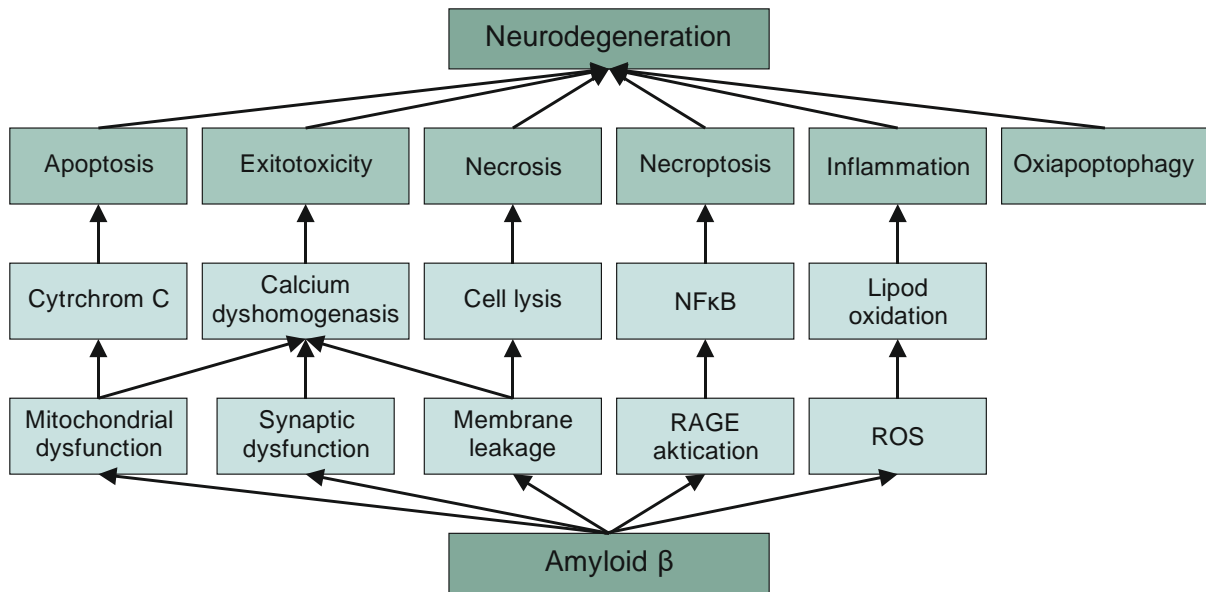


Figure 3: A β related cell death mechanisms contributing to neurodegeneration in Alzheimer's disease.

Various factors are discussed to be involved in the development of Alzheimer's disease (see Figure 2B).^{11,12} The most prominent ones are (I) environmental factors, e.g. metal ions, natural products, drugs and dietary compounds, (II) genetic factors alias inheritable mutations and (III) epidemiologic factors like cognitive and physical inactivity, hypertension, diabetes, obesity or depression.¹⁰ Only for few of these factors the functional mechanism linking them to the development of Alzheimer's disease are known, whereas for most, only correlations could be shown and the underlying effects are speculative at best. However, a large proportion can be attributed to one or a number of the pathways: metal homeostasis, neuroinflammation and reactive oxygen species, the neuronal cytoskeleton, neurotransmitter homeostasis, neurofibrillary tangles of Tau protein or amyloid plaques of A β .¹³

A large number of possible cell death mechanisms was described to be active in Alzheimer's disease. Despite the large variety, A β was identified as a central factor, which is potentially active in all major cell death variants (see Figure 3).

Although aggregation is one of the essential and best studied properties of A β , A β aggregates and especially fibrils, which are their typical aggregated form, seem to be of less importance for its pathological potential. Instead, focus shifted to soluble species as a potential target point for development of new drugs. Nonetheless, it is of utter importance to get deeper insights in the fibril formation process, not only to get a better understanding of Alzheimer's disease but also because fibril formation is a highly relevant general pathway of protein misfolding.

3.2 Proteins and their 3D structure

3.2.1 Properties of amino acids

Proteins are linear heteropolymers built of amino acids. All amino acids are composed of a carboxylic acid group and an amino group. For protein formation an amide from the carboxy group of one amino acid and the amino group of another one is formed. This is called peptide bond and the chain of peptide bonds forms the protein backbone. As this is directional, each polypeptide, including proteins, has an amino group at one end (called N-terminus) and correspondingly a carboxylic acid group at the other, called C-terminus (see Figure 4).

In the genetic code, twenty amino acids, called proteinaceous or canonical amino acids, are encoded. They differ in the side chain, which is attached to the α -carbon, which separates the carboxy from the amino group. As the α -carbon is a chirality center, D- and L-forms exist. However, exclusively the L-enantiomers are used in protein formation. The combination of the different properties of the individual amino acids is the fundament for structures and functions of the various proteins.

The easiest way to categorize amino acids is by polarity: ten are nonpolar, and ten are polar. Of the latter, five are uncharged polar, three can be positively charged and two can be negatively charged (see Figure 5). However, this simple classification is insufficient to describe the properties of the amino acids.

To structure amino acids by function, a substitution matrix can be used. This describes the frequency one amino acid is substituted by another when comparing large sets of evolutionary sequence alignments.¹⁴ As these matrices describe only propensities, they do not give the underlying reasons for this. Therefore, a description of the physicochemical and biochemical properties of amino acids is necessary. This can be achieved by amino acid indices where each index describes one property and each amino acid contributes one value to the index. Different approaches were used to structure these indices to meaningful groups but they give basically similar results. A clustering giving eight property groups identifies: (1) electrostatic properties, (2) residue properties, (3) intrinsic properties, (4) hydrophobicity, (5) α - and turn propensities, (6) physicochemical propensities, (7) composition, and (8) β structure propensity.¹⁵

For reduced complexity, an easier way to visualize the comparability of the different canonical amino acids, a Venn diagram can be used (see Figure 6).¹⁶ This is derived from a positioning of the amino acids in a matrix displaying the probabilities of amino acids substitutions and a grouping according to physicochemical properties. The two major distinguishing features are side chain size and hydrophobicity. The 'side chain size category' includes the subgroups 'small' and 'tiny'. Within the hydrophobicity group are 'hydrophobic amino acids' and 'polar amino acids'. Together with 'charge' (positive or negative) these describes the water affinity of the amino acids. Additional sets contain the aromatic and aliphatic amino acids. Some amino acids require a description by more than one category like histidine, which is an aromatic, polar amino acid, which can carry a positive charge, leading to overlaps between the amino acid categories.

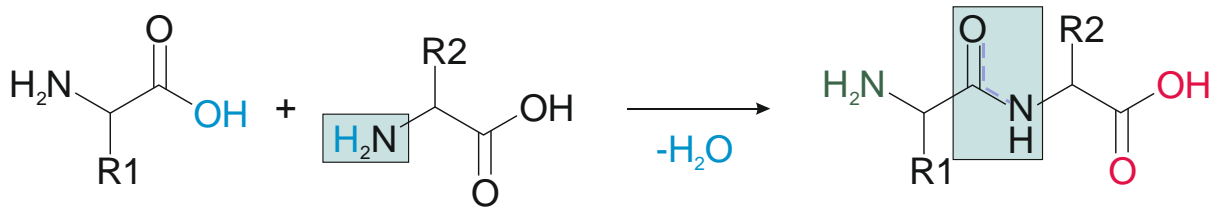


Figure 4: Peptide bond formation.

A peptide bond is formed by the condensation of a carboxy group and an amino group. The resulting peptide bond is stabilized by mesomerism (indicated by the dotted line along the peptide bond), which results in a planar conformation. The peptide bond formation causes a directionality of the formed (poly-)peptide with an amino-terminus defined by the free amino group (colored green) and a carboxy terminus defined by the free carboxy group (colored red).

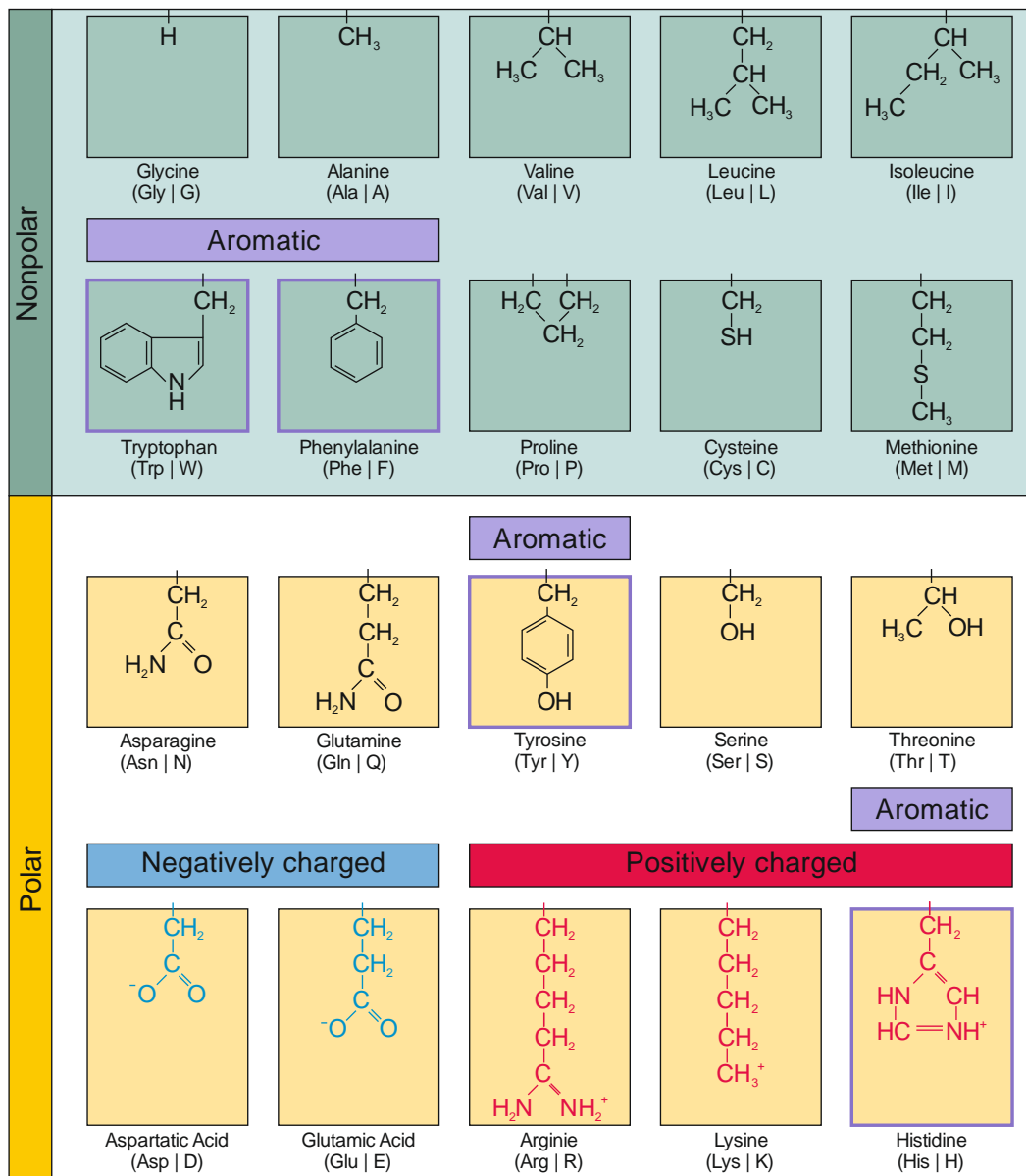


Figure 5: The 20 canonical amino acids.

Full name, three letter, and one letter code. The amino acid residues are grouped by physicochemical properties.

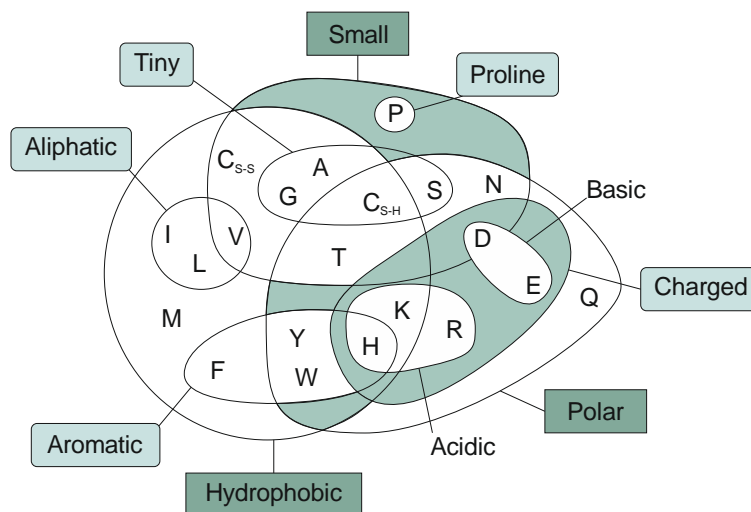


Figure 6: Venn diagram.

Visualization of amino acid cluster by properties, adapted from Taylor et al.¹⁶

Besides the canonical amino acids, proteins can contain additional amino acids. In vivo, these are mainly chemically modified residues, which can be formed physiologically, for example by posttranslational modification, or pathologically, for example by oxidation with reactive oxygen species of in case of racemization.¹⁷ In rare cases, t-RNA synthetases can accept non-proteinaceous amino acids, leading to misincorporation of these into proteins. Furthermore, using biotechnological techniques, non-proteinaceous amino acids can be incorporated intentionally, either to perform scientific experiments or to design proteins with specific functions for medical or industrial application.

3.2.2 IDPs and unstructured proteins

After or even during translation, polypeptide chains undergo a folding process leading to the native protein conformation. Some proteins or parts of proteins, however, do not form stable structures but consists mainly of random coils and are called intrinsically disordered proteins (IDPs), or IDP regions, respectively. In contrast to misfolded proteins, these show biological activity and their flexible structure is an important feature.

As the folding process depends on the properties of the amino acids, intrinsic disorder is also mediated by specific amino acid characteristics, mainly low hydrophobicity allowing unfettered interaction with the aqueous solvent and high net charge mediating repulsive forces.¹⁸ Ile, Leu, Val, Trp, Tyr, Phe, Cys, and Asn are specifically described to promote disorder. Other characteristics of amino acids often found in IDPs are flexibility, β -sheet propensity or bulkiness.¹⁹ A general feature of most IDPs is a low hydrophobicity and a high net charge. This leads to a high dehydration energy and charge repulsion, which counteracts structure formation. Especially for large IDPs a high net charge seems is frequently observed, whereas for small proteins it is less common (see Figure 7).²⁰

Whereas for enzymes or scleroproteins a stable structure is mandatory, intrinsic disorder allows for other, specific functions like adaptable and specific binding, assembling, motive presentation, target recognition, chaperone activity or allosteric coupling. Also important is the fact that the structural flexibility enable the proteins to undergo different processes like post translational modification, transit through channels or pores, alternative splicing and tolerance to mutations.²¹

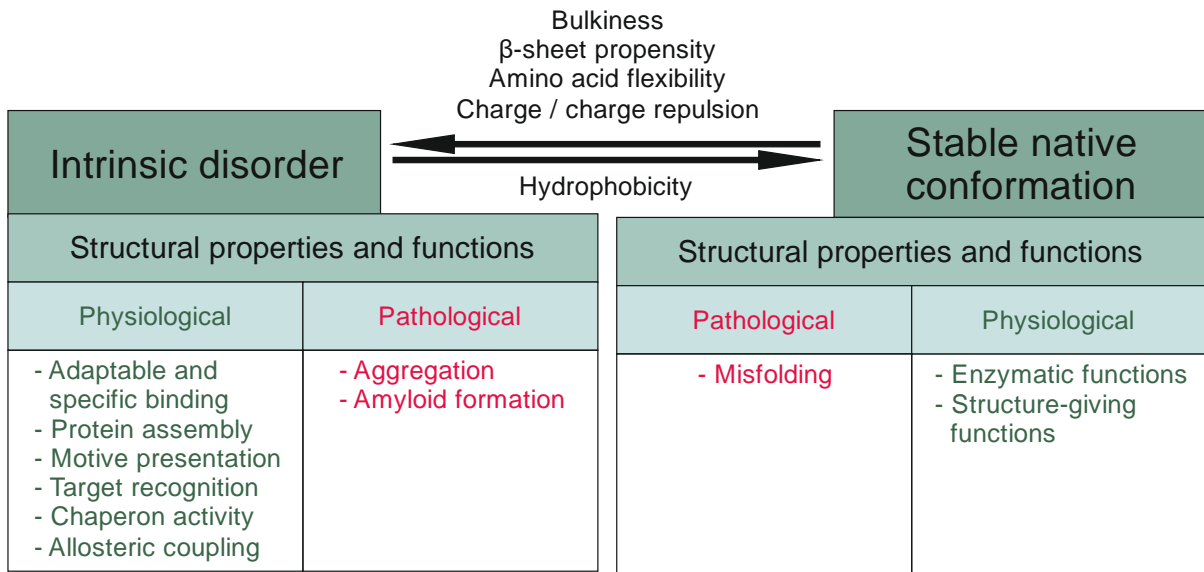


Figure 7: Comparison of structure properties and function between proteins with intrinsic disorder and a stable native conformation.

The main force stabilizing the native protein structure is hydrophobicity. Structure formation can be prevented by repulsive forces or by interactions causing entropy loss. Whereas in proteins with a native conformation function directly depends on the stability of this structure, intrinsic disorder allows for a different set of functions and properties. The main impairment of the functionality of intrinsic disordered proteins lies in their aggregation and fibril formation propensity.

As IDPs fulfill a broad spectrum of functions, they are also relevant for a variety of diseases. Therefore, many IDPs have been reported to play a role in cancer, diabetes, cardio vascular disease, and neurodegenerative diseases.²² An important aspect of IDP pathology is pathologic structure formation. Although they have no stable conformation, which can become misfolded, they are threatened by aggregation and amyloid fibril formation. Especially for various neurodegenerative diseases, the involvement of different IDPs has been shown. A prominent example is the A β peptide. When in monomeric form, this peptide shows intrinsic disorder but fibrils formed of A β are a hallmark of Alzheimer's disease. As an IDP, A β monomers show typical characteristics like a high abundance of charged amino acids compared to its size, especially at its N-terminus, and a tendency to form a hairpin conformation stabilized by charge attraction.²³

3.2.3 Native protein structure

For most proteins, a certain stable structure is mandatory to fulfill their function. Classically, four levels of structure are distinguished: primary structure, secondary structure, tertiary structure and quaternary structure (see Figure 8). The primary structure describes only the amino acid sequence. The secondary structures comprise the elemental structural building blocks, which form larger structures. The tertiary structure describes the conformation of a whole protein, and finally the quaternary structure is the result of several protein chains interacting with each other.

Secondary structures are the smallest stable elements of the polypeptide, which can be described. Besides unstructured random coil, α -helix and β -sheet are the most common folding patterns. These are complemented by short turn or bend patterns, which are linkers between α -helix and β -sheet elements.

The main force stabilizing secondary structures is the formation of hydrogen bonds within the backbone. While individual side chain interactions might be stronger, the high abundance of backbone hydrogen bonds result in a larger net energy contribution. The strongest restriction is caused by the steric limitation within the backbone. The free electron pair of the amin nitrogen is delocalized and gives the peptide bond a partial double bond character. This resonance stabilization prevents rotation. Therefore, the main flexibility within the backbone comes from the bond rotations at the C α atoms. The rotation angle around the N-C α bond is defined as ϕ angle and the angle around the C α -C bond as ψ . These rotations are restricted by the influence of the side chains. As this site differs between the individual amino acids, each amino acid has an individual range of preferred ϕ and ψ angles that is accessible. In consequence, this causes a preference for the formation of certain secondary structures for each amino acid. This can be illustrated in a Ramachandran plot (see Figure 8).²⁴ Within this plot, different regions can be defined, which represent different conformational classes used to define secondary structure classes.²⁵ Another important feature resulting from the sequence of rotation angles and reflecting the stabilizing interactions is the H-bond pattern. For example, besides the α -helix other protein helices are described, which mainly differ in the pattern of the stabilizing H-bonds.

The analysis of known protein structures lead to different libraries of commonly found structures. A widely used classification is the Dictionary of Protein Secondary Structure.²⁶ This classification differentiates between two distinct features to describe secondary structures: H-bonds and geometrical structure. Geometrical structures include four different elements: (1) Bends, which are regions with high curvature defined by backbone angles, (2) chirality, defined by the dihedral angle, (3) disulfide bonds between cysteine side chains and (4) chain breaks. The second feature deals with the H-bonds in a hierarchical way. The simplest element is a single H-bond. From this, two elemental patterns can be defined: an n-turn with an H-bond between nearby amino acids and a bridge between distant amino acids. In the latter case a parallel orientation and an antiparallel orientation can be formed depending of the relative position of the C-terminus and N-terminus. At a further level turns and bridges can form larger structures namely helices and β -sheets. A helix consists of two or more consecutive n-turns. There are three different helices, which differ on the H-bond pattern: α -helix with the H-bond between the amino acids i and $i+4$, 3_{10} -helix with the H-bond between the amino acids i and $i+3$ and π -helix with the H-bond between the amino acids i and $i+5$. A set of bridges builds a β -ladder and ladders can assemble to β -sheets. With these components eight secondary structure elements can be defined: (1) 3_{10} -helix, (2) α -helix, (3) π -helix, (4) H-bonded turn, (5) bend, (6) coil, (7) extended strand in parallel and/or anti-parallel β -sheet conformation, and (8) residue in isolated β -bridge.²⁶ Because these structures are derived from known protein structures, depending on the analyses procedure other sets of secondary structures might be derived. The main features of the classes, however, remain similar.

The native protein structure is composed by a combination of these secondary structure elements. For most proteins, this is the structure that fulfills the protein function. In case of larger proteins, a breakdown in protein domains as an intermediate level is convenient. Whereas secondary structures usually do not appear isolated, protein domains are self-contained and functional units. Therefore, they can be considered as modular units from which more complex protein functionalities can be built and often the same domain is used in different proteins to fulfill equal functions. Because they combine structure and function, structurally similar domains often fulfill similar functions and domains are often conserved between species and during evolution.

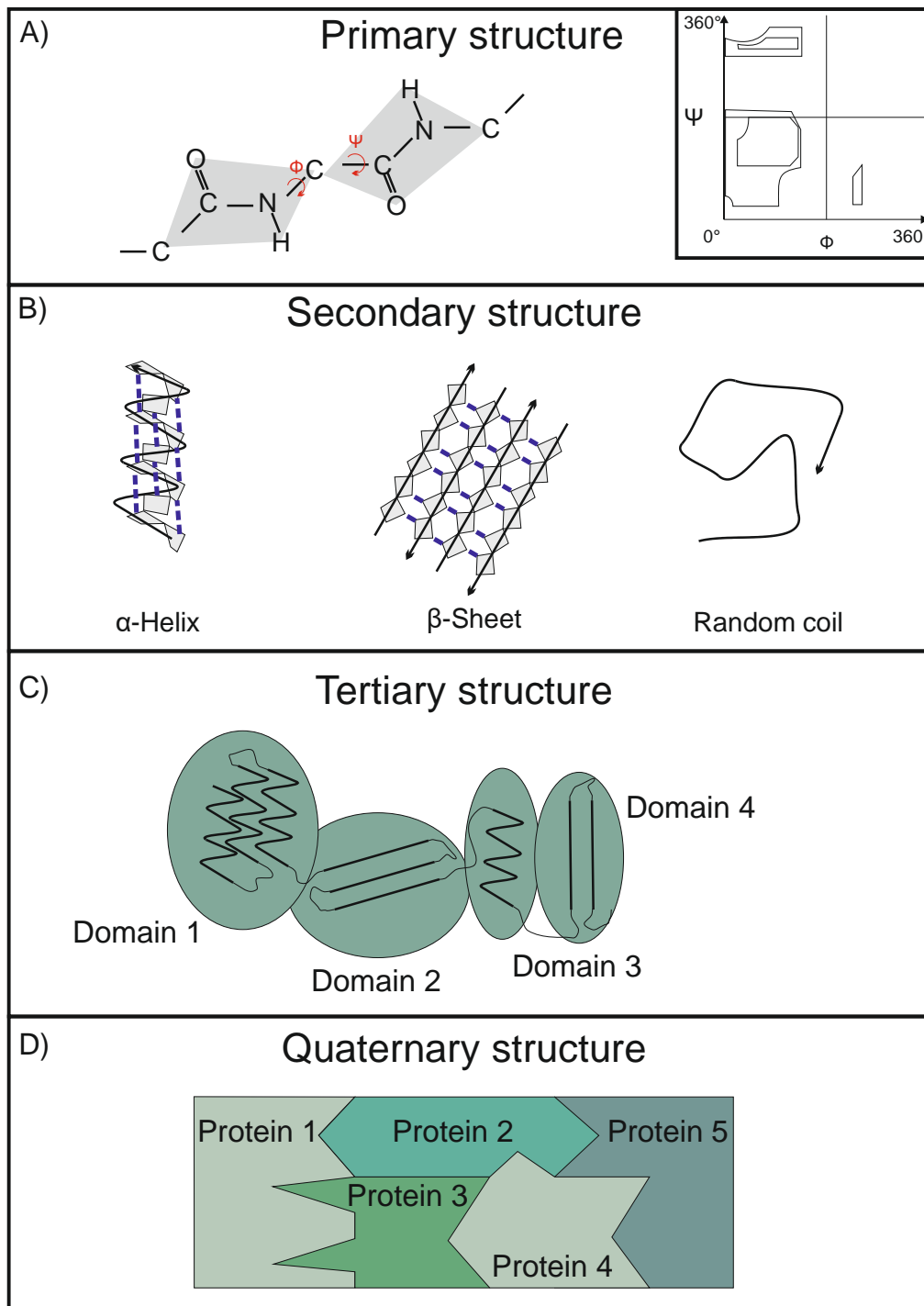


Figure 8: Structure hierarchy of proteins.

A) Primary structure. Because of mesomerism, the peptide bond is planar (indicated by grey quadrilaterals) Rotations are possible around the $C\alpha$ -CO bond and the $C\alpha$ -N bond. Accessible rotation angles are amino acid specific and can be illustrated in a Ramachandran plot (insert). B) Secondary structures can be defined by the dihedral angles between the peptide bonds and the formation of hydrogen bonds. The most predominant secondary structure elements are α -helix, β -sheet and random coil. C) The tertiary structure is formed by the assembly of secondary structural elements. Especially in larger proteins, domains can be formed by stable, separated secondary structure assemblies. D) Some proteins require the formation of homo- or heterooligomers or even larger protein complexes to become active. These are defined as quaternary structures.

The final tertiary structure is stable, but not static. Often, protein activity is accompanied by translocation of protein domains or by a reorganization within the domains, in some cases even on the level of the secondary structure, e.g. by unwinding of a helix or extension of a β -sheet. It is also common that regulatory posttranslational modifications like phosphorylation act on level of the primary structure to induce a structural reorganization and a change of function.

Some proteins require that more than one polypeptide chain associate to become active, for example by dimerization, oligomerization or complex formation. In this case the functional structure is called quaternary structure.

3.2.4 Protein misfolding: cross- β structure

As the correct fold of a protein is mandatory for its function, this process has to be highly regulated *in vivo*. Repeating folding-denaturation cycle experiments showed that the structural information of a protein contained in the amino acid sequence is sufficient for the formation of its native structure, as no cofactors are necessary for the refolding.²⁷ But also *in vitro*, correct folding is not guaranteed and misfolding and aggregation can be a problem. *In vivo*, there are additional challenges. For once, the cellular environment is highly crowded and the folding process can be influenced by interactions with close-by molecules. Furthermore, during translation, the polypeptide is formed in a relatively slow, stepwise process. Therefore, interactions between distant amino acids are not immediately possible. Furthermore, first folding processes occur in the exit tunnel of the ribosome, which provides only limited spaces and allows only the formation of structures with a narrow diameter.²⁸ These obstacles are overcome by different ways. The most dominant is the activity of molecular chaperones. These proteins interact with non-folded or misfolded peptide chain chains and induce native folding by lowering the corresponding energy barriers. Another mode of action of chaperones is, that they provide a protected folding environment (see Figure 9).²⁹

Nevertheless, misfolding occurs and if refolding is not possible misfolded proteins have to be deposited or degraded. The primary way to clear misfolded proteins is by degradation in proteasomes. When chaperones fail to induce native folding, they can recruit ligases for ubiquitination of the target peptide. This is the signal for its degradation in the proteasome, which has protease activity. A main limitation of proteasomes is their size, which is why they can only degrade single proteins.³⁰ Larger structures like aggregates have to be degraded by larger cell structures like lysosomes or aggresomes.³¹ One of the most persistent protein species are fibrils. Besides their bulkiness and conglomeration in aggregates, they possess a highly stable structural motif: the cross- β .

Conventionally, a protein fibril, also called amyloid, is defined as a large linear homopolymer of proteins. With exception of individual cases, the common hallmark of fibrils is the cross- β structure. In this structure, every protein unit supplies two or more β -strands and identical strands of the different proteins form a β -sheet. At least two sheets stack together. The strands then are arranged orthogonally to the fibril axis. The high stability of fibrils arises from mainly two forces: besides the hydrogen bonds between the individual β -strands, which form the β -sheets also the interactions between the stacked β -sheets contribute. In most cases, the inter-sheet interaction is mediated by hydrophobic contacts. During the formation of the cross- β structure, enthalpy contribution from these contacts is relatively small. Much more important is the entropic gain arising from the water molecules, which are restricted in terms of rotational, translational, and vibrational freedom when they interact with hydrophobic surfaces on the β -sheet. By stacking of the sheets, these restrictions are eliminated. The special arrangement in the cross- β structure results in the effect, that hydrogen bond formation becomes

cooperative. That means the formation of additional hydrogen bonds during fibril growth has an above-average contribution to structural stability.³² Once the cross- β structure is formed, the stacking it is mainly stabilized by van der Waals forces.³³ Further stabilizing interactions like salt bridges can occur in individual cases of specific amyloids but are not a general feature.

As the interaction between stacked β -sheets is stabilized by van der Waals forces, the amino acid residues have to organize in a close proximity structure. This is achieved by a steric zipper arrangement (see Figure 10). In the β -strands, neighboring amino acid residues are separated by a fixed distance, determined by the backbone torsion angles. Within the β -sheets, opposing amino acid residues orientate in-register resulting in an undulate topography because of the alternate orientation of the residues. When β -sheets stack they do this in an intermeshing fashion. This can result in eight possible orientations, which depend on whether the β -sheets are parallel or antiparallel, same or different surfaces interact and if the sheets are arranged in the same or in opposing directions. Not all possible orientations have been observed in protein fibrils. Furthermore, the steric zipper is an idealized model derived from crystal structures.³⁴

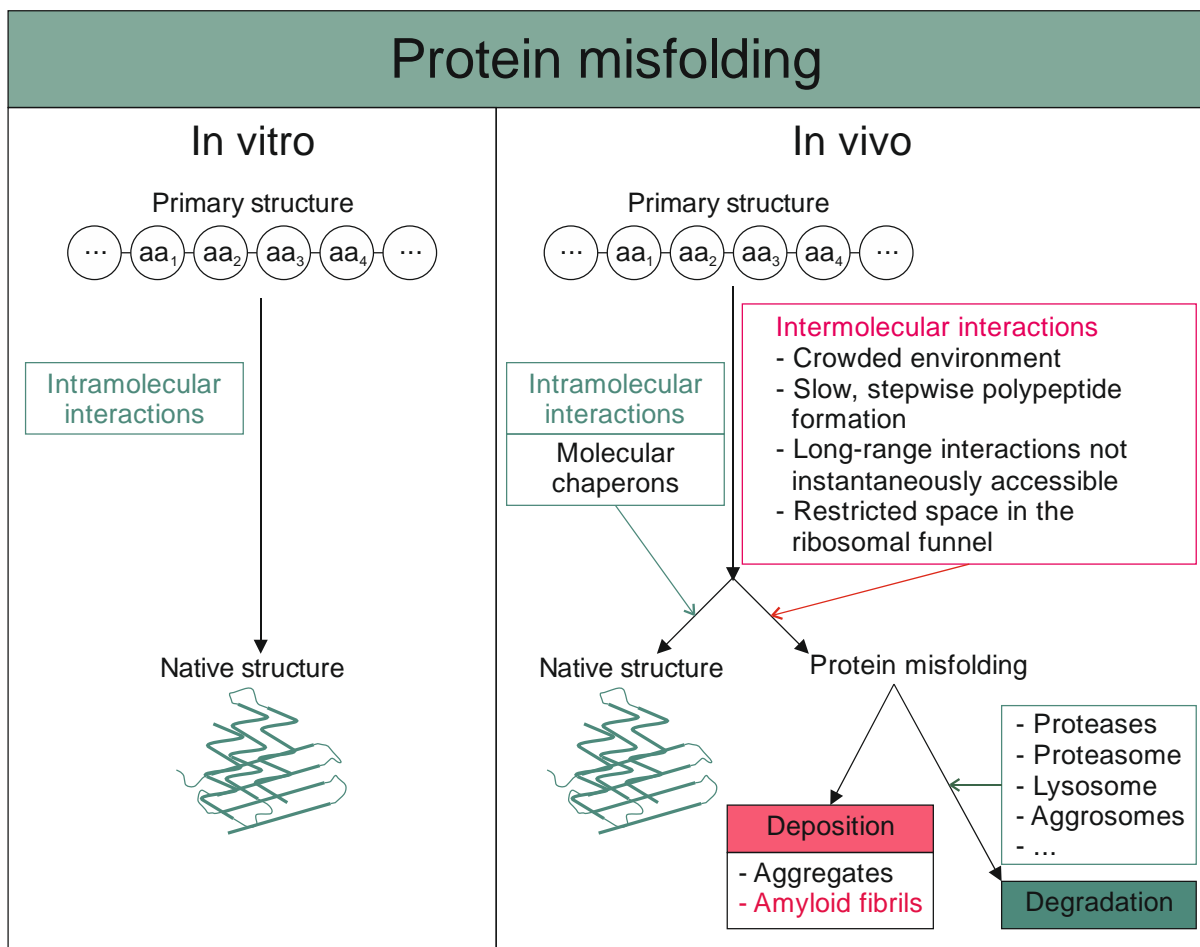


Figure 9: Protein folding and misfolding pathways.

In ideal in vitro environment, intramolecular interactions guide the folding pathway towards the native structure. In vivo, this process can be disturbed by intermolecular interactions or steric constraints. Furthermore, not all interactions are instantaneously accessible as the polypeptide is formed sequentially in the ribosome. The folding process to the native structure can be supported by molecular chaperones. Even so, some proteins adopt a misfolded structure. These can either be degraded by proteolytic enzymes and cell compartments or deposited in form of aggregates or amyloid fibrils.

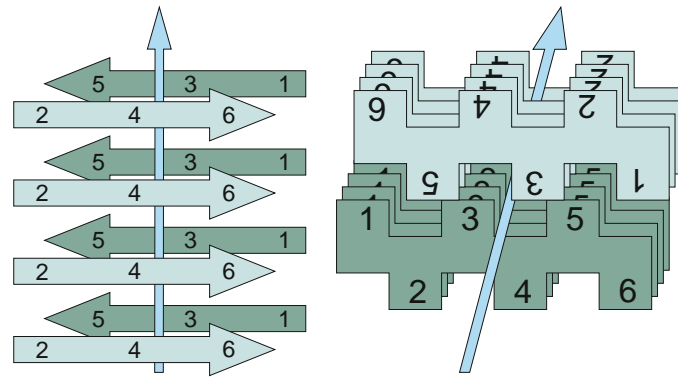


Figure 10: Top and side view of a class 1 steric zipper conformation.

Within the individual β -sheets (colored in different shades of green) the orientation of the amino acid residues alternates. In the parallel orientation, identical, opposing amino acid residues orientate in-register and form an undulate topography. Two β -sheets stack in a way, that equal surfaces interact in opposing orientation. In order to form fibrils, several stacks string together along the fibril axis (blue arrow), adapted from Sawaya et al.³⁴

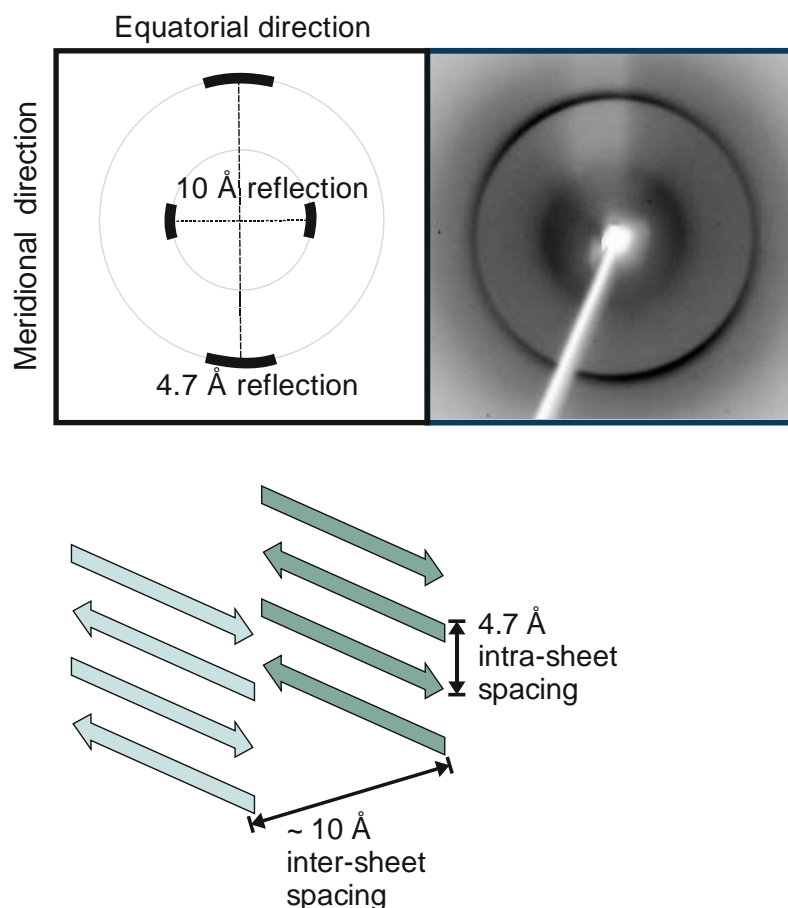


Figure 11: Cross- β structure.

Top: X-ray diffraction image of a partially oriented fiber and schematics of the characteristic 4.7 Å equatorial and ~ 10 Å meridional reflections. Bottom: Schematics of cross- β structure with characteristic 4.7 Å intra-sheet and ~ 10 Å inter-sheet spacing.

This structure is classically identified by X-ray structure analyses as it creates two characteristic reflections: one sharply demarcated at a 4.7 Å spacing, caused by the hydrogen bonds within the β -sheets between the β -strands, and one more diffuse reflection at about 10 Å corresponding to the spacing between the β -sheets (see Figure 11). When fibrils are aligned along a common axis, the 4.7 Å reflection will orient in two opposing equatorial and the 10 Å reflection in two opposing meridional signals. The term cross- β for the structure arises from this cross-like arrangement of the reflections. In this arrangement, a large number of backbone hydrogen bonds are formed and typically hydrophobic amino acid residues conglomerate in the core of the fibril whereas hydrophilic residues are exposed on the surface. Additionally, further stabilizing interactions can be developed, for example by forming three or more β -sheets within one fibril, which allow for more complex arrangements. Furthermore, several individual fibrils can align to larger fibers. This together results in a highly stable structure, which can be energetically more favorable than the native protein conformation.³⁵

Since fibril formation is considered as an innate ability of all proteins and associated with a broad spectrum of diseases, there is need to take a closer look at the individual elements of this process. For this purpose, A β is a well suited and widely used model.

3.3 Guiding physicochemical properties and interactions in protein structure formation

Refolding experiments proved that the native protein structure does not depend on the process of folding or initial conditions but only on the thermodynamic stability. Therefore, this conformation is the global energy minimum compared to all other accessible states. The energy of a state is determined by different forces acting between single atoms, chemical bonds or whole chemical groups of the polypeptide. Since also the native state typically shows pronounced dynamics, all possible forces, also weak or rare ones, contribute significantly to the native conformation. However, some forces are of particular importance as they act on greater extent, either because they are more frequent or contribute more strongly to the energy state.³⁶

The **hydrophobic effect** is the main energy contributor for conformational stability. It depends on the number of hydrophobic groups, mainly CH/CH₂/CH₃ groups, in a polypeptide chain, which get buried within the protein core upon folding and are thereby shielded from the aqueous solvent. Mutational experiments showed that a single CH₂ group can contribute 1.1 ± 0.5 kcal/mol. The exact value strongly depends on the surrounding environment of the side chains. The main contributing factors of the energy change in these mutation experiments are hydrophobicity caused by the solvent entropy at the protein surface and van der Waals interactions of the side chains acting within the solvent-shielded protein core (see Figure 12 A). The change of solute-solvent interactions contributes positively to the folding process. As the first layer of water molecules surrounding the solute are more ordered, there is a large entropy loss, which is reduced during the folding process. Because the surface area is reduced during the folding process, the entropy loss is diminished giving a positive net energy contribution. This is counterbalanced by cavity work, which is needed to bury a side chain within the protein core by displacement of other atoms and interactions. The cavity work is unfavorable and correlates with accessible surface area or molar volume. A third, smaller contribution arises from van der Waals interactions within the hydrophobic core. Depending on the number of CH_x groups, less or more van der Waals interactions can be formed, which contributes to the net energy of the process.³⁷ Taken all together, the hydrophobic effect gives the largest energy contribution to the folding process for most proteins, especially for large ones.³⁸

Hydrogen bonds make the second largest contribution to the folding energy (see Figure 12 B). Hydrogen bonds in polypeptides can be classified by the contributing part of the amino acids. In ordinary globular proteins, hydrogen bonds between the backbone peptide groups are most common. They account for over half of the hydrogen bonds within proteins and are the determinant for secondary structure. Nearly one quarter of hydrogen bonds are between side chains and peptide groups and only about every sixth is between two side chains.³⁹ Energetically more instructive is a differentiation by the involved atoms. Classically, backbone hydrogen bonds are of the heteronuclear type N-H...O as the hydrogen of one amino group interacts with the carboxy group of another peptide bond. Hydrogen bonds involving side chains can be hetero- (X-H...Y) or homonuclear (X-H...X). Heteronuclear hydrogen bonds are by default weaker than homonuclear ones as resonance is an important contribution and this is strongest when the resonance states are similar, which is the case for homonuclear hydrogen bonds. The strength of a hydrogen bond directly depends on its ability to change the nature of an asymmetric, electrostatic dipole-dipole interaction to a symmetric interaction with a covalent nature. Therefore, electrostatics driven hydrogen bonds, which are the predominant ones contributing to peptide formation, are weak by default, however, their high abundance results in a large net contribution.⁴⁰ Furthermore, the stabilization energy of a predominantly electrostatics driven hydrogen bond strongly depends on the dielectric constant of its environment. Therefore, such a hydrogen bond provides more stabilization when located in the hydrophobic core of a protein than when located at the solvent exposed surface.⁴¹ In this group resonance assisted heteronuclear hydrogen bonds are of high importance, as they induce the formation of secondary structures. There, a hydrogen is shared between the amino group of one peptide bond with the carboxy group of another. In extended secondary structures resonance stabilized chains of these interactions are formed.⁴⁰

The second exception is the hydrogen bond component of salt bridges. While salt bridges mainly depend on electrostatic interactions, they also share hydrogen bond features when the interaction is between a positively charged protonated group and a negatively charged deprotonated group. In this case they can be classified as charge assisted hydrogen bonds. This is the typical case in proteins where an anionic, deprotonated carboxylate of aspartate, glutamate or the carboxy-terminus, or a phosphate group modification and a cationic protonated ammonium from lysine or the amino-terminus, or a guanidinium of arginine. The hydrogen bond nature of these interactions is predominant in salt bridges with small proton affinity differences between donor and acceptor. In contrast, the electrostatic component, which is the main contributor for the interaction energy, is increased in cases of high proton affinity differences.⁴⁰

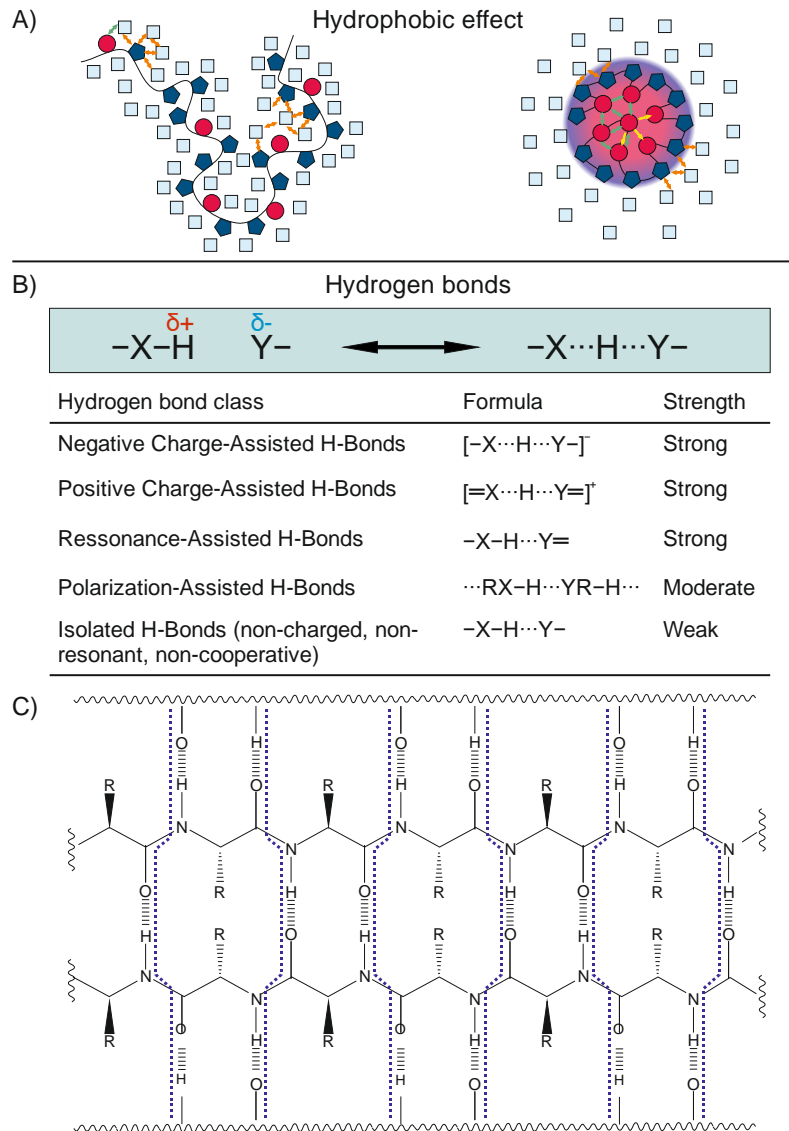


Figure 12: Forces and interactions guiding protein folding (I).

A) **Hydrophobic effect.** Proteins are composed of amino acids with hydrophobic (red circles) and hydrophilic (dark blue pentagons) side chains. In an aqueous solution solvent molecules (light blue squares) form interactions with exposed amino acids (orange arrows). This causes a loss of entropy for the solvent molecules. When the hydrophobic side chains are buried in the protein core this reduces the surface area, decreases protein-solvent interactions and subsequently increase entropy of the system resulting in stabilization of folding. Furthermore, van der Waals interactions between hydrophobic side chains are formed (green arrows), which also facilitates the folded conformation. Relocation of the hydrophobic side chains require a replacement of neighbouring amino acids and the formation of a cavity (yellow arrows), which slightly reduces the energy contribution of the hydrophobic effect. B) upper part: two-sided characteristics of a hydrogen bond with contributions of electrostatic dipole-dipole interaction and covalent bond character. The stronger the covalent character of the hydrogen bond the higher is the interaction energy. Middle part: Heteronuclear (X, Y) and homonuclear (X=Y) hydrogen bonds can be grouped in five classes, adapted from Gilli et al.⁴⁰ C) In proteins, isolated hydrogen bonds are most common. By secondary structure formation backbone hydrogen bonds can become resonance assisted, which is illustrated for the example of an extended β -sheet (lower part). Resonance stabilization strongly increases the energy contribution of hydrogen bonds during protein folding.

Electrostatics causes different effects in proteins and on protein folding (see Figure 13 A). The two major aspects are stabilization by interactions of opposing charges and destabilization by repulsion of same charges. An important aspect for both is an energy penalty for dehydration. A further discrimination has to be made between short-ranged dipole-dipole interactions and long-ranged Coulomb forces. Electrostatic interactions only marginally contribute to the total folding energy. Their importance lies in the long-range nature of electrostatic Coulomb forces. Therefore, they can induce non-local interactions, which bring distant amino acids in close proximity. Most charges including ion pairs are located at the protein surface. There, they can have a modest stabilizing effect. Localization within the hydrophobic core of the protein is accompanied by high energetic penalties. Since the energy gain by Coulomb interaction is higher in a nonpolar environment, other effects more than compensate this. The total interaction energy depends on three parts: Coulomb forces, solvation effects and interaction with mobile ions. As only the Coulomb interaction is energetically favorable, this explains why almost exclusively ion pairs can be found in the interior of proteins, but not single charges. The Coulomb forces depend on the involved charges, their distance and the dielectric constant of the environment. All three strongly change during the folding process: the charge by the pKa shift of the amino acids, the distance by conformational rearrangement and the dielectric constant by the formation of a hydrophobic core. The second part is the solvation. Charges interact more favorable with a polar solvent than with a nonpolar one. Although also in an aqueous environment the electrostatic field of charges leads to the ordering and orientation of water molecules and thereby to an entropy loss, the separation of a charge and solvating water molecules is even higher. The absolute value of this depends on the difference in the dielectric constants of the two environments. The third part accounts for the influence of mobile ions, for example salt ions. At low salt concentrations their electrostatic interaction with the charges is favorable and they act as counter ions. In contrast, at high concentrations the hydration of the salt ions competes with the hydration of the protein impairing the folding process.^{20,36}

Especially the effect on mobile ions is not only important for specific interactions, but more so for the second major aspect of electrostatics: non-specific repulsions at highly charged molecules. This considers only the repulsion effects of similar charges. Therefore, it has only negative contribution to the protein folding and stability of the folded conformation, except at the isoelectric point of the protein, where it can become neglectable as it correlates with the square of the net charge.³⁶ A high net charge is relevant for prevention of structure formation for IDPs and can also increase the solubility of a protein and prevent aggregation or fibril formation.⁴¹ The last two are also influenced by the salt concentration.

The concentration of mobile ions in the medium is one of the external factors, which are important for protein folding. Another one is the pH, which means the proton concentration of the solvent. It determines the protonation state and with this the charge of some amino acids. This is primarily important for the unfolded state and for the induction of first non-local contacts. Furthermore, it affects the folding process. The pKa of an ionizable chemical group depends on its solvent exposure and the presence of other charges. Dehydration costs favor the uncharged state whereas Coulomb interactions with other charges or polar groups favor the charged state. As both change during the folding process, also the protonation state of a chemical group can change. The third important external factor is the dielectric constant difference between the solvent and the protein core as the strength of the interaction depends on the dielectric constant of the environment. This can be dependent on the localization of the protein, for example within a membrane or by chaperone activity, or on the temperature.²⁰

Overall, it can be stated, that electrostatics is not the driving force of protein folding, but modulates the folding process and is important for the final conformation due to formation of non-local and long-range interactions and by localization of charged amino acids.

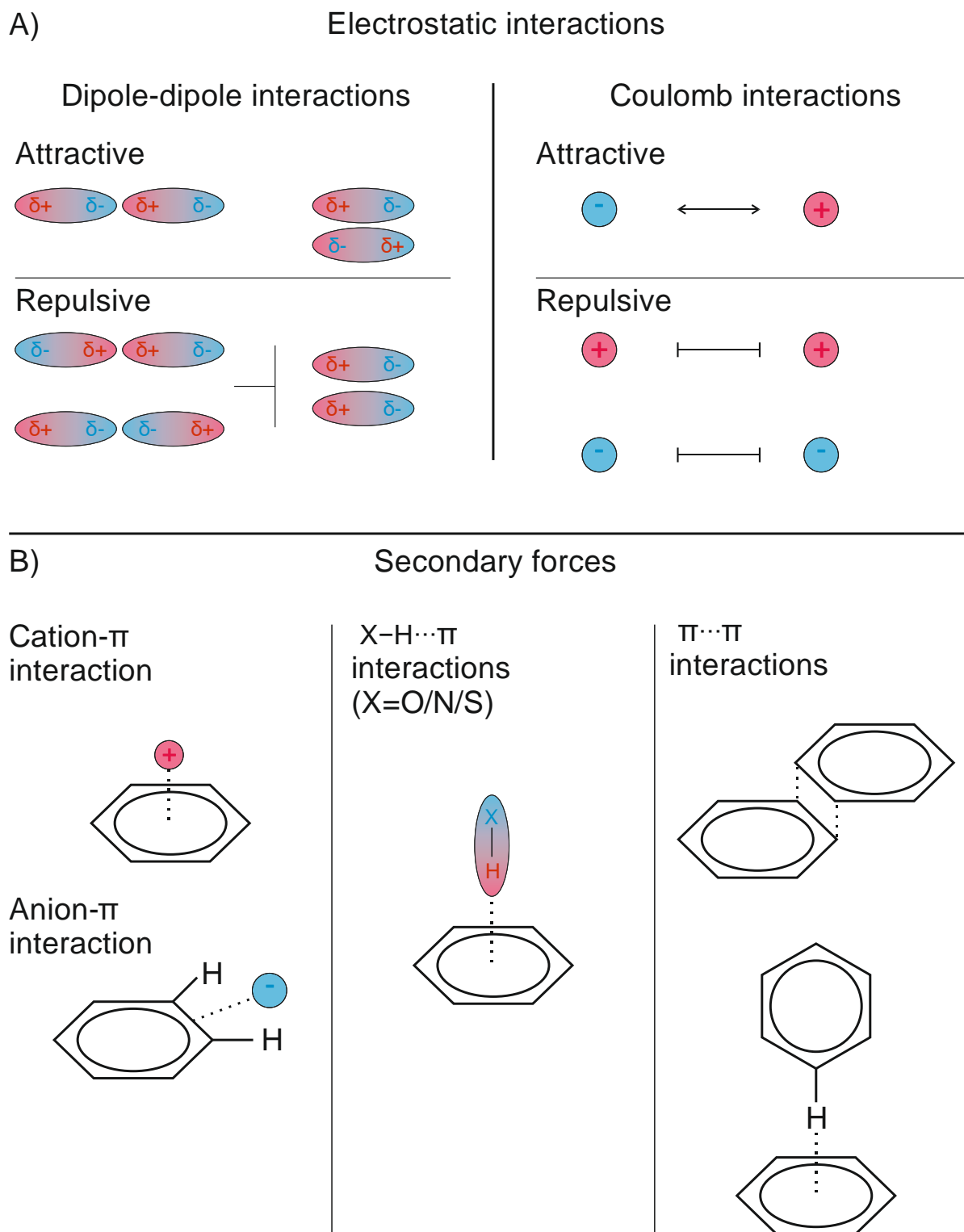


Figure 13: Forces and interactions guiding protein folding (II).

A) The predominant electrostatic interactions in proteins exist between dipoles and between charges. Attractive and repulsive forces can arise by different combinations of positive or negative charges. Additionally, interactions between dipoles and charges are also possible (not depicted).²⁰ B) The most important secondary forces in proteins involve conjugated ring systems. Mainly interactions between aromatic rings and ions, dipoles, or other aromatic moieties are relevant, adapted from Newberry et al.⁴²

The forces described above contribute the main energies guiding protein folding and stabilization of protein structures. However, further **secondary forces** are known that are important to explain the stability of some conformation or the formation of specific contacts and non-local interactions (see Figure 13 B). Stability, especially of secondary structures, is mostly mediated by additional interactions within the protein backbone. One are C-H...O hydrogen bonds, which are most frequent between backbone C α -H and carbonyl oxygens. They are similar to classical hydrogen bonds but the electrostatic contribution is larger than van der Waals interactions or charge transfer. They stabilize α -helical as well as β -sheet secondary structures. Also important for the high stability of β -sheets are C5 hydrogen bonds. They are also a variation of classical hydrogen bonds where an amide proton interacts with a neighboring carbonyl oxygen of the same amino acid. This interaction probably contributes to the formation and stability of amyloid fibrils. The last relevant prevailing backbone interaction, that is particularly important for the stabilization of the different helical secondary structures are n- π^* interactions. In this case, an interaction is formed between a free electron pair of a carbonyl group with the π^* orbital of a neighboring carbonyl group.⁴²

Secondary interactions involving amino acid side chains mainly involve aromatic rings. The strongest interaction is with cations. This is mainly mediated by electrostatic attraction between positively charged arginine or lysine with electronegative π -orbital of the ring system, which is further strengthened by dielectric dispersion and charge transfer. These interactions are special, because they are stronger than the dehydration penalty that accompany electrostatic interactions and are thereby able to form initial long-range contacts. Similar are hydrogen bonds between ring systems and hydrogens bound to oxygen, nitrogen or sulfur atoms. They follow the same principles like aromatic ring and cation interactions but are weaker. Besides interactions with electropositive partners also interactions with anions are possible. They are mediated by the electropositive lateral surface. The last relevant interaction of a ring systems is with another one. There, two conformations are possible, either T-shaped or stacked with an offset or lateral displacement. These interactions are mediated by electrostatics and instantaneous dipole-induced dipole forces. In addition to ring systems also sulfur groups are described to participate in secondary interactions. However, they are even less frequent.⁴²

3.4 The process of protein folding

Taken together, guiding physicochemical properties and interactions lead to a multitude of energetically favorable or unfavorable conformations. These can be summarized in the model of an energy landscape, which illustrates how different pathways, which lead to increasingly lower energy states result in certain structures (see Figure 14).⁴³ However, as so many interactions and transient conformations are possible, not all can be sampled in the folding process as a random search would need much longer time to reach the native state than is found in vitro and in vivo.⁴⁴ Therefore, folding has to go along specific pathways in which certain steps have to be models energy barriers need to be overcome. To describe this, four major models were created, which explain single aspects of this process (see Figure 15).

One is the diffusion-collision model that describes that, as a first step, structural microdomains are formed, depending on stochastic sampling of possible near-field interactions. By diffusion, these microdomains sequentially interact with each other, which allows for a limited set of new, more stable interactions. Progressively, the final protein structure is formed.⁴⁵

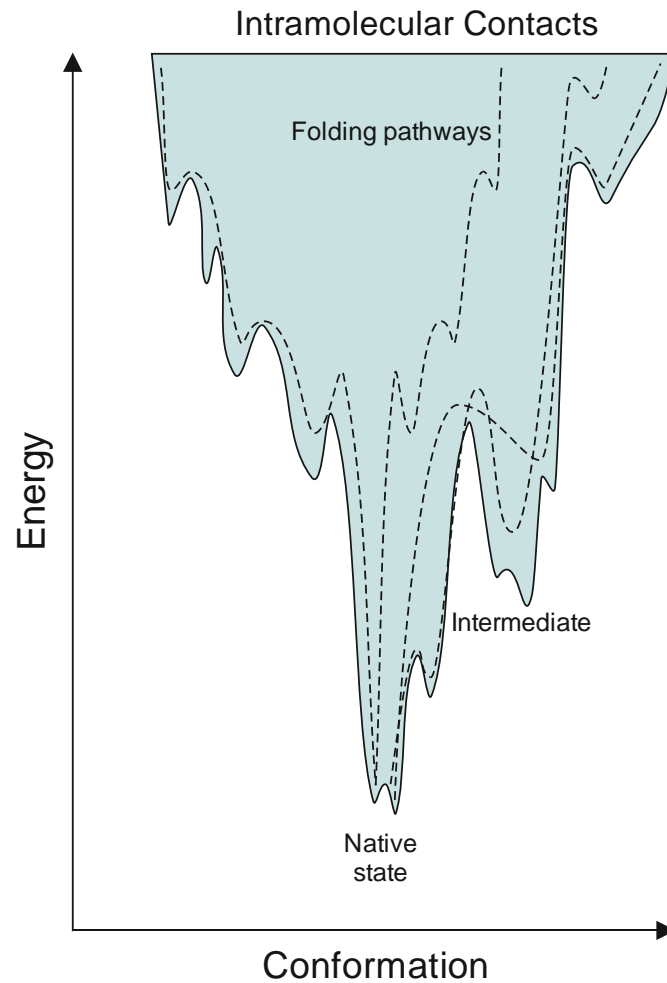


Figure 14: Schematic folding energy landscape of proteins.

Along the different possible folding pathways (dashed lines), the number of stabilizing intramolecular contacts increases, which leads to a net decrease of energy in the system. Along the pathway, semi stable intermediates at energy sinks can be formed whereas the lowest energy conformation represents the native state, adapted from Jahn et al.⁴⁶

The framework model is a limiting case of the diffusion-collision model. It describes protein folding as a hierarchical process, starting by small structural elements, which stepwise form larger structures until the final conformation is achieved. This is represented by the classical hierarchy of a succession of primary, secondary, and tertiary protein structure.⁴⁷

The hydrophobic collapse model focusses on the process, in which non-polar amino acids cluster together to build a hydrophobic core whereas polar ones arrange at water facing surfaces. This can be applied on the scale of microdomains, protein domains as well as the whole protein, especially in case of globular proteins. It is still under discussion what the specific steps are and in which order they occur, for example if the structure formation of the hydrophobic core is directly linked to the structural collapse or if the hydrophobic residues arrange in a separate step.⁴⁸

Finally, the nucleation-condensation model transfers the process of crystallization on the folding of proteins. It assumes an initial nucleus formation, which propagates the structure. Primal weak local interactions are progressively stabilized by long-range interactions, which can also lead to structural rearrangements during the process. This model is particularly applicable in case of small proteins.⁴⁹

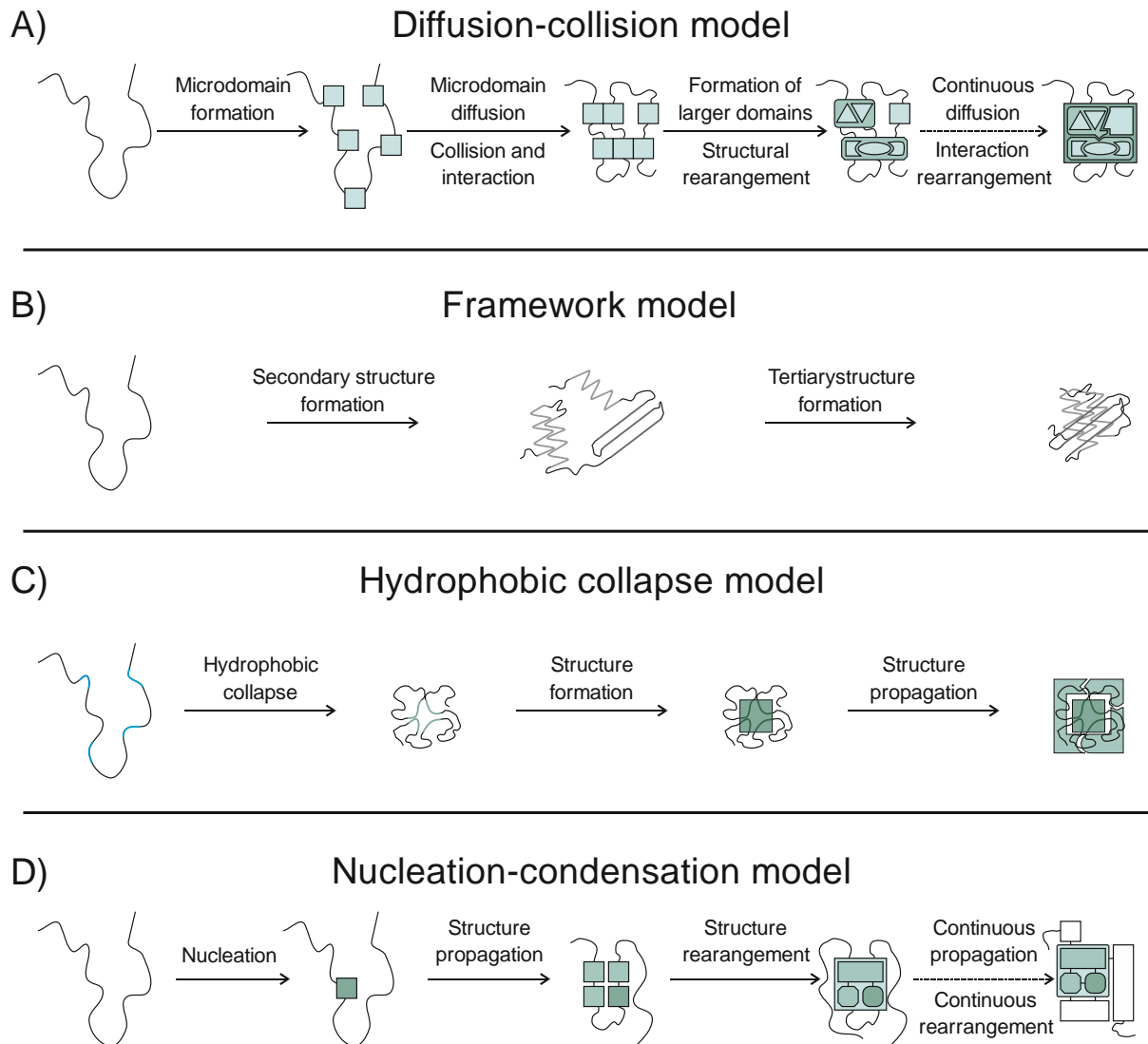


Figure 15: Structure formation models.

A) In the diffusion collision model, protein folding is initiated by the formation of microdomains due to local interactions. These microdomains diffuse and subsequently interact with each other causing structural rearrangement and the development of larger structures.⁴⁵ B) In the framework model, the first step of protein folding is the formation of secondary structures, which assemble to the native tertiary structure.⁴⁷ C) According to the hydrophobic collapse model structure formation is preceded by the interaction of hydrophobic amino acid residues and protein structures originate from this hydrophobic core.⁴⁸ D) The nucleation-condensation model resembles crystallization and is applicable especially to small proteins. There, local interactions initially cause the formation of a nucleus, which propagates to the native structure.⁴⁹

These models focus on the structure formation of a single, isolated protein and the influence of solvent and intramolecular contacts. However, also intermolecular contacts become important, especially because functionality of most proteins depends on the interaction with further molecules or particularly other proteins. Furthermore, protein aggregation, which is also caused by intermolecular contacts, is a common problem in vivo and in vitro.^{46,50} To describe these phenomena an extension of the folding energy landscape has to be made, adding intermolecular interactions (see Figure 16).

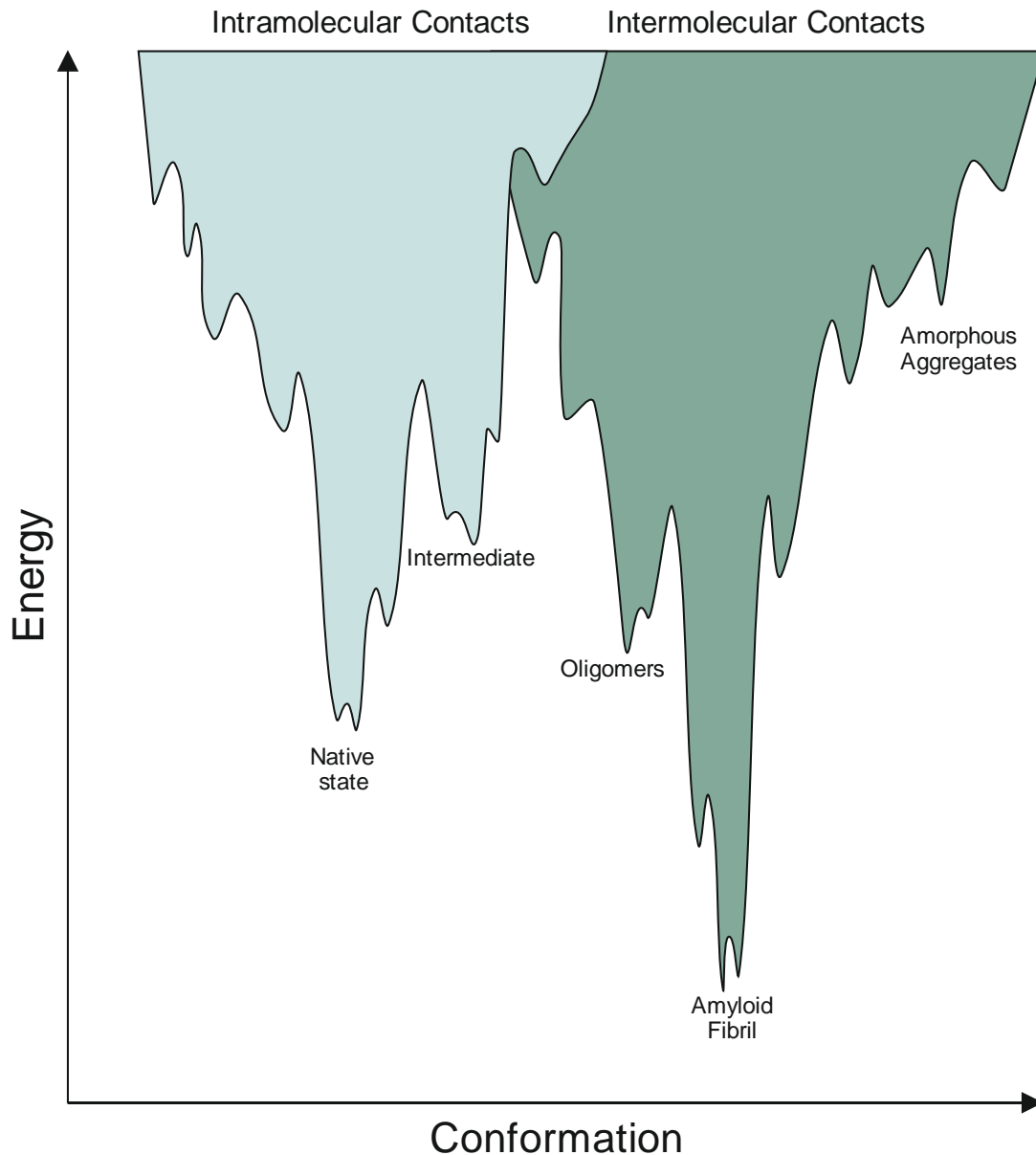


Figure 16: Extended folding energy landscape with intermolecular contacts.

Additional possible contacts result in new conformations. The highly ordered structure in amyloid fibrils represents a new global energy minimum, which is more stable than the native conformation, adapted from Jahn et al.⁴⁶

A special case of protein aggregation is the formation of protein fibrils. There, a large number of identical proteins assemble to one uniform structure. Furthermore, nearly all fibrils share common structural characteristics although different fibrils can be formed from proteins of various size and sequence. Moreover, despite fibrils often represents the energetically most stable structure and potentially all proteins are capable to form fibrils, this structure is mostly non-functional, hence a misfolding product, and associated with a range of diseases,⁵¹ albeit, some fibrils fulfil physiological functions.⁵² This is astonishing, because it implies, that the native structure of a protein is not the energetically most favorable and that protein function and with this live itself requires an energetically non-optimal conformation. The curtail point in preventing fibrillation is the energy barrier between the fibrillar state and other conformations, especially the native one. Therefore, processes or molecules, which lower the energy barrier between the native state and fibrillar state are significant risk factors in protein misfolding.

3.5 Amyloid β peptide and amyloid fibril formation

3.5.1 A β and its structure formation process

The fibrillation of A β can be described as a stepwise process with a lag phase, a fibrillation phase and a plateau phase. Each phase is characterized by different structural variants of A β , starting with monomers, oligomers, protofibrils and finally mature fibrils (see Figure 17).

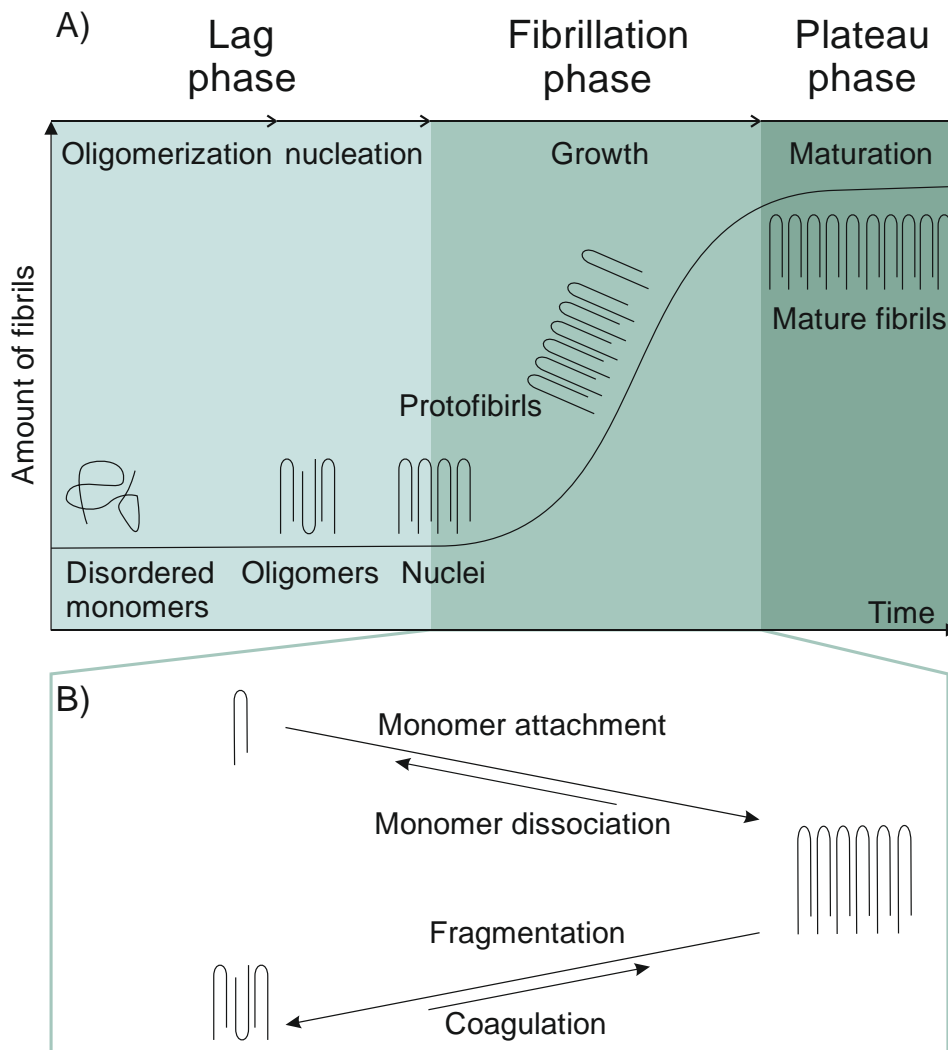


Figure 17: The fibril formation process.

A) The process can be divided into three phases, each characterized by specific structural variants. At the beginning of the process, A β shows intrinsic disorder. During the lag phase oligomers are formed. By structural reorientation oligomers can adopt a nuclei conformation, which ends the lag phase and initiates the rapid fibril growth of the fibrillation phase. First, protofibrils are formed, which mature to fibrils after further restructuring. When fibril growth is ended and an equilibrium between the different structural forms is achieved the plateau phase is reached. B) Fibril growth can be achieved by attachment of monomers or by attachment of whole oligomers, called coagulation. Coagulation is a subordinate process, as the concentration of suitable oligomers is usually considerably lower. Fibril shortening can occur by fragmentation or by monomer dissociation, whereas monomer dissociation is energetically unfavorable.

Monomers

The fibril formation process starts with single monomers. In case of $A\beta$, these are formed as a product of cleavage from a precursor protein (see “Peptide length”). This enables the occurrence of different variants, which can behave differently during fibril formation. Additionally, posttranslational modifications or mutational variants might cause further diversification.

In vivo, the most abundant alloform of $A\beta$ is the 40 amino acid long variant. Most charged amino acids are located at the N-terminus. The C-terminus is dominated by hydrophobic residues. Another accumulation of hydrophobic residues is at a region ranging from L17 till A21 (see Figure 18 A).

An important feature of fibrillation prone $A\beta$ monomers is structural flexibility. This intrinsic disorder is caused by the primary structure but can further be influenced by a structure unfavorable environment characterized by a high pH or a non-polar solvent. Whereas for some intrinsically disordered proteins this structural flexibility is an important functional feature, in case of amyloidogenic proteins, this leads to a high fibrillation propensity.^{53,54}

The large flexibility combined with the high aggregation potential represent major obstacles for experimental investigation of the structural and dynamical features of $A\beta$ monomers. Besides NMR experiments, the most profound insights were achieved by in silico investigations. These show that, as expected, the monomer structure is highly flexible (see Figure 18 B). However, distinct structural elements occur with a certain preference and probability. So, it could be shown, that in $A\beta_{(1-40)}$ monomers, besides random coil, α -helical structures can occur while β -strands are not stable. This is notable, because β -strands are by far the most dominant secondary structure in fibrils. However, these features are highly sensitive to the investigated $A\beta$ variant as well as to the experimental conditions.⁵⁵⁻⁵⁷

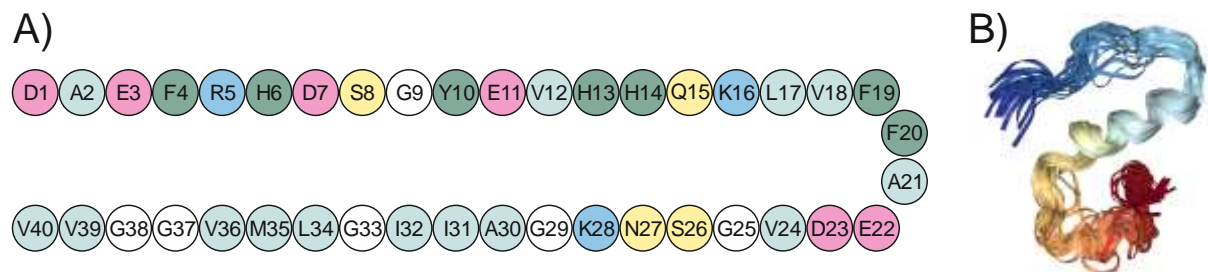


Figure 18: $A\beta$ monomer structure.

A) primary structure of the 40 amino acid allotpe of $A\beta$. Amino acid color code: yellow – polar, red – acidic, blue – basic, dark green – aromatic, light green – hydrophobic. Charged amino acids are mainly located at the N-terminus. Hydrophobic residues cluster at the C-terminus and at a hydrophobic region comprizing amino acids L17-A21. B) Simulation derived structural model of a partially folded monomeric species of $A\beta$ (PDB ID: 2LFM)⁵⁶. As an intrinsically disordered peptide monomeric $A\beta$ has no stable secondary structure. Only a small part has some tendency to form an α -helix.

Oligomers

The next step towards fibril formation is the assembly of oligomers. To this end, a number of monomers has to come in close proximity and lasting intermolecular interactions have to be established. This depends on the concentration of the protein, temperature and the energetical characteristics of possible interactions.⁵²

As is illustrated by the folding energy landscape model, the transition from unstructured monomers to mature fibrils can go via different routes, resulting in a multitude of transient oligomers of different size and structure.⁵⁸ An initial step of A β oligomerization is the formation of a turn structure, which, after structural reorganization, persist also in mature fibrils.⁵⁹ An important contact accompanying this turn formation is the hydrophobic interaction between F19 and L34, that is not only present in early oligomers, but is conserved over the further fibril formation process.⁶⁰ Even though an important characteristic of the oligomers is their heterogeneity, detailed structural analysis of single species can give valuable insights into important processes and functions. An example for an oligomer structure with atomic resolution is available for the A β ₍₁₋₄₂₎ variant in a membrane mimicking environment (see Figure 19). It shows a planar, tetrameric assembly in which the two outer peptides provide two β -strands linked by a turn and each of the inner two peptides provides a single β -strand located at their C-terminus to build an antiparallel β -sheet. With increasing protein concentration two of these tetramers stack on top of each other in a sandwich-like fashion to form an octamer.⁶¹ Another model suggest uniform U-shape strand-turn-strand structures of peptides, which assemble to hexamers.⁶² If or to what extent these features are also present in other A β variants, under different conditions, especially in a purely aqueous environment, and if these structures can nucleate fibril formation remains to be shown. Some studies suggest that this is only partially the case.⁶³

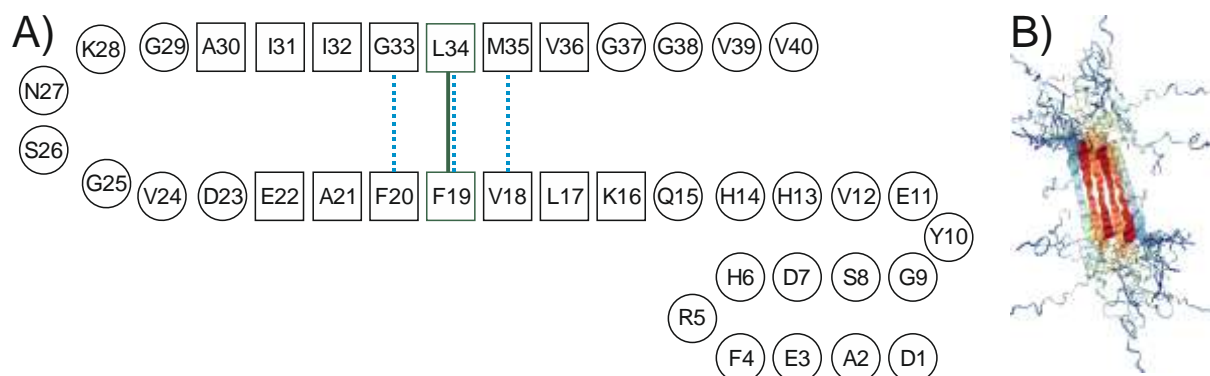


Figure 19: A β oligomer structure.

A) Models of early oligomer are typically characterized by an antiparallel, β -sheet (amino acids with β -sheet conformation are indicated by squares). The hydrogen bonds are intramolecular (blue dotted lines). In these soluble oligomers the β -sheets are not fully extended and the turn region between the β -strands remains unstructured.⁶⁴ The characteristic F19-L34 contact is already established (green colored) B) Structure of an A β tetramer within a lipid environment (lipids not depicted). The typical antiparallel β -sheet with intramolecular hydrogen bonds is recognizable. In this special case not all monomer units participate equally in the structure and the β -strands are extended, probably because of stabilization by the membrane environment. (PDB ID: 6RHY)⁶¹

The structural transition from an oligomeric state to a nucleation capable nucleus is the subsequent step in fibril formation. To initiate fibrillation, oligomers have to show three essential qualities. First, they have to have an oligomeric and a nucleating conformation. Second, they have to be able to shift between these conformations, and third, the association of further protein units has to result in a significant lower net energy of the system.⁵³ In case of A β , one crucial step in this process is the reorientation of the intramolecular antiparallel β -sheet in the oligomeric conformation to an intermolecular parallel β -sheet, which propagates in the fibril structure, by a 90° rotation of the individual β -strands.^{65,66} This then is stabilized by the formation of a new salt bridge between D23 and K28.^{67–69} Once a substantial amount of fibril structure promoting nuclei is formed, fibril elongation becomes the predominant process, which is the hallmark of the growing phase.

Protofibrils

While the structural species formed by elongation of nuclei already show the typical, energetically favorable cross- β structure, this first fibrillar conformation undergoes local rearrangement resulting in two distinct classes of fibrils: first protofibrillar intermediates and later mature fibrils.⁷⁰ Protofibrils show the same extent of the β -strands including the same amino acids like oligomers and the transition from an oligomer-like antiparallel intramolecular β -sheet to a fibril-like parallel intermolecular β -sheet conformation is not completed (see Figure 20).^{71,72} This might reflect the fibril elongation by the mechanism of coagulation instead of pure monomer association.

Monomer association by a lock and dock mechanism is the simplest way to explain fibril growth. A monomer without stable structure stochastically associates onto an existing fibril end. Formation of intermolecular interactions between monomer and fibril then result in a structural transition of the monomer that equals the fibril conformation.⁷³

In a coagulation process, on the other hand, not monomers but larger elements of several monomer units, which themselves originated from oligomeric structures attach on the fibril end. This requires a certain structural similarity, which enables the formation of appropriate interactions. The common oligomeric origin of both species might provide this fit explaining why this oligomeric characteristics is still maintained in protofibrils.⁷³

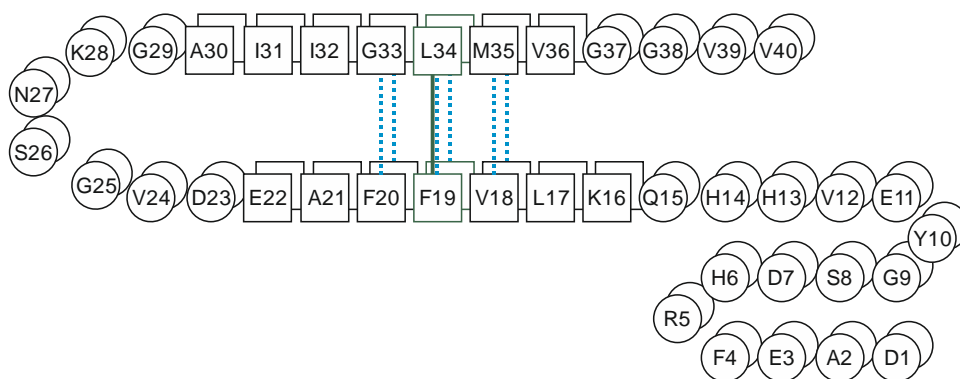


Figure 20: A β protofibril model.

The structure of the A β molecules in protofibrils is similar to their structure in soluble oligomers with not fully extended β -sheets (amino acids with β -sheet conformation are indicated by squares) and an unstructured turn region. Although the A β units string together in a fibrillar fashion, the β -sheets are still antiparallel and from intramolecular contacts (hydrogen bonds are indicated by blue dotted lines). The F19-L34 contact remains conserved (green colored).⁷¹

Fibrils

Independent of the details of the growth process, finally a maturation to the mature fibril structure occurs. In case of A β , this comprises an extension of the parallel β -sheet structure and the conversion of intermolecular contacts.^{72,74} But even on the level of mature fibrils, structural polymorphism exist. This can be due to variation of the primary sequence, for example by differential proteolytic cleavage, posttranslational modification or mutation. But also identical monomers can produce different fibril structures, depending on the folding pathway.⁷⁵ These structural varieties can reflect differences in the biological and especially pathological activity of the distinct variants.^{76,77}

Just focusing on wildtype A $\beta_{(1-40)}$, most structures and models agree on a set of characteristic elements present in conventional U-shaped structures (see Figure 21). The central element is the hydrophobic core region, which comprises approximately the amino acids 15-21 and 31-36, which form the two β -strands of the β -sheets that stack to build the cross- β structure.⁷⁸ Typically, the β -sheets extend the hydrophobic core ranging up to amino acids G9-E22 and A30-V39.⁷⁹ An important contact within the hydrophobic core region is the hydrophobic interaction between F19 and L34, as this is early forming and conserved over a large spectrum of models and A β variants.^{60,80} The two β -strands are linked by a turn domain. Especially residues 22/23 and 29/30 show a clear backbone bend. The amino acids 24-28 adopt a structured turn conformation.⁷⁸ The formation of the turn is an essential step in the structure conversion from oligomers to fibril forming nuclei.⁵⁹ An important interaction in this domain is the salt bridge between D23 and K28 because it stabilizes the turn structure.⁶⁷ Residues 37-40 and 1-14 form the unstructured C- and N-termini, respectively. However, in some models the latter is described to interact with other elements of the fibril, which can lead to an, at least partial and transient, structure formation within the N-terminus, for example by extension of the adjacent β -sheet.⁸¹ Furthermore the N-terminus comprises the metal binding site mainly including the amino acids 6, 13, and 14.⁸²

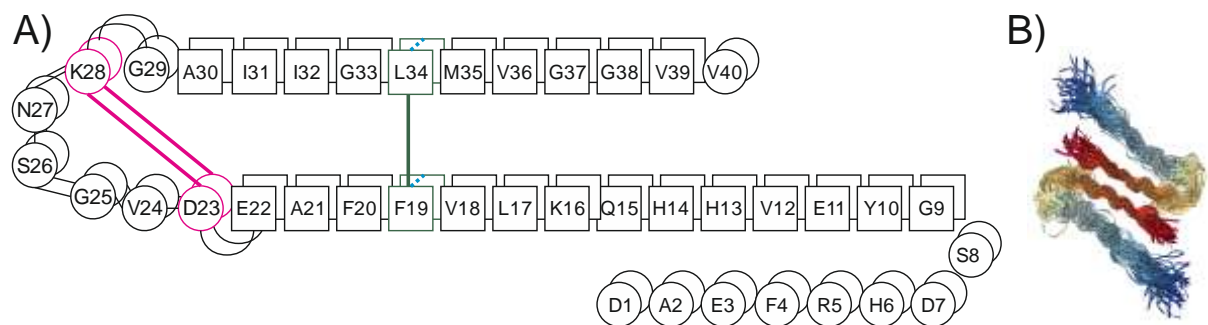


Figure 21: A β fibril structure.

A) Mature fibrils show extended, parallel β -sheets (amino acids with β -sheet conformation are indicated by squares). The F19-L34 contact (green colored) and the intermolecular hydrogen bonds (indicated by blue dotted lines) remain conserved from the protofibrillar structure. In contrast to protofibrils the structure of the turn region becomes stabilized by a salt bridge between D23-K28 (red colored). Typically, pronounced backbone bends are observable between E22-D23 and K28-G29.^{78,79} B) Structure of two stacked A β fibrils with the characteristic U-shaped and parallel, intermolecular β -sheets. (PDB ID 2LMN)⁷⁹

Although the application of this classical U-shape model is popular in the literature, newer findings suggest that other structural arrangements also showing the described contacts are possible. In an extended structural model obtained by cryo-EM the loop-region, which links the two β -sheets does not form a turn but remains straight. In this case the characteristic contacts are formed intermolecularly with a second, opposing A β peptide in inverse orientation.⁸³ Also in the U-shape model intermolecular the contacts might be intermolecular. This could be caused by an offset between the β -sheets along the fibril axis.⁷⁹

Besides linear elongation, other, secondary processes occur during the growth phase, which emanate from existing fibrils. These comprise secondary nucleation, branching, fragmentation and lateral association.

During secondary nucleation, the lateral surface of a fibril supports the formation of new, independent fibrillation nuclei by lowering the free energy barrier of this process.⁷³ In case of branching, monomers associate to the fibril and adopt the fibril conformation like in the lock and dock model described above, however, not in position of the fibril end but at the lateral surface of the fibril.⁸⁴ Fragmentation on the other hand is the opposing process to coagulation. There, a whole fragment with a fibrillar conformation separates from the original fibril. This mainly occurs by breakup when the fibril length exceeds a certain length and is affected by mechanical forces. All these processes increase the fibril formation rate as they lead to a higher number of available nuclei.⁷³

Lateral association is different in a way that there two or more mature fibrils join together to form a fiber. This decreases the fibril formation rate as it reduces the available surface for branching and secondary nucleation. Also, additional contacts are formed between the fibrils potentially leading to further structural rearrangements and new superstructures. The final fibers differ not only in the number of included fibrils but also in their microscopic topography, like in their cross section or twisting along the fibril axis.^{79,85}

Ultimately, all described processes occur simultaneously and an equilibrium is achieved, which characterizes the final plateau phase.⁷³

3.5.2 The F19-L34 contact in previous investigations

The hydrophobic core region forms the cross- β structure, the essential structural element of amyloid fibrils. A hydrophobic contact between F19 and L34 that is located in the center of the core region, marks a first and vital step in the fibril formation process. Mutations at the site of the contact investigated by a preceding study of Adler et al. have been reported to change the local structure of A β fibrils but do not affect the global fibril structure. Most strikingly, they completely abolished A β toxicity, independent of the nature of the contact.⁸⁶

Mutational studies with double mutants showed that alterations at this region are strongly location dependent. Mutant pairs with identical amino acid composition but different amino acid localization showed dramatically different effects (e.g. at position F19, F20: FF \rightarrow IG and FF \rightarrow GI). This shows, that not only the net forces and energies are important, but more so the specific interactions, which are formed between the amino acids.⁸⁷

Steric constraints

The structural flexibility of the peptide backbone is determined by the accessible ϕ and ψ torsion angles of the individual amino acids, which is influenced by the specific side chain. The two most extreme amino acids in this regard are glycine and proline. As glycine has only a proton for a side chain, there is no further steric constraint and it shows the highest degree of structural flexibility. In contrast, proline has a side chain, which is covalently attached to the

backbone by an additional bond between the C δ and the peptide amino group. This strongly reduces the backbone torsion angles that can be adapted. As a consequence, proline typically does not participate in secondary structure formation.

A F19G substitution showed only marginal differences compared to the wildtype. The times describing the fibril formation kinetics remained largely unaltered as well as the fibril morphology. The local structure within the hydrophobic core region also showed only small changes. The only observable differences were a somewhat denser packaging of the side chains that resulted in a lower motional amplitude and a reduced fibril diameter.

A F19P substitution had strong effects on all investigated features. Altogether, it induced a significant energetic penalty of the fibril formation process and the final fibril structure. This is reflected by the drastically increased fibril formation kinetic times. Also, the transition of intermediates to more mature structures was impaired resulting in a higher heterogeneity of the investigated samples and a change in fibril morphology.

Overall, it seems that a change in the steric flexibility of the protein backbone can be tolerated to some extent. Fibrils react with a local structural rearrangement, which results in a denser packaging of the core region and decreased dynamics of the contributing side chains due to higher backbone flexibility and vice versa for lower backbone flexibility. This is probably not caused by a change of side specific interactions but by a change of the net energies of the process (see Figure 22).

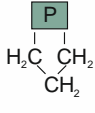
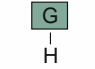
		Fibril formation kinetics	Global fibril morphology	Cross- β secondary structure	Local structure	Local dynamics
Steric constraints	Sterically constrained	 Substantially slower	Shorter fibrils	Polymorph, not completely matured	Alterations at F20 and A21	Increased
	Sterically flexible	 Similar	Shorter fibrils	Similar	Similar expect F20	Reduced

Figure 22: Sterically constrained F19 mutants.

Of all mutants, the steric alterations caused the vastest changes compared to WT and the two mutants show distinct effects. F19P impairs the fibril formation and F19G causes a denser packaging of the fibril core.

Side chain hydrogen bonds

The influence of additional side chain hydrogen bonds was tested using F19Y and F19W mutations. For both mutants, the fibril formation process is moderately slowed down and the global and local structures were similar to the wildtype with only minor deviations. In both variants additional side chain contacts could be observed. Overall, these two mutants showed the biggest similarities with the wildtype. This is striking because only these mutants still contain a ring system at position 19 whereas in all other mutants tested this gets replaced by a non-ring moiety. This might indicate that the presence of a ring system is more important for the fibril formation process and the fibril structure than other characteristics (see Figure 23).

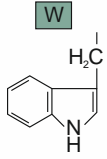
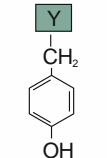
		Fibril formation kinetics	Global fibril morphology	Cross- β secondary structure	Local structure	Local dynamics
Hydrogen bonds	Indole ring group 	Slower	Similar	Similar	Similar	Similar
	Phenyle ring group 	Slower	Similar	Similar	Similar	Similar

Figure 23: F19 mutants with additional hydrogen bond donating chemical groups.

These mutants allow for the formation of additional hydrogen bonds while still possessing an amino acid residue with a conjugated ring system. These mutants resemble the WT in nearly all aspects. Only the fibril formation kinetics is slightly slower.

Electrostatic constraints

The incorporation of charged amino acids into a nonpolar environment like the fibril core structure results in a high energetic penalty. This impairs the fibril formation process in several ways. First, an additional negative charge at the monomer level can increase the repulsion of the peptides, which reduces oligomer assembly. Second, salt bridges can be formed that have to be broken in the process of fibril formation. Third, the charged amino acid has to be discharged by protonation or deprotonation at an energetical cost. Fourth, during discharging also a dehydration and rearrangement of solvent molecules is needed, which results in an additional energetical cost entropic penalty.

These effects could be demonstrated by a F19E substitution. In this variant, the fibrillation kinetics was clearly decelerated. Although the global and local structure remained largely unaltered, which speaks for an uncharged state of the glutamate, a destabilization of the structure could be observed (see Figure 24).

In case of a F19K substitution the effects are much weaker. Compensatory for the energetic costs of a charge for the fibril formation process is the reduction of the negative net charge of the soluble monomer by the introduction of an additional positive charge. Therefore, fibrillation kinetics and global morphology resemble the wildtype. Also, the free energy of the mutant shows only marginal differences. In contrast, NMR chemical shift values indicate that the local structure is clearly changed, especially at the neighboring position F20. An explanation could be that the F20 flips into the fibril core whereas the F19K forms a contact with the E22 at the fibril surface.

		Fibril formation kinetics	Global fibril morphology	Cross- β secondary structure	Local structure	Local dynamics	
Electrostatic interaction	Single charge		Slower	Similar	Similar	Strong alterations at F20	Reduced
			Slower	Similar	Similar	Similar	Similar
	Charge-charge interaction		No fibrils formed				
		Slightly slower	Similar	Similar	Strong alterations at F20	Reduced expect F20 ring	

Figure 24: F19 mutants introducing charged amino acids and F19-L34 double mutants introducing attractive or repulsive charges.

The introduction of a negative charge at position F19 is well tolerated and causes only minor alterations. In contrast, the introduction of a positive charge in the single as well as in the double mutant results in a structure rearrangement in the core region. Otherwise, the fibril characteristics remain mostly similar in comparison to the WT. The substitution of the hydrophobic contact for a salt bridge prevented fibril formation, probably because of a stabilization of the monomers.

The formation of an additional salt bridge can compensate for other energetic penalties, however, there is some evidence, that this contact is not preserved in the mature fibril.⁸⁸ In this regard, the F19K L34E double mutant is interesting. In this case the salt bridge would have to be incorporated into the nonpolar hydrophobic core and cannot be localized at the fibril surface without breaking the fibril structure. Although the salt bridge could potentially compensate for the energetic penalties, this is not the case for this double mutant. Instead, fibril formation is completely abolished, perhaps because of the formation of another structurally stable conformation that is caused by the new salt bridge. In contrast, a F19K L34K double mutant did not show such effects but resembles the wildtype with some alterations especially for the local structure at position F20 and concerning the free energy of the fibrils. Probably similar effects like in the F19K single mutation can be observed. On the one side, the reduction of the net charge of the monomers benefits fibril formation whereas the discharge or reorganization impair the stability of the fibril structure.

3.6 Biological relevance of A β modifications

As the physicochemical characteristics of A β are influenced by various factors like different peptide lengths, posttranslational modifications or mutations at diverse locations this also has influence on its biological function, as well as its role in the development of neurodegenerative diseases (see Figure 25).

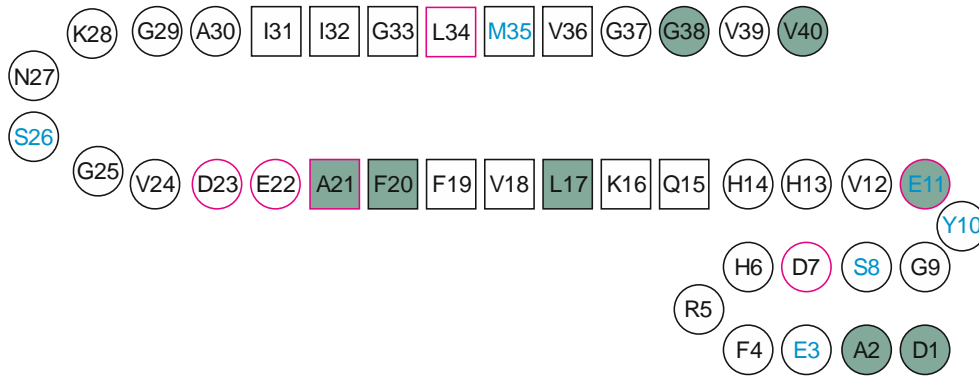


Figure 25: Selected A β mutations and modifications.

Several amino acids can undergo posttranslational modifications (blue font). Many mutations (red outline) are located within protease cleavage sites (filled green symbols).

3.6.1 A β mutations in early onset Alzheimer's disease

Various factors are discussed to be involved in the development of Alzheimer's disease. Great attention was devoted to genetic variants and gene mutations. It is possible to assign different variants of Alzheimer's diseases to two distinct types: sporadic and familial forms, correlating to late onset and early onset Alzheimer's disease, respectively (see Figure 26).

While the sporadic one counts for the majority of cases, the familial can be attributed to mutations of mainly three proteins: amyloid precursor protein, presenilin 1, and presenilin 2. Strikingly, all of these forms relate to the A β mediated pathway of Alzheimer's disease. Presenilin 1 and 2 are important for the A β release from the amyloid precursor protein. Within the precursor, many disease relevant mutations are located within the A β region (see Table 1). Most of these mutations cluster around the protease cleavage sites. Many mutations located at the N- and C-terminus affect A β cleavage, resulting in different amounts of formed A β and peptides with varying lengths that show different physicochemical and pathological properties.^{89,90} But also, a great number of mutations within the A β sequence cluster around alternative cleavage sites. Investigated mutations of this type comprise the E11K mutation at the alternative BACE1 cleavage site, A21, D23 and several E22 mutations at the BACE2 cleavage site and K16N at the α -secretase site. These mutations do not only influence the formation of non-A β cleavage products of the amyloid precursor protein but might also affect the proteolytic degradation of A β .^{91,92} Additionally, especially for the different mutations at the BACE2 cleavage site, a multitude of other, cleavage independent effects, is described like structural changes at the level of monomers, oligomers, and fibrils as well as changes in the fibril formation kinetics, cellular localization or downstream effects.^{93–98} Furthermore, there are mutations that are distant to described cleavage sited, for example at the metal binding side at the N-terminus (H6R, D7N, D7H) or within the hydrophobic core region (L34V), also resulting in diverse effects on A β properties and functions.^{99–105}

Table 1 A β variants.

Mutation (orange colored), modification (blue colored), and cleavage sites (green colored) located at the A β region of the amyloid precursor protein (approximately amino acids 1-40).⁸⁹ * β -methylamino-L-alanine (BMAA) misincorporation is under discussion but has not been shown to be present in A β in vivo.

Name	Position	Wildtype	Posttranslational modification	Mutation	Protease cleavage site
	-2			N	β -secretase, (Bace2)
Swedish	-2	K			
Swedish	-2	N		L	
	3	E	pyroglutamate formation		
Torotti	7	D		N	
	8	S	phosphorylation (BMAA misincorporation)*		
	10	Y	dityrosine mediated crosslinking		
	11				β -secretase
Leuven	11	E		K	
	11	E	pyroglutamate formation		
	17				α -secretase
	20				Bace 2 (α -secretase)
	21				Bace 2
Flemish	21	A		G	
Dutch	22	E		Q	
Arctic	22	E		G	
Italian	22	E		K	
	22	E		Δ	
Iowa	23	D		N	

	26	S	phosphorylation (BMAA misincorporation)*		
Piemont	34	L		V	
	35	M	oxidation		
	38				γ -secretase
	40				γ -secretase
	42				γ -secretase
	42	A		T	
Austrian	34	T	L		
Iranian	43	T		A	
French	44	V		M	
German	44	V		A	
Florida	45	I		V	
	45	I		T	
	45	I		F	
London	46	V		I	
	46	V		G	
	46	V		F	
	46	V		L	
	48				ϵ -secretase
	48	T		P	
	49				ϵ -secretase
Australian	52	L		P	
Belgian	K			N	

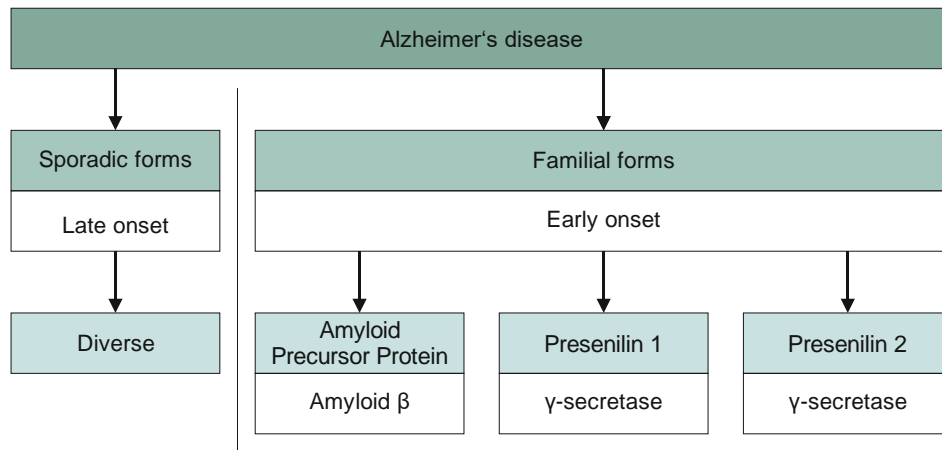


Figure 26: Genetic factors in the etiology of Alzheimer's disease.

While diverse gene mutations can also contribute to sporadic, late onset forms, familial forms are mainly caused by mutations in one of three genes: either in presenilin 1 and 2 that are elements of the APP cleaving γ -secretase enzyme complex or in the A β Precursor Protein itself.

A possible sequence changing alternative to mutation is the misincorporation of non-proteinogenic amino acids. An example might be β -methylamino-L-alanine (BMAA). However, such a mechanism is not proven and still under controversial discussion.

3.6.2 Posttranslational modification

Different posttranslational modifications of A β are described to be important for the pathology of Alzheimer's disease, namely oxidation of M35,^{106,107} nitration, dityrosine or pyroglutamate formation and glycosylation of Y10,^{108,109} as well as isomerization and racemization of D1, D7, S8 and S26.^{110–112} S8 and S26 can also undergo phosphorylation. S8 phosphorylation can occur intracellularly and extracellularly, which both lead to an amplification of the peptides aggregation propensity.^{113,114} This might increase toxicity in some aspects. However, this is counteracted by a stabilization of the non-toxic fibrillar form.^{115,116} Phosphorylation at the S26 site leads to an increase of A β oligomers and enhances toxicity, supposedly by granulovacuolar degeneration.¹¹⁷ Another toxic pathway related to S26 modification might be by excitotoxicity. It could be shown that S26 racemization enables A β to induce excitotoxicity in the presence of excitatory agents.¹¹⁸ This is reminiscent of BMAA, which is under discussion to be an excitotoxic neurotransmitter mimetic, as well as an possible substitute for serine during protein expression.^{119–122}

3.6.3 Peptide length

A β is derived by cleavage of the amyloid precursor protein (APP) (see Figure 27 A). Protein cleavage by various different proteases is an important feature of APP regulation and function. APP cleavage involves a variety of different cleavage sites, cleavage products, proteinases, and downstream effects.¹²³ The cleavage pathways of APP can be divided into canonical and non-canonical pathways, depending on the proteases involved. Regarding the pathology of Alzheimer's disease, it is most relevant, if the cleavage pathway leads to generation of the amylogenic A β peptide.

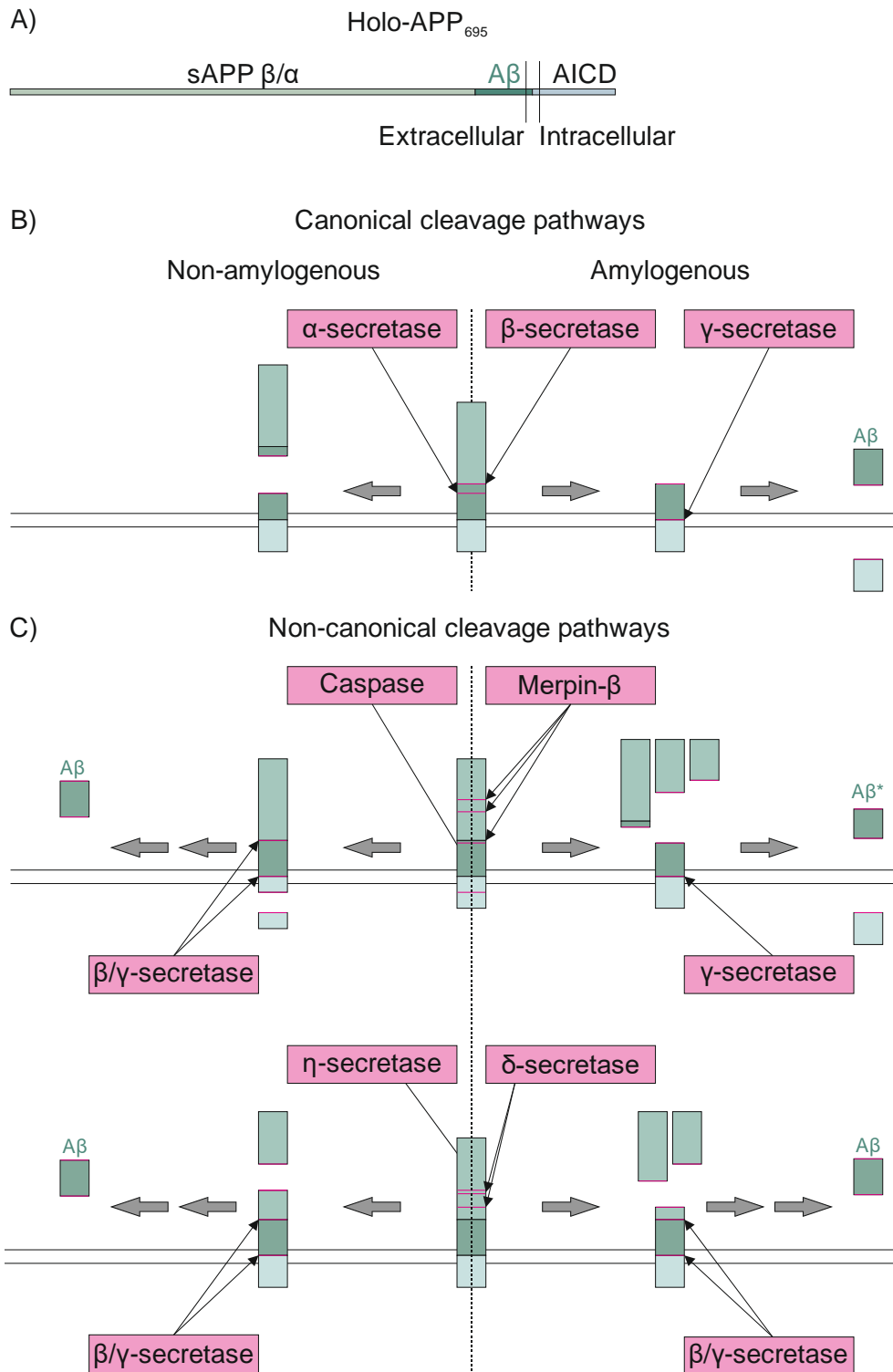


Figure 27: APP cleavage pathways.

A) A β is a cleavage product of the amyloid β precursor protein (APP). Depending on the cleavage pathway, additional extracellular and intracellular fragments besides A β are produced. B) The canonical cleavage pathway of APP is mediated by α -, β -, and γ -secretase. The β/γ branch results in the release of A β and is therefore amylogenous. A-secretase cleaves within the A β sequence, preventing A β formation and fibrillation. C) Besides the canonical pathway several other are known that comprise the proteases caspase, merpin- β , δ -secretase and η -secretase. All proteases produce different cleavage products from which at least one can undergo further canonical β/γ -cleavage. Therefore, all are potentially amylogenous. In case of merpin- β a truncated A β alloform is formed.

The canonical pathway involves the proteinase families of α -, β -, and γ -secretases (see Figure 27 B).¹²³ From all the pathways, canonical and non-canonical, only α -secretase cleavage is non-amyloidogenic because it cleaves APP within the A β sequence. The main α -secretase of the brain is A disintegrin and metalloprotease 10 (ADAM10).^{124,125} Amyloidogenic β -secretion is mainly mediated by the aspartyl proteinases β site APP cleavage enzymes 1 and 2 (BACE1, BACE2).¹²⁶ The final cleavage steps are performed by presenilin containing γ -secretase. First, it cleaves at the ϵ -site, which releases the intracellular domain into the cytosol. Then it truncates the remaining fragment till full length A β in the amyloidogenic case, or p3, a truncated A β variant, in the non-amyloidogenic case are formed.¹²⁷ This special characteristics of a step-wise cleavage of γ -secretase is caused by its ability to perform two different cleavage mechanisms, endopeptidase-like and carboxypeptidase-like, both within the lipid bilayer.¹²⁷

The best described non-canonical APP processing includes caspase cleavage, meprin β cleavage, the δ -pathway and the η -pathway,¹²⁸ whereas further cleavage possibilities are suggested (see Figure 27 C).¹²⁹ All of these can eventually lead to formation of A β variants. The δ - and η -pathways produce products, which can undergo canonical β - and γ -secretion, whereas caspase and meprin β have inherent cleavage activity at the β -site, which leads to A β secretion after subsequent γ -secretase cleavage.^{123,128}

3.7 Methods for the investigation of fibril formation and structure

To characterize the diverse mechanisms of the fibril formation process and the structure of mature fibrils a set of experiments was carried out investigating three libraries of A β mutants. The different peptides were obtained by solid phase peptide synthesis. Kinetic studies were performed using the Thioflavin T fluoresce assay. Global, secondary and local structure information were gained by transmission electron microscopy, circular dichroism spectroscopy, X-ray diffraction and NMR chemical shift measurements. Local structural information was complemented by molecular dynamics investigations by NMR DipShift experiments. The biological activity was tested in cell culture with an MTT assay. For one set of mutants, additional LDH Assay, Caspase 3 assay, neurite length measurement and Hoechst/PI staining were performed to differentiate between different ways of cell response.

3.7.1 Fibril formation kinetics

The usage of fluorescence dyes is a well-established method in detection of amyloid structures. A broad range of dyes is available, including Congo Red, Thioflavin T (ThT), Chrysin, 6-OH-BTA-1, or 2C40. Among these, Congo Red is best established for histological staining whereas ThT is most widely used for in vitro experiments.¹³⁰ As it shows an intensity increase upon specific fibril binding, this dye was used for measurements of the fibril formation kinetics.

ThT is composed of two building blocks: a benzothiazole double ring and a phenol ring (see Figure 28 A). Benzothiazole is an aromatic, heterocyclic, bicyclic compound with a sulfuric and a nitric moiety, which is dimethylated at the N3 and C5 position. The quaternary ammonium is stably positively charged. The phenyl ring carries a tertiary dimethyl amine. The two ring systems are linked between the ortho-carbon of the phenyl moiety and the C2 of the

benzothiazole. Therefore, the C2 is a reactive carbon. Furthermore, the C-C bond between the ring systems allows for rotation, which is important for its fluorescence properties.

The benzothiazole can be excited by absorption of light at about 420 nm. By electron transfer and rotation around the C-C bond to a perpendicular orientation, the excited state can relax to a Twisted Intramolecular Charge Transfer state (TICT). This state can undergo further relaxation, which is accompanied by weak emission at about 510 nm. When C-C bond rotation is inhibited, benzothiazole has to relax directly to its ground stage. This process is highly emissive and results in high intensity fluorescence at a wave length of 480 nm.¹³¹ The impairment of rotation can be achieved by binding of the dye to a surface.

The binding mode of ThT to fibrils is still under controversial discussion. At least two different modes are well accepted.¹³² The first is by electrostatic interaction of the positively charged dye to negative charges of the fibril surface. Whereas this binding mode might be the predominant one, it is not structure specific and does not result in the inhibition of the Twisted Intramolecular Charge Transfer state by rotation impairment. For this, a different binding mode is necessary. In the cross- β structure, the arrangement of successive amino acids along the fibril axis results in the formation of periodic ridges at the fibril surface. ThT can intercalate into these ridges, especially at hydrophobic areas. This strong and structure specific interaction prevents the ring rotation and results in the fluorescence increase upon fibril binding.¹³³

At the beginning of the experiment ThT is added to a freshly prepared solution of non-fibrillated peptide. As ThT cannot bind to any fibrillar structure only low background fluorescence is detected. This state is maintained over a period of time until fibrillation nuclei are formed. With this, rapid fibril growth is initiated, resulting in an increase in the amount of fibril structures, ThT binding and subsequently detectable fluorescence. When most peptide is incorporated in fibrils a steady state is reached where the fluorescence remains constant. Fibril formation independent processes can lead to a constant increase or decrease of detectable fluorescence in the final phase, for example by structural rearrangement or sedimentation.

The fibril formation process consisting of three phases, a lag phase, a fibrillation phase and a plateau phase, results in a sigmoidal curve shape of a ThT intensity plot in a fibrillation assay (see Figure 28 B). This curve can be fitted by:

$$y = F_1 + m_1 t + \frac{F_2 + m_2 t}{1 + e^{-\frac{t-h}{\tau}}} \quad (3.1)$$

where y is the fluorescence intensity at time point t , F_1 is the intercept and m_1 the slope of the initial baseline and F_2 is the intercept and m_2 the slope of the final baselines with the y -axis. The half time of the fibrillation phase is h and τ is the elongation time constant.¹³² From this, two independent time values, the lag time

$$t_{lag} = h - 2\tau \quad (3.2)$$

and the fibrillation time

$$t_{fib} = 4\tau \quad (3.3)$$

can be calculated, which characterize the fibril formation process.

This procedure is only valid, if the fitting function describes the dominating mechanisms of the fibril formation processes. Under some circumstances the process is dominated by processes like branching or secondary nucleation, which give rise to altered curve shapes. To investigate these, more sophisticated fitting procedures are needed.¹³⁴

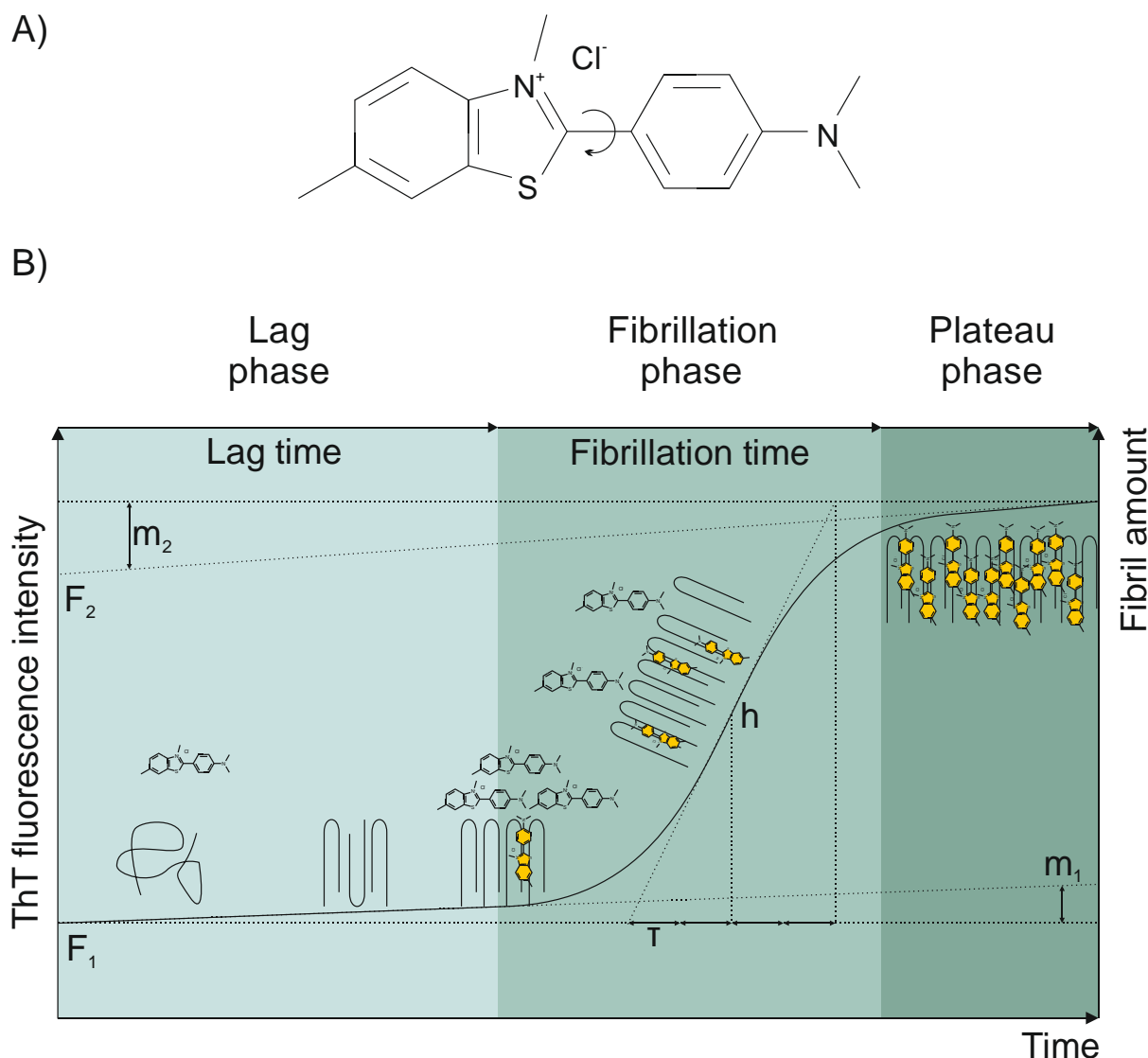


Figure 28: Thioflavin T fluorescence assay.

A) Structure of Thioflavin T showing the demethylated, charged benzothiazole bicycle and the phenyl ring carrying a dimethylamino group, which are linked by a covalent C-C bond. B) Time dependent Thioflavin T fluorescence during fibril formation and important values for sigmoidal curve fitting.

Further limitations of ThT assay mainly lie in the stability, specificity and sensitivity to other compounds of the dye. Especially protonation of the tertiary amine at low pH and hydroxylation at the reactive carbon of the benzothiazole bicycle at high pH or high temperature can reduce emission.¹³⁵ Because ThT binding mainly depends on common electrostatic and hydrophobic interactions structure unspecific binding to crude protein aggregates can be problematic as in some cases it can mimic fibril binding. The sensitivity to other compounds like phenolic molecules, DNA, polysaccharides, and β -sheet rich proteins can be problematic when these are involved.¹³² Especially β -sheet rich protein structures and crude protein aggregates exhibiting hydrophobic surfaces are problematic as they can also be formed by non-fibrillar aggregation pathways of the investigated protein and mimic fibril formation. For this fluorescence-based fibril formation assays have to be complemented by other methods.

3.7.2 Fibril morphology

In microscopic images, protein fibrils show characteristic structures. A well-suited imaging technique for amyloids is transmission electron microscopy (TEM). As the size of fibrils range from the micrometer scale for fibril length of fibril conglomerations to the nanometer scale for the diameter of individual fibrils, conventional light microscopy is insufficient because of its resolution limitations. This is circumvented in electron microscopy by the usage of an electron beam instead of visible light as the electron beam has a shorter wavelength and with this allow higher resolution. As typical fibril samples are relatively thin, this suggests the usage of transmission electron microscopy. A drawback of this method is the necessity of staining, as pure fibrils lack contrast. This procedure might alter the fibril morphology or distort the image due to staining residues. Besides showing the global morphology also more detailed information for example of fibril shape, twisting, or substructures can be obtained. This allows for a differentiation between prefibrillar structures, crude aggregates and mature fibrils.¹³⁶

3.7.3 Secondary structure composition and characteristics

The most important structural element of amyloid fibril is the cross- β structure. Its characteristics and its contribution to the global secondary structure composition can be investigated by X-ray diffraction and circular dichroism, respectively.

Circular dichroism uses the fact that in the peptide bond the $n \rightarrow \pi^*$ transition between the orbital of a free electron pair of the oxygen and the antibonding π^* orbital of another carbonyl group as well as the $\pi \rightarrow \pi^*$ transition of the amide groups within the peptide bond strongly depends on the torsion angles within the backbone as they determine the orientation and proximity of the orbitals (see Figure 29 A). These transitions can be tested with radiation in the ultraviolet spectrum. The $n \rightarrow \pi^*$ transition shows absorbance at about 220 nm and the $\pi \rightarrow \pi^*$ transition at about 200 nm.

Circularly polarized light can be described by a two-component system in which two linear polarized components are perpendicular to each other and shifted by $\pi/2$. This results in the rotation of the field vectors if the radiation along the propagation axis. When left and right circularly polarized light passes through a protein, the two components show different dipole interactions with the backbone orbitals affecting their wave length, speed, and absorption. As the orbitals are influenced by the steric orientation of the backbone, the analysis of the different components of the circular polarized light, especially the 200 nm and the 220 nm absorption corresponding to the $n \rightarrow \pi^*$ and $\pi \rightarrow \pi^*$ transitions, give information about the average secondary structure of proteins. Typical for random coil is a minimum between 190 nm-200 nm and a maximum between 210 nm-220 nm whereas β -sheet structures are characterized by a maximum between 190 nm-200 nm and a minimum between 210 nm-220 nm (see Figure 29 B).¹³⁷

As the cross- β structure is defined by two repetitive structural elements, the intermolecular, intra sheet hydrogen bonds and the intramolecular stacking of the β -sheets, X-ray diffraction images show two characteristic reflections. From the image, the spacing can be calculated by

$$s = \lambda/2 \sin \left[\frac{1}{2} \tan^{-1} \left(\frac{l}{d} \times \frac{360}{2\pi} \right) \right] \quad (3.4)$$

where, s is the spacing causing the reflection, λ is the wavelength of the X-ray beam, l is the distance between the reflection and the center of the image and d is the distance between sample and detector. In a classical fibrils two reflexes can be seen at 4.7 Å and about 10 Å corresponding to the H-bond distance and the distance between the β -sheets, respectively.³⁵

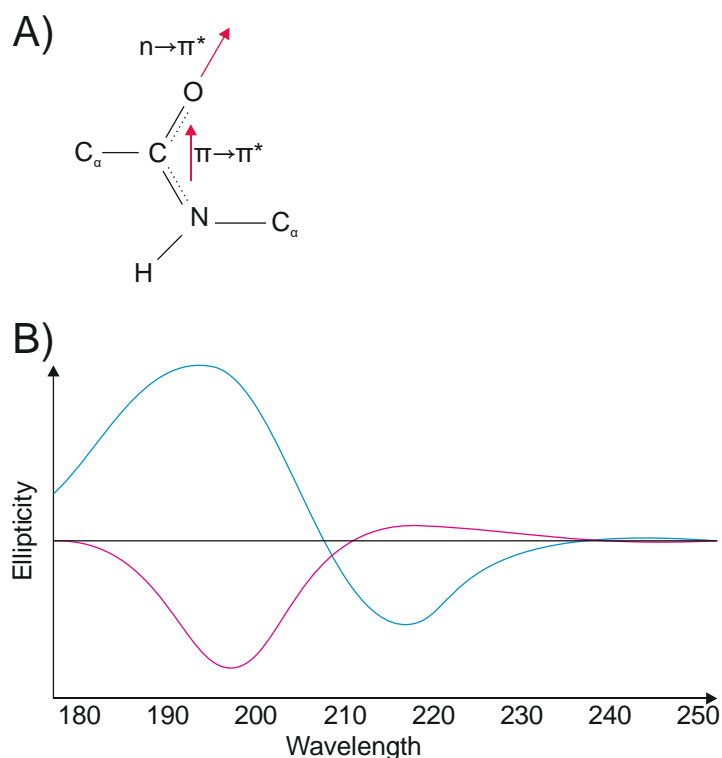


Figure 29: Circular dichroism spectroscopy.

A) Important transitions of the protein backbone. B) Characteristic spectra of proteins with predominant β -sheet (blue) and random coil (red) structure, adapted from Whitmore et al.¹³⁷

3.7.4 Local structure

The nuclear magnetic resonance (NMR) chemical shift of atoms depends on their local electric environment. As the conformation of a protein backbone also influences this environment, knowledge of the chemical shifts of backbone atoms gives site-specific insights into the secondary structure.

NMR spectroscopy uses the spin properties of atom nuclei. The spin (\vec{S}) together with the gyromagnetic ratio (γ) determine the magnetic moment ($\vec{\mu}$) of a nucleus:

$$\vec{\mu} = \gamma \vec{S} \quad (3.5)$$

For nuclei with a magnetic moment the energy states for different spins are no longer degenerated when placed in a magnetic field. Only nuclei with a non-zero spin, like ^1H , ^{13}C , or ^{15}N with a spin of $\pm\frac{1}{2}$ have a magnetic dipole moment and are NMR active. The spin \vec{S} is quantized and can only have integer or half integer multiples of \hbar :

$$\vec{S} = m\hbar \quad (3.6)$$

Where, in case of spin $\frac{1}{2}$ nuclei $m=\frac{1}{2}$ or $m=-\frac{1}{2}$. When a nucleus with a magnetic moment is placed within an external magnetic field, the energies of the $m=\frac{1}{2}$ and $m=-\frac{1}{2}$ differ, depending on a parallel ($\frac{1}{2}$) or antiparallel ($-\frac{1}{2}$) orientation of the spin with respect to the applied magnetic field (B_0) with the energy (E) being

$$E = -\vec{\mu}\vec{B}_0 \quad (3.7)$$

From (3.5), (3.6), and (3.7) results for the energy difference of the two spin states:

$$\Delta E = \gamma \hbar B_0 = -\hbar \omega_L \quad (3.8)$$

where ω_L is the Larmor frequency, which describes the precession of the magnetic moment about the magnetic field. The components of the corresponding vectors in z-orientation sum up to a measurable net magnetization, which is higher when the energy difference between the parallel and antiparallel state is greater. The relation of the populations between these states can be described by:

$$\frac{N_{-\frac{1}{2}}}{N_{\frac{1}{2}}} = \exp\left(\frac{-\hbar \gamma B_0}{k_B T}\right) \quad (3.9)$$

where N is the population of the state, k_B is the Boltzmann constant and T the temperature. Therefore, high magnetic fields are usually used for NMR spectroscopy to achieve a well detectable net magnetization. Even so it is that the term $k_B T$ is way larger than $-\hbar \gamma B_0$, which makes NMR spectroscopy a rather insensitive technique.

When such a spin system is radiated with an additional external radio-frequency pulse where the frequency of the pulse equals the Larmor frequency of the nucleus, the electromagnetic field of the pulse and the applied magnetic field combine to an effective magnetic field with an orientation, which can deviate from the z-axis. As a result, the induced field of the nuclei will orientate along the new effective field and leave the z axis and give magnetization in the x/y-plane. As this field rotated around the z-axis defined by \vec{B}_0 it can induce a detectable electric signal within a coil orientated parallel to the x/y-plane with a frequency equaling the Larmor frequency of the nuclei.

The Larmor frequency of a nucleus not only depends on the external magnetic field but is also influenced by other, internal interactions arising for example from spin-spin couplings, dipolar and quadrupolar interactions, and electromagnetic shielding by the local environment, which causes a chemical shift. These different contributions can be presented by the Hamiltonian (\widehat{H}_{int}):

$$\widehat{H}_{int} = \widehat{H}_J + \widehat{H}_D + \widehat{H}_Q + \widehat{H}_{CS} \quad (3.10)$$

where \widehat{H}_J represents spin interactions mediated by chemical bonds, \widehat{H}_D represents dipolar interactions, \widehat{H}_Q quadrupolar interactions and \widehat{H}_{CS} electromagnetic shielding by electrons. The chemical shift can be represented by the Hamiltonian

$$\widehat{H}_{CS} = -\gamma \hbar \sigma B_0 \widehat{I}_z \quad (3.11)$$

where \widehat{I}_z is the spin operator and σ the shielding tensor. This leads to an effective magnetic field (B_{eff}) of

$$B_{eff} = B_0(1 - \sigma) \quad (3.12)$$

The CSA tensor represents the influence of the local electric environment of a nucleus. This is mainly defined by the electron cloud surrounding the nucleus and is influenced by its density and shape, which directly depends on the special characteristics of the chemical bonds, which are influenced by torsion and dihedral angles. As this is changed during protein folding the shielding tensor gives information about the secondary structure of a protein.

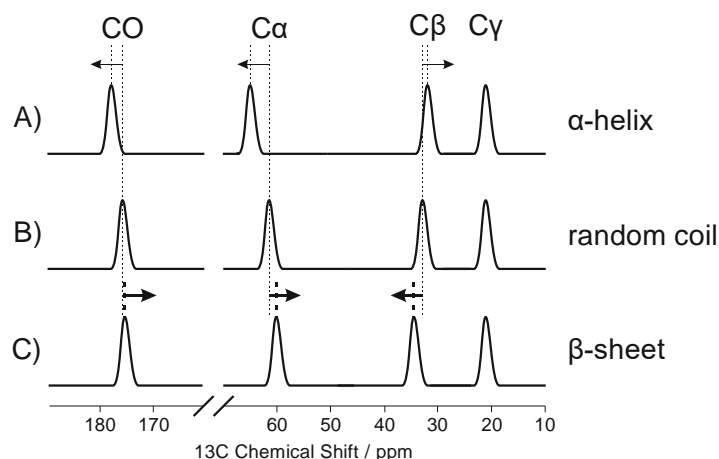


Figure 30: Schematic comparison of the carbon chemical shifts of valine in different secondary structures.

A) Especially the chemical shifts of the C_{α} and C_{β} are shifted to larger, respectively lower values compared to a random coil conformation B). In a β -sheet C) this is reverse.

Because measured resonance frequencies also depend on the applied magnetic field, for comparability between different experimental setups the chemical shift (δ) is given, which is the frequency of the nucleus of interest (ν_i) with respect to a reference frequency ν_{ref} . As the difference is orders of magnitude lower than the absolute values it is given in parts per million (ppm):

$$\delta = 10^6 \frac{\nu_i - \nu_{ref}}{\nu_{ref}} \quad (3.13)$$

As the chemical shift differs for nuclei in amino acids within different secondary structures a comparison of these values can be used for analysis of the local protein structure. The very high frequency resolution of NMR spectroscopy allows for the detection of smallest structural changes.

A nucleus well suited for site specific labeling in NMR experiments is ^{13}C . In nature the NMR-inactive ^{12}C is the predominant carbon isotope with an abundance of nearly 99 %. Therefore, the integration of NMR-active ^{13}C into samples can be used for site specific labeling. For secondary structure investigations especially the C_{α} carbon within the protein backbone as well as the C_{β} carbons are interesting as their chemical shifts differ between the different amino acids, which is important for signal assignment and the chemical shifts are directly influenced by the structural orientation of the backbone and changes during secondary structure formation. In principle the investigation of the chemical shift of CO carbons is also possible, however, these are quite similar between the amino acids and often signals overlap, which hamper data analysis.

When the chemical shifts for example of the C_{α} of amino acids are compared between different secondary structures clear differences can be seen (see Figure 30). In an α -helical conformation larger chemical shifts compared to random coil conformation are observed. In contrast, β -sheets in most cases result in lower chemical shift values. For convenience usually the C_{α} - C_{β} chemical shift differences are reported, which has the advantage, that these are independent of the used reference standards. With this, experimentally determined C_{α} - C_{β} chemical shift differences can be compared to reference values for the secondary structures and the structure of the sample protein can be estimated.

The dynamics of amino acids can be investigated by DipShift NMR experiments. Additionally to the chemical shift, this experiment gives also the dipolar coupling between ^{13}C and ^1H nuclei. In standard solid-state NMR experiments these dipolar couplings are not detectable because the corresponding anisotropic information are eliminated during the measurement. In the Dip-Shift experiment these information are recovered. For this, heteronuclear dipolar between couplings ^{13}C and ^1H are allowed to evolve for a certain time interval t_1 , which modifies the recorded signal amplitude (S_{t_1}):

$$S_{t_1} = S_0 \langle \cos \phi_{t_1} \rangle \quad (3.14)$$

with

$$\phi_{t_1} = \int_0^{t_1} \omega_{ch}(t) dt \quad (3.15)$$

where ϕ is the phase angle and ω_{ch} the angular heteronuclear coupling frequency, which can be expressed by

$$\omega_{CH}(t) = \delta_{CH} \frac{\sin 2\beta_0}{\sqrt{2}} \cos(\omega_r t + \gamma) + \delta_{CH} \frac{\sin^2 \beta}{2} \cos(2\omega_r t + 2\gamma) \quad (3.16)$$

where β and γ are angles from Euler transformation, ω_r is the MAS frequency and δ_{CH} the CH coupling constant. This results in a modulation of the recorded signal, which is periodic to the rotor period of the MAS. In the first part during one rotor period the signal is reduced and recovers at the end of the period. This can be recorded by incrementally prolongation of t_1 until a full rotor period is sampled.¹³⁸ The reduction is dependent of the coupling constant δ_{CH} .

$$\delta_{CH} = -\frac{\mu_0 \gamma_C \gamma_H h^2}{16\pi^3 r^3} \quad (3.17)$$

This shows that the dipolar coupling strongly depends on the distance of the nuclei, which is mainly determined by the chemical bond species. Furthermore, the coupling strength depends on the applied \vec{B}_0 field and the angle between the chemical bond vector and the magnetic field. When the chemical bond vector between the ^{13}C and ^1H is not rigid but shows movement, which is faster than the MAS frequency, δ_{CH} averages to

$$\overline{\delta_{CH}} = \frac{1}{2} \delta_{CH} \langle 3 \cos^2 \theta - 1 \rangle \quad (3.18)$$

This results in a reduction of $\overline{\delta_{CH}}$ with an increasing opening angle θ of the chemical bond vector movement. In consequence the dephasing of the signal becomes weaker for movements with a higher motional amplitude. With this the dipolar coupling can be calculated from the shape of the dephasing curve (see Figure 31).

Because the dipolar coupling also depends on the distance between the nuclei in the chemical bond, which differs between CH, CH₂ and CH₃ groups, usually an order parameter S with

$$S = \frac{\delta_{exp}}{\delta_{ref}} \quad (3.19)$$

is given, where δ_{exp} is the experimentally determined dipolar coupling and δ_{ref} is the dipolar coupling of a fully rigid chemical bond vector determined from a crystalline reference sample. Therefore, the order parameter is a measure for the local dynamics with $S = 0$ indicating isotropic movement and $S = 1$ full rigidity.

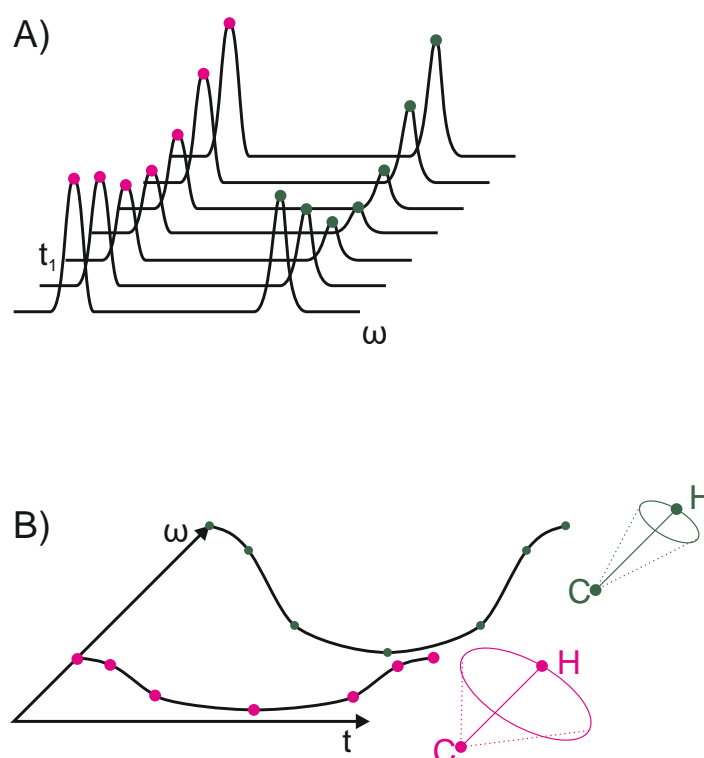


Figure 31: DipShift experiment.

A) Over one rotor period, increasing evolution times t_1 result in an initial decrease of the signal intensity and a recovery during the second half. B) This can be plotted as a dephasing curve. Large dephasing indicates a small motional amplitude of the observed C-H bond (green) whereas low dephasing indicates a high amplitude (red).

3.7.5 Biological activity

The biological activity of A β peptides can be investigated by different cell assays. In this work mainly the MTT assay was used. For selected samples, additionally LDH assays, Caspase 3 assays, Hoechst/PI staining and neurite length measurements were performed (see Figure 32). All assays test different mechanisms of cell death. It is important to be mindful about the interpretation of the results of the different assays as they test only single aspects of different cellular pathways and should not be generalized.

For all assays the choice of the cellular system is of high importance. In this work a cell culture of RN46A cells or a primary culture of neurons obtained from fetal mouse brains were used. The primary culture has the advantage of being potentially more physiological but is experimentally demanding. The RN46A cells are a neuronal cell line, which also mimics important physiological features. Both systems are well suited to investigate certain aspects of the cellular activity of A β . However, the comparison of effects between different systems is limited. Furthermore, as the pathological activity of A β in different diseases is still not known it is not clear if a used cell system reflects conditions that are medically relevant.

The MTT assay utilizes the reduction of membrane permeable MTT (3-(4,5-dimethylthiazol-2-yl)-2,5-diphenyltetrazolium bromide) to formazan by mitochondrial dehydrogenase. Formazan concentrations can be easily measured by absorbance. Dehydrogenase activity is generally stable within cells under physiological conditions but is often reduced when cells undergo cell death. For this, a reduced formazan formation shows a reduction of dehydrogenase activity, which can indicate cell death.

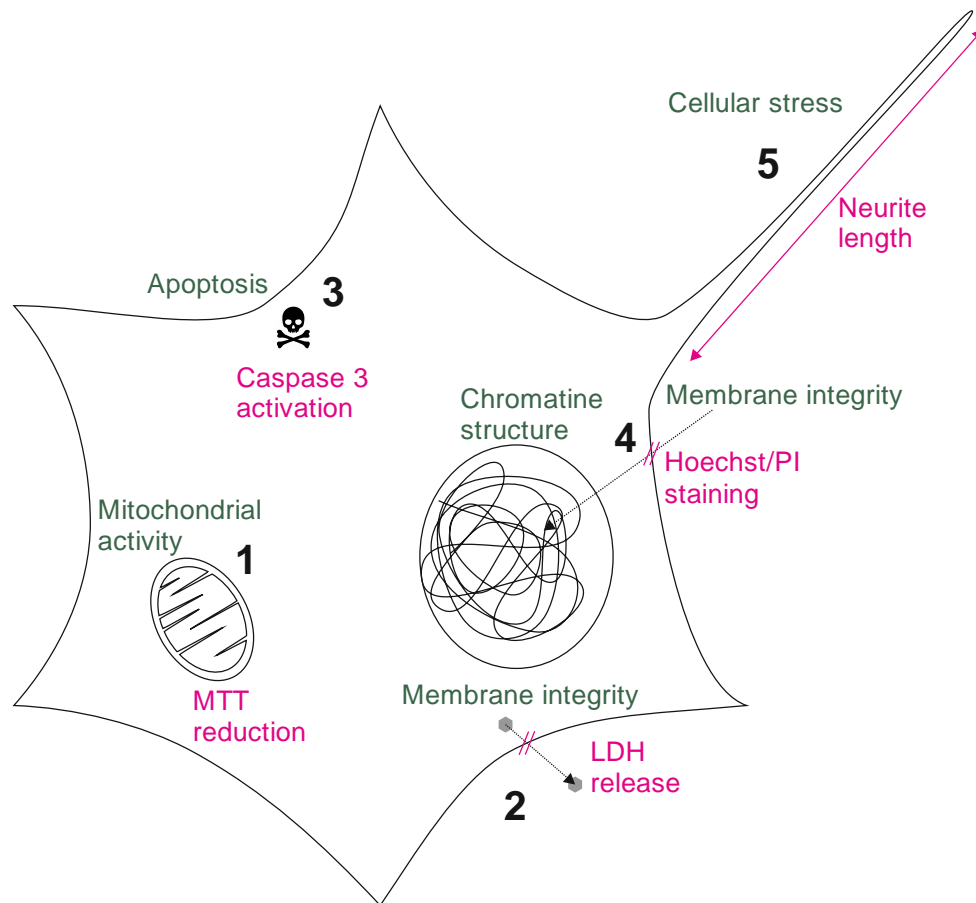


Figure 32: Cell response assays.

The response of cells to $A\beta$ exposition was tested by (1) MTT assay, (2) LDH assay, (3) caspase 3 assay, (4) Hoechst/PI staining, and (5) neurite length measurements.

The LDH assay measures the concentration of extracellular Lactate dehydrogenase (LDH). LDH a cytosolic protein, which is not membrane permeable and not secreted under physiological conditions. Therefore, extracellular LDH indicates a disintegration of the cell membrane barrier, which can also be an indicator for cell death.

Caspase 3 is a cysteine-aspartic acid protease expressed as an enzymatically inactive proenzyme. Proteolytic activation of Caspase 3 is a key step in the apoptosis activation cascade. Therefore, a detection of active Caspase 3 by immunocytochemistry is a measure for apoptotic cell death.

Hoechst/PI staining tests the integrity of the cell membrane. Propidium iodide (PI) is a dye, which is not membrane permeable can only be found intracellularly when the cell membrane integrity is impaired as is the case when cells undergo cell death. Hoechst dyes are bis-benzimidides based DNA staining reagents, which are membrane permeable and can enter the cell nucleus. They show different staining properties depending on the chromatin structure. Therefore, they stain condensed chromatin that can be an indicator for apoptosis more than the chromatin of viable cells. The combination of both dyes, Hoechst and PI, can give information of the cell viability.

Extended neurites are a hallmark of functional neurons. Cellular stress or cell death results in a shortening or even disintegration. Therefore, measurements of neurite length can be an indicator for neuronal damage.

4 Research questions and motivation

The three-dimensional structure of a protein is determined by the sequence of its amino acids and the physicochemical characteristics of the amino acid residues. However, the folding process can be error-prone and protein misfolding is a curtail factor involved in many diseases. An important risk factor of misfolding are intermolecular forces that can interfere with the usually dominating intramolecular forces and lead to the formation of protein aggregates.⁴⁶ A prevalent pathway of such an aggregation is the formation of amyloid fibrils. This fibril formation process is characterized by the assembly of a large number of equal proteins to form a characteristic structure composed of stacked, extended β -sheets, which is called a cross- β structure.³⁵ Although extensive research has been attributed to the process of fibril formation, many questions remained open, especially concerning the role of specific intra- and intermolecular interactions during structure formation. As fibril formation is a generic process for probably all polypeptides, a better understanding of the underlying mechanisms might give insights into the general structure formation processes beyond protein misfolding.

A β , the hallmark protein of Alzheimer's disease, is a well-established model peptide for fibril formation. For this peptide, the hydrophobic contact between phenylalanine 19 (F19) and leucine 34 (L34) is of high importance. It is well accepted that this contact marks an early and conserved event in the folding process.⁶⁷ However, in previous mutation studies of the F19-L34 contact it could be shown that the cross- β structure is highly stable regarding point mutations.⁸⁶ F19 was substituted with amino acids testing structural flexibility, hydrogen bond formation, and the influence of charged amino acids. All mutants showed that the cross- β structure remains conserved. Only local rearrangements and differences in the packing density of amino acid residues within the constraints of the robust intermolecular hydrogen bond network of the peptide backbones were observed. Furthermore, although the kinetics of the fibril formation process turned out to be highly sensitive not only to mutations but especially to the solvent environment, mainly the folding intermediates were influenced rather than the mature structure. The largest difference between the wildtype and the mutants was revealed in the cellular response investigated by 3-(4,5-dimethylthiazol-2-yl)-2,5-diphenyltetrazolium bromide (MTT) assay, which tests the activity of mitochondrial dehydrogenase. These experiments show that the mitochondrial activity was exclusively impaired by the wildtype whereas all mutants tested in this study were inactive regardless of the nature of the mutation.

The superior aim of this work is to characterize the principle physicochemical characteristics and interactions, which govern amyloid fibril formation (see Figure 33). For that, local changes on the primary structure by amino acid substitution were introduced. In this context, the focus was on the F19-L34 contact supplemented by investigations at positions S8 and S26. This strategy allowed for addressing the question which of the physicochemical interactions govern the amylogenic folding pathways and the cross- β structure formation and how they are influenced by local perturbations or constraints. The characterization of the fundamental forces acting in this process will give a better understanding of the self-organization of a polypeptide during folding and secondary structure formation. Furthermore, we ask the question how these mechanisms translate to protein function and biological activity. In the following, the central questions of this dissertation are specified:

What are the physicochemical interactions, which govern the amylo-genic folding pathway and the cross- β structure formation?

How are they influenced by local perturbations and constraints in the primary structure?

How do they affect the self-organization of the polypeptide chain?

How do these mechanisms translate to protein function and activity?

In order to contribute answers to these questions the work was divided into three working packages. (1) First, investigations on the L34 position of the F19-L34 contact were performed as for this position no systematic mutational investigations, analogous to the study on F19, were available from literature. A conservative mutation strategy was used to test the specificity of the interaction between F19 and L34 and the sensitivity of its biological activity in MTT cell viability assays. Whereas the global morphology and the cross- β structure were expected to be stable in any case, independent of the nature of the mutation, the local structure and dynamics are known to be more sensitive and might react even to minor constraints. First, leucine was substituted by one of the other members of the branched chain amino acids: the isomer isoleucine, where the position of one methyl group is shifted, and valine, which is one methylene group shorter. The isoleucine was supposed to nearly exclusively change the shape of the amino acid and conserve all other properties. The valine has a different length and volume and therefore was supposed to mainly change the contributions of van der Waals forces in the contact. Secondly, the leucine was replaced by its non-proteinogenic stereoisomer *D*-leucine, which was supposed to exclusively change the steric properties of the amino acid. Summarizing, this part of the work addresses the following questions:

How important are the steric features of the amino acid at position L34?

What effects are related to a change of the van der Waals volume or side chain length?

How does the L34 position contribute to the F19-L34 contact?

(2) In the second part, the focus was shifted back to the F19 position. Substitutions with non-proteinogenic amino acids were introduced, which caused rather conservative changes of the local properties of this position. This was analogous to the L34 mutation study, which showed that already minor modifications at the F19-L34 contact cause clear effects. This allowed for a more specific characterization of the influence of the ring system properties, which were previously shown to be important for the fibril formation pathway.⁸⁶ Furthermore, it was investigated how sensitive the impact of these modification is on the biological activity of A β . The two most closely related canonical amino acids of phenylalanine, tyrosine and tryptophane, were already investigated. While being highly similar to the wildtype in terms of structure and kinetics, both caused a complete loss of function in the MTT cell viability assay. Therefore, non-proteinogenic amino acids, which are more similar to phenylalanine than tyrosine and tryptophane, were chosen. The first amino acids of this set are phenylglycine (Phg) and the homophenylalanine (S)-2-amino-4-phenyl-butyric acid (hPhe), which lack one methylene group or have an additional one, respectively. These modifications change the amino acid length and volume and therefore the contribution of van der Waals interactions. Additionally, the benzene ring was replaced, on the one hand by a saturated cyclohexane group in case of

cyclohexylalanine (Cha) resulting in the loss of π -aromaticity but increasing the 3D steric demand, and on the other hand by a naphthalene in case of (1-naphtyl)-alanine (Nal), increasing the 2D steric demand but maintaining the aromaticity. Both change the π -ring system of the amino acid. In case of (1-naphtyl)-alanine it is extended and in cyclohexylalanine it is replaced by a saturated ring. Furthermore, the (1-naphtyl)-alanine again changes the volume of the amino acid and the van der Waals interactions. Furthermore, the cyclohexylalanine exchanges the planar ring system with a ring system, which shows different conformers. Summarizing, this second part of the work addresses the following questions:

How important is the π -ring system and the planarity of the residue?

What effects are caused by a change of the van der Waals volume or side chain length?

How does the L34 position contribute to the contact?

(3) In working package three, the influence of the introduction of β -methylamino-L-alanine (BMAA) at the positions F19, S8, and S26 were compared to WT A β . Microbial BMAA is a non-canonical amino acid that is of interest, because, as a neurotoxin, it is speculated to be a risk factor for neurodegenerative diseases. One of the hypothetical pathologic pathways is the misincorporation of this amino acid probably in place of serins.¹¹⁹ As it is shown to be accepted by the serine t-RNA synthetase, it shares biologically important properties of serine and might be misincorporated into proteins during translation. In this regard, a serine-BMAA substitution can be evaluated as a moderate modification. We consecutively substituted S8 and S26 with BMAA to investigate potential effects of this mutations on structure and biological activity of A β and compared these mutants to a F19BMAA mutation and to the wildtype. Additionally, we compared the F19BMAA substitution with the other F19 mutants as mutational effects at this position are well described.⁸⁶ For these mutants a broad set of cell assays was performed to investigate the effects of the different A β variants on different cell toxicity pathways comprising mitochondrial activity, plasma membrane integrity, apoptosis, and neuronal stress. Summarizing, the third part of the work addresses the following questions:

How do substitutions of serine affect A β structure and biological activity?

Are effects on A β structure formation and biological activity caused by mutations at the F19-L34 contact comparable to substitutions at the N-terminus or the turn region?

Are different cell toxicity pathways affected differentially by A β mutations?

What effects could be expected, when BMAA is indeed misincorporated into A β in place of serine?

Is BMAA misincorporation a plausible risk factor for A β fibril formation?

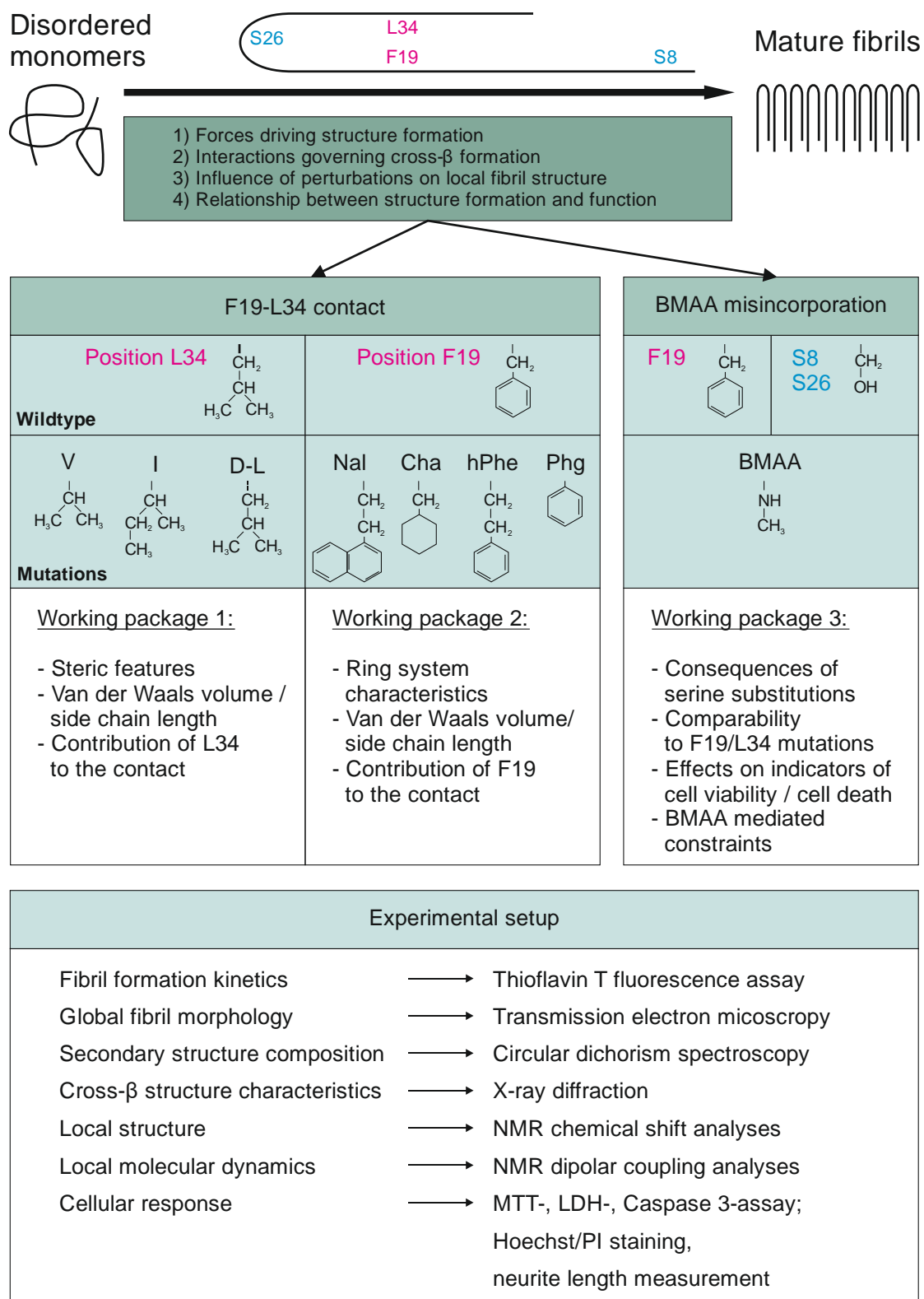


Figure 33: Research questions and experimental setup.

The aim of this work was to get a better understanding of the structure formation process during fibril formation and the individual role of different physical forces. For this, the work was divided into three packages. The first two addressed the amino acids L34 and F19 with their F19-L34 contact, which is important for the fibril formation. In the third package the influence of β-methylamino-L-alanine (BMAA) substitution on position F19, S8 or S26 was investigated. The study addressed different aspects of the fibril formation process using a set of complementary experiments (lower panel).

All questions raised above could be treated using an extensive set of biophysical and biochemical methods and their complementary interpretation. Kinetics of the fibril formation, morphology of fibrils and cellular activity were investigated to get insights into different structural and functional properties of different A β variants. The kinetics of the fibril formation process is highly sensitive to the local field and interactions with the solvent, especially concerning folding intermediates. The global fibril morphology was investigated using transmission electron microscopy (TEM). Secondary structure composition and the cross- β structure were characterized using circular dichroism (CD) and x-ray diffraction, respectively. The local structure and dynamics were investigated by NMR experiments for which uniformly isotopically labeled amino acids functioned as local reporters at selected positions. Based on this knowledge, a better understanding of the physicochemical forces driving protein folding and fibril formation as an element of misfolding can be achieved.

In addition to structural and physicochemical properties, cellular activity and potential pathological consequences of the introduced modifications were also addressed. As it is still unknown which cellular pathways are responsible for cellular A β activity, only selected mechanisms were tested. For all mutants MTT assays were performed investigating their influence on mitochondrial activity. For selected mutants additional assays were performed: (1) lactate dehydrogenase (LDH) assays to test the integrity of the plasma membrane, (2) Hoechst/PI staining alternative test for plasma membrane integrity and status of the cellular chromatin, (3) caspase 3 activity assays to detect a possible apoptosis pathway, and (4) measurements of the neurite length, which can be an indicator for neuronal damage.

Of special interest was the fact, that in previous studies all investigated mutants at the F19-L34 contact showed distinct biological activities compared to the wildtype.⁸⁶ With the mutations selected for this work, it should be possible to investigate how sensitive this effect is to minor alterations, and if any effect is attributed to the F19-L34 contact, which response mechanisms play a distinct role specific to the respective modifications.

5 Articles

5.1 Amyloid β (1-40) Toxicity Depends on the Molecular Contact between Phenylalanine 19 and Leucine 34⁹⁹

Attestation of authors contribution

Journal: ACS CHEMICAL NEUROSCIENCE

Authors: Korn, A., McLennan, S., Adler, J., Krueger, M., Surendran, D., Maiti, S., & Huster, D.

Contributions Korn, Alexander: Fibril preparation, NMR investigations, fibrillation kinetics assays, X-ray diffraction studies, CD-spectroscopy experiments, data analyses, writing of the publication

Contributions McLennan, Steffane: Fibril preparation, NMR investigations, fibrillation kinetics assays, data analyses

Contributions Adler, Juliane: Fibril preparation, NMR investigations, fibrillation kinetics assays, X-ray diffraction studies, data analyses

Contributions Krueger, Martin: TEM imaging

Contributions Surendran, Dayana: Cell culture, biological activity assays, data analyses, writing of the publication

Contributions Maiti, Sudipta: Conception, writing of the publication

Contributions Huster, Daniel: Project idea, conception, writing of the publication

Amyloid β (1–40) Toxicity Depends on the Molecular Contact between Phenylalanine 19 and Leucine 34

Alexander Korn,[†] Steffane McLennan,[†] Juliane Adler,[†] Martin Krueger,[‡] Dayana Surendran,[§] Sudipta Maiti,[§] and Daniel Huster^{*,†,§}

[†]Institute for Medical Physics and Biophysics, Leipzig University, Härtelstr. 16-18, D-04107 Leipzig, Germany

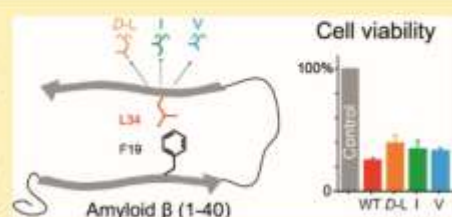
[‡]Institute of Anatomy, Leipzig University, Liebigstr. 13, D-04103 Leipzig, Germany

[§]Department of Chemical Sciences, Tata Institute of Fundamental Research, Homi Bhabha Road, Colaba, Mumbai 400 005, India

Supporting Information

ABSTRACT: The formation of the hydrophobic contact between phenylalanine 19 (F19) and leucine 34 (L34) of amyloid β (1–40) ($A\beta$ (1–40)) is known to be an important step in the fibrillation of $A\beta$ (1–40) peptides. Mutations of this putatively early molecular contact were shown to strongly influence the toxicity of $A\beta$ (1–40) (Das et al. (2015) ACS Chem. Neurosci. 6, 1290–1295). Any mutation of residue F19 completely abolished the toxicity of $A\beta$ (1–40), suggesting that a proper F19–L34 contact is crucial also for the formation of transient oligomers. In this work, we investigate a series of isomeric substitutions of L34, namely, D-leucine, isoleucine, and valine, to study further details of this molecular contact. These replacements represent very minor alterations in the $A\beta$ (1–40) structure posing the question how these alterations challenge the fibrillation kinetics, structure, dynamics, and toxicity of the $A\beta$ (1–40) aggregates. Our work involves kinetic studies using thioflavin T, transmission electron microscopy, X-ray diffraction for the analysis of the fibril morphology, and nuclear magnetic resonance experiments for local structure and molecular dynamics investigations. Combined with cell toxicity assays of the mutated $A\beta$ (1–40) peptides, the physicochemical and biological importance of the early folding contact between F19 and L34 in $A\beta$ (1–40) is underlined. This implies that the F19–L34 contact influences a broad range of different processes including the initiation of fibrillation, oligomer stability, fibril elongation, local fibril structure, and dynamics and cellular toxicity. These processes do not only cover a broad range of diverse mechanisms, but also proved to be highly sensitive to minor modulations of this crucial contact. Furthermore, our work shows that the contact is not simply mediated by general hydrophobic interactions, but also depends on stereospecific mechanisms.

KEYWORDS: Amyloid fibrils, hydrophobic contact, fibril structure, fibril dynamics, fibril morphology, mutation



INTRODUCTION

Correct three-dimensional folding is essential to ensure protein functionality. During protein evolution, structural integrity proved to be far more crucial than the amino acid sequence. In many protein families, less than 5% of the sequence but over 50% of the structure is conserved.^{1,2} Therefore, protein folding is a pivotal and highly regulated process. Even though protein misfolding regularly occurs, in most cases cells are able to refold or degrade misfolded proteins. Failure of this process can lead to severe diseases like Alzheimer's disease, cerebral amyloid angiopathy, diabetes, and others.³ One distinct misfolding pathway for proteins is that of amyloid fibrillation.

Amyloid formation is a ubiquitously occurring process undergone by a large variety of proteins with distinct amino acid sequences. Under specific conditions, all these different proteins tend to form the energetically favorable, highly stable cross- β structure. This structure is composed of two β -strands lying on top of each other. The stability can be attributed to intermolecular backbone hydrogen bond formation within the β -sheets and intramolecular hydrophobic contacts between the

side chains of the amino acid residues in the opposing β -strands.^{3,4}

A commonly used model to study fibrillation and fibril structure is the amyloid β peptide ($A\beta$). It is a peptide with typically 40 or 42 amino acids that comprises four domains: a flexible N-terminus, the hydrophobic core region, a turn region, and the hydrophobic C-terminus.^{5–7} $A\beta$ monomers are intrinsically disordered and do not form any stable secondary structure.^{8,9} $A\beta$ fibrillation is a multistep process initiated by monomer interaction and oligomerization.¹⁰ $A\beta$ oligomers are very heterogeneous and different oligomer sizes and structures have been identified.¹¹ One general feature of many $A\beta$ oligomers and protofibrils is their predominant β -sheet structure.^{12–15} At a certain, still not well characterized point, many oligomers can act as fibrillation seeds, which induce rapid linear accretion of further monomers, which results in the formation of first protofibrils and finally mature fibrils that

Received: September 15, 2017

Accepted: December 12, 2017

Published: December 12, 2017

show the characteristic cross- β structure.^{16,17} For $A\beta$, this process is still not fully understood, but several characteristic intermediate steps could be identified.^{12,18–20}

One such step is the formation of β -sheet structure. Early forming oligomers show antiparallel β -sheets.^{5–7} By contrast, the β -sheets in mature fibrils have a parallel orientation in most $A\beta$ variants. Another important step during fibrillation of $A\beta$ is the formation of a salt bridge between the amino acid residues D23 and K28. This salt bridge stabilizes the turn linking the hydrophobic core region and the hydrophobic N-terminus that builds the cross- β structure.^{21,22} Within this structure, another important interaction is found: the hydrophobic contact between phenylalanine 19 (F19) and leucine 34 (L34).

The F19–L34 contact is formed at an early stage of fibrillation and marks the first interaction between the two hydrophobic domains which later build the cross- β structure.^{7,20,23,24} This contact was found in different $A\beta(1–40)$ preparations and various oligomeric structures.^{7,20,23,24} Therefore, it seems to be a ubiquitous feature in the otherwise versatile amyloid formation process. Perturbation of this contact has severe effects on the fibrillation and the characteristics of oligomers and fibrils. Adler and co-workers investigated different constraints of the F19–L34 contact by mutational studies.^{25,24} The chosen mutants allowed to address the question as to how a change of conformational flexibility, introduction of fixed charges inside the cross- β structure, altered hydrogen bonding, or an exchange of the hydrophobic contact by a salt bridge would influence fibril structure and the kinetics of fibrillation. Whereas the general fibril morphology and the cross- β structure were found to be remarkably robust against any of these introduced perturbations, local structure and dynamics were altered in many of the mutant peptide variants. Also, the fibrillation kinetics were different for nearly all mutants up to the point where no efficient fibril formation could be observed for one $A\beta(1–40)$ variant. In spite of the robustness of the $A\beta(1–40)$ structure against most of these introduced perturbations, a striking feature was observed when looking at the toxicity of these $A\beta(1–40)$ variants to primary rat neurons.²⁶ Although the mutated $A\beta(1–40)$ preparations had a very similar overall morphology compared to the wildtype $A\beta(1–40)$, all mutations nearly completely prevented interaction with lipid bilayers and the $A\beta(1–40)$ toxicity was completely abolished. This provokes the question as to how sensitive alterations of the correct hydrophobic contact between L34 and F19 are with regard to the pathobiology of $A\beta(1–40)$. To investigate this point further, we set out to explore what minimal structural alteration of the F19–L34 contact would be possible that both retains most structural and dynamic features of $A\beta(1–40)$ fibrils and would also exhibit the full toxicity of the $A\beta(1–40)$ aggregates.

To address these questions, a small library of mutated $A\beta(1–40)$ peptides was created. We intended to alter the hydrophobic contact between F19 and L34 as little as possible by introducing mutations to structurally very similar amino acids. The amino acids structurally most similar to phenylalanine are tyrosine and tryptophan. Both mutations had been probed in our previous work and yielded fibrils with very similar structural features,²⁴ but no toxicity was observed for these variants.²⁶ In the current study, three mutations at position L34 were studied that were structurally very similar to leucine. These comprise the *D*-isomer of leucine $A\beta(1–40)$ in mutant L34*D*-L, already previously introduced,²⁷ and two new $A\beta(1–40)$ mutants, where L34 is replaced by isoleucine

(L34I) or valine (L34V). All mutated residues are hydrophobic and have a branched side chain. They feature very similar van der Waals volumes and hydrophobicity.^{28,29} The isoleucine in the L34I mutant is the isomer of the wildtype leucine, where only one methyl group is shifted from the γ to the β position. The *D*-L is the chiral counterpart of the proteinogenic (*L*-) leucine and differs only in the stereochemic center at *C* α . The β -branched chain amino acid valine is also hydrophobic and one methylene group shorter than leucine. Clinically interesting, the L34V mutation is known to be associated with cerebral amyloid angiopathy, a disease where $A\beta$ fibrils form deposits in the wall of blood vessels in the central nervous system which can cause brain bleeding.^{30,31}

To compare the findings of this work to the results of the previous library of $A\beta(1–40)$ peptides, we performed fibrillation kinetics measurements, X-ray diffraction, NMR chemical shift, and NMR order parameter studies to confirm that these very mild mutations only very insignificantly alter the wildtype amyloid fibril structure. The interesting question we then ask is the impact of these mild mutations on cell toxicity, using a neuronal cell line. If cell toxicity of these peptides was still influenced, it would further demonstrate the biological importance of the specific contact between F19 and L34 in $A\beta(1–40)$ pathology.

RESULTS

CD Spectroscopy. For an initial characterization of the secondary structure of all samples, we used UV circular dichroism (CD) spectroscopy of all $A\beta$ peptide variants before and after aggregation, i.e., for a fresh preparation and a peptide preparation incubated for 7 days, undergoing gentle shaking. CD spectra are reported in Figure 1. All freshly dissolved peptides showed a most prominent negative minimum at ~ 198 nm, characteristic of disordered peptides. After incubation and shaking for 7 days, the CD spectra changed drastically, now exhibiting strong negative peaks at 217–219 nm indicating the structural transition from random coil to extended β -sheet structure.

Fibrillation Kinetics. In a basic model, amyloid fibrillation can be described in a three step process consisting of a lag phase, a fibrillation phase, and a plateau phase.³² During the lag phase, intrinsically disordered monomers form heterogeneous oligomers. At a specific time point, which marks the ending of the lag phase and the beginning of the fibrillation phase, seeds are formed. These low molecular weight species initiate rapid growth of fibrils, which show the characteristic cross- β structure. In the final plateau phase, equilibrium between fibrillar and soluble amyloid is reached. The duration of the lag and fibrillation phase strongly depends on intrinsic properties of the amyloid peptide.³³

To investigate fibrillation kinetics, we used ThT fluorescence measurements. ThT is a dye that shows bright fluorescence intensity at 482 nm after binding to β -sheet structures, which are the predominant secondary structural motifs in amyloid fibrils.^{34,35} The intensity plots of all investigated variants are reported in Figure 2 and showed typical sigmoidal curves.³³ The wildtype $A\beta(1–40)$ peptide showed the longest lag phase and shortest fibrillation phase with 4.4 ± 0.2 and 1.2 ± 0.3 h, respectively. The lag phases of the mutants were relatively similar comprising 2.3 ± 0.6 h for L34*D*-L, 2.4 ± 0.1 h for L34I, and 2.5 ± 0.5 h for L34V. The fibrillation time of the L34I and L34*D*-L mutants were 2.2 ± 0.2 and 2.2 ± 0.8 h, respectively, which is nearly twice as long as for the wildtype $A\beta(1–40)$

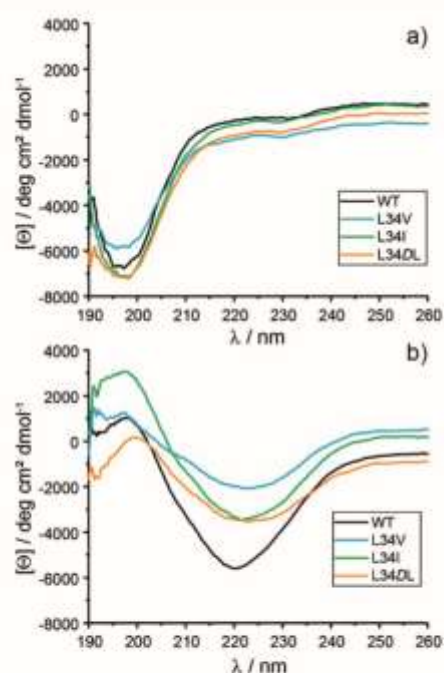


Figure 1. UV-CD spectra of $A\beta(1-40)$ wildtype and the respective mutants before (a) and after aggregation (b). CD spectra of freshly dissolved $A\beta$ peptides are characterized by random coil secondary structure (a), while $A\beta$ peptides, incubated and gently shaken for 7 days, exhibited clear characteristics of an extended β -sheet secondary structure (b).

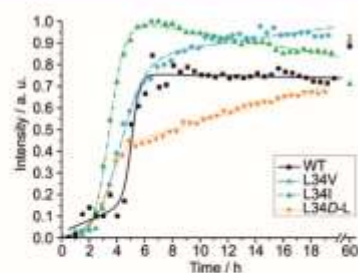


Figure 2. Fibrillation kinetics of $A\beta(1-40)$ wildtype and mutant $A\beta(1-40)$ peptides determined by fluorescence of ThT bound to fibrils.

peptide. The L34V mutation shows the longest fibrillation time (3.6 ± 0.6 h). All experimental errors were determined from data obtained in triplicate. Within the set of experiments, carried out in parallel, ThT fibrillation curves were well reproducible.

General Fibril Morphology. To investigate the global fibril structure, X-ray diffraction (XRD) images and TEM images were recorded. The TEM images shown in Figure 3, showed that all variants formed well-structured fibrils. Wildtype, L34I, and L34D-L fibrils were characterized by nearly identical morphology. Differences in the intensity are staining artifacts caused by sample preparation and from differences of the thickness of the underlying carbon film (Formvar film). The $A\beta(1-40)$ L34V fibrils were significantly shorter, which could be caused by differences in fibril growth or due to fibril fragmentation by shearing forces during

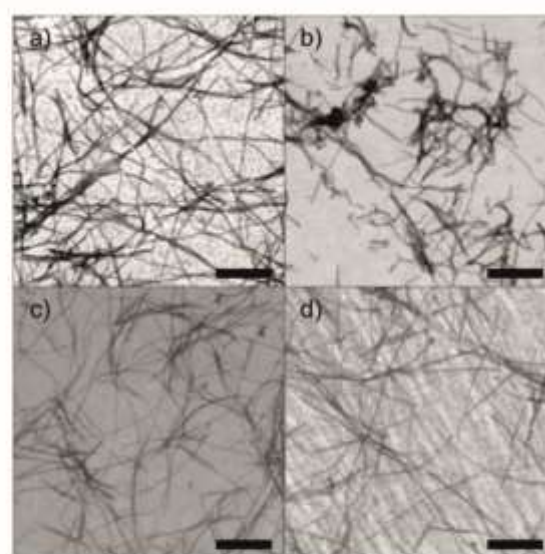


Figure 3. TEM images of the $A\beta(1-40)$ variants: (a) wildtype; (b) L34V; (c) L34I; (d) L34D-L; scale bars represents 400 nm.

pipetting when the samples were prepared. All fibrils showed partial twisting and were sometimes attached to each other. From the TEM images, diameters of the different fibrils were determined. The thinnest fibrils were formed from wildtype $A\beta(1-40)$ peptides (13.8 ± 2.5 nm) followed by L34D-L (14.5 ± 2.5 nm), L34V (14.7 ± 2.7 nm), and L34I fibrils (14.9 ± 3.1 nm). Experimental errors represent the standard deviations ($n = 50$). Values for wildtype and the L34D-L variant are slightly larger than reported before.²⁷

A more detailed view of the global fibril structure was provided from the X-ray diffraction data. The universal amyloid cross- β structure is formed by two stacked β -sheets that show two distinct reflections in XRD spectra. The first refers to the intrasheet distance that is defined by the hydrogen bond length between the β -strands of 4.7 Å. The second reflection corresponds to the intersheet distance that is defined by the interacting amino acid residues inside the fibril. This reflection is typically less well-defined at approximately 10–11 Å.¹⁶ XRD diffraction data for the four peptide variants are shown in Figure 4. The more defined reflection corresponding

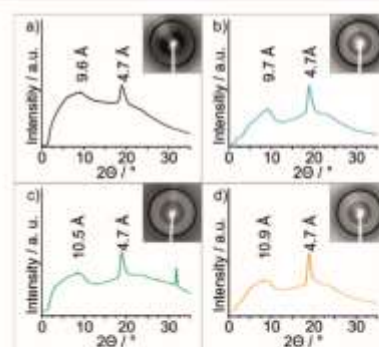


Figure 4. X-ray diffraction pattern of the $A\beta(1-40)$ variants: (a) wildtype; (b) L34V; (c) L34I; (d) L34D-L; insets show corresponding diffraction images.

to the intrasheet distance was 4.7 Å and identical for all variants. The meridian reflection corresponding to the intersheet distance was less well-defined and indicated by a broader peak in the XRD spectra. Also, this peak corresponded to similar distances (wildtype: 9.6 Å; L34D-L: 10.9 Å; L34V: 9.7 Å; L34I: 10.5 Å), which indicates slight differences in the packing of the opposing β -strands.

Local A β (1–40) Fibril Structure. Local fibril structure was investigated in specific positions using 1D and 2D ^{13}C MAS NMR spectroscopy. Typical ^{13}C solid-state NMR spectra are shown in Figures S2 and S3. Uniformly $^{13}\text{C}/^{15}\text{N}$ -labeled amino acids were introduced at certain positions of the peptides, mainly in the central cross- β -core in the vicinity of the F19–L34 contact. From the NMR spectra, isotropic ^{13}C NMR chemical shifts were extracted. These chemical shifts are influenced by the dihedral angles of the peptide backbones providing a measure of local secondary structure.³⁷ Especially the $C\alpha$, $C\beta$, and CO chemical shifts contain secondary structure information. Particularly useful are $C\alpha$ – $C\beta$ chemical shift differences as they are independent of external referencing and can readily be used to identify local secondary structure elements in proteins and peptides. An exception is the amino acid glycine which lacks a $C\beta$ atom. In this case, the ^{13}CO chemical shift is more informative.³⁸

A summary of the chemical shift data obtained for all A β (1–40) fibrils investigated in this study is displayed in Figure 5. According to the structural models of A β (1–40) fibrils, all labeled amino acids except G25 should be localized in the central cross- β structure. Accordingly, we detected very typical β -sheet-like chemical shifts for all labeled positions. However, although the general secondary structure indicated β -sheet character, some small alterations were detected.

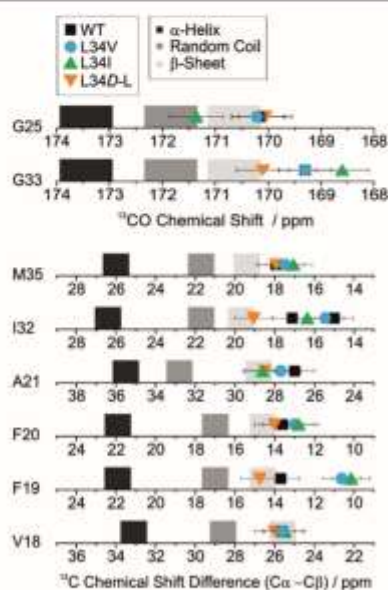


Figure 5. ^{13}C NMR chemical shift data of the A β (1–40) variants and corresponding secondary structure information as derived from the NMR chemical shifts: gray boxes represent reference values for α -helix, random coil, and β -sheet secondary structure; symbols represent measured values for V18, F19, F20, A21, I32, and M35 as $^{13}\text{C}\alpha$ – $^{13}\text{C}\beta$ chemical shift differences. For G33 and G25, ^{13}CO chemical shifts are reported as glycine is missing a $^{13}\text{C}\beta$ carbon.

For instance, at position I32 in the wildtype A β (1–40) fibrils, two cross peaks with different chemical shifts were detected indicating two distinct A β (1–40) polymorphs. The major polymorph has a contribution of 68% ($\delta C\alpha = 57.5$ ppm) and the minor polymorph a contribution of 32% ($\delta C\alpha = 55.5$ ppm). Polymorphism is not uncommon in A β (1–40) fibrils.^{39,40} However, all investigated mutants were lacking the polymorphism at this position. Furthermore, the L34D-L variant showed a significant alteration compared to the L34I, L34V, and at least one of the two wildtype A β (1–40) polymorphs. More striking were the chemical shift differences at position F19, directly involved in the hydrophobic contact to L34.^{7,23,24} In this case, only the L34D-L variant resembled the wildtype. Both the L34I and the L34V variant showed a clear upfield shift.

The only labeled amino acid outside the cross- β core was G25. This amino acid is positioned in the turn region between the two β -sheets. Therefore, it is expected to show local structure characteristics of random coil or even α -helix.³⁸ This could only be shown for the L34I variant. The wildtype as well as all other variants show a nearly identical local structure with β -sheet character.

Overall, it can be summarized that the local secondary structure in the backbone of the A β (1–40) fibrils is stable and mainly undisturbed by the introduced mutations. Only at single positions, namely, G25, I32, and predominantly F19, smaller alterations could be detected.

Molecular Dynamics of Mutated A β (1–40) Fibrils. It was previously shown that perturbations of the local A β (1–40) fibril structure introduced by mutation of the F19–L34 contact can influence the local packing inside the fibril, which leads to an alteration of the molecular dynamics and in particular the motional amplitudes of the residues in the vicinity of the mutated site.⁵⁴ Alterations of the molecular dynamics on a single residue level can be investigated by determining motional averaging of the dipolar coupling of ^1H – ^{13}C bond vectors.⁴¹ This was done by DIPSHIFT separated local field experiments, allowing to determine order parameters expressing motional amplitudes with correlation times shorter than about 40 μs .⁴² Typical dipolar dephasing curves from which the motionally averaged dipolar couplings and order parameters were determined are shown in Figure S4.

The cross- β structure of amyloid fibrils is well-defined and stabilized by numerous hydrogen bonds.^{3,4} Therefore, the peptide backbone is highly confined, leading to high order parameters for the $C\alpha$ – $\text{H}\alpha$ bond vectors. $C\alpha$ – $\text{H}\alpha$ order parameters of wildtype and mutated A β (1–40) variants are shown in Figure 6. Most backbone sites showed high order parameters of >0.9 indicative of a very rigid structure. Notable exceptions are F19 and F20 directly opposing the mutated site. In particular, in the L34V variant, the $C\alpha$ – $\text{H}\alpha$ order parameter dropped rather drastically to ~ 0.8 . In contrast, G33 showed a significantly increased order parameter in all three mutated peptides compared to wildtype A β (1–40) fibrils. In the side chain, M35 and F19 showed the most pronounced differences. In the L34D-L variant, $C\beta$ and $C\gamma$ order parameters of M35 significantly decrease, while these bond vectors are more ordered in the other two variants compared to the wildtype. Strikingly, the F19 ring directly opposing the mutated site showed a tremendous increase in the motional amplitude indicated by a strong decrease in order parameters for all mutated peptides.

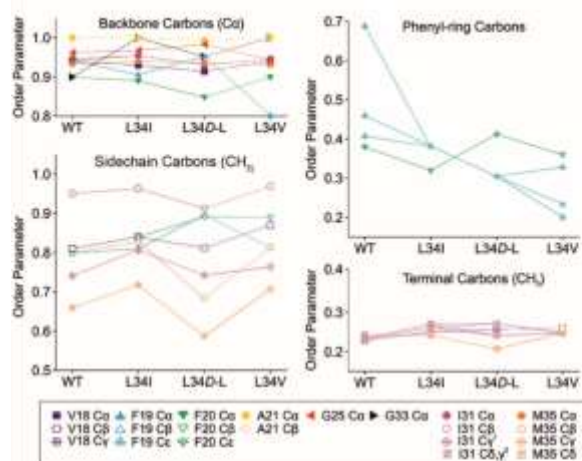


Figure 6. Molecular dynamics of the $A\beta(1-40)$ variants represented by DIPSHIFT derived order parameters for all labeled ^{13}C atoms in wildtype and the mutated $A\beta(1-40)$ peptides

Influence of $A\beta(1-40)$ Variants on Cell Toxicity. To test the toxicity of the $A\beta(1-40)$ mutants, standard MTT experiments were performed using the neuronal RN46A cell line. Cells were incubated with wildtype and mutated $A\beta(1-40)$ peptides, freshly prepared by dissolving lyophilized peptide powder. Thus, $A\beta(1-40)$ peptides were added as monomers/small oligomers. As a control, vehicle treated cells were used. As already known, wildtype $A\beta(1-40)$ was highly toxic and reduced cell viability to $25.5 \pm 1.8\%$ compared to control. Also, the mutants L34D-L, L34I and L34V proved to be toxic, but to a significantly lesser extent. Cells treated with $A\beta(1-40)$ L34V showed the lowest viability ($33.0 \pm 2.2\%$), followed by the L34I ($34.4 \pm 7.2\%$) and L34D-L mutant ($39.4 \pm 6.2\%$) as shown in Figure 7. Qualitatively very similar results were observed using Hoechst/PI staining of RN46A cells treated with the respective peptides. Hoechst/PI staining revealed highest toxicity of wildtype $A\beta(1-40)$ ($52.3 \pm 3.4\%$ cell viability), followed by the L34D-L mutant ($77.9 \pm 5.9\%$), L34I ($86.9 \pm 1.5\%$), and L34V ($87.6 \pm 3.0\%$). While the differences between the individual mutated peptide variants were not

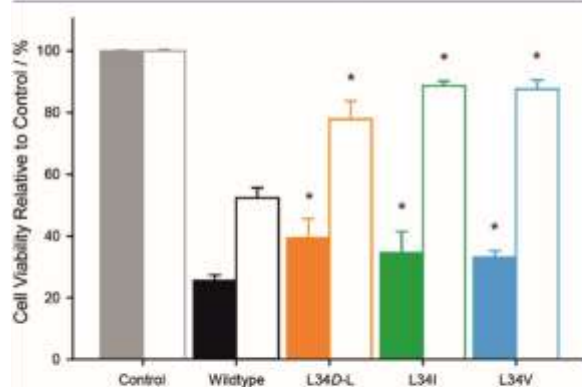


Figure 7. MTT (filled bars) and Hoechst/PI (empty bars) cytotoxicity assay of RN46A cells treated with wildtype and mutated $A\beta(1-40)$ peptides. * $p < 0.05$ between wild type $A\beta(1-40)$ and each mutated variant. Error bars represent the standard deviation of three independent experiments with 6 wells each.

statistically significant, the difference between wildtype $A\beta(1-40)$ and the mutated variants was significant ($p < 0.05$).

DISCUSSION

The hydrophobic contact between amino acids F19 and L34 has been shown to be of fundamental importance for the toxicity of fibrillar $A\beta(1-40)$ aggregates.²⁶ While mutations at F19 caused only minor alterations in fibril morphology,²⁴ all mutations completely abolished the toxicity of the $A\beta(1-40)$ peptides,²⁶ suggesting a significant importance of the unaltered F19–L34 contact, most likely on the transient oligomer level. The lacking toxicity of all F19 mutations provokes the question as to what is the minimal tolerated chemical modification of the F19–L34 contact that restores full or at least partial toxicity. On the F19 site, the side chains that are also aromatic, but more polar are tyrosine and tryptophan. Both variants of $A\beta(1-40)$ carrying either tryptophan or tyrosine in position 19 were studied before and showed no toxicity.²⁶ Here, we turned our attention to residue L34 and investigated three mutants with residues in position 34 that are structurally most similar to the wildtype leucine. This was motivated by the fact that the aliphatic side chain of leucine could be less demanding than the aromatic benzene ring of phenylalanine. Having L34 exchanged for isoleucine, valine, or D-leucine introduces the most minimal structural alterations of the contact conceivable.

To first obtain insights in the early processes of the fibrillation, measurements of the fibrillation kinetics were performed providing two parameters. The first value is the lag time required for fibrillation seeds to form, which initiate rapid fibril formation. During the lag time, the predominant species are oligomers of different sizes and characteristics. Compared to the wildtype, all investigated $A\beta(1-40)$ mutants showed a shorter lag time. The F19–L34 contact is one of the first interactions described for oligomer formation.⁴³ However, it is not clear if this interaction can still be formed by other amino acids and the process of contact formation itself cannot be investigated by the performed kinetic measurements. The experiments only show the point of transition between the oligomeric and fibrillary state. Therefore, an explanation of the shortening of the lag time could be that the F19–L34 contact stabilizes a specific oligomeric structure. Stabilization of oligomeric structures can have significant consequences for toxicity and has been the focus of previous research.⁴⁴ If this stabilization was weakened by mutation, the transition to the even more stable fibrillary structure would be accelerated. All of the here investigated substitutions show minor physicochemical effects. Therefore, it is possible that for the mutants, the initial oligomer formation is only slightly delayed. The transition to the fibrillary state, however, would be accelerated, which leads to an overall shortening of the lag time. It is striking that all previously investigated mutations of the F19–L34 contact led to a clear increase in the lag time.²⁴ This indicates that the two different sets of mutations address different mechanisms. The previous variants clearly changed the physicochemical characteristics of the hydrophobic core, which led to a disturbance of fibril formation. Here, the hydrophobic character was conserved, but the minor alterations caused a shortening of the lag time indicating a reduced lifetime of the oligomeric states.

The second characteristic parameter of fibrillation kinetics is the fibrillation time. This is the time between the initiation of rapid fibril formation and the end of fibrillation, characterized by the beginning of the plateau phase. There, equilibrium

between fibrillary and nonfibrillary states is achieved. All mutants show an elongated fibrillation time. This shows that the L34 is not only important for the formation of an initial contact, but also influences fibril growth.

The next aspect that was studied in detail was fibril morphology. TEM images as well as X-ray diffraction pattern showed no significant differences between mutants and wildtype. The X-ray diffraction patterns show reflections typical of the fibril-characteristic cross- β structure. These observations resemble the results of the previously investigated series of mutants concluding that none of the investigated mutations has an effect on global fibril structure.

To get more atomistic insights into the structure of the fibrils formed by the mutated $A\beta(1-40)$ peptides, NMR experiments were performed. The determined chemical shifts provide information on the local secondary structure. All mutants showed clear β -sheet characteristics for all investigated residue positions in the cross- β region. One of the minor differences is the observation of some polymorphism, which is a common feature of many $A\beta(1-40)$ fibril preparations. However, these polymorphisms seem to be not conserved, hardly reproducible, and also influenced by experimental procedures. The most striking structural differences occurred at position F19, where the L34V and the L34I mutants induced a small chemical shift change compared to the wildtype and L34D-L. Even if the chemical shift differences show a β -sheet characteristic for all variants, the absolute values indicate a change in the local structure. It seems that the F19–L34 contact not only is mediated by unspecific hydrophobic interactions, but also exhibits a more specific mechanism. Because the L34D-L substitution does not show this difference to wildtype $A\beta(1-40)$, the specificity seems to be mediated more by atomic interactions than by steric aspects. The NMR experiments were only performed on mature fibrils; therefore, the question of how the initial contact formation and its influence on oligomers is influenced by minor mutations remains open. Nevertheless, the ability of the L34I and L34V mutations to affect the highly stable cross- β structure to such a degree underlines the sensitivity of the F19–L34 contact as an essential step in fibrillation.

Another aspect that is directly related to the local structure is molecular dynamics, here studied by means of order parameters, which provide a measure of the amplitudes of the fast segmental motions. High order parameters correspond to small motional amplitudes, and low order parameters indicate high motional amplitudes on a correlation time much faster than ~ 40 μ s. In general, the cross- β structure is well-defined and strongly stabilized by hydrophobic interactions and hydrogen bonds. Therefore, it is highly rigid, which is reflected by the high DIPSHIFT order parameters of the backbone carbons.

In the backbone, there are two important observations worth mentioning. One is the reduced mobility of G33 in all variants indicated by the higher order parameters for the $C\alpha$ site of G33. G33 is a direct neighbor of the mutated residue L34. This could indicate that the substitution and structural rearrangement inside the cross- β structure causes a constraint that restricts the motion of G33. This could come about by denser fibril packing. The second observation is that the motional amplitude of the F19 $C\alpha$ –H bond vector is increased exclusively for the L34V mutation. Apparently, the smaller side chain of valine compared to leucine provides free volume that is filled by larger amplitude motions of F19. It is striking

that the minor alteration of a hydrophobic contact has a quite substantial influence on the highly rigid and strongly stabilized backbone of the opposing β -strand. This observation is more pronounced in the ring moiety of F19. The benzene ring also shows larger motional amplitudes in all other mutated peptides indicating packing differences within the hydrophobic core of the mutated fibrils. Although the difference in the van der Waals volumes of the mutated residues valine (105 \AA^3) and isoleucine (124 \AA^3) is very similar to that of the wildtype residue leucine (124 \AA^3),²⁶ apparently the altered hydrophobic contact results in a looser packing with more free volume for phenylalanine ring motions. This is also expressed in the resolution of the ring carbons, which varies between the mutants. If the altered motions enable additional wagging of the ring, it would cause a decline of the order parameter and collapse of the three carbon signals from the ring into a single peak by signal averaging, which could explain our observations. In contrast, the side chain of F20, which is facing out of the fibrillary core in most models of $A\beta(1-40)$ fibrils remains largely uninfluenced by the mutation at position 34. Overall, the DIPSHIFT experiments show that the strongest effects of the investigated L34 substitutions are not on the neighboring amino acids but on the F19 of the opposing β -strand, underlining the importance and sensitivity of the F19–L34 interaction.

The final part of this work addresses the question of how the disturbance of the F19–L34 contact influences the cellular toxicity of $A\beta(1-40)$. The experiments performed on the L34 mutated peptides show a more differentiated picture compared to the F19 mutants.²⁶ All mutants decreased toxicity, but to a lower extent than wildtype $A\beta(1-40)$. Assuming that oligomeric species mainly mediate cell toxicity, this behavior correlates with the finding that the lag time is shortened. The fibrillation time, where oligomer concentration decreases, is accelerated in mutant $A\beta(1-40)$.

After the wildtype $A\beta(1-40)$, the highest toxicity was observed for the stereoisomer L34D-L. $A\beta(1-40)$ L34D-L showed the smallest structural deviations that are most predominant in the F19 position. Therefore, it may be assumed that the fibril structure shows characteristics that are important for oligomer toxicity. However, the difference of toxicity between the different mutants is only small and not significant and correlations between the individual structural characteristics and toxicity are highly speculative. Nevertheless, it is clear that only major disturbances of the F19–L34 contact result in complete loss of toxicity. $A\beta$ peptides with minor mutations, as probed here, remain toxic, but to a lesser degree than wildtype $A\beta(1-40)$, demonstrating the high specificity of the toxicity mediating structure.

The toxicity assays using the two different protocols were qualitatively very similar, but quantitatively rather different. The MTT assay reports lower cell viability on the average. Propidium iodide, a DNA intercalating dye that labels only the dead cells, penetrates only the cells whose membrane integrity is compromised, while the Hoechst is another DNA intercalating dye that can freely pass through intact cell membranes. PI majorly stains necrotic and late apoptotic cells where there is loss of cell membrane integrity. On the other hand, MTT is a mitochondrial enzyme-activity dependent simple colorimetric assay, but not a specific test for apoptosis. If there is a decrease in the MTT reduction product formazan, it does not necessarily mean there is cell death, but rather decrease of cell viability or metabolic activity. The assays

therefore report different aspects of cell toxicity, but within each assay it is confirmed that the mutated variants are less toxic than the wildtype $A\beta$.

Taken together, our work demonstrates that the F19–L34 contact is not only important as a first interaction step in $A\beta$ (1–40) fibrillation, but also influences oligomer stability, fibril elongation, local structure, and dynamics as well as neuronal toxicity. Some of these aspects confirm the previously reported findings of the importance of the F19–L34 contact.^{24,26,45,48} While all alterations of position F19 completely abolished $A\beta$ toxicity, here, we show that even minor alterations of the L34 also have direct impacts on the $A\beta$ toxicity, confirming the biological role of the F19–L34 contact in $A\beta$ (1–40) aggregates. Specifically, we demonstrate that the F19–L34 contact is not only mediated by a general hydrophobic interaction, but depends on a highly specific mechanism. This mechanism affects various aspects of $A\beta$ (1–40) including toxicity, and further investigations will not only lead to a deeper understanding of $A\beta$ (1–40) fibrillation and amyloid formation in general, but may also open new ways to target the problem of neurodegenerative diseases. Possibly, a small molecule that specifically interferes with the proper F19–L34 contact formation may carry high pharmacological potency.

On a final note, we would like to comment on the very recent high resolution structures of the more toxic $A\beta$ (1–42) variant.^{47–50} These structures do not show the F19–L34 contact due to a completely different fold. However, even in $A\beta$ (1–42), any mutation of residue L34 renders the peptide quite harmless.⁵¹ Furthermore, the most recent structure of the Osaka mutant $A\beta$ (1–40) Δ 22 presents the F19–L34 contact,⁵² although the overall fold differs from the wildtype structural models of $A\beta$ (1–40).⁵⁷ This supports the idea that the F19–L34 contact in $A\beta$ (1–40) is of biological importance. However, especially our understanding of the oligomeric aggregates of $A\beta$ is still incomplete; some studies have shown a F19–L34 contact in $A\beta$ oligomers,^{43,53} but others do not.^{54,55} Clearly, only high resolution structures of $A\beta$ oligomers will likely provide fundamental new insights into the toxicity of $A\beta$ peptides.

METHODS

Peptide Synthesis. $A\beta$ (1–40) wildtype with the sequence DAEFRHDSGY EVHHQKLVFF AEDVGSNKGAIIGLMVGGVV and three single mutants L34D-L (R-form enantiomer), L34I, and L34V (the mutated L34 is underlined in the peptide sequence) were synthesized using standard F-moc solid phase synthesis. For each peptide, two variants with U-¹³C/¹⁵N labeled amino acids at the following positions were produced: peptide (1) V18, F20, A21, G33; peptide (2) F19, G25, I32, M35 (highlighted in italic and bold, respectively, in the structure shown above). Peptide purity was assessed from HPLC to be higher than 98%. A typical mass spectrum of the synthesized wildtype $A\beta$ (1–40) peptide is shown in Figure S1.

$A\beta$ (1–40) Fibril Preparation. Lyophilized peptides were dissolved in alkaline phosphate buffer (25 mM sodium phosphate, 150 mM sodium chloride, 0.01% sodium azide, pH 9.5) at a concentration of 1 mg/mL. After complete dissolution, the samples were dialyzed twice using 1000 Da MWCO dialysis tubes (Zellu Trans, Roth) and 2 L of the same buffer at pH 7.4 for 2 h each. Afterward, the peptide solutions were transferred into reaction tubes and incubated in a thermoshaker for at least 14 days at 37 °C and 450 rpm. At selected time points, aliquots for transmission electron microscopy (TEM), X-ray diffraction experiments, and fluorescence measurements of the ThT kinetics were taken.

For NMR measurements, mature fibrils were centrifuged at 86 000g for 1 h at 4 °C. Pellets were lyophilized for at least 48 h using an Alpha 1-4 lyophilizer (Martin Christ Gefriertrocknungsanlagen GmbH; Osterode, Germany). Finally, pellets were rehydrated with 50% (w/w) H₂O, homogenized by ten freeze thaw cycles (freezing in liquid nitrogen and heating to 37 °C) and transferred into a 4 mm MAS rotor and sealed.

Thioflavin T (ThT) Fluorescence Measurements 96-Well Plate format. Lyophilized peptides were dissolved in phosphate buffer containing 25 μ M ThT (25 mM sodium phosphate, 150 mM sodium chloride, 0.01% sodium azide, pH 7.4) at a concentration of 1 mg/mL. A triplet of peptide solutions of a volume of 150 μ L each was transferred into a 96-well plate (Nunc) and fluorescence was measured on a Tecan Infinite M200 Microplate Reader (Tecan Group AG, Männedorf, Switzerland) using the following measurement protocol: temperature at 37 °C, excitation at 450 nm, emission at 485 nm, 5 min shaking/5 min waiting cycle, measurement every 30 min.

ThT Kinetics Data Evaluation. ThT fluorescence experiments were carried out in triplicate. Intensity data were normalized by subtraction of the minimal intensity value at the lag phase and division by the maximum intensity. Data were fitted using a sigmoidal curve

$$I = y + m_f t + \frac{y_f + m_f t}{1 + e^{-(t-t_0)/\tau}} \quad (1)$$

where I is the fluorescence intensity, t is the time, and t_0 is the time at half maximal intensity. From this, the lag time is calculated by $t_0 - 2\tau$ and fibrillation time is calculated by 4τ . The other symbols in the formula are fitting parameters.³² In eq 1, m refers to the slope of the graph during the lag time and plateau phase and τ represents a measure of the fibrillation time.

Circular Dichroism Spectroscopy. CD spectra were recorded on a Jasco 710 spectrometer using a 2 mm quartz cuvette. For sample preparation, a stock solution with a concentration of 1 mg/mL peptide in phosphate buffer (25 mM sodium phosphate, 150 mM sodium chloride, 0.01% sodium azide, pH 7.4) was prepared and used either directly for CD measurements on monomers, or for measurements of fibrils after 7 days of incubation at 37 °C and 450 rpm using a thermoshaker. For CD measurements, the stock solution was diluted to a final peptide concentration of 10 μ M with H₂O. All measurements were performed in triplicate.

Transmission Electron Microscopy (TEM). The mature fibril solution was diluted 1:20 with H₂O. Here, 2 μ L of this solution was transferred onto a Formvar film-coated copper grid. After drying, the sample was stained with 1% uranyl acetate solution. TEM images were recorded on a Zeiss SIGMA microscope equipped with a STEM detector and Atlas Software (Zeiss NTS; Oberkochen, Germany).

X-ray Diffraction Measurements. An aliquot of mature fibril solution was spun down using a table top centrifuge (using approximately 16 060g for 10 s) and washed with H₂O three times. Then 10 μ L of highly concentrated fibril solution was pipetted between two paraffin coated glass capillaries and slowly dried in a desiccator. The fibrils on the capillary were positioned in the X-ray beam of the diffractometer (Rigaku, Tokyo, Japan; X-ray source: copper rotating anode MM007 with 0.8 kW) and diffraction patterns were recorded with an exposure time of 5 min at 24 °C.

Solid-State NMR Measurements. All NMR spectra were acquired on a Bruker 600 MHz Avance III NMR spectrometer (Bruker BioSpin GmbH, Rheinstetten, Germany) operating at a resonance frequency of 600.1 MHz for ¹H, 150.9 MHz for ¹³C, and 60.8 MHz for ¹⁵N. A triple channel 3.2 mm MAS probe was used, the temperature for all experiments was set to 30 °C. The ¹H 90° pulse length was 4 μ s, and the ¹⁵N 90° pulse length was 5 μ s; ¹H-X CP contact time was 1000 μ s at a spin lock field of about 50 kHz, the relaxation delay was 2.5 s, and ¹H decoupling was applied with an rf amplitude of 65 kHz using Spinal 64 decoupling.

Two dimensional NMR spectra were acquired using single ¹³C–¹³C DARR experiments or ¹³C–¹⁵C DARR and ¹⁵N–¹³C α correlation dual acquisition experiments, where during each DARR

experiment eight or four ^{13}C – ^{15}N correlation experiments were acquired simultaneously.⁵⁶ The DARR mixing time was 50 or 500 ms and MAS frequency was set to 11 777 Hz. In the double CP ^{15}N – ^{13}C correlation experiments, the CP contact time was 1 and 4 ms for ^1H – ^{15}N and ^{13}C – ^{15}N transfer steps, respectively.

^1H – ^{13}C dipolar couplings were measured using constant time DIPSHIFT experiments.⁴² The MAS frequency was set to 5 kHz, homonuclear decoupling during dipolar evolution was achieved using the frequency switched Lee–Goldburg sequence⁵⁷ with an effective rf field of 80 kHz. Motionally averaged dipolar couplings were determined from numerical simulation of the experimental dephasing curves over one rotor period. Simulations of the DIPSHIFT time domain data $g(t)$ were performed using a program written in C++ according to $g(t) = \exp(i \int_0^t \omega(t') dt')$ with $\omega(t) = C_1 \cos(\gamma + \omega_r t) + C_2 \cos(2\gamma + 2\omega_r t)$. $C_1 = -\delta_{\text{CH}} \sqrt{2} / 2 \sin(2\beta)$ and $C_2 = 1/2 \delta_{\text{CH}} \sin^2 \beta$, with the dipolar coupling strength δ_{CH} , the MAS angular frequency ω_r , and the Euler angles β and γ for powder averaging.⁵⁸ Simulations were performed with 1° increment for the β and γ angles. Motionally averaged dipolar coupling values $\langle \delta_{\text{CH}} \rangle$ were determined from the best fit of the dephasing curve to the experimental data. Order parameters were obtained from the equation $S_{\text{CH}} = \langle \delta_{\text{CH}} \rangle / \delta_{\text{CH}}$ where δ_{CH} represents the rigid limit value for the dipolar coupling as determined experimentally from frozen amino acids.^{42,59}

3-(4,5-Dimethylthiazol-2-yl)-2,5-diphenyltetrazoliumbromide (MTT) and Hoechst/PI Assays. The MTT assay was used as a quantitative measure to determine the viability of cells treated with different A β (1–40) peptides. The assay is based on the MTT (3-(4,5-dimethylthiazol-2-yl)-2,5-diphenyltetrazolium bromide) reduction to formazan, which occurs in the mitochondria of living cells due to the activity of mitochondrial dehydrogenases. Briefly, neuronal RN46A cells were seeded into 96-well plates at a density of 1×10^4 cells/well and left for 24 h. After attachment, the cells were treated with the following: vehicle control (serum-free DMEM/F-12 alone), wild type, L340-L, L34L, and L34V A β (1–40) mutant at 100 μM for 60 h at 37 $^\circ\text{C}$. After corresponding A β (1–40) treatment, MTT solution (1 mg/mL in PBS) was added into each well and cells were incubated at 37 $^\circ\text{C}$ for 4 h. Afterward, the MTT solution was aspirated and 100 μL of acidified isopropanol was added to each well. The plate was gently shaken on an orbital shaker for 20 min to completely dissolve the formazan precipitation. Absorbance was detected at 570 nm using a microplate reader (TECAN Infinite M200, USA). Absorbance was normalized with respect to the untreated control cultures to calculate changes in cell viability. We prepared 3 replicates, i.e. three different experiments, with 6 wells each for each A β peptide.

In addition, a Hoechst/PI staining cell viability assay was also performed on RN46A cells grown on poly-L-lysine coated glass coverslips which were incubated with 100 μM each of the wildtype and the mutant peptides. The extent of cell death was assessed after 60 h using Hoechst/PI staining. In brief, the cells were treated with 0.01 mg/mL propidium iodide (PI, DNA intercalating dye that labels only the dead cells) and 0.01 mg/mL of Hoechst 33342 (DNA intercalating dye that labels both live and dead cells) in Thomson's buffer (TB, consisting of 20 mM sodium HEPES, 146 mM NaCl, 5.4 mM KCl, 1.8 mM CaCl₂, 0.8 mM MgSO₄, 0.4 mM KH₂PO₄, 0.3 mM Na₂HPO₄, and 5 mM dextrose; pH adjusted to 7.4) for 10 min followed by washing with TB. The cells were imaged for Hoechst 33342 and PI fluorescence in a confocal microscope setup (LSM-710, Zeiss, Germany) using a 20 \times objective. Two photon excitation of Hoechst 33342 was performed using 740 nm pulsed light from a mode-locked Ti:sapphire laser (MaiTai, Spectra-Physics, Santa Clara, CA). The fluorescence was separated from the excitation using a 690 nm dichroic mirror and detected using a photomultiplier tube (with a bandpass filter 385–535 nm). PI was excited using a 543 nm laser (He–Ne, Zeiss), the fluorescence was separated using a dichroic mirror and detected between 565 and 720 nm. Image analysis was performed for several fields (at least 12 per dish) for three dishes per peptide and assessed for the total number of cells (i.e., Hoechst 33342 fluorescent spots) and the number of dead cells (i.e., PI fluorescent spots) using an automated particle counter in ImageJ software. Cell viability was reported as the ratio of cells which were live (PI

negative) to the total number of cells. The cell viability expressed as percentage was normalized with respect to control cell viability assumed to be 100%.

Statistical significance was analyzed using Student's *t* test, and significance was assumed for probability values of $p < 0.05$.

■ ASSOCIATED CONTENT

Supporting Information

The Supporting Information is available free of charge on the ACS Publications website at DOI: 10.1021/acschemneuro.7b00360.

Mass spectrum of synthesized wildtype A β (1–40) peptide, characteristic 1D and 2D NMR spectra of amyloid fibrils, DIPSHIFT dephasing curves, and best fit simulations (PDF)

■ AUTHOR INFORMATION

Corresponding Author

*Phone: +49 (0) 341/97-15701. Fax: +49 (0) 341/97-15709. E-mail: daniel.huster@medizin.uni-leipzig.de.

ORCID

Sudipta Maiti: 0000-0002-6540-7472

Daniel Huster: 0000-0002-3273-0943

Author Contributions

A.K. S.M.L., J.A., M.K., and D.S. performed the research, analyzed data, and provided graphs and text sections for the manuscript. S.M. supervised the cell experiments and contributed to manuscript writing and the revision. D.H. conceived the study, supervised all research, wrote the manuscript with the contributions of all coauthors, and provided the revision with contributions of all coauthors.

Funding

The study was supported by the Deutsche Forschungsgemeinschaft (DFG, TRR-SFB 102, A06).

Notes

The authors declare no competing financial interest.

■ REFERENCES

- Chothia, C., and Lesk, A. M. (1986) The relation between the divergence of sequence and structure in proteins. *EMBO J.* 5, 823–826.
- Orengo, C. A., and Thornton, J. M. (2005) Protein families and their evolution—a structural perspective. *Annu. Rev. Biochem.* 74, 867–900.
- Chiti, F., and Dobson, C. M. (2006) Protein misfolding, functional amyloid, and human disease. *Annu. Rev. Biochem.* 75, 333–366.
- Chiti, F., and Dobson, C. M. (2009) Amyloid formation by globular proteins under native conditions. *Nat. Chem. Biol.* 5, 15–22.
- Petkova, A. T., Ishii, Y., Balbach, J. J., Antzutkin, O. N., Leapman, R. D., Delaglio, F., and Tycko, R. (2002) A structural model for Alzheimer's beta-amyloid fibrils based on experimental constraints from solid state NMR. *Proc. Natl. Acad. Sci. U. S. A.* 99, 16742–16747.
- Torok, M., Milton, S., Kaye, R., Wu, P., McIntire, T., Glabe, C. G., and Langen, R. (2002) Structural and dynamic features of Alzheimer's Abeta peptide in amyloid fibrils studied by site-directed spin labeling. *J. Biol. Chem.* 277, 40810–40815.
- Bertini, I., Gonnelli, L., Luchinat, C., Mao, J., and Nesi, A. (2011) A new structural model of A β 40 fibrils. *J. Am. Chem. Soc.* 133, 16013–16022.
- Xu, Y., Shen, J., Luo, X., Zhu, W., Chen, K., Ma, J., and Jiang, H. (2005) Conformational transition of amyloid beta-peptide. *Proc. Natl. Acad. Sci. U. S. A.* 102, 5403–5407.

- (9) Cote, S., Derreumaux, P., and Mousseau, N. (2011) Distinct Morphologies for Amyloid Beta Protein Monomer: Abeta1-40, Abeta1-42, and Abeta1-40(D23N). *J. Chem. Theory Comput.* 7, 2584–2592.
- (10) Fawzi, N. L., Ying, J., Torchia, D. A., and Clore, G. M. (2010) Kinetics of amyloid beta monomer-to-oligomer exchange by NMR relaxation. *J. Am. Chem. Soc.* 132, 9948–9951.
- (11) Prangkio, P., Yusko, E. C., Sept, D., Yang, J., and Mayer, M. (2012) Multivariate analyses of amyloid-beta oligomer populations indicate a connection between pore formation and cytotoxicity. *PLoS One* 7, e47261.
- (12) Chimoni, S., Shaibat, M. A., Jones, C. R., Calero, D. C., Aizezi, B., and Ishii, Y. (2007) Evidence of fibril-like beta-sheet structures in a neurotoxic amyloid intermediate of Alzheimer's beta-amyloid. *Nat. Struct. Mol. Biol.* 14, 1157–1164.
- (13) Losic, D., Martin, L. L., Mechler, A., Aguilar, M.-I., and Small, D. H. (2006) High resolution scanning tunnelling microscopy of the beta-amyloid protein (Abeta1-40) of Alzheimer's disease suggests a novel mechanism of oligomer assembly. *J. Struct. Biol.* 155, 104–110.
- (14) Yun, S., Urbanc, B., Cruz, L., Bitan, G., Teplow, D. B., and Stanley, H. E. (2007) Role of electrostatic interactions in amyloid beta-protein (A beta) oligomer formation: a discrete molecular dynamics study. *Biophys. J.* 92, 4064–4077.
- (15) Yu, L., Edalji, R., Harlan, J. E., Holzman, T. F., Lopez, A. P., Labkovsky, B., Hillen, H., Barghorn, S., Ebert, U., Richardson, P. L., Miesbauer, L., Solomon, L., Bartley, D., Walter, K., Johnson, R. W., Hajduk, P. J., and Olejniczak, E. T. (2009) Structural characterization of a soluble amyloid beta-peptide oligomer. *Biochemistry* 48, 1870–1877.
- (16) Hortschansky, P., Schroeckh, V., Christopeit, T., Zandomenighi, G., and Fändrich, M. (2005) The aggregation kinetics of Alzheimer's beta-amyloid peptide is controlled by stochastic nucleation. *Protein Sci.* 14, 1753–1759.
- (17) Harper, J. D., and Lansbury, P. T. JR (1997) Models of amyloid seeding in Alzheimer's disease and scrapie: mechanistic truths and physiological consequences of the time-dependent solubility of amyloid proteins. *Annu. Rev. Biochem.* 66, 385–407.
- (18) Scheidt, H. A., Morgado, I., and Huster, D. (2012) Solid-state NMR reveals a close structural relationship between amyloid- β protofibrils and oligomers. *J. Biol. Chem.* 287, 22822–22826.
- (19) Sarroukh, R., Cerf, E., Derclaye, S., Dufrene, Y. F., Goormaghtigh, E., Ruyschaert, J.-M., and Raussens, V. (2011) Transformation of amyloid beta(1-40) oligomers into fibrils is characterized by a major change in secondary structure. *Cell. Mol. Life Sci.* 68, 1429–1438.
- (20) Ahmed, M., Davis, J., Aucoin, D., Sato, T., Ahuja, S., Aimoto, S., Elliott, J. I., van Nostrand, W. E., and Smith, S. O. (2010) Structural conversion of neurotoxic amyloid-beta(1-42) oligomers to fibrils. *Nat. Struct. Mol. Biol.* 17, 561–567.
- (21) Anand, P., and Hansmann, U. H. E. (2011) Internal and environmental effects on folding and dimerization of the Alzheimer's beta amyloid peptide. *Mol. Simul.* 37, 440.
- (22) Paparcone, R., Pires, M. A., and Buehler, M. J. (2010) Mutations alter the geometry and mechanical properties of Alzheimer's Abeta(1-40) amyloid fibrils. *Biochemistry* 49, 8967–8977.
- (23) Paravastu, A. K., Leapman, R. D., Yau, W.-M., and Tycko, R. (2008) Molecular structural basis for polymorphism in Alzheimer's beta-amyloid fibrils. *Proc. Natl. Acad. Sci. U. S. A.* 105, 18349–18354.
- (24) Adler, J., Scheidt, H. A., Krüger, M., Thomas, L., and Huster, D. (2014) Local interactions influence the fibrillation kinetics, structure and dynamics of A β (1-40) but leave the general fibril structure unchanged. *Phys. Chem. Chem. Phys.* 16, 7461–7471.
- (25) Adler, J., Baumann, M., Voigt, B., Scheidt, H. A., Bhowmik, D., Häupl, T., Abel, B., Madhu, P. K., Balbach, J., Maiti, S., and Huster, D. (2016) A detailed analysis of the morphology of fibrils of selectively mutated amyloid β (1-40). *ChemPhysChem* 17, 2744–2753.
- (26) Das, A. K., Rawat, A., Bhowmik, D., Pandit, R., Huster, D., and Maiti, S. (2015) An early folding contact between Phe19 and Leu34 is critical for amyloid-beta oligomer toxicity. *ACS Chem. Neurosci.* 6, 1290–1295.
- (27) Chandra, B., Korn, A., Maity, B. K., Adler, J., Rawat, A., Krueger, M., Huster, D., and Maiti, S. (2017) Stereoisomers probe steric zippers in Amyloid- β . *J. Phys. Chem. B* 121, 1835–1842.
- (28) Creighton, T. E. (1996) *Proteins: Structures and molecular principles*, 2nd ed., W. H. Freeman and Company, New York.
- (29) Wimley, W. C., and White, S. H. (1996) Experimentally determined hydrophobicity scale for proteins at membrane interfaces. *Nat. Struct. Mol. Biol.* 3, 842–848.
- (30) Obici, L., Demarchi, A., de Rosa, G., Bellotti, V., Marciano, S., Donadei, S., Arbustini, E., Palladini, G., Diegoli, M., Genovese, E., Ferrari, G., Coverlizza, S., and Merlini, G. (2005) A novel AbetaPP mutation exclusively associated with cerebral amyloid angiopathy. *Ann. Neurol.* 58, 639–644.
- (31) Fossati, S., Cam, J., Meyerson, J., Mezhericher, E., Romero, I. A., Couraud, P. O., Weksler, B. B., Ghiso, J., and Rostagno, A. (2010) Differential activation of mitochondrial apoptotic pathways by vasculotropic amyloid-beta variants in cells composing the cerebral vessel walls. *FASEB J.* 24, 229–241.
- (32) Nielsen, L., Khurana, R., Coats, A., Frokjaer, S., Brange, J., Vyas, S., Uversky, V. N., and Fink, A. L. (2001) Effect of environmental factors on the kinetics of insulin fibril formation: elucidation of the molecular mechanism. *Biochemistry* 40, 6036–6046.
- (33) Michaels, T. C. T., Liu, L. X., Meisl, G., and Knowles, T. P. J. (2017) Physical principles of filamentous protein self-assembly kinetics. *J. Phys.: Condens. Matter* 29, 153002.
- (34) Freire, S., de Araujo, M. H., Al-Soufi, W., and Novo, M. (2014) Photophysical study of Thioflavin T as fluorescence marker of amyloid fibrils. *Dyes Pigm.* 110, 97–105.
- (35) Murugan, N. A., Olsen, J. M. H., Kongsted, J., Rinkevicius, Z., Aidas, K., and Agren, H. (2013) Amyloid fibril-induced structural and spectral modifications in the thioflavin-T optical probe. *J. Phys. Chem. Lett.* 4, 70–77.
- (36) Sunde, M., Serpell, L. C., Bartlam, M., Fraser, P. E., Pepys, M. B., and Blake, C. C. (1997) Common core structure of amyloid fibrils by synchrotron X-ray diffraction. *J. Mol. Biol.* 273, 729–739.
- (37) Spera, S., and Bax, A. (1991) Empirical correlation between protein backbone conformation and C.alpha. and C.beta. ¹³C nuclear magnetic resonance chemical shifts. *J. Am. Chem. Soc.* 113, 5490–5492.
- (38) Luca, S., Filippov, D. V., van Boom, J. H., Oschkinat, H., de Groot, H., and Baldus, M. (2001) Secondary chemical shifts in immobilized peptides and proteins: A qualitative basis for structure refinement under magic angle spinning. *J. Biomol. NMR* 20, 325–331.
- (39) Petkova, A. T., Leapman, R. D., Guo, Z., Yau, W.-M., Mattson, M. P., and Tycko, R. (2005) Self-propagating, molecular-level polymorphism in Alzheimer's beta-amyloid fibrils. *Science* 307, 262–265.
- (40) Agopian, A., and Guo, Z. (2012) Structural origin of polymorphism of Alzheimer's amyloid beta-fibrils. *Biochem. J.* 447, 43–50.
- (41) Scheidt, H. A., Morgado, I., Rothmund, S., and Huster, D. (2012) Dynamics of amyloid beta fibrils revealed by solid-state NMR. *J. Biol. Chem.* 287, 2017–2021.
- (42) Huster, D., Xiao, L., and Hong, M. (2001) Solid-state NMR investigation of the dynamics of the soluble and membrane-bound colicin Ia channel-forming domain. *Biochemistry* 40, 7662–7674.
- (43) Sarkar, B., Mithu, V. S., Chandra, B., Mandal, A., Chandrakesan, M., Bhowmik, D., Madhu, P. K., and Maiti, S. (2014) Significant structural differences between transient amyloid- β oligomers and less-toxic fibrils in regions known to harbor familial Alzheimer's mutations. *Angew. Chem., Int. Ed.* 53, 6888–6892.
- (44) Sahoo, B., Nag, S., Sengupta, P., and Maiti, S. (2009) On the stability of the soluble amyloid aggregates. *Biophys. J.* 97, 1454–1460.
- (45) Chandrakesan, M., Bhowmik, D., Sarkar, B., Abhyankar, R., Singh, H., Kallianpur, M., Dandekar, S. P., Madhu, P. K., Maiti, S., and Mithu, V. S. (2015) Steric crowding of the turn region alters the

tertiary fold of Amyloid- β 18–35 and makes it soluble. *J. Biol. Chem.* 290, 30099–30107.

(46) Hoffmann, F., Adler, J., Chandra, B., Mote, K. R., Bekçioğlu-Neff, G., Sebastiani, D., and Huster, D. (2017) Perturbation of the F19-L34 contact in Amyloid β (1–40) fibrils induces only local structural changes but abolishes cytotoxicity. *J. Phys. Chem. Lett.* 8, 4740–4745.

(47) Xiao, Y., Ma, B., McElheny, D., Parthasarathy, S., Long, F., Hoshi, M., Nussinov, R., and Ishii, Y. (2015) A β (1–42) fibril structure illuminates self-recognition and replication of amyloid in Alzheimer's disease. *Nat. Struct. Mol. Biol.* 22, 499–505.

(48) Colvin, M. T., Silvers, R., Ni, Q. Z., Can, T. V., Sergeev, I., Rosay, M., Donovan, K. J., Michael, B., Wall, J., Linse, S., and Griffin, R. G. (2016) Atomic resolution structure of monomorphic A β 42 amyloid fibrils. *J. Am. Chem. Soc.* 138, 9663–9674.

(49) Wälti, M. A., Ravotti, F., Arai, H., Glabe, C. G., Wall, J. S., Böckmann, A., Güntert, P., Meier, B. H., and Riek, R. (2016) Atomic-resolution structure of a disease-relevant A β (1–42) amyloid fibril. *Proc. Natl. Acad. Sci. U. S. A.* 113, E4976–84.

(50) Gremer, L., Schölzel, D., Schenk, C., Reinartz, E., Labahn, J., Ravelli, R. B. G., Tusche, M., Lopez-Iglesias, C., Hoyer, W., Heise, H., Willbold, D., and Schröder, G. F. (2017) Fibril structure of amyloid- β (1–42) by cryo-electron microscopy. *Science* 358, 116–119.

(51) Vignaud, H., Bobo, C., Lascu, I., Sörgjerd, K. M., Zako, T., Maeda, M., Salin, B., Lecomte, S., and Cullin, C. (2013) A structure-toxicity study of A β 42 reveals a new anti-parallel aggregation pathway. *PLoS One* 8, 1–13.

(52) Schütz, A. K., Vagt, T., Huber, M., Ovchinnikova, O. Y., Cadalbert, R., Wall, J., Güntert, P., Böckmann, A., Glockshuber, R., and Meier, B. H. (2015) Atomic-resolution three-dimensional structure of amyloid β fibrils bearing the Osaka mutation. *Angew. Chem., Int. Ed.* 54, 331–335.

(53) Chandra, B., Bhowmik, D., Maity, B. K., Mote, K. R., Dhara, D., Venkatramani, R., Maiti, S., and Madhu, P. K. (2017) Major reaction coordinates linking transient Amyloid- β oligomers to fibrils measured at atomic level. *Biophys. J.* 113, 805–816.

(54) Vivekanandan, S., Brender, J. R., Lee, S. Y., and Ramamoorthy, A. (2011) A partially folded structure of amyloid-beta(1–40) in an aqueous environment. *Biochem. Biophys. Res. Commun.* 411, 312–316.

(55) Prade, E., Barucker, C., Sarkar, R., Althoff-Ospelt, G., Lopez del Amo, J. M., Hossain, S., Zhong, Y., Multhaup, G., and Reif, B. (2016) Sulindac sulfide induces the formation of large oligomeric aggregates of the Alzheimer's disease Amyloid- β peptide which exhibit reduced neurotoxicity. *Biochemistry* 55, 1839–1849.

(56) Gopinath, T., and Veglia, G. (2012) Dual acquisition magic-angle spinning solid-state NMR spectroscopy: simultaneous acquisition of multidimensional spectra of biomacromolecules. *Angew. Chem., Int. Ed.* 51, 2731–2735.

(57) Bielecki, A., Kolbert, A. C., and Levitt, M. H. (1989) Frequency-switched pulse sequences: Homonuclear decoupling and dilute spin NMR in solids. *Chem. Phys. Lett.* 155, 341–346.

(58) Schmidt-Rohr, K., and Spiess, H. W. (1994) *Multidimensional solid-state NMR and polymers*, Academic Press, London.

(59) Barre, P., Zschornig, O., Arnold, K., and Huster, D. (2003) Structural and dynamical changes of the bindin B18 peptide upon binding to lipid membranes. A solid-state NMR study. *Biochemistry* 42, 8377–8386.

5.2 Ring structure modifications of phenylalanine 19 increase fibrillation kinetics and reduce toxicity of amyloid β (1-40)¹³⁹

Attestation of authors contribution

Journal: CHEMICAL COMMUNICATIONS

Authors: Korn, A., Surendran, D., Krueger, M., Maiti, S., & Huster, D.

Contributions Korn, Alexander: Fibril preparation, NMR investigations, fibrillation kinetics assays, X-ray diffraction studies, CD-spectroscopy experiments, data analyses, writing of the publication

Contributions Surendran, Dayana: Cell culture, biological activity assays, data analyses, writing of the publication

Contributions Krueger, Martin: TEM imaging

Contributions Maiti, Sudipta: Conception, writing of the publication

Contributions Huster, Daniel: Project idea, conception, writing of the publication



Ring structure modifications of phenylalanine 19 increase fibrillation kinetics and reduce toxicity of amyloid β (1-40)[†]

Alexander Korn,^a Dayana Surendran,^b Martin Krueger,^c Sudipta Maiti^b and Daniel Huster^{b,*}

Cite this: *Chem. Commun.*, 2018, 54, 5430

Received 2nd March 2018,
Accepted 1st May 2018

DOI: 10.1039/c8cc01733f

rsc.li/chemcomm

We investigated the influence of the chemical structure of the phenylalanine side chain in position 19 of the 40 residue amyloid β peptide. Side chain modifications in this position yielded fibrils of essentially unaltered morphology, structure, and dynamics, but significantly increased fibrillation kinetics and diminished the toxicity of the peptides.

Protein stability is encoded in sequential and long range interactions between individual amino acids.¹ Mutations in the sequence can lead to destabilization resulting in a shift of the equilibrium from the native or unfolded state towards aggregated misfolded states.² The latter are characterized by thermodynamically stable interchain contacts made with other molecules. Such misfolding is associated with numerous diseases, particularly in neurobiology. For instance, a number of mutations render amyloid β ($A\beta$) peptides highly aggregation prone, leading to early onset Alzheimer's disease.³ Thermodynamic stability of $A\beta$ peptides has been analyzed in detail.⁴ Recent studies demonstrated that perturbing an early folding contact of $A\beta_{40}$ leads to drastic alterations of the toxicity of these mutants,^{5,6} while the structure and dynamics of the fibrils was only marginally influenced.⁷⁻⁹ In this work, the hydrophobic contact between phenylalanine 19 (F19) and leucine 34 (L34) was altered by rather conservative mutations. Similarly, mutations were introduced into position L34 and flanking residues of $A\beta_{42}$, yielding essentially non-toxic species in *in vivo* models.^{10,11}

It has been suggested that the F19-L34 interaction represents an early folding contact in the misfolding of $A\beta_{40}$.⁵ However, the exact mechanism by which even minor alterations of the sequence render specifically the oligomeric aggregates of these mutated peptides harmless is not understood, but probably

related to the structural details of the F19-L34 contact. Here, we study chemical alterations of the phenylalanine side chain in four non-natural analogs in position 19 of $A\beta_{40}$ peptides addressing (i) the importance of the aromatic ring system of F19, (ii) the spatial proximity of the F19-L34 contact, and (iii) the size and hydrophobicity of the ring system. The structures of the mutated side chains are given in Fig. 1. As the role of aromatic side chains in amyloid formation has been highlighted,¹² such modifications may help understanding the specificities of molecular contacts that lead to $A\beta$ oligomer and fibril formation.

In the first variant, the aromatic benzene ring of F19 was replaced by a cyclohexane moiety using cyclohexyl-L-alanine (Cha) in the F19Cha mutant. Second, the proximity of the molecular contact between F19 and L34 was altered by either removing the CH_2 group in the side chain using phenylglycine (Phg) in the F19Phg mutant, or by adding one CH_2 group into the side chain using 4-phenylbutyric acid L-homophenylalanine (Homophe) in the F19Homophe mutant. Third, the size of the aromatic sidechain of phenylalanine was increased by replacing the benzene by a naphthalene ring in (1-naphthyl)-L-alanine (Nal) in the F19Nal mutant. Thus, a small library of $A\beta$ peptide variants was created that addresses the specificity of side chain packing for the fibrillation kinetics, the structure and dynamics of the $A\beta_{40}$ fibrils as well as their toxicity.

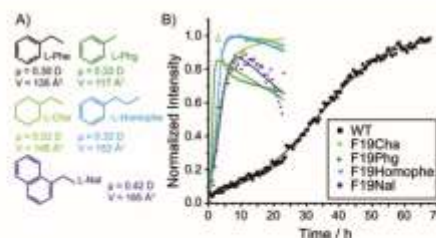


Fig. 1 (A) Structures, dipole moments (μ), and van der Waals volumes (V) of the mutated F19 side chains and (B) ThT fluorescence intensities as a function of fibrillation time of each $A\beta$ peptide variant.

^a Institute for Medical Physics and Biophysics, Leipzig University, Härtelstr. 16-18, Leipzig D-04107, Germany. E-mail: daniel.huster@medizin.uni-leipzig.de

^b Department of Chemical Sciences, Tata Institute of Fundamental Research, Homi Bhabha Road, Colaba, Mumbai, 400 005, India

^c Institute of Anatomy, Leipzig University, Liebigstr. 13, Leipzig D-04103, Germany

[†] Electronic supplementary information (ESI) available: Detailed materials & methods, CD spectra, TALOS+ torsions angles, and ¹H-¹³C order parameters. See DOI: 10.1039/c8cc01733f

Quantum chemical calculations of these side chains revealed relatively similar values for dipole moment and van der Waals volume (Fig. 1A). Somewhat remarkable differences arise in the F19Cha substitution, where the phenyl ring is replaced by a saturated cyclohexyl moiety. As a result, the ring system is no longer planar, which leads to a $\sim 10\%$ increased volume and, most importantly, nearly completely abolishes its dipole moment. The two mutations that probe the proximity of the contact of the phenylalanine ring with L34 (Phg and Homophe) show altered van der Waals volumes, but similar dipole moments. The naphthalene ring in the Nal variant is sterically most demanding, resulting in the largest volume and introduces the biggest dipole moment of 0.42 D.

We investigated the fibrillation kinetics of all mutated A β peptide variants in comparison to the wildtype (WT) peptide using the standard ThT assay.¹³ While we detected the often reported sigmoidal increase in ThT fluorescence intensity for WT A β peptides,¹⁴ all A β variants with altered F19 ring structure showed essentially no lag time and a drastically reduced fibrillation time in these ThT fluorescence intensity curves (Fig. 1B).

We determined the kinetic parameters¹⁴ for the fibrillation of the various peptide variants. WT A β_{40} preparations showed typical lag and fibrillation times of 12.6 ± 1.5 h and 45.4 ± 0.8 h, respectively. It should be noted that the assays were carried out at pH 9.2 to slow down the fibrillation of the mutated peptides. In all mutated peptides, the lag time is nearly completely abolished and cannot be resolved with our assay that involves a dead time of ~ 20 min for sample preparation before the first data point can be acquired. In contrast, the fibrillation time can safely be determined from the ThT fluorescence data. In all A β variants, the fibrillation time was drastically reduced (6.7 ± 0.6 h for the F19Cha variant, 6.0 ± 0.7 h for F19Nal, 3.6 ± 0.2 for F19Homophe, and 1.2 ± 0.2 h for F19Phg). Comparing the fibrillation times among the analogs, the variation of the side chain length (as probed in the Phg and Homophe variants) showed a greater influence than the modifications in the ring system (as probed in the Cha and Nal variants).

We next looked at the secondary structure in the mutated A β peptides using circular dichroism (CD) spectroscopy. Fibrillation causes a secondary structure transition from random coil monomers to β -sheet-rich fibrils. The monomers of all investigated peptides show characteristic random coil CD spectra with a minimum at ~ 200 nm (Fig. S1, ESI[†]). Upon fibrillation, the CD spectra of the A β peptides reveal the typical β -sheet character with a maximum at ~ 200 nm and a minimum at ~ 220 nm. The CD spectrum of F19Nal features two additional local positive peaks at ~ 210 nm and 230 nm located within the negative 220 nm peak region. The β -sheet character of the CD spectrum of F19Phg is only weakly developed, with the positive peak at 200 nm completely missing, but showing a negative peak at ~ 225 nm.

The morphology of the fibrils of mutated A β peptides was analyzed using transmission electron microscopy (TEM). All peptides formed amyloid fibrils that are in agreement with the characteristic cross- β structure (Fig. 2) and showed fibrillar structures of somewhat varying morphology. The measured diameters for WT A β fibrils and the fibrils formed by the

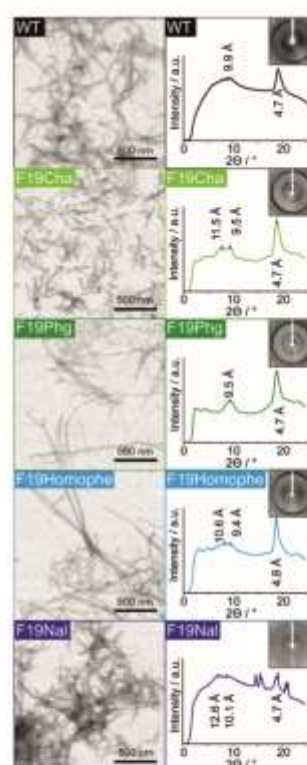


Fig. 2 TEM images (left) and X-ray diffraction pattern (right) of the A β_{40} variants.

peptides with altered ring morphology were of comparable size (WT: 15.7 ± 4 nm, F19Cha: 15.1 ± 3.2 nm, F19Nal: 15.0 ± 3.7 nm). However, when the length of the phenylalanine side chain was altered, somewhat thinner fibrils resulted (F19Homophe: 12.5 ± 2.7 nm, F19Phg: 10.4 ± 2.1 nm). More apparent were differences in the fibril lengths. Whereas the F19Cha mutant fibrils were short and needle-shaped, the side chain lengths altered variants F19Homophe and F19Phg formed a distinct class with particularly long fibrils. Only the F19Nal mutant showed a similar fibril length as the WT.

All fibril preparations showed the typical X-ray reflections at ~ 4.7 Å and ~ 10 – 12 Å (Fig. 2), which are caused by the hydrogen bond mediated intersheet distance and the side-chain contact mediated distance between opposing β -strands, respectively.¹⁵ The 4.7 Å reflections are relatively well-defined in the fibril preparations of all analogs and only the F19Homophe mutant showed a slightly longer distance of 4.8 Å. The intra-sheet spacing was less well-defined. WT and F19Phg fibrils showed a single reflection at 9.9 Å and 9.5 Å, respectively. The other mutated peptides formed fibrils that were somewhat more heterogeneous. For these molecules, two reflections were detected (F19Cha: 11.5 Å and 9.5 Å, F19Nal 12.6 Å and 10.1 Å, F19Homophe: 10.6 Å and 9.4 Å). Partially, also higher order reflections were recorded, but could not be associated with distinct structural features. The additional peaks detected for the F19Nal sample were caused by salt residua.

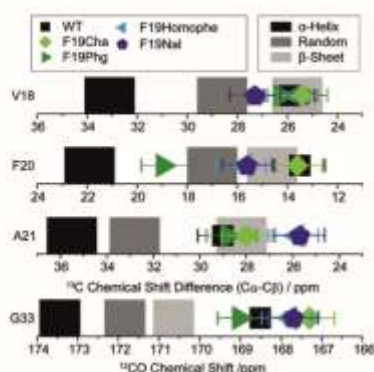


Fig. 3 ^{13}C MAS NMR chemical shifts of the labeled residues in WT and mutated $\text{A}\beta_{40}$ fibrils determined from ^{13}C - ^{13}C correlation experiments and corresponding secondary structure information as derived from the NMR chemical shifts. Gray boxes represent reference values for α -helix, random coil, and β -sheet secondary structure. Symbols represent experiment.

To study the local secondary structure in the fibrils, isotopic labels for solid-state NMR measurements were introduced in selected positions (valine (V18), phenylalanine (F20), alanine (A21), and glycine (G33)). ^{13}C chemical shifts, determined in ^{13}C - ^{13}C DARR NMR experiments, represent a measure for local secondary protein structure. In Fig. 3, we plot the $^{13}\text{C}\alpha$ - $^{13}\text{C}\beta$ chemical shift differences and provide reference values for the canonical secondary structure elements for the respective amino acid in the examined protein fibrils. As there is no $^{13}\text{C}\beta$ chemical shift for glycine, the ^{13}CO chemical shift is the preferred indicator for this amino acid.

At position V18, all peptides formed β -sheet structures irrespective of the mutation. Only the F19Nal variant showed some tendency for coil structure in this position. More clearly, the mutated position 19 influenced the secondary structure of residue F20. While in the F19Cha mutant, F20 showed WT chemical shifts, F19Homophe and F19Nal exhibited a tendency for coil structure, which was very solidly manifested in the F19Phg mutant. In positions A21 and G33, the influence of the mutated position 19 showed no structural impact and essentially WT chemical shifts are detected. We used TALOS+ to convert the chemical shift data into backbone torsion angles,¹⁶ which are reported in Table S1 and Fig. S2 (ESI[†]). As suggested by the chemical shift data, structurally very homogeneous $\text{A}\beta$ fibrils were obtained.

In addition to structural alterations, the mutations may also influence the local dynamics in the fibrils as a consequence of altered side chain packing in the fibril core. Here, we measured the amplitude of segmental C-H bond vector fluctuations in the protein backbone and side chain of the fibrils. These bond vector fluctuations are expressed as order parameters for all resolved sites, an order parameter of 1 is obtained for completely rigid ^1H - ^{13}C bond vectors, while an order parameter of 0 indicates isotropic reorientation.¹⁷ Order parameters are plotted in the Fig. S3 (ESI[†]).

Overall, the influence of the F19 ring modifications on the order parameters of the labeled amino acids was moderate.

Noteworthy examples were the backbone segments of V18 and G33 in the F19Nal variant, which became more mobile compared to the WT. Apparently, the naphthalene ring led to some local packing differences that were compensated for by larger amplitude motions of G33 and V18. Also, residue A21 in the F19Phg variant experiences more motional freedom expressed by lower segmental order parameter in the backbone. The shorter side chain of Phg creates some void volume that causes the A21 backbone to increase its motional amplitudes. Within experimental error, also the side chains only showed very moderate responses to the introduction of the altered ring structures. Most notably, the F20 ring became more ordered in the variants F19Nal, F19Homophe, and F19Phg, which may be related to tertiary contacts in these mutated $\text{A}\beta$ fibrils.

Finally, we studied how the mutations influenced the toxicity of the $\text{A}\beta$ variants using a neuronal cell line. Cell toxicity was tested using the standard MTT assay. As expected WT $\text{A}\beta$ peptides reduced cell viability to $40 \pm 2\%$ compared to vehicle treated control cells (Fig. 4). All analogs still showed toxicity, but at a significantly lower level than the WT (F19Cha: $76 \pm 4\%$, F19Nal: $54 \pm 4\%$, F19Homophe: $76 \pm 2\%$, F19Phg: $72 \pm 5\%$ cell viability).

Amyloid fibrils are proven to be very robust against variations of local perturbations and the introduction of local physical fields.⁶⁻⁹ However, the toxicity of these mutated $\text{A}\beta$ peptides is a very sensitive parameter that appears to depend heavily on the proper molecular contacts within the sequence.^{5,6,10,11} The F19 and L34 contact appears to represent an important interaction point in $\text{A}\beta_{40}$ fibrils, which crucially modulates the toxicity of oligomeric species of $\text{A}\beta_{40}$.⁵ After establishing that minimal perturbations of L34 already reduce the toxicity of the $\text{A}\beta$ peptides,⁶ here, we systematically altered the chemical structure of the F19 side chain. Only moderate alterations of the structure and dynamics of mature $\text{A}\beta$ fibrils were observed when (i) the aromatic character of the phenylalanine side chain is abolished, (ii) the proximity of the hydrophobic contact between the side chains of L34 and F19 is altered, or (iii) the benzene moiety of F19 is replaced by a naphthalene ring.

From the structural point of view of mature $\text{A}\beta$ fibrils, the aromaticity of the F19 side chain does not seem crucial as the local secondary structure, dynamics, and fibril morphology remained largely uninfluenced in the F19Cha mutant. The fibrils obtained were just somewhat shorter, exhibiting a slightly increased

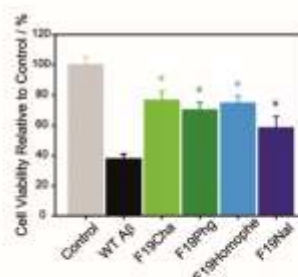


Fig. 4 MTT cell viability assay of RN46A cells treated with WT and mutated $\text{A}\beta_{40}$. * represents $p < 0.05$ between WT $\text{A}\beta_{40}$ and each variant. Error bars represent the standard deviation of 3 independent experiments. 6 wells each.

packing of the opposing β strands. The proximity between the L34 side chain and the F19 benzene ring, probed by the Phg and Homophe mutants, also only moderately influenced the structure and morphology of mature A β fibrils. Fibrils were a bit smaller in diameter, and the shorter Phg side chain induces local coil structure for residue F20. Furthermore, residue A21 experienced more motional freedom indicative of a looser packing density induced by the smaller side chain of Phg. The additional methylene group in the side chain of Homophe seemed to be tolerated very well in A β fibrils. The larger naphthalene ring in the F19Nal mutant was also astonishingly well accommodated in the fibril core structure. The amyloid structure locally became a bit more mobile and the F20 ring was more rigid.

These very moderate structural and morphological consequences of the introduction of altered F19 ring structures were contrasted by two very significant alterations concerning the fibrillation kinetics and the toxicity of the peptide variants: (i) none of the peptide variants showed a detectable lag time that exceeded the dead time of the experiment, which is about 20 min. Also, fibrillation was about 7 to 38 times faster in the mutated A β fibrils, suggesting significant alterations in the oligomer formation process. This may be a consequence of modified solubility, which could alter the seeding and thus enable a faster pathway for A β fibrillation. Consequently, also (ii) the toxicity of the A β variants is altered compared to the WT peptides. The modifications of the F19 ring structure as probed here rendered the peptides less toxic than the WT. We previously investigated F19X mutants (X = glycine, proline, tyrosine, tryptophan, glutamate, lysine), which showed no toxicity anymore.³ In contrast, mild mutations of L34X (X = valine, isoleucine, and D-leucine) retained most of the toxicity of the A β fibrils.⁶

Previous work has also studied the importance of the Phe₁₉Phe₂₀ motif for A β ₄₂ fibril formation showing that mutations to Leu or Ile enhance fibrillation.¹⁸ The authors concluded that aromaticity does not seem to play a critical role, but the toxicity of these mutated peptides was not tested.¹⁸

In summary, perturbations at F19 alter the pathway of A β aggregation. This changes the toxicity, possibly by disturbing the metastability of the toxic WT oligomers, and/or by steering the aggregation process through different, less-toxic, oligomers.^{19,20} This suggests that a benzene ring in position 19 combined with exactly the right structural proximity to L34 is required to form A β ₄₀ oligomers of the correct structure to exert full cell toxicity. Even marginal differences such as the addition or removal of a single methylene group in the sidechain are critical for the toxicity of A β . This was not encountered in the previous F19X mutants of proteinogenic amino acids,⁵ which rendered A β ₄₀ completely non-toxic. In the previous library of L34X A β ₄₀ mutants,⁶ the

peptide variants exhibited the correct F19 side chain structure and consequently, the peptides showed pronounced toxicity. The metastability of the WT oligomer may enhance its toxicity, so the faster aggregation kinetics and the lower toxicity of the mutants may be related. Therefore, the present data suggests that residue F19 is a crucial amino acid for the formation of toxic oligomers, which could represent a promising site for pharmacological intervention as inhibitors often feature and possibly target aromatic moieties.²¹

The study was supported by the Deutsche Forschungsgemeinschaft (DFG, TRR-SFB 102, A06).

Conflicts of interest

There are no conflicts to declare.

Notes and references

- C. B. Anfinsen, *Science*, 1973, **181**, 223.
- C. M. Dobson, *Nature*, 2003, **426**, 884.
- D. J. Selkoe and M. B. Podlisny, *Annu. Rev. Genomics Hum. Genet.*, 2002, **3**, 67.
- R. Wetzel, S. Shivaprasad and A. D. Williams, *Biochemistry*, 2007, **46**, 1.
- A. K. Das, A. Rawat, D. Bhowmik, R. Pandit, D. Huster and S. Maiti, *ACS Chem. Neurosci.*, 2015, **6**, 1290.
- A. Korn, S. McLennan, J. Adler, M. Krueger, D. Surendran, S. Maiti and D. Huster, *ACS Chem. Neurosci.*, 2018, **9**, 790.
- J. Adler, H. A. Scheidt, M. Krueger, L. Thomas and D. Huster, *Phys. Chem. Chem. Phys.*, 2014, **16**, 7461.
- J. Adler, M. Baumann, B. Voigt, H. A. Scheidt, D. Bhowmik, T. Haupt, B. Abel, P. K. Madhu, J. Balbach, S. Maiti and D. Huster, *ChemPhysChem*, 2016, **17**, 2744.
- F. Hoffmann, J. Adler, B. Chandra, K. R. Mote, G. Bekcioglu-Neff, D. Sebastiani and D. Huster, *J. Phys. Chem. Lett.*, 2017, **8**, 4740.
- H. Vignaud, C. Bobo, I. Lascu, K. M. Sorgjerd, T. Zako, M. Maeda, B. Salin, S. Lecomte and C. Cullin, *PLoS One*, 2013, **8**, e80262.
- L. M. Luheshi, G. G. Tartaglia, A. C. Brorsson, A. P. Pawar, I. E. Watson, F. Chiti, M. Vendruscolo, D. A. Lomas, C. M. Dobson and D. C. Crowther, *PLoS Biol.*, 2007, **5**, e290.
- E. Gazit, *FASEB J.*, 2002, **16**, 77.
- H. Naiki, K. Higuchi, M. Hosokawa and T. Takeda, *Anal. Biochem.*, 1989, **177**, 244.
- L. Nielsen, R. Khurana, A. Coats, S. Frokjaer, J. Brange, S. Vyas, V. N. Uversky and A. L. Fink, *Biochemistry*, 2001, **40**, 6036.
- M. Sunde, L. C. Serpell, M. Bartlam, P. E. Fraser, M. B. Pepys and C. C. Blake, *J. Mol. Biol.*, 1997, **273**, 729.
- Y. Shen, F. Delaglio, G. Cornilescu and A. Bax, *J. Biomol. NMR*, 2009, **44**, 213.
- H. A. Scheidt, I. Morgado, S. Rothermund and D. Huster, *J. Biol. Chem.*, 2012, **287**, 2017.
- A. H. Armstrong, J. Chen, A. Fortner McKoy and M. H. Hecht, *Biochemistry*, 2011, **50**, 4058.
- V. S. Mithu, B. Sarkar, D. Bhowmik, A. K. Das, M. Chandrakesan, S. Maiti and P. K. Madhu, *J. Biol. Chem.*, 2014, **289**, 11122.
- B. Chandra, D. Bhowmik, B. K. Maity, K. R. Mote, D. Dhara, R. Venkatramani, S. Maiti and P. K. Madhu, *Biophys. J.*, 2017, **113**, 805.
- Y. Porat, A. Abramowitz and E. Gazit, *Chem. Biol. Drug Des.*, 2006, **67**, 27–37.

5.3 Incorporation of the Nonproteinogenic Amino Acid β -Methylamino-alanine Affects Amyloid β Properties and Toxicity¹⁴⁰

Attestation of authors contribution

Journal: CHEMICAL COMMUNICATIONS

Authors: Korn, A., Höfling, C., Zeitschel, U., Krueger, M., Roßner, S., & Huster, D.

Contributions Korn, Alexander: Fibril preparation, NMR investigations, fibrillation kinetics assays, X-ray diffraction studies, CD-spectroscopy experiments, data analyses, writing of the publication

Contributions Hoefling, Corinna: Cell culture, biological activity assays, immunochemistry, data analyses, writing of the publication

Contributions Zeitschel, Ulrike: Cell culture, biological activity assays, immunochemistry, data analyses, writing of the publication

Contributions Krueger, Martin: TEM imaging

Contributions Rossner, Steffen: Conception, writing of the publication

Contributions Huster, Daniel: Project idea, conception, writing of the publication

Incorporation of the Nonproteinogenic Amino Acid β -Methylamino-alanine Affects Amyloid β Fibril Properties and Toxicity

Alexander Korn, Corinna Höfling, Ulrike Zeitschel, Martin Krueger, Steffen Roßner, and Daniel Huster*



Cite This: *ACS Chem. Neurosci.* 2020, 11, 1038–1047



Read Online

ACCESS |



Metrics & More



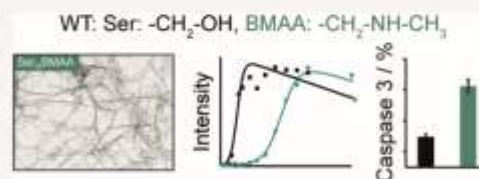
Article Recommendations



Supporting Information

ABSTRACT: The nonproteinogenic amino acid β -methylamino alanine (BMAA) is a neurotoxin and represents a potential risk factor for neurodegenerative diseases. Despite intense research over the last years, the pathological mechanism of BMAA is still unclear. One of the main open questions is whether BMAA can be misincorporated into proteins, especially as a substitute for serine, and whether this has structural and functional consequences for the afflicted proteins leading to early onset neurodegeneration. In this study, we hypothesize that BMAA was indeed incorporated into $A\beta_{40}$ molecules and study the structural and dynamical consequences of such misincorporation along with the effect such mutated $A\beta_{40}$ peptides have on neuronal cells. We used the synthetic β -amyloid peptide ($A\beta_{40}$), a known key player in the development of Alzheimer's disease, to incorporate BMAA substitutions at three different positions in the peptide sequence: Ser₆BMAA at the peptide's N-terminus, Phe₁₀BMAA in the hydrophobic core region, and Ser₂₆BMAA in the flexible turn region of $A\beta_{40}$ fibrils. We performed a set of biophysical experiments including fluorescence, circular dichroism, solid-state NMR spectroscopy, transmission electron microscopy, and X-ray diffraction to investigate structural and functional aspects of the mutated peptides compared to wildtype $A\beta_{40}$. All variants showed high structural tolerance to BMAA misincorporation. In contrast, the cellular response and neuronal survival were affected in a mutation site-specific manner. As a consequence, we can state from the physicochemical point of view that, if BMAA was misincorporated into proteins, it could indeed represent a risk factor that could potentially play a role in neurodegeneration. Further research addressing the role of BMAA, especially its protein-associated form, should be performed to obtain a better understanding of neurodegenerative diseases and to develop new therapeutic strategies.

KEYWORDS: Amyloid β toxicity, BMAA, amyloid structure, amyloid dynamics, nonproteinaceous amino acid mutation



INTRODUCTION

Environmental factors, infections, exposure to toxins, food poisoning, water contamination, and other conditions have threatened mankind from the very beginning until this day and age. Most insidious are agents that exert their destructive potential in a severely time delayed manner, which often renders pharmacological intervention and medical treatment impossible. One prominent example for such conditions are prion diseases, which were originally referred to as “slow virus diseases”¹ before their molecular mechanisms were discovered.² A relevant example for environmental hazards are nonproteinogenic amino acids, which are produced by cyanobacteria and can have devastating effects on the exposed population once they make it into the food chain.^{3,4} This is particularly relevant, as intense lake phytoplankton blooms have increased since the 1980s.⁵

One of the most spectacular epidemiological findings in this aspect was the discovery that the nonproteinogenic amino acid β -methylamino-L-alanine (BMAA) caused amyotrophic lateral sclerosis-parkinsonism-dementia (ALS-PDC), a neurodegenerative disease that shares specific characteristics with Alzheimer's disease (AD).^{6,7} It was conspicuous because it

was one of the leading death causes of the native Chamorro population on the island of Guam and also affected U.S. marines garrisoned on this island.^{6,7} Today, it is well accepted that the disease was caused by BMAA produced by cyanobacteria and accumulated in the local diet at this time, mostly through flour tortillas for which cycad seeds were used. However, the specific pathological mode of action of BMAA on a molecular level is still unclear. Currently, there are two possible mechanisms under consideration. First, BMAA may act as a neurotransmitter mimetic and thereby change neurological signaling pathways, which results in neurodegeneration.⁸ Second, the nonproteinogenic amino acid BMAA may be misincorporated into neuronal proteins and peptides, which then causes neurodegeneration, most likely because of protein malfunction or misfolding.⁹

Received: December 11, 2019

Accepted: March 6, 2020

Published: March 6, 2020

In particular, two studies provide some support for the latter hypothesis. The first publication claims that BMAA is accepted as a substrate instead of serine by its specific tRNA synthetase,¹⁰ but this view is subject to significant controversy.¹¹ The second study showed that BMAA downregulates PP2A activity and induces tau hyperphosphorylation.¹² As tau protein is highly relevant for the development of AD, it is interesting in that context that BMAA was detected in the brain tissue of AD patients both in the free form and in the protein-bound form.¹³ Later, this study was contradicted further questioning the significance of BMAA in neurodegenerative diseases.¹⁴ To underline the physiological relevance of BMAA, *in vivo* studies in zebrafish embryos exposed to BMAA revealed several effects such as the production of reactive oxygen species, decrease in protective capacity against excitotoxicity and oxidative stress, inhibition of developmental energetic and metabolic transitions, and inhibition of biosynthetic pathways.^{15–17}

In a more theoretical/physicochemical approach, the question of whether BMAA can associate with proteins has been tackled by quantum mechanical calculations and subsequent molecular dynamics simulations.¹⁸ It was found that BMAA can indeed bind to proteins with high affinity. Furthermore, BMAA was incorporated *in silico* into amyloid β peptides ($A\beta_{42}$), which represents the toxic agent in AD, to replace the natural residues Ser₅ or Ser₂₆, but these simulations did not reveal any altered conformational dynamics of the $A\beta$ peptides/fibrils.¹⁸

It should be emphasized at this point that there is absolutely no evidence that BMAA is incorporated into $A\beta$ peptides under physiological or pathological conditions. Nevertheless, based on the aforementioned results and studies, the link between BMAA and AD is intriguing and plausible. Therefore, we decided to study $A\beta$ peptides that carry BMAA substitutions experimentally. To investigate the possible effects of BMAA misincorporation in $A\beta$, we used solid phase peptide synthesis to generate two serine substitutions, *i.e.*, Ser₅BMAA and Ser₂₆BMAA. Furthermore, as our previous studies suggest a high relevance of the $A\beta_{40}$ residue Phe₁₉ for toxicity,^{19–21} we also generated the mutant Phe₁₉BMAA and included it into our studies of $A\beta$ fibrillation kinetics, fibril morphology, structure, and dynamics as well as toxicity toward mouse primary neurons.

With the aforementioned peptide variants, we can address the question whether BMAA misincorporation affects the characteristic structure formation and fibrillation processes, the amyloid specific fibril structure, and the mode of toxicity of β amyloid. Our data suggest that $A\beta_{40}$ by and large tolerates BMAA misincorporation at positions 8, 19, and 26. However, the fibrillation kinetics of the $A\beta$ peptides is sensitive to these substitutions. Consequently, all peptide mutants show different cellular response and toxicity not only compared to the wildtype (WT) $A\beta_{40}$ but also between the individual variants. As is well-known from the single amino acid mutations leading to the devastating familial early onset AD cases, small modifications in the $A\beta$ peptide sequence may affect the onset, progression, and treatability of AD.

RESULTS AND DISCUSSION

Fibrillation Kinetics Using Fluorescence Assays. The fibrillation kinetics of $A\beta$ peptides reports the influence of small alterations in the peptide sequence on the kinetics of the structure formation process. To this end, two different kinetics

experiments, involving either ThT dye or intrinsic tyrosine (Tyr) fluorescence, were performed to investigate the influence of the BMAA substitutions on the fibrillation process of the modified $A\beta$ peptides in comparison to WT $A\beta_{40}$. Both assays showed that $A\beta_{40}$ peptides carrying the N-terminal Ser₅BMAA substitution follow similar fibrillation kinetics as that of WT $A\beta$, whereas the Phe₁₉BMAA mutant shows a slight and the Ser₂₆BMAA mutant shows a pronounced prolongation of fibrillation and lag times (see Figure 1).

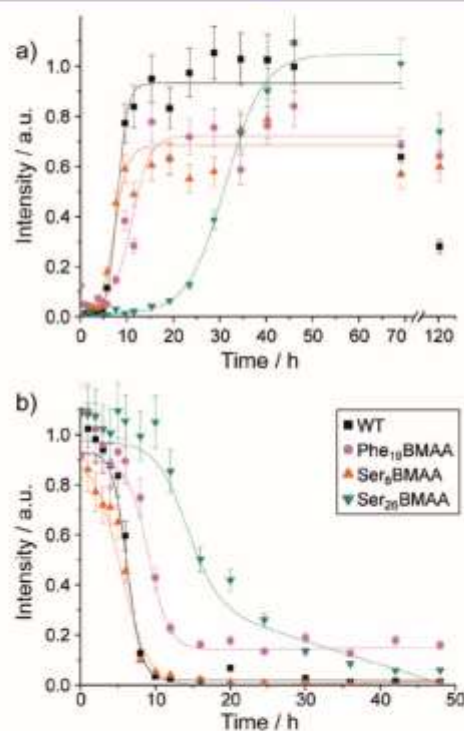


Figure 1. Fibrillation kinetics of WT and mutated $A\beta$ peptides measured by (a) ThT fluorescence and (b) intrinsic Tyr fluorescence. The peptide concentration was 1 mg/mL at pH 7.4 and a temperature of 37 °C. Experimental data were fitted to sigmoidal functions as described in Materials and Methods. In (a), only data points for times up to 70 h were considered in the fit, as sedimentation of large fibrillary aggregates occurs for longer experimental times.²³ Experimental errors in the determination of the lag time and fibrillation time were calculated from fitting errors.

In the ThT assay, thioflavin T fluorescence is increased by intercalation of the dye into amyloid fibrils.²² All $A\beta$ variants show the typical sigmoidal fluorescence intensity curve as a function of time featuring the three distinct phases: the lag phase, the fibrillation phase, and the plateau phase (Figure 1a). After reaching a plateau value, for some samples, the fluorescence intensity decreases, which is attributed to sedimentation of large fibrillary aggregates.^{23,24} WT $A\beta_{40}$ shows a lag time of 6.0 ± 1.6 h. This time constant is slightly extended for Phe₁₉BMAA (7.5 ± 2.5 h), slightly reduced for Ser₅BMAA (4.6 ± 2.7 h), but significantly longer for Ser₂₆BMAA (24.1 ± 1.1 h). Furthermore, the fibrillation time is shortest for WT $A\beta_{40}$ (4.6 ± 1.7 h), slightly longer for Ser₅BMAA (5.8 ± 3.4 h), and longer for Phe₁₉BMAA ($8.1 \pm$

3.3 h). Again, Ser₂₆BMAA showed the longest fibrillation time with 17.0 ± 1.3 h.

The Tyr fluorescence results using the intrinsic tyrosine residues yielded comparable results (Figure 1b). In this assay, the fibrillation mixture is centrifuged at different time points and the tyrosine fluorescence of the soluble fraction in the supernatant is measured, which provides a signal decrease proportional to the number of formed fibrils.²⁵ The Phe₁₉BMAA variant showed a slightly prolonged lag time and the Ser₂₆BMAA variant showed a considerably prolonged lag time (6.4 ± 1.0 and 9.8 ± 1.8 h, respectively) compared to WT (4.3 ± 0.4 h). The lag time of the Ser₉BMAA substitution was reduced to 1.8 ± 1.6 h. The fibrillation time was shortest for the WT with 3.8 ± 0.5 h. The fibrillation times of the mutants were, in increasing order, 5.5 ± 1.2 h for Phe₁₉BMAA, 7.3 ± 2.1 h for Ser₉BMAA, and 8.3 ± 2.1 h for Ser₂₆BMAA.

The largest difference in the fibrillation kinetics compared to WT A β ₄₀ was observed for the Ser₂₆BMAA substitution. It showed a longer lag time as well as an elongated fibrillation time. This indicates that this mutation is on the one hand less fibrillation prone, but on the other hand there is a longer time where oligomers are present. Nevertheless, it is not possible to predict if this mutation is more or less toxic. The kinetic data allow for both assumptions. The reason for the change in the kinetics might be due to an impairment of the turn formation caused by the weaker dipole moment of BMAA and the additional methyl group which might lead to steric constraints. The Phe₁₉BMAA mutation has only slight effects on the kinetics which is in agreement with various other mutational studies for the Phe₁₉ position. The Ser₉BMAA mutation shows nearly identical lag and fibrillation times compared to the WT. The Ser₉ position is located at the N-terminus and with this probably not relevant for the formation of an oligomer core structure. Also, Rauk discusses that his observed interaction between Ser₉BMAA and Asp₇ in the A β ₄₂ monomers has no significant influence.¹⁸

A β ₄₀ Fibril Morphology Investigated by Transmission Electron Microscopy. To investigate the morphology of the A β fibrils on a mesoscopic length scale and to compare the fibril morphology between WT and mutated A β ₄₀ peptides, transmission electron microscopy (TEM) images were recorded and fibril diameters were compared. All peptide variants showed typical fibril morphology and fibril diameters in agreement with previous studies on mutated A β ₄₀ fibrils^{19–21} (see Figure 2). However, statistically significant differences could be observed. The diameters for the various variants are as follows: (1) WT, 14.7 ± 2.6 nm; (2) Phe₁₉BMAA, 12.6 ± 1.9 nm; (3) Ser₉BMAA, 13.3 ± 2.3 nm; and (4) Ser₂₆BMAA, 11.8 ± 2.4 nm. Using statistical methods (ANOVA), it could be shown that all mutants have a smaller diameter than the WT and also Ser₉BMAA and Ser₂₆BMAA fibrils differ significantly ($p = 0.05$). In spite of the statistical significance, the interquartile ranges are large and there is no clear indication that these differences in the fibril diameters are of physiological importance.

Mesoscopic Cross- β Structure Investigated by X-ray Diffraction. To prove that the observed filaments showed the characteristic cross- β structure of amyloid fibrils, X-ray diffraction experiments were carried out. If fibrils with the characteristic cross- β structure are formed, two X-ray reflections are expected, one at 4.7 Å and one at about 10–11 Å originating from backbone hydrogen bonds and inter sheet spacing, respectively.²⁶ All investigated A β ₄₀ peptide

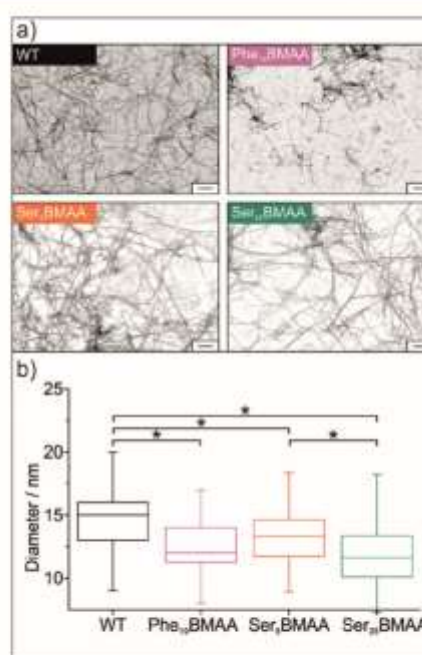


Figure 2. (a) TEM images of WT and mutant A β ₄₀ fibrils. Scale bars represent 250 nm. (b) Box plots of measured fibril diameters ($n = 100$, a total of 100 measurements from two independent preparations). Statistical significance ($p = 0.05$) was calculated using analysis of variance (ANOVA).

variants showed the two expected reflections indicative of the canonical cross- β structure (see Figure 3). The well-defined

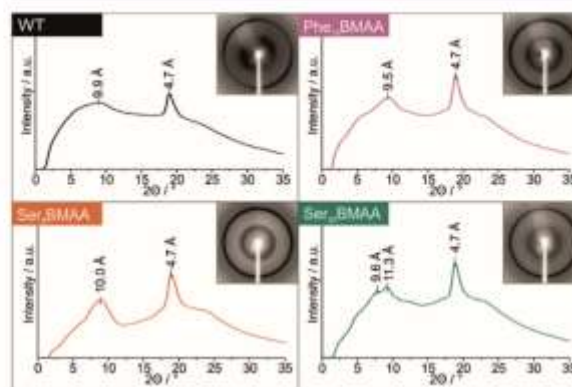


Figure 3. Intensity plots of the X-ray diffraction patterns of WT and mutant A β ₄₀ fibrils. Insets show the corresponding diffraction images.

hydrogen bond spacing was 4.7 Å for all variants. The inter sheet spacing is by nature less well-defined and was 9.9 Å for WT, 9.5 Å for Phe₁₉BMAA, 10.0 Å for Ser₉BMAA, and 9.6 Å/11.3 Å for Ser₂₆BMAA, with the latter indicating some structural polymorphism in the Ser₂₆BMAA A β ₄₀ fibrils.

Investigation of the Local Molecular Structure of the Mutated A β ₄₀ Fibrils Investigated by CD and Solid-State NMR Spectroscopy. For an overall assessment of the peptide's secondary structures, we carried out CD experiments in solution. The CD spectra are reported in Supporting

Information Figure S01. Freshly prepared peptide monomers in solution showed the typical signature of a random coil secondary structure with a pronounced minimum at 195 nm. After 7 days of incubation for fibrillation, the minimum in the CD spectrum is shifted to 220 nm, indicating a β -strand secondary structure.

For a more site-specific investigation of the secondary structure of the mutated peptides, solid-state NMR spectroscopy measurements were performed. The local protein fold influences the NMR chemical shift, which is particularly well observable when the chemical shift differences between the $^{13}\text{C}\alpha$ and $^{13}\text{C}\beta$ atoms of the amino acid residues are analyzed. For glycine, lacking a $^{13}\text{C}\beta$ atom, the ^{13}CO chemical shift is more informative. To determine the ^{13}C chemical shifts of WT and mutated $A\beta_{40}$ fibrils, one- and two-dimensional solid-state MAS NMR experiments of $A\beta_{40}$ peptides bearing $^{13}\text{C}/^{15}\text{N}$ isotopic labels in positions Gly₉, Phe₂₀, Val₂₄, and Asn₂₇, positioned in the characteristic structural elements of $A\beta_{40}$ fibrils (Gly₉ in the flexible N-terminus, Phe₂₀ and Val₂₄ in the first β -strand, and Asn₂₇ in the turn between the two β -strands), were recorded. Results of the structural analysis based on the NMR results are shown in Figure 4.

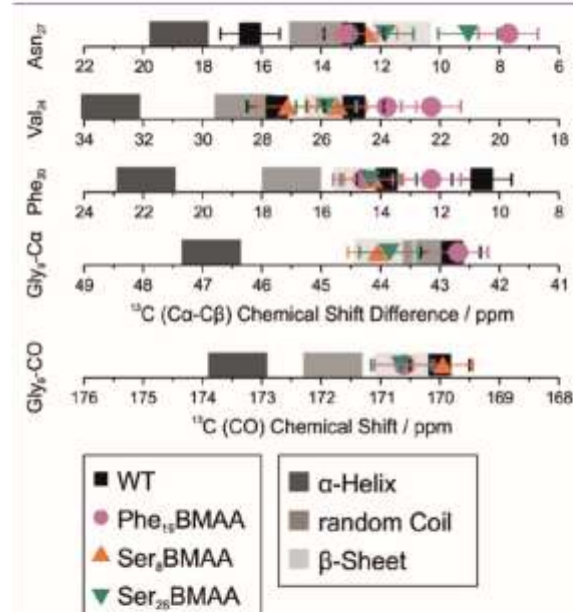


Figure 4. ^{13}C solid-state MAS NMR ^{13}CO chemical shift of Gly₉ and $^{13}\text{C}\alpha$ - $^{13}\text{C}\beta$ chemical shift differences of Phe₂₀, Val₂₄, and Asn₂₇ as compared to reference values for secondary structures (gray boxes). Plotted are the values for all labeled amino acids: Gly₉, Phe₂₀, Val₂₄, and Asn₂₇.

In this set of experiments, a relatively high degree of structural polymorphism in the $A\beta_{40}$ fibrils was detected, which is often described in the literature.^{27–29} The WT shows typical β -sheet structure for two polymorphs in the hydrophobic core region at position Phe₂₀. In the turn region, it also shows two polymorphs but with a different secondary structure. For Val₂₄, one polymorph shows a β -sheet and the other a random coil structure. For the second position in the turn region at Asn₂₇, one polymorph shows a random coil with a tendency to the β -sheet structure, whereas the other one tends to express partially

α -helical torsion angles in the backbone. For the N-terminus, sampled at position Gly₉, the $^{13}\text{C}\alpha$ chemical shift indicates a random coil and the ^{13}CO chemical shift β -sheet.

All $A\beta_{40}$ mutants showed a similar structure at the N-terminus according to the Gly₉ ^{13}CO chemical shift, for Ser₈BMAA and Ser₂₆BMAA and also the Gly₉ $^{13}\text{C}\alpha$ chemical shifts indicate β -sheet structure. At position Phe₂₀, all mutants showed a chemical shift difference nearly identical to that of one of the WT polymorphs; Phe₁₉BMAA shows a polymorph more similar to the second WP polymorph. Also, in the turn region at position Asn₂₇, the three mutants exhibited some polymorphism. The WT polymorph with partial α -helical tendencies was without counterpart for the mutants. In contrast, Phe₁₉BMAA and Ser₂₆BMAA showed a polymorph with a very low $^{13}\text{C}\alpha$ - $^{13}\text{C}\beta$ chemical shift difference indicating a clear β -sheet structure.

Local Dynamics of Mutated $A\beta_{40}$ Fibrils Investigated by Solid-State NMR Order Parameters. The NMR order parameters, determined from the motionally averaged ^1H - ^{13}C dipolar coupling values reflect the motional amplitude of the corresponding ^1H - ^{13}C bond vector. An order parameter of 1 represents full rigidity, and an order parameter of 0 indicates isotropic motion. Thus, NMR order parameters provide information on the local dynamics of the bond vectors in the respective amino acid. The NMR order parameters of the labeled amino acids in mutated $A\beta_{40}$ fibrils are reported in Figure 5.

As is expected, the backbone of all amyloid fibrils grown from the various peptide variants is very rigid, reflected by order parameters for the $\text{C}\alpha$ carbons of ~ 0.9 without

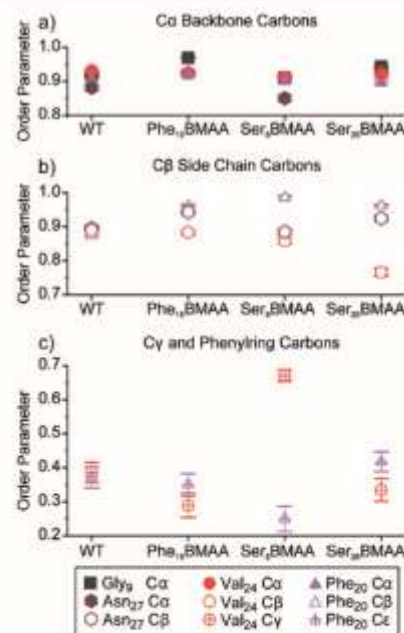


Figure 5. Order parameters derived from solid-state NMR DIP-SHIFT experiments representing the amplitude of the molecular motions of the respective bond vector. A value of 1 represents absolute rigidity, and a value of 0 indicates isotropic motion. Values for (a) $\text{C}\alpha$, (b) $\text{C}\beta$, and (c) other side chain carbons are plotted separately for better clarity. Error bars were estimated as 10% of $(1 - S)$.

substantial variations between the individual variants. Also, the $C\beta$ order parameters are high, indicating only slightly higher mobility. At position Phe₂₀, all mutants show a minor increase in rigidity compared to WT, and for the Val₂₀ of Ser₂₆BMAA an order parameter lower than that for the other peptides could be observed. The Val₃₀ $C\gamma$ and the phenyl ring order parameters are significantly lower as is typical for the terminal carbons. Also here the order parameters for Phe₃₀ are similar for all investigated variants. Only for Val₃₄ is a clear shift toward higher values observed for the Ser₉BMAA variant.

Cellular Toxicity Assays of Mutated $A\beta$ Fibrils. A set of four different cell culture experiments was performed to assess the toxicity of the WT and BMAA mutated $A\beta_{40}$ peptides (Figure 6). First, to analyze the integrity of the cellular

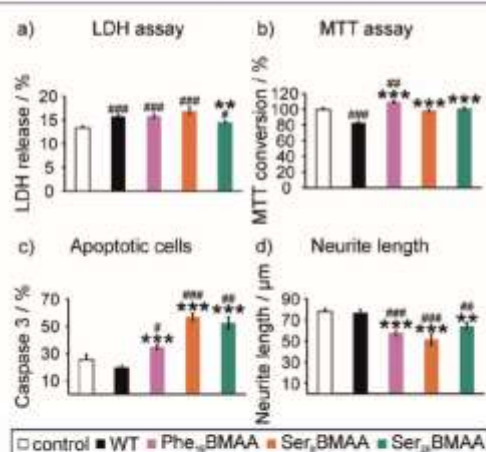


Figure 6. Results of cell culture experiments performed with primary mouse neurons. (a) LDH activity in the supernatants of cells exposed to all $A\beta$ variants is significantly increased compared to control. (b) Measurement of MTT conversion shows that WT $A\beta$ leads to a significant reduction of cell viability whereas mutant $A\beta$ shows no significant difference compared to the control. (c) Quantification of the appearance of activated caspase-3 as an intracellular marker for apoptotic cells shows that the mutant $A\beta$ variants initiate the apoptotic pathway in significantly more cells than WT $A\beta$ does. (d) Neurite length as a marker for viability of neurons is consistently reduced in neurons exposed to mutant $A\beta$. Plotted are mean values \pm SEM. Significances were tested using one-way ANOVA, $p \leq 0.05$, * vs WT, # vs control.

membrane, LDH released into the culture medium was quantified by an enzymatic activity assay. This assay demonstrated that all $A\beta$ variants caused cellular membrane disintegration leading to LDH release (Figure 6a). Second, a standard MTT assay was carried out to quantify the metabolic activity of primary mouse neurons. MTT is converted by mitochondria to formazan and an indicator of metabolically active cells. Only WT $A\beta_{40}$ caused a reduction in MTT conversion to formazan, whereas the BMAA mutant $A\beta_{40}$ variants did not affect glycolytic activity compared to control cells (Figure 6b). Third, the activation of caspase-3 by cleavage of its pro-form is an initial step in the induction of the apoptotic cell death pathway, which can be monitored immunocytochemically by antibodies that recognize the neopeptide of activated caspase-3. Quantification of activated caspase-3 immunoreactive cells revealed that WT $A\beta$ did not activate caspase-3, whereas all BMAA substituted $A\beta_{40}$ variants

robustly induced caspase-3 activation (Figure 6c). Finally, fourth, the retraction of neurites, i.e., reductions in neurite length, is an early indicator of neuronal damage and was measured after exposure to different $A\beta_{40}$ peptides. As for caspase-3 activation, only the $A\beta$ mutants but not the WT $A\beta$ affected neurite length (Figure 6d).

Thus, in general, both WT $A\beta$ and BMAA $A\beta$ damage cells, leading to membrane disintegration and LDH release. However, there appears to be different cellular mechanisms active with WT $A\beta$ acting via impairment of the mitochondrial glycolytic activity and all BMAA $A\beta$ peptides via induction of caspase-3 activation and retraction of neurites. This is in line with distinct pathogenic pathways activated by WT $A\beta$ and BMAA $A\beta$ variants.

Structural Consequences of BMAA Incorporation into $A\beta_{40}$ Peptides and Fibrils. From looking in detail at the structural level, we show that BMAA incorporation induces local constraints that lead to small structural alterations of different structural elements of $A\beta_{40}$ fibrils.

Hydrophobic Core Region. Several previous studies showed that the hydrophobic core region of $A\beta_{40}$ fibrils is structurally stable and tolerates a large variety of mutational constraints at the level of mature fibrils.^{20,21,30–35} In contrast, mutations at Phe₁₉ and/or Leu₃₄ can strongly affect the oligomerization and fibrillation process as well as the pathological properties of $A\beta_{40}$.^{19–21,30} We addressed this contact by introducing U-¹³C/¹⁵N labeling at position Phe₃₀. In agreement with our previous studies,^{20,21,30,31} the β -sheet structure of this region remained conserved for all mutants. Neither the Ser substitutions nor the Phe₁₉BMAA mutation showed structural effects at the hydrophobic core region. This is in agreement with mutational studies that show that this region tolerates a large variety of introduced constraints like differences of charges, backbone flexibility, ring systems, and hydrogen bonding.^{20,21,30–35}

Turn Region. The formation of the turn region is critical for the transition from monomers to oligomers and finally fibrils.³⁶ A structural hallmark of this site is the formation of a salt bridge between Asp₂₃ and Lys₂₈ which stabilizes the turn in $A\beta_{40}$ fibrils.³⁷ In this region, we introduced two isotopic labels at Val₂₄ and Asn₂₇. For all investigated variants, one polymorph with a β -sheet structure extent to Val₂₄ could be detected. This indicates that in these variants the turn starts at position Gly₂₅, which suggests torsional angle variability. Only the WT and the Ser₉BMAA mutation formed fibrils of a single polymorph with a turn that already comprises Val₂₄. Looking at position Asn₂₇, all mutants showed a WT-like polymorph with random coil-like chemical shifts. Furthermore, the Ser substitutions had an additional polymorph with lower $C\alpha$ - $C\beta$ chemical shift difference. Assigning this finding to the $A\beta_{40}$ structure derived from AD patients published by Tycko et al.,³⁸ a potential interaction between residues 8 and 26 can be assumed. In the structure, Ser₂₆ is pointing out of the turn and has no intramolecular contact. However, in this 3-fold symmetry structure, where three fibril strands align to a trigonal assembly, there is an interaction between Ser₂₆ of one fibril and the Ser₈ of the neighboring fibril.³⁸ This interaction is mediated by a hydrogen bond between the side chain OH of the Ser₂₆ and the backbone NH of the Ser₈. This interaction might be still possible in the Ser₂₆BMAA mutant, where the diamine group of the BMAA side chain substitutes the OH side chain group of the original serine side chain. However, the interaction of BMAA should be weaker because of its lower dipole moment

(BMAA: $\mu = 1.07$ D; Ser: $\mu = 2.06$ D) and its larger volume due to the terminal methyl group (BMAA, $V = 82.7$ Å³; Ser, $V = 59.2$ Å³) (dipole moment and volume were calculated by quantum mechanical calculation using SPARTAN). The steric clash caused by the methyl group may also cause a relocation of the whole N-terminus of the neighboring fibril which can explain the Gly₉ C α chemical shift change for both serine substitutions.

In addition to the chemical shifts, we also measured order parameters for all labeled carbon atoms, which provide a measure for the molecular mobility at these positions. From all investigated sites, only the terminal methyl group carbon of Val₂₄ showed an increased order parameter, meaning a lower motional amplitude, in the case of the Ser₈BMAA substitution. This might be surprising because the BMAA₈ and Val₂₄ are rather distant from each other. In the Tycko model,³⁸ Val₂₄ points out of the fibril and can interact with the N-terminus of the neighboring fibril, especially with Arg₅ and Asp₇.

N-Terminus. According to Tycko's structural model,³⁸ residue Asp₇ is in close proximity to both positions 8 (intramolecular) and 26 (interfibrillar) but shows no direct interactions with Ser₈. However, Rauk published a computer model of mutated fibrils where the Ser₈BMAA side chain interacts with Asp₇ in case of A β ₄₂ (the second predominant A β form with two additional C-terminal valines),¹⁸ an interaction not observed for the WT. This makes it likely that the Ser₈BMAA mutation has an effect on the whole N-terminal structure formation and with this might influence the interaction between the Val₂₄ and the N-terminus which can be seen by the increased order parameter of the terminal valine methyl group. In addition to the contact between Val₂₄ and the N-terminus and the direct interactions of positions 26 and 8, an intraterminal structural reorganization might be important. The N-terminus is described to be flexible in most A β ₄₀ models.^{39–41} In the patient derived structure from Tycko et al.,³⁸ the N-terminus participates in an elongated β -sheet. In our experiments, the Gly₉ ¹³C α chemical shift also indicates a β -sheet structure in this region. The Gly₉ ¹³C α chemical shifts indicate a distinct structure of the serine substitutions compared to WT and the Phe₁₉BMAA mutant. For Ser₂₆BMAA, this can be explained by the altered interaction with Ser₈ and the rearrangement due to the additional methyl group. Ser₈ shows no specific interactions in the fibril model, but also here the pure increase in volume caused by BMAA substitution might change the structural organization of the N-terminus. Additionally, the potentially new interaction between BMAA₈ and Asp₇ in the monomers might cause a different terminal packaging in the fibrils. Summarizing our structural data in comparison to structural models, we can assume that all three positions can be directly influenced by a Ser-BMAA substitution and might play a crucial role in oligomer formation and pathological potential of A β .

CONCLUSIONS

The nonproteinogenic amino acid BMAA is controversially discussed as a potential risk factor for the development of neurodegenerative diseases.^{12–14} Out of various biochemical effects, the substitution of BMAA for serine might represent a possible pathological mechanism.¹⁰ However, until this day, it was neither proved nor disproved that BMAA can be incorporated into A β or any other protein. However, such a scenario could indeed be relevant as a consequence of the

exposure of individuals with environmental toxins, for instance produced by cyanobacteria.^{4,12,13}

Regardless if in principle BMAA can finally be incorporated into A β peptides through the food chain, we were interested to study how such substitutions would influence the fibrillation formation kinetics of A β ₄₀ as well as the structure, dynamics and toxicity of these mutated aggregates in comparison to WT A β ₄₀. We have chosen A β ₄₀ as maternal molecule in this study, because it is less toxic than A β ₄₂ and, therefore, allows detecting modifications posing higher toxic potential. Moreover, since A β ₄₀ is more abundant than A β ₄₂ the chance for misincorporation of amino acids is higher. To this end, we used the possibilities of solid phase peptide synthesis and incorporated BMAA into crucial positions of A β ₄₀ peptides. First, we substituted the two serine residues in A β ₄₀, one in the N-terminal region at position 8 and one in the turn region at position 26, because serine substitution seems the most likely pathologically relevant possibility. It was described before that increased BMAA levels in the body could result in mischarging of tRNA originally loaded with Ser resulting in the false incorporation of BMAA instead of Ser in proteins important in neurodegeneration, which could seed aggregation and fibril formation of proteins in neuronal tissue.¹⁰ Interestingly, Ser₈ and Ser₂₆ phosphorylation have been demonstrated to be associated with aspects of amyloid pathology in AD.^{42,43} Furthermore, we substituted position Phe₁₉, which is highly relevant for the formation of an early folding contact with Leu₃₄ and was shown to be of high relevance for the toxicity of A β ₄₀ fibrils.^{19–21,30–32} With this small library of BMAA containing A β ₄₀ peptides, we evaluated the biophysical properties and the toxicity of BMAA containing A β ₄₀ peptides/fibrils.

Our results show that, if BMAA is incorporated into A β ₄₀, it has some curtailed and pathologically relevant effects. The fibril core structure remains mainly unaffected but the Ser-BMAA substitution suggests an interaction between the turn region and the N-terminus by a direct contact between Ser₂₆ and Ser₈ that is also conserved after the Ser-BMAA substitution. This contact is in agreement with the AD A β ₄₀ model previously described by Tycko et al.³⁸ The fibrillation kinetics is only substantially affected in the case of the Ser₂₆BMAA substitution, which shows an elongation of the lag and fibrillation time. However, significant changes of the cellular response were observed for the different variants. With this, it is conceivable that BMAA can potentially affect the properties of A β and is a relevant risk factor for AD. In previous computational work on BMAA-substituted A β ₄₂, Rauk claims that BMAA is not involved in AD.¹⁸ Our experimental data on A β ₄₀ show that effects can be observed. Which of the A β species could be relevant for AD still remains an open question. The A β ₄₂ form is more toxic, but the A β ₄₀ variant shows higher concentrations in brain tissue. Different studies also demonstrated that posttranslational A β modifications including N-truncation,⁴⁴ pyroglutamate formation,⁴⁵ tyrosine nitration,⁴⁶ and serine phosphorylation^{42,43} are important.^{47–50} That provides another function of the Ser-BMAA substitution as serine residues are potential phosphorylation sites that would no longer be available after substitution or can mimic aspects of phosphorylation.^{47,51,52} Additionally, Rauk focuses on the structure of monomers.¹⁸ However, the structure of the pathologically relevant toxic oligomers is still unresolved and the potential influence of BMAA misincorporation is therefore unknown. Our data suggest an influence also

at the oligomeric level. As of now, our understanding of $A\beta$ oligomers is very limited⁵³ and structural investigations and modeling range from very dynamic and disordered structures with a high degree of turns and twists and the lack of secondary structure^{54,55} all the way to relatively well described structural models of precise stoichiometry.^{56,57} Another aspect still unaddressed is that BMAA misincorporation might also affect the degradation of $A\beta$, which is also a relevant aspect for its biological activity and consequently for its role in AD.

MATERIAL AND METHODS

Peptide Synthesis. Standard Fmoc solid phase synthesis was used to produce the $A\beta_{40}$ peptides with the WT sequence DAEFRHDSGY EVHHQKLVFV AEDVGSNKGAIIGLMVGGVV and three mutants with the BMAA substitutions Ser₅BMAA, Phe₁₉BMAA, and Ser₂₆BMAA (the mutated residues are underlined in the peptide sequence). For NMR measurements, U-¹³C/¹⁵N labeled amino acids were introduced at positions Gly₉, Phe₂₀, Val₂₄, and Asn₂₇ (highlighted in bold in the peptide sequence). Peptide synthesis was performed by the Peptide Synthesis Core Unit of the University of Leipzig (https://home.uni-leipzig.de/tzkf/index_peptide.html).

$A\beta_{40}$ Fibril Preparation. Peptide powder was dissolved in aqueous buffer (25 mM sodium phosphate, 150 mM NaCl, 0.01% sodium azide, pH 9.5) at a concentration of 1 mg/mL. Subsequently, the solution was dialyzed using a 1000 Da MWCO dialysis membrane (Zellu Trans, Roth) two times against 1 L of fibrillation buffer (25 mM sodium phosphate, 150 mM sodium chloride, 0.01% sodium azide, pH 7.4) for 2 h each. For fibrillation, the sample was transferred into 1.5 mL reaction tubes and incubated for at least 7 days at 37 °C and 450 rpm in a thermoshaker. Fibrils prepared by this procedure were used for transmission electron microscopy, X-ray diffraction, and NMR-measurements.

Thioflavin T (ThT) Fluorescence Measurements. Peptide powder was dissolved in fibrillation buffer (25 mM sodium phosphate, 150 mM NaCl, 0.01% sodium azide, pH 7.4) at a concentration of 1 mg/mL applying vigorous shaking and vortexing. Three times, 150 μ L of this solution was transferred into a 96-well plate (Nunc, flat bottom, black) and 25 μ M ThT was added. Triplicates of WT and mutant $A\beta_{40}$ peptides were measured in parallel on the same plate. ThT fluorescence was measured with a microplate reader (Tecan Infinite M200, Tecan Group AG, Männedorf, Switzerland) at 37 °C, 450 nm excitation wavelength, 485 nm emission detection, and 5 min shaking/5 min waiting cycle. Measurements were performed every 30 min for at least 72 h.

Tyr Fluorescence Measurements. Aliquots of peptide solution were centrifuged at 2000g for 20 min at 4 °C. Subsequently, 50 μ L of supernatant was diluted in 450 μ M H₂O and transferred into a quartz cuvette (Hellma). Tyrosine fluorescence spectra (emission at 300–380 nm) were recorded on a FluoroMax-2 spectrometer (Jobin Yvon, Edison NJ) at room temperature with excitation at 265 nm. Peak intensity was determined by fitting the data with a Gaussian function.

Fluorescence Intensity Data Evaluation. Intensity data were normalized by $I = (I_t - I_{min})/I_{max}$ where I is the normalized intensity, I_t is the measured intensity value at the corresponding time point, and I_{min} and I_{max} are the minimal and maximal intensity measured for the corresponding well, respectively. Normalized data were fitted using a simple sigmoidal curve model, $I = \gamma + \frac{\beta}{1 + e^{-(t-t_0)/\tau}}$, for the ThT intensities, where I is the normalized intensity, t is the time, t_0 is the time at half maximal intensity, and τ is a measure for the fibrillation time. For the Tyr data, the fit function was $I = -\left(\gamma + m_1 + \frac{\beta + m_1}{1 + e^{-(t-t_0)/\tau}}\right) + I_0$, which is mirrored at the abscissa and shifted along the ordinate by the parameter I_0 .

For both assays, the lag time was derived by $t_{lag} = t_0 - 2\tau$ and the fibrillation time by $t_{fib} = 4\tau$. Reported mean values and standard deviations were calculated from the different fit values. For the

displayed graphs, intensities were averaged before plotting and calculation of the fit curves.

Transmission Electron Microscopy (TEM). A volume of 2 μ L of diluted fibril solution (1:20 with H₂O) was transferred onto a formvar film-coated copper grid. After evaporation of the solvent, the sample was stained with 1% uranyl acetate. Images were recorded on a transmission electron microscope (Zeiss SIGMA) equipped with a STEM detector and operated with Atlas software (Zeiss NTS, Oberkochen, Germany).

X-ray Diffraction Measurements. Mature fibrils were washed three times with H₂O. After the last centrifugation step (approximately 16,000g, 10 s) and removal of the supernatant, a droplet of concentrated fibril solution was placed between two paraffin sealed glass capillaries and slowly dried in a humid environment. Partially aligned fibrils on top of the sealed capillaries were mounted in the X-ray beam of a diffractometer (Rigaku, Tokio, Japan, copper rotating anode X-ray source MM007 with 0.8 kW). Diffraction images were recorded with 1 min exposure time at room temperature.

CD Spectroscopy. For stock solution preparation, approximately 1 mg of lyophilized peptide powder was presolubilized in 25 μ L of NaOH solution at pH 11 and diluted to a concentration of 1 mg/mL using standard phosphate buffer (25 mM sodium phosphate, 150 mM sodium chloride, 0.01% sodium azide, pH 7.4). For recording CD spectra, the stock solution was diluted to a final peptide concentration of 10 μ M with H₂O and transferred to a 2 mm quartz cuvette. Monomers were diluted 10 min after stock solution preparation. For fibril measurements, the stock solution was incubated for 7 days at 37 °C and 450 rpm using a thermoshaker prior to dilution to measuring concentration. Before dilution to the measuring concentration, fibrils were ultrasonicated in a water bath for 30 min and vigorously vortexed. CD spectra were recorded on a Jasco spectrometer at 25 °C, in continuous scanning mode with 50 nm/min, 4 s response time, 2.0 nm bandwidth, and an accumulation number of 5.

Solid-State NMR Measurements. After fibrillation, the peptide solution was centrifuged at 86,000g for 1 h at 4 °C. After removal of the supernatant, the pellets were frozen in liquid nitrogen and lyophilized for at least 48 h using an Alpha 1-4 lyophilizer (Martin Christ Gefriertrocknungsanlagen GmbH, Osterode, Germany). For NMR measurements, the fibril pellets were rehydrated to 50% (w/w) H₂O. For homogenization, 10 freeze/thaw cycles were applied (liquid nitrogen –37 °C water bath/centrifugation at 16,000g for 3 s) and the sample was transferred into 3.2 mm MAS rotors.

Solid-state MAS NMR spectra were recorded on a 600 MHz Avance III NMR spectrometer (Bruker BioSpin GmbH, Rheinstetten, Germany) operated at resonance frequencies of 600.1, 150.9, and 60.8 MHz for ¹H, ¹³C, and ¹⁵N, respectively. A triple channel 3.2 mm MAS probe operated at a temperature of 30 °C was used for all experiments. The 90° pulse length was set to 4 μ s for ¹H and ¹³C and to 5 μ s for ¹⁵N. For cross-polarization, a contact time of 1 ms and a spin lock field of 50 kHz were used. Relaxation delay was set to 2.5 s and the Spinal 64 sequence with an rf amplitude of 65 kHz was applied for ¹H decoupling.

Two-dimensional NMR spectra were recorded using a dual acquisition pulse sequence,⁵⁸ where one ¹³C–¹⁵C DARR⁵⁹ and four ¹⁵N–¹³C α correlation spectra were acquired simultaneously. The mixing time for the DARR experiments was 500 ms, MAS frequency was set to 11,777 Hz, and double CP contact times were 1 ms for ¹H–¹⁵N and 4 ms for ¹³C–¹⁵N transfer step.

To determine the motionally averaged ¹H–¹³C dipolar couplings, constant time DIPSHIFT experiments with 5 kHz MAS frequency and 80 kHz rf field frequency switched Lee–Goldberg homonuclear decoupling⁶⁰ were performed.⁶¹ Using numerical simulation of the experimental dephasing curves over one rotor period, motional averaged dipolar couplings were determined. For DIPSHIFT time domain data simulation, a C++ program was used. Euler angles for powder averaging were incremented in 1° steps in the simulations. The best fit of the dephasing curve to the experimental data was used to determine motional averaged dipolar coupling values $\langle\delta_{CH}\rangle$. Order parameters S_{CH} were calculated according to $S_{CH} = \langle\delta_{CH}\rangle/\delta_{CH0}$ where

δ_{CH} is the dipolar coupling rigid limit value derived frozen amino acid samples.^{62,63}

Cell Culture. Primary neuronal cultures were established from fetal mouse brains of C57Bl/6 mice at gestation day 16 and grown under standard conditions.^{64,65} Briefly, fetal brains were prepared and neurons were dissociated into single cells by triturating the brains by means of a pipet and passing the cell suspensions through sterile nylon meshes (20 μ m). Suspensions were then grown in seeding medium (DMEM/Ham's F-12 supplemented with 5% fetal horse serum (FHS) and 1% penicillin–streptomycin–neomycin (PSN) antibiotic mixture) in 96-well culture plates (for MTT and LDH assays) or on poly-L-lysine-coated glass coverslips in 24-well culture plates (for immunocytochemistry), respectively. The cells were cultured at 37 °C in a humidified atmosphere containing 5% CO₂. On the following day, the seeding medium was exchanged by neuronal medium (DMEM/Ham's F-12 supplemented with 1% PSN, 1% N-2 supplement and 20% astrocyte conditioned medium). After 3 days *in vitro*, cultures were stimulated with A β_{40} peptides at concentrations of 10 μ M for 18 h.

Neuronal survival was analyzed using the 3-(4,5-dimethylthiazol-2-yl)-2,5-diphenyltetrazolium bromide (MTT) assay which measures glycolytic activity. Briefly, MTT was solvated in cell culture media without serum and added to the primary neurons for 2 h. After addition of 50% DMSO/50% ethanol and shaking for 10 min, the absorbance was measured at 592 nm.

Neuronal cell death was measured in cell culture supernatant by lactate dehydrogenase (LDH) assay (Promega, CytoTox96) according to the manufacturer's protocol. LDH is a cytosolic protein, which is not normally secreted but can be detected extracellularly under conditions of membrane leakage.

Immunocytochemistry. Cells grown on coverslips were stained with primary antibodies against activated caspase-3 (1:100, AF835, R&D) and neurofilament M and H (1:1,000, AB5539, AB5735, Millipore) in TBS (0.1 M, pH 7.4) containing 0.1% Triton X-100 and 5% normal donkey serum at 4 °C overnight. On the next day, coverslips were washed thrice with TBS and then incubated with the respective secondary antibodies donkey anti-rabbit-Cy3 (1:400, 711-225-152, Dianova), donkey anti-chicken-biotin (1:400, cat. no. 703-066-155, Dianova) followed by streptavidin-Cy2 (1:200, 016-220-084, Dianova) in TBS containing 2% BSA for 60 min at room temperature. After rinsing with TBS, cell nuclei were stained with Hoechst 33342 in TBS (1:10,000) for 10 min at room temperature. The coverslips were washed, air-dried, embedded with Entellan/Toluol on glass slides, and stored at 4 °C in the dark. Fluorescence images were acquired with an inverted fluorescence phase-contrast microscope using a 10 \times objective (Bioevo BZ-9000E, Keyence, Neu-Isenburg, Germany). BZ-II Analyzer 2.1 software (Keyence, Osaka, Japan) was used for quantification of activated caspase-3 and measurement of neurite length in neurofilament stainings.

Control experiments were performed by omitting the primary antibody. All controls were negative, indicating that the observed fluorescence signals were specific. For quantification, four regions of interest from each coverslip were randomly selected and caspase-3 positive cells were counted with regard to all cells indicated by Hoechst staining. The same procedure was applied for quantifying neurite length under experimental conditions.

■ ASSOCIATED CONTENT

Supporting Information

The Supporting Information is available free of charge at <https://pubs.acs.org/doi/10.1021/acschemneuro.9b00660>.

CD spectra of freshly dissolved and fibrillated A β_{40} peptides, analytical data for all synthesized A β_{40} peptides by HPLC and mass spectrometry (PDF)

■ AUTHOR INFORMATION

Corresponding Author

Daniel Huster – Institute for Medical Physics and Biophysics, Leipzig University, D-04107 Leipzig, Germany; orcid.org/0000-0002-3273-0943; Phone: +49 (0) 341 9715701; Email: daniel.huster@medizin.uni-leipzig.de; Fax: +49 (0) 341 9715709

Authors

Alexander Korn – Institute for Medical Physics and Biophysics, Leipzig University, D-04107 Leipzig, Germany
Corinna Höfling – Paul Flechsig Institute for Brain Research, Leipzig University, D-04103 Leipzig, Germany
Ulrike Zeitschel – Paul Flechsig Institute for Brain Research, Leipzig University, D-04103 Leipzig, Germany
Martin Krueger – Institute of Anatomy, Leipzig University, D-04103 Leipzig, Germany
Steffen Roßner – Paul Flechsig Institute for Brain Research, Leipzig University, D-04103 Leipzig, Germany

Complete contact information is available at:

<https://pubs.acs.org/doi/10.1021/acschemneuro.9b00660>

Author Contributions

A.K. and D.H. designed research, A.K. prepared the samples, carried out fluorescence, X-ray diffraction, and NMR experiments, and analyzed data, M.K. carried out and analyzed the TEM measurements, C.H., U.Z., and S.R. carried out and analyzed the toxicity experiments. D.H. and A.K. wrote the manuscript with the contributions of all coauthors.

Funding

The study was supported by the Deutsche Forschungsgemeinschaft, DFG, Project Number 189853844-SFB TRR 102 (A06).

Notes

The authors declare no competing financial interest.

■ REFERENCES

- Thormar, H. (1971) Slow infections of the central nervous system. II. *J. Neurol.* 199, 151–166.
- Prusiner, S. B. (1998) Prions. *Proc. Natl. Acad. Sci. U. S. A.* 95, 13363–13383.
- Gantar, M., and Svircev, Z. (2008) Microalgae and cyanobacteria: food for thought. *J. Phycol.* 44, 260–268.
- Cox, P. A., Banack, S. A., Murch, S. J., Rasmussen, U., Tien, G., Bidigare, R. R., Metcalf, J. S., Morrison, L. F., Codd, G. A., and Bergman, B. (2005) Diverse taxa of cyanobacteria produce beta-N-methylamino-L-alanine, a neurotoxic amino acid. *Proc. Natl. Acad. Sci. U. S. A.* 102, 5074–5078.
- Ho, J. C., Michalak, A. M., and Pahlevan, N. (2019) Widespread global increase in intense lake phytoplankton blooms since the 1980s. *Nature.*, 10–1648.
- Spencer, P. S., Nunn, P. B., Hugon, J., Ludolph, A., and Roy, D. N. (1986) Motoneurone disease on Guam: possible role of a food neurotoxin. *Lancet* 327, 965–9736.
- Spencer, P. S., Nunn, P. B., Hugon, J., Ludolph, A. C., Ross, S. M., Roy, D. N., and Robertson, R. C. (1987) Guam amyotrophic lateral sclerosis-parkinsonism-dementia linked to a plant excitant neurotoxin. *Science* 237, 517–522.
- Chiu, A. S., Braid, N., Marcal, H., Welch, J. H., Gehring, M. M., Guillemain, G. J., and Neilan, B. A. (2015) Global cellular responses to beta-methyl-amino-L-alanine (BMAA) by olfactory ensheathing glial cells (OEC). *Toxicol.* 99, 136–145.
- Rodgers, K. J. (2014) Non-protein amino acids and neurodegeneration: the enemy within. *Exp. Neurol.* 253, 192–196.

- (10) Dunlop, R. A., Cox, P. A., Banack, S. A., and Rodgers, K. J. (2013) The non-protein amino acid BMAA is misincorporated into human proteins in place of L-serine causing protein misfolding and aggregation. *PLoS One* 8, No. e75376.
- (11) Chernoff, N., Hill, D. J., Diggs, D. L., Faison, B. D., Francis, B. M., Lang, J. R., Larue, M. M., Le, T. T., Loftin, K. A., Lugo, J. N., Schmid, J. E., and Winnik, W. M. (2017) A critical review of the postulated role of the non-essential amino acid, beta-N-methylamino-L-alanine, in neurodegenerative disease in humans. *J. Toxicol. Environ. Health, Part B* 20, 183.
- (12) Arif, M., Kazim, S. F., Grundke-Iqbal, I., Garruto, R. M., and Iqbal, K. (2014) Tau pathology involves protein phosphatase 2A in parkinsonism-dementia of Guam. *Proc. Natl. Acad. Sci. U. S. A.* 111, 1144–1149.
- (13) Pablo, J., Banack, S. A., Cox, P. A., Johnson, T. E., Papapetropoulos, S., Bradley, W. G., Buck, A., and Mash, D. C. (2009) Cyanobacterial neurotoxin BMAA in ALS and Alzheimer's disease. *Acta Neurol. Scand.* 120, 216–225.
- (14) Meneely, J. P., Chevallier, O. P., Graham, S., Greer, B., Green, B. D., and Elliott, C. T. (2016) beta-methylamino-L-alanine (BMAA) is not found in the brains of patients with confirmed Alzheimer's disease. *Sci. Rep.* 6, 36363.
- (15) Froyset, A. K., Khan, E. A., and Fladmark, K. E. (2016) Quantitative proteomics analysis of zebrafish exposed to sub-lethal dosages of beta-methyl-amino-L-alanine (BMAA). *Sci. Rep.* 6, 29631.
- (16) Powers, S., Kwok, S., Lovejoy, E., Lavin, T., and Sher, R. B. (2017) Editor's Highlight: Embryonic Exposure to the Environmental Neurotoxin BMAA Negatively Impacts Early Neuronal Development and Progression of Neurodegeneration in the Sod1-G93R Zebrafish Model of Amyotrophic Lateral Sclerosis. *Toxicol. Sci.* 157, 129–140.
- (17) Roy, U., Conklin, L., Schiller, J., Matysik, J., Berry, J. P., and Alia, A. (2017) Metabolic profiling of zebrafish (*Danio rerio*) embryos by NMR spectroscopy reveals multifaceted toxicity of beta-methylamino-L-alanine (BMAA). *Sci. Rep.* 7, 17305–17409.
- (18) Rauk, A. (2018) beta-N-Methylamino-l-alanine (BMAA) Not Involved in Alzheimer's Disease. *J. Phys. Chem. B* 122, 4472–4480.
- (19) Das, A. K., Rawat, A., Bhowmik, D., Pandit, R., Huster, D., and Maiti, S. (2015) An Early Folding Contact between Phe19 and Leu34 is Critical for Amyloid-beta Oligomer Toxicity. *ACS Chem. Neurosci.* 6, 1290–1295.
- (20) Korn, A., Surendran, D., Krueger, M., Maiti, S., and Huster, D. (2018) Ring structure modifications of phenylalanine 19 increase fibrillation kinetics and reduce toxicity of amyloid beta (1–40). *Chem. Commun.* 54, 5430–5433.
- (21) Hoffmann, F., Adler, J., Chandra, B., Mote, K. R., Bekcioglu-Neff, G., Sebastiani, D., and Huster, D. (2017) Perturbation of the F19-L34 Contact in Amyloid beta (1–40) Fibrils Induces Only Local Structural Changes but Abolishes Cytotoxicity. *J. Phys. Chem. Lett.* 8, 4740–4745.
- (22) Biancalana, M., and Koide, S. (2010) Molecular mechanism of Thioflavin-T binding to amyloid fibrils. *Biochim. Biophys. Acta, Proteins Proteomics* 1804, 1405–1412.
- (23) Adler, J., Scheidt, H. A., Lemmnitzer, K., Krueger, M., and Huster, D. (2017) N-terminal lipid conjugation of amyloid β (1–40) leads to the formation of highly ordered N-terminally extended fibrils. *Phys. Chem. Chem. Phys.* 19, 1839–1846.
- (24) Hayden, E. Y., Hoi, K. K., Lopez, J., Inayathullah, M., Condron, M. M., and Teplow, D. B. (2017) Identification of key regions and residues controlling Abeta folding and assembly. *Sci. Rep.* 7, 12434–10845.
- (25) Sengupta, P., Garai, K., Sahoo, B., Shi, Y., Callaway, D. J., and Maiti, S. (2003) The amyloid beta peptide (Abeta(1–40)) is thermodynamically soluble at physiological concentrations. *Biochemistry* 42, 10506–10513.
- (26) Sunde, M., Serpell, L. C., Bartlam, M., Fraser, P. E., Pepys, M. B., and Blake, C. C. (1997) Common core structure of amyloid fibrils by synchrotron X-ray diffraction. *J. Mol. Biol.* 273, 729–739.
- (27) Tycko, R. (2014) Physical and structural basis for polymorphism in amyloid fibrils. *Protein Sci.* 23, 1528–1539.
- (28) Fandrich, M., Meinhardt, J., and Grigorieff, N. (2009) Structural polymorphism of Alzheimer Abeta and other amyloid fibrils. *Prion* 3, 89–93.
- (29) Walti, M. A., Ravotti, F., Arai, H., Glabe, C. G., Wall, J. S., Bockmann, A., Guntert, P., Meier, B. H., and Riek, R. (2016) Atomic-resolution structure of a disease-relevant Abeta(1–42) amyloid fibril. *Proc. Natl. Acad. Sci. U. S. A.* 113, E4976–E4984.
- (30) Adler, J., Scheidt, H. A., Kruger, M., Thomas, L., and Huster, D. (2014) Local interactions influence the fibrillation kinetics, structure and dynamics of Abeta(1–40) but leave the general fibril structure unchanged. *Phys. Chem. Chem. Phys.* 16, 7461–7471.
- (31) Adler, J., Baumann, M., Voigt, B., Scheidt, H. A., Bhowmik, D., Haupt, T., Abel, B., Madhu, P. K., Balbach, J., Maiti, S., and Huster, D. (2016) A Detailed Analysis of the Morphology of Fibrils of Selectively Mutated Amyloid beta (1–40). *ChemPhysChem* 17, 2744–2753.
- (32) Korn, A., McLennan, S., Adler, J., Krueger, M., Surendran, D., Maiti, S., and Huster, D. (2018) Amyloid beta (1–40) Toxicity Depends on the Molecular Contact between Phenylalanine 19 and Leucine 34. *ACS Chem. Neurosci.* 9, 790–799.
- (33) Mao, Y., Zlatic, C. O., Griffin, M. D., Howlett, G. J., Todorova, N., Yarovsky, L., and Gooley, P. R. (2015) Hydrogen/Deuterium Exchange and Molecular Dynamics Analysis of Amyloid Fibrils Formed by a D69K Charge-Pair Mutant of Human Apolipoprotein C-II. *Biochemistry* 54, 4805–4814.
- (34) Wetzel, R., Shivaprasad, S., and Williams, A. D. (2007) Plasticity of amyloid fibrils. *Biochemistry* 46, 1–10.
- (35) Vignaud, H., Bobo, C., Lascu, I., Sorgjerd, K. M., Zako, T., Maeda, M., Salin, B., Lecomte, S., and Cullin, C. (2013) A structure-toxicity study of Abeta42 reveals a new anti-parallel aggregation pathway. *PLoS One* 8, No. e80262.
- (36) Chandra, B., Bhowmik, D., Maiti, B. K., Mote, K. R., Dhara, D., Venkatramani, R., Maiti, S., and Madhu, P. K. (2017) Major Reaction Coordinates Linking Transient Amyloid-beta Oligomers to Fibrils Measured at Atomic Level. *Biophys. J.* 113, 805–816.
- (37) Chandrakesan, M., Bhowmik, D., Sarkar, B., Abhyankar, R., Singh, H., Kallianpur, M., Dandekar, S. P., Madhu, P. K., Maiti, S., and Mithu, V. S. (2015) Steric Crowding of the Turn Region Alters the Tertiary Fold of Amyloid-beta18–35 and Makes It Soluble. *J. Biol. Chem.* 290, 30099–30107.
- (38) Lu, J. X., Qiang, W., Yau, W. M., Schwieters, C. D., Meredith, S. C., and Tycko, R. (2013) Molecular Structure of beta-Amyloid Fibrils in Alzheimer's Disease Brain Tissue. *Cell* 154, 1257–1268.
- (39) Scheidt, H. A., Morgado, I., Rothemund, S., and Huster, D. (2012) Dynamics of amyloid beta fibrils revealed by solid-state NMR. *J. Biol. Chem.* 287, 2017–2021.
- (40) Petkova, A. T., Ishii, Y., Balbach, J. J., Antzutkin, O. N., Leapman, R. D., Delaglio, F., and Tycko, R. (2002) A structural model for Alzheimer's beta-amyloid fibrils based on experimental constraints from solid state NMR. *Proc. Natl. Acad. Sci. U. S. A.* 99, 16742–16747.
- (41) Bertini, I., Gonnelli, L., Luchinat, C., Mao, J., and Nesi, A. (2011) A new structural model of Abeta40 fibrils. *J. Am. Chem. Soc.* 133, 16013–16022.
- (42) Kumar, S., Rezaei-Ghaleh, N., Terwel, D., Thal, D. R., Richard, M., Hoch, M., Mc Donald, J. M., Wullner, U., Glebov, K., Heneka, M. T., Walsh, D. M., Zweckstetter, M., and Walter, J. (2011) Extracellular phosphorylation of the amyloid beta-peptide promotes formation of toxic aggregates during the pathogenesis of Alzheimer's disease. *EMBO J.* 30, 2255–2265.
- (43) Kumar, S., Wirths, O., Stuber, K., Wunderlich, P., Koch, P., Theil, S., Rezaei-Ghaleh, N., Zweckstetter, M., Bayer, T. A., Brustle, O., Thal, D. R., and Walter, J. (2016) Phosphorylation of the amyloid beta-peptide at Ser26 stabilizes oligomeric assembly and increases neurotoxicity. *Acta Neuropathol.* 131, 525–537.
- (44) Kummer, M. P., and Heneka, M. T. (2014) Truncated and modified amyloid-beta species. *Alzheimer's Res. Ther.* 6, 28.
- (45) Schilling, S., Zeitschel, U., Hoffmann, T., Heiser, U., Francke, M., Kehlen, A., Holzer, M., Hutter-Paier, B., Prokesch, M., Windisch, M., Jagla, W., Schlenzig, D., Lindner, C., Rudolph, T., Reuter, G.,

Cynis, H., Montag, D., Demuth, H. U., and Rossner, S. (2008) Glutamyl cyclase inhibition attenuates pyroglutamate Abeta and Alzheimer's disease-like pathology. *Nat. Med.* 14, 1106–1111.

(46) Kummer, M. P., Hermes, M., Delekarte, A., Hammerschmidt, T., Kumar, S., Terwel, D., Walter, J., Pape, H. C., König, S., Roeber, S., Jessen, F., Klockgether, T., Korte, M., and Heneka, M. T. (2011) Nitration of tyrosine 10 critically enhances amyloid beta aggregation and plaque formation. *Neuron* 71, 833–844.

(47) Rezaei-Ghaleh, N., Amininasab, M., Kumar, S., Walter, J., and Zweckstetter, M. (2016) Phosphorylation modifies the molecular stability of beta-amyloid deposits. *Nat. Commun.* 7, 11359.

(48) Barykin, E. P., Petrushanko, I. Y., Burnysheva, K. M., Makarov, A. A., and Mitkevich, V. A. (2016) Isomerization of Asp7 increases the toxic effects of amyloid beta and its phosphorylated form in SH-SY5Y neuroblastoma cells. *Mol. Biol. (Moscow, Russ. Fed., Engl. Ed.)* 50, 762.

(49) Scheidt, H. A., Adler, J., Zeitschel, U., Hofling, C., Korn, A., Krueger, M., Rossner, S., and Huster, D. (2017) Pyroglutamate-Modified Amyloid beta (11–40) Fibrils Are More Toxic than Wildtype Fibrils but Structurally Very Similar. *Chem. - Eur. J.* 23, 15834–15838.

(50) Scheidt, H. A., Adler, J., Krueger, M., and Huster, D. (2016) Fibrils of Truncated Pyroglutamyl-Modified Abeta Peptide Exhibit a Similar Structure as Wildtype Mature Abeta Fibrils. *Sci. Rep.* 6, 33531.

(51) Rezaei-Ghaleh, N., Kumar, S., Walter, J., and Zweckstetter, M. (2016) Phosphorylation Interferes with Maturation of Amyloid-beta Fibrillar Structure in the N Terminus. *J. Biol. Chem.* 291, 16059–16067.

(52) Hu, Z. W., Vugmeyster, L., Au, D. F., Ostrovsky, D., Sun, Y., and Qiang, W. (2019) Molecular structure of an N-terminal phosphorylated beta-amyloid fibril. *Proc. Natl. Acad. Sci. U. S. A.* 116, 11253–11258.

(53) Hayden, E. Y., and Teplow, D. B. (2013) Amyloid beta-protein oligomers and Alzheimer's disease. *Alzheimer's Res. Ther.* 5, 60.

(54) Kotler, S. A., Brender, J. R., Vivekanandan, S., Suzuki, Y., Yamamoto, K., Monette, M., Krishnamoorthy, J., Walsh, P., Cauble, M., Holl, M. M., Marsh, E. N., and Ramamoorthy, A. (2015) High-resolution NMR characterization of low abundance oligomers of amyloid-beta without purification. *Sci. Rep.* 5, 11811.

(55) Brender, J. R., Ghosh, A., Kotler, S. A., Krishnamoorthy, J., Bera, S., Morris, V., Sil, T. B., Garai, K., Reif, B., Bhunia, A., and Ramamoorthy, A. (2019) Probing transient non-native states in amyloid beta fiber elongation by NMR. *Chem. Commun. (Cambridge, U. K.)* 55, 4483–4486.

(56) Serra-Batiste, M., Ninot-Pedrosa, M., Bayoumi, M., Gairi, M., Maglia, G., and Carulla, N. (2016) Aβ42 assembles into specific barrel pore-forming oligomers in membrane-mimicking environments. *Proc. Natl. Acad. Sci. U. S. A.* 113, 10866–10871.

(57) Lendel, C., Bjerring, M., Dubnovitsky, A., Kelly, R. T., Filippov, A., Antzutkin, O. N., Nielsen, N. C., and Hard, T. (2014) A hexameric peptide barrel as building block of amyloid-beta protofibrils. *Angew. Chem., Int. Ed.* 53, 12756–12760.

(58) Gopinath, T., and Veglia, G. (2012) Dual acquisition magic-angle spinning solid-state NMR-spectroscopy: simultaneous acquisition of multidimensional spectra of biomacromolecules. *Angew. Chem., Int. Ed.* 51, 2731–2735.

(59) Takegoshi, K., Nakamura, S., and Terao, T. (2001) C-13-H-1 dipolar-assisted rotational resonance in magic-angle spinning NMR. *Chem. Phys. Lett.* 344, 631–637.

(60) Bielecki, A., Kolbert, A. C., and Levitt, M. H. (1989) Frequency-switched pulse sequences: homonuclear decoupling and dilute spin NMR in solids. *Chem. Phys. Lett.* 155, 341–345.

(61) Huster, D., Yamaguchi, S., and Hong, M. (2000) Efficient-sheet identification in proteins by solid-state NMR spectroscopy. *J. Am. Chem. Soc.* 122, 11320–11327.

(62) Barré, P., Zschörnig, O., Arnold, K., and Huster, D. (2003) Structural and dynamical changes of the bindin B18 peptide upon binding to lipid membranes. A solid-state NMR study. *Biochemistry* 42, 8377–8386.

(63) Huster, D., Xiao, L., and Hong, M. (2001) Solid-state NMR investigation of the dynamics of soluble and membrane-bound colicin Ia channel-forming domain. *Biochemistry* 40, 7662–7674.

(64) Hartlage-Rubsamen, M., Waniek, A., Meissner, J., Morawski, M., Schilling, S., Jäger, C., Kleinschmidt, M., Cynis, H., Kehlen, A., Arendt, T., Demuth, H. U., and Rossner, S. (2015) Isoglutamyl cyclase contributes to CCL2-driven neuroinflammation in Alzheimer's disease. *Acta Neuropathol.* 129, 565–583.

(65) Heiland, T., Zeitschel, U., Puchades, M. A., Kuhn, P. H., Lichtenthaler, S. F., Bjaalie, J. G., Hartlage-Rubsamen, M., Rossner, S., and Hofling, C. (2019) Defined astrocytic expression of human amyloid precursor protein in Tg2576 mouse brain. *Glia.* 67, 393–403.

6 References

1. Bradbury, J. Chaperones: keeping a close eye on protein folding. *THE LANCET* **361**, 1194–1195; 10.1016/S0140-6736(03)12975-3 (2003).
2. Chaudhuri, T. K. & Paul, S. Protein-misfolding diseases and chaperone-based therapeutic approaches. *THE FEBS JOURNAL* **273**, 1331–1349; 10.1111/j.1742-4658.2006.05181.x (2006).
3. Levenson, R. W., Sturm, V. E. & Haase, C. M. Emotional and behavioral symptoms in neurodegenerative disease: a model for studying the neural bases of psychopathology. *ANNUAL REVIEW OF CLINICAL PSYCHOLOGY* **10**, 581–606; 10.1146/annurev-clinpsy-032813-153653 (2014).
4. Dugger, B. N. & Dickson, D. W. Pathology of Neurodegenerative Diseases. *COLD SPRING HARBOR PERSPECTIVES IN BIOLOGY* **9**; 10.1101/cshperspect.a028035 (2017).
5. World Health Organization. World Health Organization The Global Health Observatory. Causes of death. Available at <https://www.who.int/data/gho/data/themes/topics/causes-of-death>.
6. M. Prince, A. Wimo, M. Guerchet, G.C. Ali, Y.-T. Wu and M. Prina. World Alzheimer Report 2015. The Global Impact of Dementia. An analysis of prevalence, incidence, costs and trends. *ALZHEIMER'S DISEASE INTERNATIONAL* (2015).
7. Jia, J. *et al.* The cost of Alzheimer's disease in China and re-estimation of costs worldwide. *ALZHEIMER'S & DEMENTIA : THE JOURNAL OF THE ALZHEIMER'S ASSOCIATION* **14**, 483–491; 10.1016/j.jalz.2017.12.006 (2018).
8. Lane, C. A., Hardy, J. & Schott, J. M. Alzheimer's disease. *EUROPEAN JOURNAL OF NEUROLOGY* **25**, 59–70; 10.1111/ene.13439 (2018).
9. Jost, B. C. & Grossberg, G. T. The natural history of Alzheimer's disease: a brain bank study. *JOURNAL OF THE AMERICAN GERIATRICS SOCIETY* **43**, 1248–1255; 10.1111/j.1532-5415.1995.tb07401.x (1995).
10. Xu, W. *et al.* Meta-analysis of modifiable risk factors for Alzheimer's disease. *JOURNAL OF NEUROLOGY, NEUROSURGERY, AND PSYCHIATRY* **86**, 1299–1306; 10.1136/jnnp-2015-310548 (2015).
11. A Armstrong, R. Risk factors for Alzheimer's disease. *FOLIA NEUROPATHOLOGICA* **57**, 87–105; 10.5114/fn.2019.85929 (2019).
12. Guo, T. *et al.* Molecular and cellular mechanisms underlying the pathogenesis of Alzheimer's disease. *MOLECULAR NEURODEGENERATION* **15**, 40; 10.1186/s13024-020-00391-7 (2020).
13. Milà-Alomà, M., Suárez-Calvet, M. & Molinuevo, J. L. Latest advances in cerebrospinal fluid and blood biomarkers of Alzheimer's disease. *THERAPEUTIC ADVANCES IN NEUROLOGICAL DISORDERS* **12**, 1756286419888819; 10.1177/1756286419888819 (2019).
14. Henikoff, S. & Henikoff, J. G. Performance evaluation of amino acid substitution matrices. *PROTEINS* **17**, 49–61; 10.1002/prot.340170108 (1993).

15. Saha, I., Maulik, U., Bandyopadhyay, S. & Plewczynski, D. Fuzzy clustering of physico-chemical and biochemical properties of amino acids. *AMINO ACIDS* **43**, 583–594; 10.1007/s00726-011-1106-9 (2012).
16. Taylor, W. R. The classification of amino acid conservation. *JOURNAL OF THEORETICAL BIOLOGY* **119**, 205–218; 10.1016/S0022-5193(86)80075-3 (1986).
17. RITZTIMME, S. & COLLINS, M. Racemization of aspartic acid in human proteins. *AGEING RESEARCH REVIEWS* **1**, 43–59; 10.1016/S0047-6374(01)00363-3 (2002).
18. Uversky, V. N., Gillespie, J. R. & Fink, A. L. Why are 'natively unfolded' proteins unstructured under physiologic conditions? *PROTEINS* **41**, 415–427; 10.1002/1097-0134(20001115)41:3<415::AID-PROT130>3.0.CO;2-7 (2000).
19. Uversky, V. N. Intrinsically disordered proteins from A to Z. *THE INTERNATIONAL JOURNAL OF BIOCHEMISTRY & CELL BIOLOGY* **43**, 1090–1103; 10.1016/j.biocel.2011.04.001 (2011).
20. Zhou, H.-X. & Pang, X. Electrostatic Interactions in Protein Structure, Folding, Binding, and Condensation. *CHEMICAL REVIEWS* **118**, 1691–1741; 10.1021/acs.chemrev.7b00305 (2018).
21. Oldfield, C. J. & Dunker, A. K. Intrinsically disordered proteins and intrinsically disordered protein regions. *ANNUAL REVIEW OF BIOCHEMISTRY* **83**, 553–584; 10.1146/annurev-biochem-072711-164947 (2014).
22. Uversky, V. N. *et al.* Unfoldomics of human diseases: linking protein intrinsic disorder with diseases. *BMC GENOMICS* **10 Suppl 1**, S7; 10.1186/1471-2164-10-S1-S7 (2009).
23. Das, R. K. & Pappu, R. V. Conformations of intrinsically disordered proteins are influenced by linear sequence distributions of oppositely charged residues. *PROCEEDINGS OF THE NATIONAL ACADEMY OF SCIENCES OF THE UNITED STATES OF AMERICA* **110**, 13392–13397; 10.1073/pnas.1304749110 (2013).
24. Ramachandran, G. N., Ramakrishnan, C. & Sasisekharan, V. Stereochemistry of polypeptide chain configurations. *JOURNAL OF MOLECULAR BIOLOGY* **7**, 95–99; 10.1016/S0022-2836(63)80023-6 (1963).
25. Nagy, G. & Oostenbrink, C. Dihedral-based segment identification and classification of biopolymers I: proteins. *JOURNAL OF CHEMICAL INFORMATION AND MODELING* **54**, 266–277; 10.1021/ci400541d (2014).
26. Kabsch, W. & Sander, C. Dictionary of protein secondary structure: pattern recognition of hydrogen-bonded and geometrical features. *BIOPOLYMERS* **22**, 2577–2637; 10.1002/bip.360221211 (1983).
27. Anfinsen, C. B. Principles that govern the folding of protein chains. *SCIENCE (NEW YORK, N. Y.)* **181**, 223–230; 10.1126/science.181.4096.223 (1973).
28. Hartl, F. U. & Hayer-Hartl, M. Converging concepts of protein folding in vitro and in vivo. *NATURE STRUCTURAL & MOLECULAR BIOLOGY* **16**, 574–581; 10.1038/nsmb.1591 (2009).
29. Feldman, D. E. & Frydman, J. Protein folding in vivo: the importance of molecular chaperones. *CURRENT OPINION IN STRUCTURAL BIOLOGY* **10**, 26–33; 10.1016/S0959-440X(99)00044-5 (2000).

30. Ciechanover, A. The ubiquitin-proteasome pathway: on protein death and cell life. *THE EMBO JOURNAL* **17**, 7151–7160; 10.1093/emboj/17.24.7151 (1998).
31. Johnston, H. E. & Samant, R. S. Alternative systems for misfolded protein clearance: life beyond the proteasome. *THE FEBS JOURNAL*; 10.1111/febs.15617 (2020).
32. Tsemekhman, K., Goldschmidt, L., Eisenberg, D. & Baker, D. Cooperative hydrogen bonding in amyloid formation. *PROTEIN SCIENCE : A PUBLICATION OF THE PROTEIN SOCIETY* **16**, 761–764; 10.1110/ps.062609607 (2007).
33. Cohen, N. & Eisenbach, C. D. Molecular Mechanics of Beta-Sheets. *ACS BIOMATERIALS SCIENCE & ENGINEERING* **6**, 1940–1949; 10.1021/acsbiomaterials.9b01983 (2020).
34. Sawaya, M. R. *et al.* Atomic structures of amyloid cross-beta spines reveal varied steric zippers. *NATURE* **447**, 453–457; 10.1038/nature05695 (2007).
35. Makin, O. S. & Serpell, L. C. Structures for amyloid fibrils. *THE FEBS JOURNAL* **272**, 5950–5961; 10.1111/j.1742-4658.2005.05025.x (2005).
36. Dill, K. A. Dominant forces in protein folding. *BIOCHEMISTRY* **29**, 7133–7155; 10.1021/bi00483a001 (1990).
37. Nick Pace, C., Scholtz, J. M. & Grimsley, G. R. Forces stabilizing proteins. *FEBS LETTERS* **588**, 2177–2184; 10.1016/j.febslet.2014.05.006 (2014).
38. Baldwin, R. L. The new view of hydrophobic free energy. *FEBS LETTERS* **587**, 1062–1066; 10.1016/j.febslet.2013.01.006 (2013).
39. Sticke, D. F., Presta, L. G., Dill, K. A. & Rose, G. D. Hydrogen bonding in globular proteins. *JOURNAL OF MOLECULAR BIOLOGY* **226**, 1143–1159; 10.1016/0022-2836(92)91058-W (1992).
40. Gilli, G. & Gilli, P. Towards an unified hydrogen-bond theory. *JOURNAL OF MOLECULAR STRUCTURE* **552**, 1–15; 10.1016/S0022-2860(00)00454-3 (2000).
41. Gao, J., Bosco, D. A., Powers, E. T. & Kelly, J. W. Localized thermodynamic coupling between hydrogen bonding and microenvironment polarity substantially stabilizes proteins. *NATURE STRUCTURAL & MOLECULAR BIOLOGY* **16**, 684–690; 10.1038/nsmb.1610 (2009).
42. Newberry, R. W. & Raines, R. T. Secondary Forces in Protein Folding. *ACS CHEMICAL BIOLOGY* **14**, 1677–1686; 10.1021/acscchembio.9b00339 (2019).
43. Dobson, C. M. Protein folding and misfolding. *NATURE* **426**, 884–890; 10.1038/nature02261 (2003).
44. Zwanzig, R., Szabo, A. & Bagchi, B. Levinthal's paradox. *PROCEEDINGS OF THE NATIONAL ACADEMY OF SCIENCES* **89**, 20–22; 10.1073/pnas.89.1.20 (1992).
45. Karplus, M. & Weaver, D. L. Protein folding dynamics: the diffusion-collision model and experimental data. *PROTEIN SCIENCE : A PUBLICATION OF THE PROTEIN SOCIETY* **3**, 650–668; 10.1002/pro.5560030413 (1994).
46. Jahn, T. R. & Radford, S. E. Folding versus aggregation: polypeptide conformations on competing pathways. *ARCHIVES OF BIOCHEMISTRY AND BIOPHYSICS* **469**, 100–117; 10.1016/j.abb.2007.05.015 (2008).
47. Daggett, V. & Fersht, A. R. Is there a unifying mechanism for protein folding? *TRENDS IN BIOCHEMICAL SCIENCES* **28**, 18–25; 10.1016/S0968-0004(02)00012-9 (2003).

48. Brylinski, M., Konieczny, L. & Roterman, I. Hydrophobic collapse in (in silico) protein folding. *COMPUTATIONAL BIOLOGY AND CHEMISTRY* **30**, 255–267; 10.1016/j.compbiolchem.2006.04.007 (2006).
49. Fersht, A. R. Nucleation mechanisms in protein folding. *CURRENT OPINION IN STRUCTURAL BIOLOGY* **7**, 3–9; 10.1016/S0959-440X(97)80002-4 (1997).
50. Kiefhaber, T., Rudolph, R., Kohler, H. H. & Buchner, J. Protein aggregation in vitro and in vivo: a quantitative model of the kinetic competition between folding and aggregation. *BIO/TECHNOLOGY (NATURE PUBLISHING COMPANY)* **9**, 825–829; 10.1038/nbt0991-825 (1991).
51. Merlini, G. & Bellotti, V. Molecular mechanisms of amyloidosis. *THE NEW ENGLAND JOURNAL OF MEDICINE* **349**, 583–596; 10.1056/NEJMra023144 (2003).
52. Chiti, F. & Dobson, C. M. Protein misfolding, functional amyloid, and human disease. *ANNUAL REVIEW OF BIOCHEMISTRY* **75**, 333–366; 10.1146/annurev.biochem.75.101304.123901 (2006).
53. Scollo, F. & La Rosa, C. Amyloidogenic Intrinsically Disordered Proteins: New Insights into Their Self-Assembly and Their Interaction with Membranes. *LIFE (BASEL, SWITZERLAND)* **10**; 10.3390/life10080144 (2020).
54. Uversky, V. N. Intrinsically Disordered Proteins and Their “Mysterious” (Meta)Physics. *FRONT. PHYS.* **7**; 10.3389/fphy.2019.00010 (2019).
55. Côté, S., Derreumaux, P. & Mousseau, N. Distinct Morphologies for Amyloid Beta Protein Monomer: A β 1-40, A β 1-42, and A β 1-40(D23N). *JOURNAL OF CHEMICAL THEORY AND COMPUTATION* **7**, 2584–2592; 10.1021/ct1006967 (2011).
56. Vivekanandan, S., Brender, J. R., Lee, S. Y. & Ramamoorthy, A. A partially folded structure of amyloid-beta(1-40) in an aqueous environment. *BIOCHEMICAL AND BIOPHYSICAL RESEARCH COMMUNICATIONS* **411**, 312–316; 10.1016/j.bbrc.2011.06.133 (2011).
57. Hou, L. *et al.* Solution NMR studies of the A beta(1-40) and A beta(1-42) peptides establish that the Met35 oxidation state affects the mechanism of amyloid formation. *JOURNAL OF THE AMERICAN CHEMICAL SOCIETY* **126**, 1992–2005; 10.1021/ja036813f (2004).
58. Ono, K., Condrón, M. M. & Teplow, D. B. Structure-neurotoxicity relationships of amyloid beta-protein oligomers. *PROCEEDINGS OF THE NATIONAL ACADEMY OF SCIENCES* **106**, 14745–14750; 10.1073/pnas.0905127106 (2009).
59. Lazo, N. D., Grant, M. A., Condrón, M. C., Rigby, A. C. & Teplow, D. B. On the nucleation of amyloid beta-protein monomer folding. *PROTEIN SCIENCE : A PUBLICATION OF THE PROTEIN SOCIETY* **14**, 1581–1596; 10.1110/ps.041292205 (2005).
60. Sarkar, B. *et al.* Significant structural differences between transient amyloid- β oligomers and less-toxic fibrils in regions known to harbor familial Alzheimer's mutations. *ANGEWANDTE CHEMIE (INTERNATIONAL ED. IN ENGLISH)* **53**, 6888–6892; 10.1002/anie.201402636 (2014).
61. Ciudad, S. *et al.* A β (1-42) tetramer and octamer structures reveal edge conductivity pores as a mechanism for membrane damage. *NATURE COMMUNICATIONS* **11**, 3014; 10.1038/s41467-020-16566-1 (2020).

62. Lendel, C. *et al.* A hexameric peptide barrel as building block of amyloid- β protofibrils. *ANGEWANDTE CHEMIE (INTERNATIONAL ED. IN ENGLISH)* **53**, 12756–12760; 10.1002/anie.201406357 (2014).
63. Huang, T. H. *et al.* Structural studies of soluble oligomers of the Alzheimer beta-amyloid peptide. *JOURNAL OF MOLECULAR BIOLOGY* **297**, 73–87; 10.1006/jmbi.2000.3559 (2000).
64. Chimon, S. *et al.* Evidence of fibril-like β -sheet structures in a neurotoxic amyloid intermediate of Alzheimer's β -amyloid. *NATURE STRUCTURAL & MOLECULAR BIOLOGY* **14**, 1157–1164; 10.1038/nsmb1345 (2007).
65. Sandberg, A. *et al.* Stabilization of neurotoxic Alzheimer amyloid-beta oligomers by protein engineering. *PROCEEDINGS OF THE NATIONAL ACADEMY OF SCIENCES OF THE UNITED STATES OF AMERICA* **107**, 15595–15600; 10.1073/pnas.1001740107 (2010).
66. Hoyer, W., Grönwall, C., Jonsson, A., Ståhl, S. & Härd, T. Stabilization of a beta-hairpin in monomeric Alzheimer's amyloid-beta peptide inhibits amyloid formation. *PROCEEDINGS OF THE NATIONAL ACADEMY OF SCIENCES* **105**, 5099–5104; 10.1073/pnas.0711731105 (2008).
67. Chandra, B. *et al.* Major Reaction Coordinates Linking Transient Amyloid- β Oligomers to Fibrils Measured at Atomic Level. *BIOPHYSICAL JOURNAL* **113**, 805–816; 10.1016/j.bpj.2017.06.068 (2017).
68. Sarroukh, R. *et al.* Transformation of amyloid β (1-40) oligomers into fibrils is characterized by a major change in secondary structure. *CELLULAR AND MOLECULAR LIFE SCIENCES : CMLS* **68**, 1429–1438; 10.1007/s00018-010-0529-x (2011).
69. Cerf, E. *et al.* Antiparallel beta-sheet: a signature structure of the oligomeric amyloid beta-peptide. *THE BIOCHEMICAL JOURNAL* **421**, 415–423; 10.1042/BJ20090379 (2009).
70. Walsh, D. M. *et al.* Amyloid beta-protein fibrillogenesis. Structure and biological activity of protofibrillar intermediates. *THE JOURNAL OF BIOLOGICAL CHEMISTRY* **274**, 25945–25952; 10.1074/jbc.274.36.25945 (1999).
71. Scheidt, H. A., Morgado, I., Rothmund, S., Huster, D. & Fändrich, M. Solid-state NMR spectroscopic investigation of A β protofibrils: implication of a β -sheet remodeling upon maturation into terminal amyloid fibrils. *ANGEWANDTE CHEMIE (INTERNATIONAL ED. IN ENGLISH)* **50**, 2837–2840; 10.1002/anie.201007265 (2011).
72. Scheidt, H. A., Morgado, I. & Huster, D. Solid-state NMR reveals a close structural relationship between amyloid- β protofibrils and oligomers. *THE JOURNAL OF BIOLOGICAL CHEMISTRY* **287**, 22822–22826; 10.1074/jbc.M112.367474 (2012).
73. Gillam, J. E. & MacPhee, C. E. Modelling amyloid fibril formation kinetics: mechanisms of nucleation and growth. *JOURNAL OF PHYSICS. CONDENSED MATTER : AN INSTITUTE OF PHYSICS JOURNAL* **25**, 373101; 10.1088/0953-8984/25/37/373101 (2013).
74. Kheterpal, I., Chen, M., Cook, K. D. & Wetzel, R. Structural differences in Abeta amyloid protofibrils and fibrils mapped by hydrogen exchange--mass spectrometry with on-line proteolytic fragmentation. *JOURNAL OF MOLECULAR BIOLOGY* **361**, 785–795; 10.1016/j.jmb.2006.06.066 (2006).

75. Evason, K., Huang, C., Yamben, I., Covey, D. F. & Kornfeld, K. Anticonvulsant medications extend worm life-span. *SCIENCE (NEW YORK, N. Y.)* **307**, 258–262; 10.1126/science.1105299 (2005).
76. Qiang, W., Yau, W.-M., Lu, J.-X., Collinge, J. & Tycko, R. Structural variation in amyloid- β fibrils from Alzheimer's disease clinical subtypes. *NATURE* **541**, 217–221; 10.1038/nature20814 (2017).
77. Paravastu, A. K., Qahwash, I., Leapman, R. D., Meredith, S. C. & Tycko, R. Seeded growth of beta-amyloid fibrils from Alzheimer's brain-derived fibrils produces a distinct fibril structure. *PROCEEDINGS OF THE NATIONAL ACADEMY OF SCIENCES* **106**, 7443–7448; 10.1073/pnas.0812033106 (2009).
78. Williams, A. D. *et al.* Mapping abeta amyloid fibril secondary structure using scanning proline mutagenesis. *JOURNAL OF MOLECULAR BIOLOGY* **335**, 833–842; 10.1016/j.jmb.2003.11.008 (2004).
79. Paravastu, A. K., Leapman, R. D., Yau, W.-M. & Tycko, R. Molecular structural basis for polymorphism in Alzheimer's beta-amyloid fibrils. *PROCEEDINGS OF THE NATIONAL ACADEMY OF SCIENCES OF THE UNITED STATES OF AMERICA* **105**, 18349–18354; 10.1073/pnas.0806270105 (2008).
80. Das, A. K. *et al.* An early folding contact between Phe19 and Leu34 is critical for amyloid- β oligomer toxicity. *ACS CHEMICAL NEUROSCIENCE* **6**, 1290–1295; 10.1021/acschemneuro.5b00074 (2015).
81. Söldner, C. A., Sticht, H. & Horn, A. H. C. Role of the N-terminus for the stability of an amyloid- β fibril with three-fold symmetry. *PLOS ONE* **12**, e0186347; 10.1371/journal.pone.0186347 (2017).
82. Streltsov, V. X-ray absorption and diffraction studies of the metal binding sites in amyloid beta-peptide. *EUROPEAN BIOPHYSICS JOURNAL : EBJ* **37**, 257–263; 10.1007/s00249-007-0232-5 (2008).
83. Ghosh, U., Thurber, K. R., Yau, W.-M. & Tycko, R. Molecular structure of a prevalent amyloid- β fibril polymorph from Alzheimer's disease brain tissue. *PROCEEDINGS OF THE NATIONAL ACADEMY OF SCIENCES OF THE UNITED STATES OF AMERICA* **118**; 10.1073/pnas.2023089118 (2021).
84. Andersen, C. B. *et al.* Branching in amyloid fibril growth. *BIOPHYSICAL JOURNAL* **96**, 1529–1536; 10.1016/j.bpj.2008.11.024 (2009).
85. Meinhardt, J., Sachse, C., Hortschansky, P., Grigorieff, N. & Fändrich, M. Abeta(1-40) fibril polymorphism implies diverse interaction patterns in amyloid fibrils. *JOURNAL OF MOLECULAR BIOLOGY* **386**, 869–877; 10.1016/j.jmb.2008.11.005 (2009).
86. Adler, J., Scheidt, H. A., Krüger, M., Thomas, L. & Huster, D. Local interactions influence the fibrillation kinetics, structure and dynamics of A β (1-40) but leave the general fibril structure unchanged. *PHYSICAL CHEMISTRY CHEMICAL PHYSICS : PCCP* **16**, 7461–7471; 10.1039/c3cp54501f (2014).
87. Hilbich, C., Kisters-Woike, B., Reed, J., Masters, C. L. & BEYREUTHER, K. Substitutions of hydrophobic amino acids reduce the amyloidogenicity of Alzheimer's disease β A4 peptides. *JOURNAL OF MOLECULAR BIOLOGY* **228**, 460–473; 10.1016/0022-2836(92)90835-8 (1992).

88. Hoffmann, F. *et al.* Perturbation of the F19-L34 Contact in Amyloid β (1-40) Fibrils Induces Only Local Structural Changes but Abolishes Cytotoxicity. *THE JOURNAL OF PHYSICAL CHEMISTRY LETTERS* **8**, 4740–4745; 10.1021/acs.jpcclett.7b02317 (2017).
89. Bateman, R. J. *et al.* Autosomal-dominant Alzheimer's disease: a review and proposal for the prevention of Alzheimer's disease. *ALZHEIMER'S RESEARCH & THERAPY* **3**, 1; 10.1186/alzrt59 (2011).
90. Zhou, L. *et al.* Amyloid precursor protein mutation E682K at the alternative β -secretase cleavage β '-site increases A β generation. *EMBO MOLECULAR MEDICINE* **3**, 291–302; 10.1002/emmm.201100138 (2011).
91. Tsubuki, S., Takai, Y. & Saido, T. C. Dutch, Flemish, Italian, and Arctic mutations of APP and resistance of A β to physiologically relevant proteolytic degradation. *THE LANCET* **361**, 1957–1958; 10.1016/S0140-6736(03)13555-6 (2003).
92. Kaden, D. *et al.* Novel APP/A β mutation K16N produces highly toxic heteromeric A β oligomers. *EMBO MOLECULAR MEDICINE* **4**, 647–659; 10.1002/emmm.201200239 (2012).
93. Chong, S.-H., Yim, J. & Ham, S. Structural heterogeneity in familial Alzheimer's disease mutants of amyloid-beta peptides. *MOLECULAR BIOSYSTEMS* **9**, 997–1003; 10.1039/c2mb25457c (2013).
94. Hubin, E. *et al.* Two distinct β -sheet structures in Italian-mutant amyloid-beta fibrils: a potential link to different clinical phenotypes. *CELLULAR AND MOLECULAR LIFE SCIENCES : CMLS* **72**, 4899–4913; 10.1007/s00018-015-1983-2 (2015).
95. Päiviö, A., Jarvet, J., Gräslund, A., Lannfelt, L. & Westlind-Danielsson, A. Unique physicochemical profile of beta-amyloid peptide variant Abeta1-40E22G protofibrils: conceivable neuropathogen in arctic mutant carriers. *JOURNAL OF MOLECULAR BIOLOGY* **339**, 145–159; 10.1016/j.jmb.2004.03.028 (2004).
96. Rönnbäck, A. *et al.* Mitochondrial dysfunction in a transgenic mouse model expressing human amyloid precursor protein (APP) with the Arctic mutation. *JOURNAL OF NEUROCHEMISTRY* **136**, 497–502; 10.1111/jnc.13410 (2016).
97. Rönnbäck, A. *et al.* Amyloid neuropathology in the single Arctic APP transgenic model affects interconnected brain regions. *NEUROBIOLOGY OF AGING* **33**, 831.e11-9; 10.1016/j.neurobiolaging.2011.07.012 (2012).
98. Kumar-Singh, S. *et al.* In vitro studies of Flemish, Dutch, and wild-type beta-amyloid provide evidence for two-staged neurotoxicity. *NEUROBIOLOGY OF DISEASE* **11**, 330–340; 10.1006/nbdi.2002.0529 (2002).
99. Korn, A. *et al.* Amyloid β (1-40) Toxicity Depends on the Molecular Contact between Phenylalanine 19 and Leucine 34. *ACS CHEMICAL NEUROSCIENCE* **9**, 790–799; 10.1021/acschemneuro.7b00360 (2018).
100. Obici, L. *et al.* A novel AbetaPP mutation exclusively associated with cerebral amyloid angiopathy. *ANNALS OF NEUROLOGY* **58**, 639–644; 10.1002/ana.20571 (2005).
101. Hori, Y. *et al.* The Tottori (D7N) and English (H6R) familial Alzheimer disease mutations accelerate Abeta fibril formation without increasing protofibril formation. *THE JOURNAL OF BIOLOGICAL CHEMISTRY* **282**, 4916–4923; 10.1074/jbc.M608220200 (2007).

102. Ono, K., Condrón, M. M. & Teplow, D. B. Effects of the English (H6R) and Tottori (D7N) familial Alzheimer disease mutations on amyloid beta-protein assembly and toxicity. *THE JOURNAL OF BIOLOGICAL CHEMISTRY* **285**, 23186–23197; 10.1074/jbc.M109.086496 (2010).
103. Chen, W.-T. *et al.* Amyloid-beta (A β) D7H mutation increases oligomeric A β 42 and alters properties of A β -zinc/copper assemblies. *PLOS ONE* **7**, e35807; 10.1371/journal.pone.0035807 (2012).
104. Xu, L., Chen, Y. & Wang, X. Dual effects of familial Alzheimer's disease mutations (D7H, D7N, and H6R) on amyloid β peptide: correlation dynamics and zinc binding. *PROTEINS* **82**, 3286–3297; 10.1002/prot.24669 (2014).
105. Fossati, S. *et al.* Differential activation of mitochondrial apoptotic pathways by vasculotropic amyloid-beta variants in cells composing the cerebral vessel walls. *FASEB JOURNAL : OFFICIAL PUBLICATION OF THE FEDERATION OF AMERICAN SOCIETIES FOR EXPERIMENTAL BIOLOGY* **24**, 229–241 (2010).
106. Ali, F. E. *et al.* Methionine regulates copper/hydrogen peroxide oxidation products of A β . *JOURNAL OF PEPTIDE SCIENCE : AN OFFICIAL PUBLICATION OF THE EUROPEAN PEPTIDE SOCIETY* **11**, 353–360; 10.1002/psc.626 (2005).
107. Ciccotosto, G. D. *et al.* Methionine oxidation: Implications for the mechanism of toxicity of the β -amyloid peptide from Alzheimer's disease. *INT J PEPT RES THER* **10**, 413–417; 10.1007/s10989-004-2394-7 (2003).
108. Kummer, M. P. *et al.* Nitration of tyrosine 10 critically enhances amyloid β aggregation and plaque formation. *NEURON* **71**, 833–844; 10.1016/j.neuron.2011.07.001 (2011).
109. Halim, A. *et al.* Site-specific characterization of threonine, serine, and tyrosine glycosylations of amyloid precursor protein/amyloid beta-peptides in human cerebrospinal fluid. *PROCEEDINGS OF THE NATIONAL ACADEMY OF SCIENCES OF THE UNITED STATES OF AMERICA* **108**, 11848–11853; 10.1073/pnas.1102664108 (2011).
110. Roher, A. E. *et al.* Structural alterations in the peptide backbone of beta-amyloid core protein may account for its deposition and stability in Alzheimer's disease. *THE JOURNAL OF BIOLOGICAL CHEMISTRY* **268**, 3072–3083 (1993).
111. Fukuda, H., Shimizu, T., Nakajima, M., Mori, H. & Shirasawa, T. Synthesis, aggregation, and neurotoxicity of the Alzheimer's A β 1-42 amyloid peptide and its isoaspartyl isomers. *BIOORGANIC & MEDICINAL CHEMISTRY LETTERS* **9**, 953–956; 10.1016/S0960-894X(99)00121-3 (1999).
112. Inoue, K. *et al.* Simultaneous determination of post-translational racemization and isomerization of N-terminal amyloid- β in Alzheimer's brain tissues by covalent chiral derivatized ultraperformance liquid chromatography tandem mass spectrometry. *ANALYTICAL CHEMISTRY* **86**, 797–804; 10.1021/ac403315h (2014).
113. Kumar, S. *et al.* Early intraneuronal accumulation and increased aggregation of phosphorylated A β in a mouse model of Alzheimer's disease. *ACTA NEUROPATHOLOGICA* **125**, 699–709; 10.1007/s00401-013-1107-8 (2013).
114. Kumar, S. *et al.* Extracellular phosphorylation of the amyloid β -peptide promotes formation of toxic aggregates during the pathogenesis of Alzheimer's disease. *THE EMBO JOURNAL* **30**, 2255–2265; 10.1038/emboj.2011.138 (2011).

115. Rezaei-Ghaleh, N., Amininasab, M., Kumar, S., Walter, J. & Zweckstetter, M. Phosphorylation modifies the molecular stability of β -amyloid deposits. *NATURE COMMUNICATIONS* **7**, 11359; 10.1038/ncomms11359 (2016).
116. Jamasbi, E., Separovic, F., Hossain, M. A. & Ciccotosto, G. D. Phosphorylation of a full length amyloid- β peptide modulates its amyloid aggregation, cell binding and neurotoxic properties. *MOLECULAR BIOSYSTEMS* **13**, 1545–1551; 10.1039/c7mb00249a (2017).
117. Kumar, S. *et al.* Phosphorylation of the amyloid β -peptide at Ser26 stabilizes oligomeric assembly and increases neurotoxicity. *ACTA NEUROPATHOLOGICA* **131**, 525–537; 10.1007/s00401-016-1546-0 (2016).
118. Kubo, T., Nishimura, S., Kumagae, Y. & Kaneko, I. In vivo conversion of racemized beta-amyloid (D-Ser 26A beta 1-40) to truncated and toxic fragments (D-Ser 26A beta 25-35/40) and fragment presence in the brains of Alzheimer's patients. *JOURNAL OF NEUROSCIENCE RESEARCH* **70**, 474–483; 10.1002/jnr.10391 (2002).
119. Cox, P. A., Kostrzewa, R. M. & Guillemin, G. J. BMAA and Neurodegenerative Illness. *NEUROTOXICITY RESEARCH* **33**, 178–183; 10.1007/s12640-017-9753-6 (2018).
120. Chiu, A. S. *et al.* Excitotoxic potential of the cyanotoxin β -methyl-amino-L-alanine (BMAA) in primary human neurons. *TOXICON: OFFICIAL JOURNAL OF THE INTERNATIONAL SOCIETY ON TOXICOLOGY* **60**, 1159–1165; 10.1016/j.toxicon.2012.07.169 (2012).
121. van Onselen, R., Venables, L., van de Venter, M. & Downing, T. G. β -N-Methylamino-L-Alanine Toxicity in PC12: Excitotoxicity vs. Misincorporation. *NEUROTOXICITY RESEARCH* **33**, 15–23; 10.1007/s12640-017-9743-8 (2018).
122. Chiu, A. S., Gehringer, M. M., Welch, J. H. & Neilan, B. A. Does α -amino- β -methylaminopropionic acid (BMAA) play a role in neurodegeneration? *INTERNATIONAL JOURNAL OF ENVIRONMENTAL RESEARCH AND PUBLIC HEALTH* **8**, 3728–3746; 10.3390/ijerph8093728 (2011).
123. Müller, U. C., Deller, T. & Korte, M. Not just amyloid: physiological functions of the amyloid precursor protein family. *NATURE REVIEWS. NEUROSCIENCE* **18**, 281–298; 10.1038/nrn.2017.29 (2017).
124. Prox, J. *et al.* Postnatal disruption of the disintegrin/metalloproteinase ADAM10 in brain causes epileptic seizures, learning deficits, altered spine morphology, and defective synaptic functions. *THE JOURNAL OF NEUROSCIENCE: THE OFFICIAL JOURNAL OF THE SOCIETY FOR NEUROSCIENCE* **33**, 12915–28, 12928a; 10.1523/JNEUROSCI.5910-12.2013 (2013).
125. Kuhn, P.-H. *et al.* ADAM10 is the physiologically relevant, constitutive alpha-secretase of the amyloid precursor protein in primary neurons. *THE EMBO JOURNAL* **29**, 3020–3032; 10.1038/emboj.2010.167 (2010).
126. Vassar, R. *et al.* Function, therapeutic potential and cell biology of BACE proteases: current status and future prospects. *JOURNAL OF NEUROCHEMISTRY* **130**, 4–28; 10.1111/jnc.12715 (2014).
127. Tomita, T. Molecular mechanism of intramembrane proteolysis by γ -secretase. *JOURNAL OF BIOCHEMISTRY* **156**, 195–201; 10.1093/jb/mvu049 (2014).

128. Andrew, R. J., Kellett, K. A. B., Thinakaran, G. & Hooper, N. M. A Greek Tragedy: The Growing Complexity of Alzheimer Amyloid Precursor Protein Proteolysis. *THE JOURNAL OF BIOLOGICAL CHEMISTRY* **291**, 19235–19244; 10.1074/jbc.R116.746032 (2016).
129. Bayer, T. A. & Wirths, O. Focusing the amyloid cascade hypothesis on N-truncated Abeta peptides as drug targets against Alzheimer's disease. *ACTA NEUROPATHOLOGICA* **127**, 787–801; 10.1007/s00401-014-1287-x (2014).
130. Nesterov, E. E. *et al.* In vivo optical imaging of amyloid aggregates in brain: design of fluorescent markers. *ANGEWANDTE CHEMIE (INTERNATIONAL ED. IN ENGLISH)* **44**, 5452–5456; 10.1002/anie.200500845 (2005).
131. Sasaki, S., Drummen, G. P. C. & Konishi, G. Recent advances in twisted intramolecular charge transfer (TICT) fluorescence and related phenomena in materials chemistry. *J. MATER. CHEM. C* **4**, 2731–2743; 10.1039/C5TC03933A (2016).
132. Gade Malmos, K. *et al.* ThT 101: a primer on the use of thioflavin T to investigate amyloid formation. *AMYLOID : THE INTERNATIONAL JOURNAL OF EXPERIMENTAL AND CLINICAL INVESTIGATION : THE OFFICIAL JOURNAL OF THE INTERNATIONAL SOCIETY OF AMYLOIDOSIS* **24**, 1–16; 10.1080/13506129.2017.1304905 (2017).
133. Biancalana, M. & Koide, S. Molecular mechanism of Thioflavin-T binding to amyloid fibrils. *BIOCHIMICA ET BIOPHYSICA ACTA* **1804**, 1405–1412; 10.1016/j.bbapap.2010.04.001 (2010).
134. Buell, A. K. The growth of amyloid fibrils: rates and mechanisms. *THE BIOCHEMICAL JOURNAL* **476**, 2677–2703; 10.1042/BCJ20160868 (2019).
135. Hackl, E. V., Darkwah, J., Smith, G. & Ermolina, I. Effect of acidic and basic pH on Thioflavin T absorbance and fluorescence. *EUROPEAN BIOPHYSICS JOURNAL : EBJ* **44**, 249–261; 10.1007/s00249-015-1019-8 (2015).
136. Andersen, C. B., Otzen, D., Christiansen, G. & Rischel, C. Glucagon amyloid-like fibril morphology is selected via morphology-dependent growth inhibition. *BIOCHEMISTRY* **46**, 7314–7324; 10.1021/bi6025374 (2007).
137. Whitmore, L. & Wallace, B. A. Protein secondary structure analyses from circular dichroism spectroscopy: methods and reference databases. *BIOPOLYMERS* **89**, 392–400; 10.1002/bip.20853 (2008).
138. Cobo, M. F., Achilles, A., Reichert, D., Deazevedo, E. R. & Saalwächter, K. Recoupled separated-local-field experiments and applications to study intermediate-regime molecular motions. *JOURNAL OF MAGNETIC RESONANCE (SAN DIEGO, CALIF. : 1997)* **221**, 85–96; 10.1016/j.jmr.2012.05.003 (2012).
139. Korn, A., Surendran, D., Krueger, M., Maiti, S. & Huster, D. Ring structure modifications of phenylalanine 19 increase fibrillation kinetics and reduce toxicity of amyloid β (1-40). *CHEMICAL COMMUNICATIONS (CAMBRIDGE, ENGLAND)* **54**, 5430–5433; 10.1039/c8cc01733f (2018).
140. Korn, A. *et al.* Incorporation of the Nonproteinogenic Amino Acid β -Methylamino-alanine Affects Amyloid β Fibril Properties and Toxicity. *ACS CHEMICAL NEUROSCIENCE* **11**, 1038–1047; 10.1021/acschemneuro.9b00660 (2020).

Acknowledgement

This work would not have come into being in the form it has without the support of a number of people, whom I would like to thank at this point.

Prof. Daniel Huster for supervising the work, the great freedom he gave me in working on the project, and the honest and direct feedback he gave me, which was a necessary point of reference for my work.

Prof. Dr. Tilo Pompe for supervising and reviewing the work at the Faculty of Life Sciences.

PD Dr. Scheidt and, above all, Dr. Juliane Adler for the instruction in the most important experiments, the technical support and especially the friendly cooperation.

Dr. Juliane Adler, PD Dr. Holger Scheidt and Steffane McLennan for collaboration on individual experiments.

PhD Dayana Surendran from the research group of Prof. Dr. Sudipta Maiti and Dr. Corinna Hoefling and Dr. Ulrike Zeitschel from the research group of Prof. Dr. Steffen Roßner for the contribution of the cell culture experiments.

PD Dr. Martin Krüger for taking the TEM images.

Dr. Christoph Parthier for measurement time and supervision at the X-ray diffractometer.

PD Dr. Holger Scheidt, Dr. Juliane Adler, Dr. Anja Penk, Dr. Benedikt Schwarze and Dr. David Ulbricht for feedback on the dissertation manuscript and my cousin Maike Wohlfarth for proof-reading in English.

The entire Huster working group and colleagues at the Institute of Medical Physics and Biophysics for the open, appreciative, and supportive work environment.

Prof. Dr. Sudipta Maiti for the opportunity to spend part of my PhD period in his group at TIFR and to gain insights into experimental methods and ways of working new to me, and to the whole Maiti group for warmly welcoming me into the group, especially Anirban Das, PhD Dayana Surendran and Dr. Barun Kumar Maity.

The SFB / TRR 102 for funding my position and the professional exchange as well as the iRTG for the training opportunities and the exchange with other PhD students.

To my friends for the in large parts constructive leisure, especially from Campus Inform, KV7, JBO und m.l.b.B.TJ!

My family, who supports me at all times, stands by me in every way possible and provides a safe haven for all my undertakings.

Curriculum vitae

Name: Alexander Korn

Date of birth: 15. May 1990

- 2018 Scientific stay, Tata Institute of Fundamental Research, Mumbai
- Since 2015 Research associate, Institute for Medical Physics and Biophysics, Leipzig University
- 2012 – 2014 Master program: Molecular Life Science, Friedrich-Schiller-Universität, Jena
Master Thesis: Investigations of the interaction of EGF-receptor (EGFR) and protein kinase C ϵ (PKC ϵ) in different cellular models
- 2009 – 2012 Bachelor program: Molecular Biomedicine, Rheinische Friedrich-Wilhelms-Universität of Bonn
Bachelor Thesis: Influence of saponins from *Hedera helix* L. on PKA dependent phosphorylation of β 2-adrenergic receptors
- 2008 – 2009 Federal voluntary service at Institute for Hydrosience, Laboratory for Hydraulic Experimentation, Water Protection and Ecology (Hydrolabor Schleusingen)
- 2000 – 2008 Abitur, Staatliches Gymnasium "Christian-Gottlieb-Reichard" Bad Lobenstein

Publications, presentations, posters

Publications

Schwarze, B., **Korn, A.**, Höfling, C., Zeitschel, U., Krueger, M., Roßner, S., & Huster, D. (2021). Peptide backbone modifications of amyloid β (1-40) impact fibrillation behavior and neuronal toxicity. *Scientific reports*, 11(1), 23767.

Fritzsche, J., **Korn, A.**, Surendran, D., Krueger, M., Scheidt, H. A., Mote, K. R., Madhu, P. K., Maiti, S., & Huster, D. (2021). Probing the Influence of Single-Site Mutations in the Central Cross- β Region of Amyloid β (1-40) Peptides. *Biomolecules*, 11(12), 1848.

Scheidt, H. A., Das, A., **Korn, A.**, Krueger, M., Maiti, S., & Huster, D. (2020). Structural characteristics of oligomers formed by pyroglutamate-modified amyloid β peptides studied by solid-state NMR. *Physical chemistry chemical physics: PCCP*, 22(29), 16887–16895.

Korn, A., Höfling, C., Zeitschel, U., Krueger, M., Roßner, S., & Huster, D. (2020). Incorporation of the Nonproteinogenic Amino Acid β -Methylamino-alanine Affects Amyloid β Fibril Properties and Toxicity. *ACS chemical neuroscience*, 11(7), 1038–1047.

Korn, A., Surendran, D., Krueger, M., Maiti, S., & Huster, D., (2018). Ring structure modifications of phenylalanine 19 increase fibrillation kinetics and reduce toxicity of amyloid β (1-40). *Chemical communications*, 54(43), 5430–5433.

Korn, A., McLennan, S., Adler, J., Krueger, M., Surendran, D., Maiti, S., & Huster, D. (2018). Amyloid β (1-40) Toxicity Depends on the Molecular Contact between Phenylalanine 19 and Leucine 34. *ACS chemical neuroscience*, 9(4), 790–799.

Scheidt, H. A., Adler, J., Zeitschel, U., Höfling, C., **Korn, A.**, Krueger, M., Roßner, S., & Huster, D. (2017). Pyroglutamate-Modified Amyloid β (11- 40) Fibrils Are More Toxic than Wildtype Fibrils but Structurally Very Similar. *Chemistry*, 23(62), 15834–15838.

Chandra, B., Haider, S., Adler, J., **Korn, A.**, Huster, D., & Maiti, S. (2017). Emerging structural details of transient amyloid-beta oligomers suggest designs for effective small molecule modulators. *Chemical Physics Letters*, 675, 51-55

Chandra, B., **Korn, A.**, Maity, B. K., Adler, J., Rawat, A., Krueger, M., Huster, D., & Maiti, S. (2017). Stereoisomers Probe Steric Zippers in Amyloid- β . *The journal of physical chemistry. B*, 121(8), 1835–1842.

Presentations

Effects of Minor Mutations of the F19-L34 Contact in Amyloid β Fibril Formation. SFB-TRR 102. Mini Symposium. Leipzig. 2016 Dec 2

Self-Organization and Dynamics of Mutated Amyloid- β Protein Fibrils. SFB-TRR 102. 7th retreat. Bad Schandau. 2021 Sep 13-15

Posters

Adler, J., **Korn, A.**, Baumann, M., Scheidt, H., Balbach, J., & Huster, D. Small Changes - Large Effects? The Influence of A β (1-40) L34I and L34d-L on Fibril -Kinetics, -Structure, and -Dynamics. 3rd SFB/TRR 102. Miniworkshop. Halle. 2015 Oct 2

Korn, A., Krueger, M., Haeupl, T., & Huster, D. Influence of BMAA Incorporation on β -Amyloid Structure. The Unusual Suspects in Neurodegeneration: Role of Non-Proteinogenic Amino Acids. Leiden. 2016 May 17-20

Adler, J., **Korn, A.**, Scheidt, H. A., & Huster, D. Investigations of the Influence of conjugated polymers, artificial amino acids & nanoparticles on kinetics, structure and dynamics of A β (1-40). 5th SFB/TRR 102. retreat. Lomhen. 2016 Sept 29

Adler, J., **Korn, A.**, Scheidt, H. A., & Huster, D. Investigations of alterations within the A β (1-40) structure. 4th SFB/TRR 102. Miniworkshop. Leipzig. 2017 May 12

Korn, A., Krüger, M., Roßner, S., & Huster, D. Serine substitution in Amyloid- β – a possible link between β -Methylamino-L-alanine and Alzheimer's disease? International Discussion Meeting on Polymer Crystallization. Wittenberg. 2017 Sept 18

Adler, J., **Korn, A.**, Scheidt, H. A., & Huster, D. Self-Organization and Dynamics of Amyloid Protein Fibrils. 6th SFB/TRR 102. Miniworkshop. Halle. 2018 Jul 9

Scheidt, H. A., **Korn, A.**, Krueger, M., & Huster, D. The oligomeric structure of pyroglutamyl-modified Ab peptides studied by solid-state NMR. 7th SFB/TRR 102. Miniworkshop. Leipzig. 2019 Nov 8

Korn, A., & Huster, D. Incorporation of the Non-proteinaceous Amino Acid β -Methyl-Amino-Alanine Affects Amyloid β Fibril Properties and Toxicity. 6th SFB/TRR 102. retreat. Bad Schandau. 2020 Mar 11

Declaration of independent work

The presented work was carried out in the period from July 2015 to February 2022 at the Institute of Medical Physics and Biophysics of the Medical Faculty of the Leipzig University in the group of Prof. Dr. Daniel Huster.

I hereby certify that I have written this paper independently and have not used any sources other than those listed in the bibliography. All persons involved in the creation of this work have been named by me. Apart from the persons named, no other persons were involved in the intellectual production of the present dissertation, in particular, the assistance of a doctoral advisor was not utilized and third parties have not received any monetary benefits, either directly or indirectly, for work related to the content of the submitted thesis.

All passages taken verbatim or in spirit from published or as yet unpublished sources are identified as such. The figures and illustrations in this paper have been created by myself or have an appropriate source reference. I have sole authorship of monographically added chapters.

This work has not been submitted in the same or similar form to any other audit authority.

Date, signature